

Synthesis and Characterization of
Dissymmetric Gemini Surfactants for Gene Delivery Applications

by

Aula Al Muslim

A thesis

presented to the University of Waterloo

in fulfillment of the

thesis requirement for the degree of

Doctor of Philosophy

in

Chemistry

Waterloo, Ontario, Canada, 2016

© Aula Al Muslim 2016

Author`s declaration

I hereby declare that I am the sole author of this thesis. This is a true copy of the thesis, including any required final revisions, as accepted by my examiners. I understand that my thesis may be made electronically available to the public.

Abstract

The lack of safe and efficient gene- delivery methods has been constantly a limiting obstacle to human gene therapy. Viral vectors have been superior in delivering exogenous DNA or RNA into a foreign cell due to their ability to integrate and generate their genetic material within a cell. However, their immunogenicity and the unfortunate deaths came as a consequence to these trials and shifted gears toward a safer realm. Histones are able to complex and compact DNA inside the nucleus. In the same manner, cationic polymers, lipids and gemini surfactants are able to complex DNA. Tremendous efforts have been made to enhance gene delivery with cationic moieties, such efforts are development of more compounds, and investigation of structure-activity correlation to improve transfection. Gemini surfactants are made of two surfactant monomers which are connected at the head group area with a spacer linker. They are able to compact and complex DNA efficiently and they can be synthesized at the bench top, with relatively low cost.

Two series of dissymmetric gemini surfactants, pyrene-based surfactants, pyr-3-n (n= 8, 12, 14, 16, and 18), and 12-3-n surfactants with n= 14, 16, and 18 were rationally designed and synthesized. Due to the bulky nature of pyrene ring and the increased hydrophobicity due to its presence, these surfactants exhibited lower values of critical micelle concentrations (CMC) with early onset of micellization compared to their symmetric m-3-m gemini surfactants. The dissymmetry with increased hydrophobicity with increasing the alkyl tail in 12-3-n surfactants caused dramatic reductions in CMC values. These dissymmetric surfactants have higher aggregation abilities due to increased intermolecular hydrophobic interactions within the micelle. Both of the groups showed higher degrees of micelle ionization, which is advantageous to gene delivery applications. This is mainly due to the easier access of anions to the surfactants

within the micelle in order to reduce the electrostatic repulsion caused by the ammonium head groups.

The lack of understanding of how DNA influences the arrangement of vector components during the complexation of DNA, as well as their interaction with biological membranes is still a major barrier hindering the transfection abilities of non-viral vectors. Hence in this work we characterized the arrangement of the gemini surfactants and phospholipids that make up the transfection vector (both in the presence and absence of DNA) as well as the effect of these components on model biological membranes using Brewster's Angle Microscopy (BAM).

Two model membrane systems were characterized, DPPC/Cholesterol and POPC/Cholesterol. The first monolayer system exhibited a rigid solid phase at the biological surface pressure threshold (30-35mN/m). The latter is more flexible due to the presence of unsaturation within the POPC alkyl chains, which makes it more fluid than the first system. In this study, in the presence or absence of DNA, structural arrangement within the gemini surfactant alone or within the vector components led to interactions with the model membranes, hence affecting its fluidity. All the gemini-DNA complexes from both groups caused the membranes to become more fluid, thus internalization of the vector may become possible.

Further characterization of the nanoparticles (polyplexes) formed by formulating the GS and the DNA into aqueous solution was conducted through the measurement of the particle size and the zeta potential to determine the stability of the complexes at higher charge ratio. Smaller particles were formed at higher charge ratios with net positive charge, indicating the complete and successful complexation of DNA with the gemini surfactants. These nanoparticles were tested in the presence or absence of DOPE in MG-63 bone cancer cells, and HEK-293 kidney cells. Unfortunately, Pyrene-3-n surfactants transfection results obtained from flow cytometer were not useful due to the interference of the pyrene emission peak with the GFP signal. However, the

pyrenyl surfactants were tested by ELISA in COS-7 cell lines, and showed poor transfection, with the highest protein expression was that of pyrene-3-8, which gave better results than the positive control itself (Lipofectamine plus). This can be attributed to the loose packing of the DNA which was shown in the physical characterization results (the zeta potential= <30mV) and the average size was below 200 nm at 1:10 and 1:5 ratios. The 12-3-n transfection complexes showed high toxicity imparted by these dissymmetric gemini surfactants, with relatively good transfection results were shown by 12-3-16 in the presence of DOPE and in its absence. DOPE's presence did not improve the transfection and it increased the overall toxicity of the complex with a significance of 0.985.

Over all, the level of the *in vitro* transfection observed by ELISA assay for the pyr-3-m gemini surfactants proved to be generally poor, with the exception of pyr-3-8, which showed remarkable transfection ability with protein expression of 8000pg and 15000pg after 48 h, and 72 h incubation periods, respectively. In addition to that, low toxicity was observed for all of the pyr-3-m surfactant complexes. These two surfactants (pyr-3-8 and 12-3-16) have emerged as promising candidates for non-viral gene delivery in different cell lines.

Acknowledgement

My appreciation and gratitude goes first to my supervisor, Dr. Shawn Wettig for giving me the opportunity to pursue a Ph.D degree in a diverse program and welcoming environment. I also appreciate his patience and mentorship during the course of the program. I would also like to extend my thanks to the committee members, Drs. Praveen Rao, Adrian Schwan, and Pavle Rodovanovic for their continuous help and guidance, especially Dr. Praveen Nekkar for providing me assistance in $^1\text{HNMR}$ interpretation.

Apart from that, I would like to thank Dr. Paul Spagnoulo from (Pharmacy, University of Waterloo) for allowing me to use his Guava easycyteTM flow cytometer to run my transfection experiments and Janet Venne (Chemistry, University of Waterloo) for helping me with the NMR instrument.

Special thanks to my colleague, George Mekhail for his valuable help and guidance in my BAM and transfection experiments, our struggle in the optimization of the transfection process and his encouragement is what kept me motivated and engaged in the research. I would like to also extend my thanks to Samantha Shortall for her friendship and help throughout the program. I will always cherish brain storming for answers together.

I would also like to thank my lab colleagues Shannon Callender, Osama Madkhali, Taksim Ahmed, and Hitang (Lizzie) Wang. I am grateful for the help I got from different labs; Tarek Mohamed, Wesseem Osman, Sarbjeet Gujral-Singh, and Arash Shakeri from Dr. Nekkar's lab, Nawaz Ahmed, Alessia Roma, and Rowena Rodrigo from Dr. Spagnoulo's lab, and Shirley Wong from Dr. Roderick Slavcev.

Dedication

To my beloved husband; Adam Celejewski and my family

Table of Contents

Author`s declaration.....	ii
Abstract	iii
Acknowledgement.....	vi
Table of Contents	viii
List of Figures	xi
List of Tables.....	xiv
List of Schemes	xv
List of Abbreviations.....	xvi
Chapter 1: Introduction	1
1.1 Gene therapy.....	1
1.2 Gene delivery.....	2
1.2.1 Naked DNA delivery	3
1.2.2. Viral Vectors.....	4
1.2.2.1 Retroviruses	6
1.2.2.2 Adenoviruses	6
1.2.3. Non-viral vectors	7
1.2.3.1 Barriers to non-viral gene delivery	8
1.2.3.2 Cationic Polymers.....	10
1.2.3.2.1 Polylysine (PLL).....	10
1.2.3.2.2 Polyethylenimine (PEI)	10
1.2.3.2.3 Membrane-disruptive peptides and Polymers	11
1.2.3.2.4 Cyclodextrin-containing polymers	12
1.2.3.2.5 Chitosan	13
1.2.3.2.5.1 Lactosylation	13
1.2.3.2.5.2 Galactosylation	14
1.2.3.2.5.3 Quaternization of oligomeric chitosan	14
1.2.4 Cationic Lipids	16
1.2.4.1 Hydrophobic chains.....	17
1.2.4.2 Hydrophilic head groups	18
1.2.4.3 Linker bonds	19
1.2.4.4 Helper Lipids	19

1.3 Gemini surfactants	21
1.3.1 Structural variations in Gemini surfactants	23
1.3.1.1 Variations in the alkyl tail	23
1.3.1.2 Variations in the head groups	27
1.3.1.3 Variations in the spacer group	29
1.3.2 Transfection efficiency <i>in vitro</i> and <i>in vivo</i>	38
1.3.3 Gemini surfactants-DNA lipoplex and the interaction with cell membranes.....	40
1.4 Langmuir-Blodgett (LB) monolayer studies and Brewster Angle Microscopy technique (BAM)	41
1.4.1 Lipid membrane composition	44
1.4.2 Model membranes	46
1.4.2.1 Types of model membranes.....	47
1.4.2.1.1 Langmuir monolayers.....	48
1.4.2.1.2 Liposomes / Lipid vesicles	48
1.4.2.1.3 Supported lipid membranes	48
Chapter 2: Hypothesis and objectives	53
2.1 Rational design of gemini surfactants and the focus of this research.....	53
2.2 Hypothesis	55
2.3 Objectives	55
Chapter 3: Synthesis and characterization of dissymmetric Gemini surfactants	57
3.1 Introduction	57
3.2 Methods and Materials	59
3.2.1.1 Synthesis of 5-bromohexane-1-pyrenyl ketone	59
3.2.1.2 Synthesis of 6-(1-pyrenylbromohexane) ¹⁹¹	59
3.2.1.3 Synthesis of pyr-3(N-(3-dimethylaminopropyl)-N, N-dimethyl-6-(pyren-6-yl)-hexan-1-ammonium bromide)	60
3.2.1.4 Synthesis of pyr-3-m (m = 8, 12, 14, 16 & 18).....	61
3.1.2 Synthesis of m-3-n surfactants	62
3.1.3 Determination of the Krafft temperatures	63
3.1.4 Surface tension measurement	63
3.1.5 Specific conductivity	64
3.1.6 Fluorescence studies	64
3.2 Results and Discussion	65
3.2.1 Krafft temperature	65

3.2.2 Surface tension analysis and favored interactions	69
3.2.3 Conductivity measurements	80
3.3 Conclusion	90
Chapter 4 Characterization of the Gemini Surfactant-DNA complexes.....	92
Langmuir-Blodgett (LB) and Brewster`s Angle Microscopy (BAM)	92
4.1 Introduction	92
4.2 Materials and Methods	94
4.2.1 Materials	94
4.2.2 Preparation of Langmuir monolayer.....	94
4.2.3 Brewster`s Angle Microscopy (BAM)	95
4.3 Analysis of Surface pressure-Area isotherms (π -A).....	95
4.4 Results and discussion	96
4.4.1 Langmuir isotherms of pyrene-based Gemini surfactants	97
4.4.2 Langmuir monolayer studies of dissymmetric gemini surfactants (12-3-n).....	121
Chapter 5: Transfection and structural properties of dissymmetrical gemini surfactant based transfection complexes	135
5.1 Introduction	135
5.2 Materials and Methods	136
5.2.1 Particle size and Zeta potential	137
5.2.2 Plasmid DNA (<i>pTGINF-GFP</i>)	137
5.2.3 <i>In vitro</i> transfection	139
5.2.4 Enzyme-Linked Immunosorbent Assay (ELISA)	141
5.2.5 3-(4,5-Dimethylthiazol-2-yl)-2,5-diphenyltetrazolium bromide (MTT) assay	142
5.3 Results and Discussion	143
5.3.1 Particle size and zeta potential measurement	143
5.3.2 Evaluation of transfection efficiency <i>in vitro</i>	146
5.4 Conclusion	151
Chapter 6: Conclusion and future studies	155
References	160
Appendices	173

List of Figures

Figure 1.1 Geographical distribution of gene therapy clinical trials up to 2013.....	6
Figure 1.2. Barriers to successful delivery of nucleic acid using non-viral vectors.....	9
Figure 1.3. The proton-sponge hypothesis.	11
Figure 1.4 Chemical structure of the <i>N,N'</i> -bis (dimethylalkyl)-alkane-diammonium-bromide or m-s-m.....	21
Figure 1.5 Chemical structure of phytanyl-3- <i>n</i> surfactants, where <i>n</i> = 1-bromododecane, 1-bromohexadecane, or 1-bromooctadecane.....	25
Figure 1.6 Structure of serine-derived gemini surfactants.....	29
Figure 1.7 structure of bispyridinium gemini surfactants with <i>s</i> = 4, 8, and 12.....	35
Figure 1.8. Molecular structures of cholesterol-based cationic gemini surfactants. (A) Hydroxyethyl spacer ($R = -CH_3$ or $-CH_2CH_2OH$), (B) oligo-oxyethylene spacer $n = 1-4$	37
Figure 1.9 Peptide-based gemini surfactants with thioether linkage (PSG).....	39
Figure 1.10 An π -A isotherm obtained by compressing an insoluble lipid monolayer formed at an air-water interface.....	43
Figure 1.11 Glycerophospholipid structure and their diversity.....	46
Figure 1.12 Chemical structures of phosphatidylchole (glycerophospholipids.....	50
Figure 1.13 Scheme representing the interactions of DNA (~200bp) with BGTC and DOPE at two surface pressures.....	51
Figure 1.14 A) Surface pressure isotherm of POPC (a), SS-1(b), and their mixed monolayer.....	52
Figure.3.1. Krafft temperatures (T_K) and Krafft points (K_P) of pyr-3-12 (●), pyr-3-14 (x), pyr-3-16(+), pyr-3-18 (▲), pyr-3-8 (■).....	66
Figure.3.2 Krafft temperatures (T_K) and Krafft points (T_P) of 12-3-14 (▶), 12-3-16 (▼), 12-3-18 (●).....	69
Figure.3.3 Surface tension measurements of pyr-3-8 (■), pyr-3-12(x), pyr-3-14 (+), pyr-3-16(●), and pyr-3-18 (▲).....	73
Figure.3.4 Surface tension plots of asymmetric gemini surfactants; 12-3-14 (x), 12-3-16(+), and 12-3-18(●).....	74
Figure.3.5 A) Pi-Pi stacking between two pyrene rings in two monomers of pyr-3-8 surfactants. B) Pi-cation and Pi-sigma are other means of interactions.....	76
Figure.3.6. Self-aggregation behavior in pyrene-3-18 in the presence of water.....	77

Figure 3.7. Fluorescence spectra of pyrenyl gemini surfactants, a) before the CMC. b) Post the CMC.....	77
Figure 3.8. Effect of dissymmetry m/m on the log C.....	78
Figure 3.9a Specific conductivity (κ) – concentration (C) studies for Pyrene-based surfactants at 25C°	87
Figure 3.9b Specific conductivity (κ) – concentration (C) studies for Pyrene-based surfactants at 30C°	87
Figure 3.9c Specific conductivity (κ) – concentration (C) studies for Pyrene-based surfactants at 35C°	88
Figure 3.10a Specific conductivity (κ) – concentration (C) studies for 12-3-n gemini surfactants at 25C°	88
Figure 3.10b Specific conductivity (κ) – concentration (C) studies for 12-3-n gemini surfactants at 30C°	89
Figure 3.10c Specific conductivity (κ) – concentration (C) studies for 12-3-n gemini surfactants at 35C°	89
Figure 3.11 The variation of ($\Delta G_m^{\circ}(\text{CH}_2)$) with the degree of dissymmetry m/n from the conductivity studies for Pyr-3-n (\blacktriangle), and 12-3-n (\bullet).....	92
Figure 4.1 Compression isotherms (π -A) of pyrene-3-8 with DPPC/Cholesterol 75:25% monolayer and POPC/Cholesterol 75:25%	101
Figure 4.2. BAM images of Pyrene-3-8 with DPPC/Cholesterol monolayer with or without DNA, and of pyrene-3-8 with POPC/Cholesterol monolayer with or without DNA.....	107
Figure 4.3 Compression isotherms (π -A) of pyrene-3-12 with DPPC/Cholesterol 75:25% monolayer and POPC/Cholesterol 75:25%	109
Figure 4.4 BAM images of Pyrene-3-12 with DPPC/Cholesterol monolayer with or without DNA, and of pyrene-3-12 with POPC/Cholesterol monolayer with or without DNA.....	112
Figure 4.5 Compression isotherms (π -A) of pyrene-3-14 with DPPC/Cholesterol 75:25% monolayer and POPC/Cholesterol 75:25%	113
Figure 4.6 BAM images of Pyrene-3-14 with DPPC/Cholesterol monolayer with or without DNA, and of pyrene-3-14 with POPC/Cholesterol monolayer with or without DNA.....	114
Figure 4.7 Compression isotherms (π -A) of pyrene-3-16 with DPPC/Cholesterol 75:25% monolayer and POPC/Cholesterol 75:25%	117
Figure 4.8 Compression isotherms (π -A) of pyrene-3-18 with DPPC/Cholesterol 75:25% monolayer and POPC/Cholesterol 75:25%	118
Figure 4.9 BAM images of Pyrene-3-16 with DPPC/Cholesterol monolayer with or without DNA, and of pyrene-3-16 with POPC/Cholesterol monolayer with or without DNA.....	119
Figure 4.10 BAM images of Pyrene-3-18 with DPPC/Cholesterol monolayer with or without DNA, and of pyrene-3-18 with POPC/Cholesterol monolayer with or without DNA.....	120

Figure 4.11 Compression isotherms (π -A) of 12-3-14 with DPPC/Cholesterol 75:25% monolayer and POPC/Cholesterol 75:25%	126
Figure 4.12 BAM images of 12-3-14 with DPPC/Cholesterol monolayer with or without DNA, and of 12-3-14 with POPC/Cholesterol monolayer with or without DNA.....	127
Figure 4.13 Compression isotherms (π -A) of 12-3-16 with DPPC/Cholesterol 75:25% monolayer and POPC/Cholesterol 75:25%	129
Figure 4.14 BAM images of 12-3-16 with DPPC/Cholesterol monolayer with or without DNA, and of 12-3-16 with POPC/Cholesterol monolayer with or without DNA.....	130
Figure 4.15 Compression isotherms (π -A) of 12-3-18 with DPPC/Cholesterol 75:25% monolayer and POPC/Cholesterol 75:25%	132
Figure 4.16 BAM images of 12-3-18 with DPPC/Cholesterol monolayer with or without DNA, and of 12-3-18 with POPC/Cholesterol monolayer with or without DNA.....	133
Figure 5.1. Gel electrophoresis of the plasmid (pGTINF-GFP) extracted after the treatment with restriction enzymes (xba-1 and HINDIII-HF). Three bands (751kb, 1095kb, and 3742kb) can be seen in the image.....	141
Figure 5.2. Particle size and Zeta potential of Pyrene-based gemini surfactants: A) Pyrene-3-8, B) Pyrene-3-12, C) Pyrene-3-14, D) Pyrene-3-16, and E) Pyrene-3-18.....	147
Figure 5.3. Particle size and Zeta potential of dissymmetric gemini surfactants (12-3-n): A) 12-3-14, B) 12-3-16, and C) 12-3-18.....	148
Figure 5.4 A) Transfection efficiency of dissymmetric gemini surfactant complexes (12-3-n) in HEK-293 cell-line (orange) and in MG-63 cell-line (blue) and B) cell viability (same colors) with Lipofectamine 2000 as the positive control.....	149
Figure 5.5 A) Transfection efficiency of pyrenyl gemini surfactant complexes in HEK-293 cell-line (orange) and in MG-63 cell-line (blue) and B) cell viability (same colors) with Lipofectamine 2000 as the positive control.....	152
Figure 5.6 ELIZA Transfection efficiency results of Pyrene-based gemini surfactant complexes in COS-7 cell line after two incubation times (48h and 72h).....	155
Figure 5.7 Results of cytotoxicity of the formulations of the pyrene-based gemini surfactants with pGT-INF-GFP-DOPE complex in COS-7 cell line.....	156

List of Tables

Table 1.1 the structure of common studied Cationic Polymers.....	15
Table 1.2 the structure of common cationic lipids used in gene delivery.....	21
Table 1.3 Packing parameter and expected aggregates` structures.....	32
Table 2.1 Gemini surfactants synthesized and used in this study.....	57
Table 3.1. Krafft points (TP) and the Krafft temperatures (TK) of the dissymmetric gemmini surfactants.....	70
Table 3.2 Critical micelle concentration (CMC), head group area (a_h), packing parameter (P), and surface excess concentrations (Γ_i) of Pyrene-based and 12-3-n surfactants.....	72
Table 3.3 Values of symmetric and dissymmetric gemini surfactants` head group areas (a_h)...81	
Table 3.4 Critical micelle concentration (CMC), and the degree of micelle ionization values (α) obtained from the conductivity measurements at three different temperatures (25C°, 30C°, and 35C°).....	86
Table 3.5 Gibbs free energy of micellization (ΔG_m°), enthalpy of micellization (ΔH_m°), and the entropy of micellization (ΔS_m°) of pyrene-based gemini surfactants and 12-3-n surfactants at different temperatures.....	91
Table 4.1 Monolayer properties for the DPPC-Chol (75-25) and POPC-Chol (75-25) monolayers at 20C° treated with pyr-3m or pyr-3-m/DNA complex.....	102
Table 4.2 Monolayer properties for the DPPC-Chol (75-25) and POPC-Chol (75-25) monolayers at 20C treated with 12-3-n or 12-3-n/DNA complex	125

List of Schemes

Scheme 3.1 Synthesis of 5-bromohexane-1-pyrene ketone.....	60
Scheme 3.2 Synthesis of 6-(1pyrenebromohexane).....	61
Scheme 3.3 Synthesis of pyr3.....	62
Scheme 3.4 Synthesis of pyr-3n.....	62
Scheme 3.5 Synthesis of 12-3-n.....	63

List of Abbreviations

12-3-12.....	1,3-propanediyl-bis(dimethyldodecylammonium) dibromide
16-3-16.....	1,3-propanediyl-bis(dimethylhexadecylammonium) dibromide
18-3-18.....	1,3-propanediyl-bis(dimethyl-octadecylammonium) dibromide
α	degree of micelle ionization
a_0	head group area
CHO.....	Chinese hamster ovary
CMC.....	Critical micelle concentration
COS.....	CV-1 in Origin, and carrying the SV40
Dc-chol.....	3 β -[<i>N</i> -(<i>N</i> ', <i>N</i> -dimethylethylenediamine)-carbamoyl] cholesterol
DMEM.....	Dulbecco's Modified Eagle's Medium
DNA.....	deoxyribonucleic acid
DOPC.....	1,2-dioleoyl-sn-glycero-3-phosphocholine
DOPE.....	1,2-Dioleoyl-sn-glycerophosphatidylethanolamine
DOSAP....	2,3-dioleyloxy- <i>N</i> -[2-(sperminecarboxamido)ethyl]- <i>N,N</i> -dimethyl-1-propanaminium
DOTAP.....	1,2-dioleoyl-3-trimethylammonium propane
DOTMA.....	<i>N</i> -[1-(2,3-dioleyoxy)propyl]- <i>N,N,N</i> ,trimethylammonium chloride
12-3-14.....	<i>N</i> -dodecyl- <i>N</i> -tetradecyl-1, 3-propanediammonium dibromide
12-3-16.....	<i>N</i> -dodecyl- <i>N</i> -hexadecyl-1, 3-propanediammonium dibromide
12-3-18.....	<i>N</i> -dodecyl- <i>N</i> -octadecyl-1, 3-propanediammonium dibromide
Pyr-3-8.....	<i>N</i> ¹ -octyl- <i>N</i> ¹ , <i>N</i> ¹ , <i>N</i> ³ , <i>N</i> ³ -tetramethyl-N3-(6-pyren-6yl)-hexyl)-propane-1,3- diammonium dibromide
Pyr-3-12.....	<i>N</i> ¹ -dodecyl- <i>N</i> ¹ , <i>N</i> ¹ , <i>N</i> ³ , <i>N</i> ³ -tetramethyl-N3-(6-pyren-6yl)-hexyl)-propane-1,3- diammonium dibromide
Pyr-3-14.....	<i>N</i> ¹ -tetradecyl- <i>N</i> ¹ , <i>N</i> ¹ , <i>N</i> ³ , <i>N</i> ³ -tetramethyl-N3-(6-pyren-6yl)-hexyl)-propane-1,3- diammonium dibromide
Pyr-3-16.....	<i>N</i> ¹ -hexadecyl- <i>N</i> ¹ , <i>N</i> ¹ , <i>N</i> ³ , <i>N</i> ³ -tetramethyl-N3-(6-pyren-6yl)-hexyl)-propane-1,3-diammonium dibromide
Pyr-3-18.....	<i>N</i> ¹ -octdecyl- <i>N</i> ¹ , <i>N</i> ¹ , <i>N</i> ³ , <i>N</i> ³ -tetramethyl-N3-(6-pyren-6yl)-hexyl)-propane-1,3- diammonium dibromide
LB.....	Langmuir-Blodgett

GS.....	Gemini Surfactant
RES.....	Reticuloendothelial system
BGTC.....	(bis(guanidinium)-tris(2-amino ethyl)amine-cholesterol
DMPC.....	1,2-Dimyristoyl-sn-glycero-3-phosphocholine
DPPG.....	1,2-dipalmitoyl-sn-glycero-3-phospho(1'-rac glycerol) sodium salt
BAM.....	Brewster Angle Microscopy
SAX.....	Small Angle X-ray scattering
PC.....	Phosphocholine
DPPC.....	1,2-dipalmitoyl-sn-glycero-3-phosphocholine
POPC.....	1,2-palmitoyl-2-oleoyl phosphocholine
PEI.....	Polyethylenimine
PLL.....	Polylysine
CD.....	Cyclodextrin
GFP.....	Green fluorescence protein gene
P.....	Packing parameter
T _P	Krafft's point
T _K	Krafft's temperature
C _S ⁻¹	Compressibility modulus
TEM.....	Transmission Electrom Microscopy
PBS.....	phosphate buffered saline
PEG.....	polyethylene glycol
Phy-3-12.....	N ¹ -dodecyl,N ¹ ,N ³ ,N ³ -tetramethyl-N ³ -(3,7,11,15-tetramethylhexadecyl) propane- 1,3-diammonium dibromide
PI.....	propidium iodide
HEK.....	Human embryonic Kidney cell-line
MG-63.....	Human osteosarcoma cell line
DMEM.....	Dulbecco's modified eagle medium
EMEM.....	Eagle's minimum essential medium
GDP.....	Gemini-DOPE-Plasmid complex
LC.....	liquid condensed phase

LE.....liquid expanded phase
LE-LC.....liquid expanded- liquid condensed phase

Chapter 1: Introduction

1.1 Gene therapy

Toward the end of the twentieth century, geneticists managed to sequence the entire human genome.¹ With this seminal tool, scientists and researchers have been able to elucidate the nature and the histology of diseases, and link them to precise genes. With this breakthrough researchers realized obstacles and hurdles to curing these genetic diseases or cancers of malignant nature. Further investigation led to the idea of possibly introducing a foreign piece of DNA into cells.² This simple concept is known as gene therapy and it includes the introduction of an exogenous gene, by means of viral or non-viral vectors or, to produce a desirable result. This result can correct an existing defect through the translation of a missing protein, or by repressing or inhibiting an existing function, thus eliminating the disease.³ The first trial goes back to 1970 when Rogers & colleagues, introduced the Shope papilloma virus that encodes arginase, which is an enzyme that degrades arginine to ornithine in patients with hyperargininemia, a rare genetic disease. Despite the lack of safety measures, the introduced gene segment led to the desired outcome without the development of adverse effects.⁴ This study, however, proved to be unsuccessful later. However, in 1999, a gene therapy clinical trial to treat Jesse Gelsinger, a patient with ornithine transcarbamylase deficiency, led to the death of a youth after a severe immune response caused by the injected adenoviral vector.⁵ This tragedy led to a substantial setback in the field. However, in the new millennium, with the advancement in the field of gene therapy, it became possible to use it to treat people and improve their life.

To develop a gene therapy, several parameters should be considered, including the likelihood of a disease to be treated by gene therapy, the successful choice of a particular gene, regulatory signals, upstream or downstream effectors, the ability of a particular cell to be transfected, whether this cell is active or not, the delivery vehicle, and the route of administration.⁶ A crucial

factor to the success of gene therapy is the means by which DNA is delivered to a nucleus in order to be expressed and to exert the desired action. However, this can be a difficult process because of the bulky nature of the DNA or the stability of RNA. In addition, the hydrophobic nature of cell membranes act as barriers to most foreign materials.⁷

1.2 Gene delivery

Deoxy ribonucleic acid (DNA) is the genetic material that is passed down from one generation to the next. DNA is contained within the nucleus of the cells and it is made of nucleotide units, which are composed of a nucleobase, a sugar, and a phosphate. According to the variations in the nucleobases, which are adenine, thiamine, cytosine, and guanine (A,T,C,G), trillions of combinations are possible, and it is from this code that essential compounds are made in the body.⁸ Peptides, proteins, enzymes and receptors are the result of the precise sequence of DNA base-pairing between the DNA nucleotides. All these proteins are required to function normally. If there is an incorrect pairing or a full sequence deletion, dramatic health consequences can ensue ranging from hair loss to life threatening conditions such as cystic fibrosis and certain forms of cancer⁹. These errors happen at the level of the genomic material and are called mutations. These mutations can occur either naturally or be caused by chemical damage by UV light (photochemical damage) or exposure to certain types of pesticides.^{10,11} The need for a strategy or a treatment for inherited diseases as well as acquired disorders led to the development of gene therapy, which requires gene delivery vehicles that can be used specifically to deliver a segment of DNA, absent or deficient. Several methods are being utilized to introduce genetic material to cells, whether *in vitro* or *ex vitro*. These range from physical methods (electroporation, heat gun or high pressure) for delivery of DNA not complexed by chemical or biological components, to biological methods (mainly viruses), and chemical methods (cationic

lipids, polymers, dendrimers, and gemini surfactants), each of which will be described in details below:

1.2.1 Naked DNA delivery

Plasmid DNA is a large polymer that cannot cross cell membranes freely. In order to facilitate its passage, assisted methods of delivery are required. DNA has been introduced to various cells by means of different physical methods that generally operate on the principle of creating a hole in cell membranes through which DNA can pass and gain access to the interior of the cell. This concept of injecting DNA was first introduced by Wolff et al.¹² in 1990. He injected a reporter gene into mouse muscle and its expression. This technique delivers a transgene by causing transient membrane damage.¹³ A "heat gun" has been used to transfer genes to skin, mucosa and exposed tissues within a limited area.¹⁴ In this technique, DNA is deposited on the surface of gold nanoparticles, which are then fired out of the gun by pressurized gas and expelled onto targeted cells. The heat gun method is able to bypass physical barriers including cell membranes, but has a number of limitations. For example, the nanoparticles only manage to penetrate few millimeters into the target tissues. In addition, the size of the delivered DNA is limited by the size of the gold nanoparticles, and inconsistencies of the coated nanoparticles may interfere with the release of the DNA, and the delivery efficacy. However, delivery of DNA was made possible to a wide range of cell types and cell environments using this technique. Delivery of naked DNA has also been introduced to cells by application of either electrical or magnetic field to a specific area. This method has more potential than the heat gun and direct injection, as it has demonstrated to increase gene expression by several orders of magnitude compared to heat gun efficacy.¹⁵ Electroporation is an example of applying an electric potential to increase gene or drug delivery. Electroporation involves applying an electrical pulse to permeate the cell membrane, whether *in vitro* or *ex vivo*.¹⁶ This technique involves the insertion of two electrodes with a space

(approximately ~1cm) between them. Applying an electric pulse temporarily disrupts the structure of the cell membrane, and allows the DNA to actually permeate into cells. Successful gene delivery using electroporation both, in *in vitro* and *in vivo* studies has been reported by a number of groups. Titomirov et al.¹⁷ placed surface electrodes to deliver a plasmid coded for a reporter gene into new-born mouse skin. A transient and long term transfection of isolated and cultured cells were reported. Hansson et al.¹⁸ also demonstrated increased transient expression of DNA in an isolated lung tissue in *ex vivo* setting. They treated lung muscles with hyaluronidase prior to electroporation and injection of the DNA, which enhanced the transfection significantly because of the ability of hyaluronidase to relax the muscles, which improved distribution of the plasmid in the tissue.¹⁹ Although electroporation was applied and used in numerous delivery studies, both *in vitro* and *in vivo*, it still has major drawbacks. First, its effective range is limited to approximately 1cm. Second, in some organs, electroporation requires a surgical procedure to insert the electrodes. Third, high voltages are required. Moreover, irreversible damage (cell death) was seen as a result of thermal heating.²⁰ With all these drawbacks, it is very difficult to apply such an invasive method into humans.

1.2.2. Viral Vectors

Viruses have evolved to become highly efficient in the delivery of exogenous nucleic acids (DNA, RNA) to various tissues.²¹ Researchers have created mutated viruses that retain their ability to deliver genetic materials to cells/organisms, but without the subsequent pathogenicity.²² Currently, viral vectors are used in more than 70% of human gene delivery clinical trials (see Figure 1.1), mainly because of their efficiency in delivering genes to numerous cell lines²³. In addition, there are commercially available gene therapy products of viral origins, Gendicine™, Oncorine™, and Glybera™. Gendicine is recombinant Human Ad-p53 Injection, trademarked as Gendicine and developed independently by Sibiono successfully obtained a Drug

license. At the beginning of 2004, Production Approval and GMP Certification were obtained from the China State Food & Drug Administration (SFDA). Gendicine is a gene therapy drug that has been approved to treat head and neck squamous cell carcinoma (HNSCC)²⁴. Oncorine which is also used to treat head and neck sarcoma is another oncolytic viral based gene therapeutic. These two drugs are mainly composed of replication-incompetent recombinant Ad5-p53 virus particles, which are based on adenovirus serotype 5 and human wild-type p53 tumor suppressor gene, a key housekeeping gene, coding human wild-type p53 protein. These two medications have been approved by the China state food and drug administration, but has not been approved in neither Europe nor North America. However, Glybera is a gene therapy that is designed to restore the LPL enzyme activity required to enable the processing, or clearance, of fat-carrying chylomicron particles formed in the intestine after a fat-containing meal. This drug consists of an engineered copy of the human LPL gene packaged with a tissue-specific promoter in a non-replicating AAV1 vector, which has a particular affinity for muscle cells. The latter product has been approved by the European Medicines agency (EMA), but not by the Food and drug agency (FDA) in America. The presence of three different drugs that might be deemed safe and are the result of viral gene therapy holds a promise of better and more options of treatments in the near future.²⁵ In the following section, we discuss some of the viruses that have been used in gene delivery and gene therapy application:

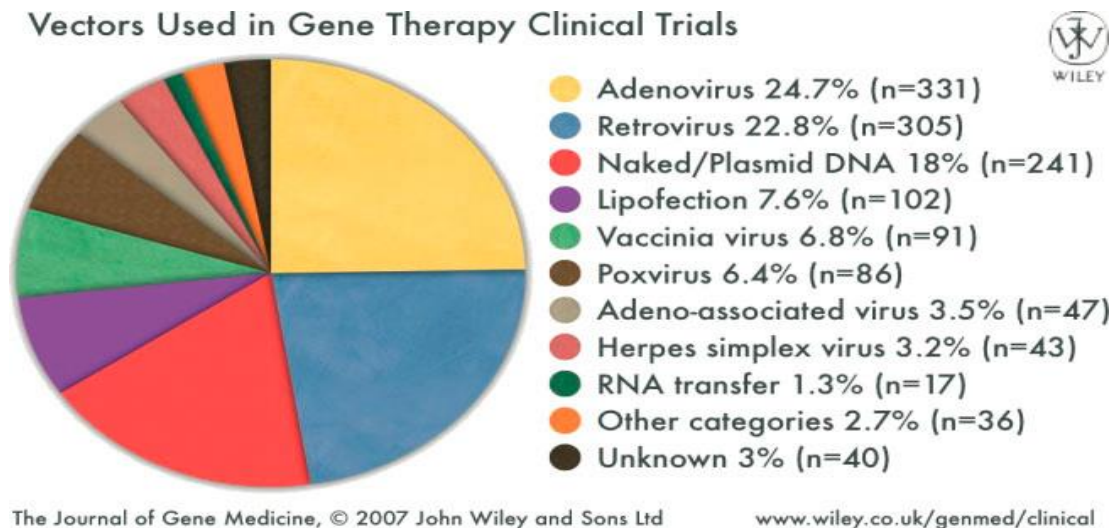


Figure 1.1 Gene therapy vectors in clinical trials up to 2013²⁶

1.2.2.1 Retroviruses

Retroviruses are small RNA viruses that replicate through a DNA intermediary through specific interactions between the viral envelope and a specific cell receptor. Once internalized by the cell, the RNA is reverse-transcribed into double stranded-DNA (dsDNA). Retroviral DNA has the ability to integrate into the host DNA, which makes it a sustainable source for the expression of an exogenous DNA for the life of the cell. However, in order for this integration to happen, mitosis is required, which limits the use of these vectors to cells capable of division. Some of the cells that can be used for this kind of application are rapidly-dividing hepatocytes following partial hepatectomy and tumor cells.²⁷

1.2.2.2 Adenoviruses

Adenoviruses are double-stranded linear DNA viruses of approximately 30-35kb in length.²⁸ Adenovirus binds to integrin protein via its penton-base protein and unlike retroviruses, adenoviruses can infect non-dividing cells, an advantage over retroviruses. Defective adenoviruses are used for gene delivery applications by removing the E1 gene, however, this

appears to affect the level of expression. Also, use of adenoviral gene products often stimulates the immune response, resulting in loss of gene expression 1-2 weeks after the injection.²⁹ The diminishing activity can be explained by the depletion of CD₄ CTL and/ or NK cells. In one study, Leopold et al.³⁰ covalently linked a fluorophore adenoviral vector to be able to track the gene transfer to A549 human epithelial lung cell line using a fluorescence microscopy. Cy3-Ad vector was co-administered with FITC-dextran to A549 cells and the vector was only co-localized when endosome-acidification was blocked by bafilomycin A1, which suggests that Ad vectors rapidly escaped the endosomes, without evidence of endosome-endosome fusion. The event of endosome-endosome infusion is important to deliver the cargo from outside of the cell to the inside of it. Moreover, through this mechanism, the endocytosed gene delivery or drug delivery vector is capable of being internalized and protected³¹. Adenoviral and retroviral vectors are associated with numerous clinical trials.

Due to their reported immunogenicity, third class of viruses is now being used, which is the adeno-associated viruses (AAV). AAV is a single stranded DNA virus that causes no current pathology in humans.³² A retroviral vector based gene therapy used to treat X-linked severe combined immunodeficiency (X-SCID) disease was a successful application of gene therapy (several patients cured of the disorder) until an unfortunate outcome happened when several children developed leukemia as a result of insertion mutation, which led to the suspension of the clinical trial with a setback that affected the entire field.³³ Safety concerns, after the reported deaths, led to the development of other possible vectors.

1.2.3. Non-viral vectors

A fundamental engineering challenge to gene therapy is the development of a safe and efficient delivery vehicle for guaranteed gene expression.³⁴ Viral vectors are far advanced in this field due to their ability to utilize the host replicating machinery to integrate and replicate its own DNA

or RNA. However, pre-immune responses are triggered with viruses and they can be oncogenic as well. Furthermore, they have limited DNA capacity, and working with viruses is quite expensive.³⁵ Beside the physical methods mentioned above, chemical methods involving the formulation of DNA into condensed particles by using cationic lipids, cationic polymers and cationic surfactants are the most frequently studied methods (see Figure 1.1).³⁶ DNA binds electrostatically to the cationic components of the particle, which compacts the DNA in order to protect it from the degradation by various endonucleases in the body. Unlike viral vectors, non-viral vectors are less immunogenic and less toxic, with no limitation of the DNA cargo. Also, these compounds are less costly. Some of these non-viral vectors can be easily synthesized at the bench top and stored for a long time according to good manufacturing practice (GMP) methods.³⁷ However, non-viral vectors are less effective than viral vectors and for that, a series of measures should be taken into consideration when designing them.

1.2.3.1 Barriers to non-viral gene delivery

Entrapment of the genetic materials into a nanoparticle is important because DNA is susceptible to degradation by endonucleases present in the extracellular space.³⁸ Zwitterionic lipids have been used in gene delivery studies and shown to form stable nanoparticles, which is an indication of a longer half-life of the DNA in the blood stream in *in vivo* study.³⁹ However, aggregation of the polyplex or the lipoplex by interacting with serum proteins occurs. Also, high salt concentration increases the recognition of the polyplex by the immune systems, which leads to its clearance by the reticuloendothelial system (RES).⁴⁰ Vector unpacking is assumed to be an important step in releasing DNA and gene expression. In a lipoplex, it has been proposed that fusion occurs between the cationic lipid of the lipoplex and the endosomal membrane lipids, hence, facilitating endosomal escape and DNA release.⁴¹ The most critical and the probably the success-limiting step in gene delivery using a non-viral vector is the passage through the nuclear

membrane.⁴² The nuclear envelope consists of two nuclear membranes and an underlying nuclear lamina and nuclear pore complex. The critical function of the nuclear membranes is to act as barriers that separate the nucleus from the cytoplasm, and the nuclear pores are the sole channel through which small polar molecules and macromolecules are able to travel, which signifies the importance of the size of the cargo and the ultimate release of the DNA from the nanoparticles.⁴³ An illustration of the physical barriers facing the non-viral vectors in gene therapy are summarized in Figure 1.2.

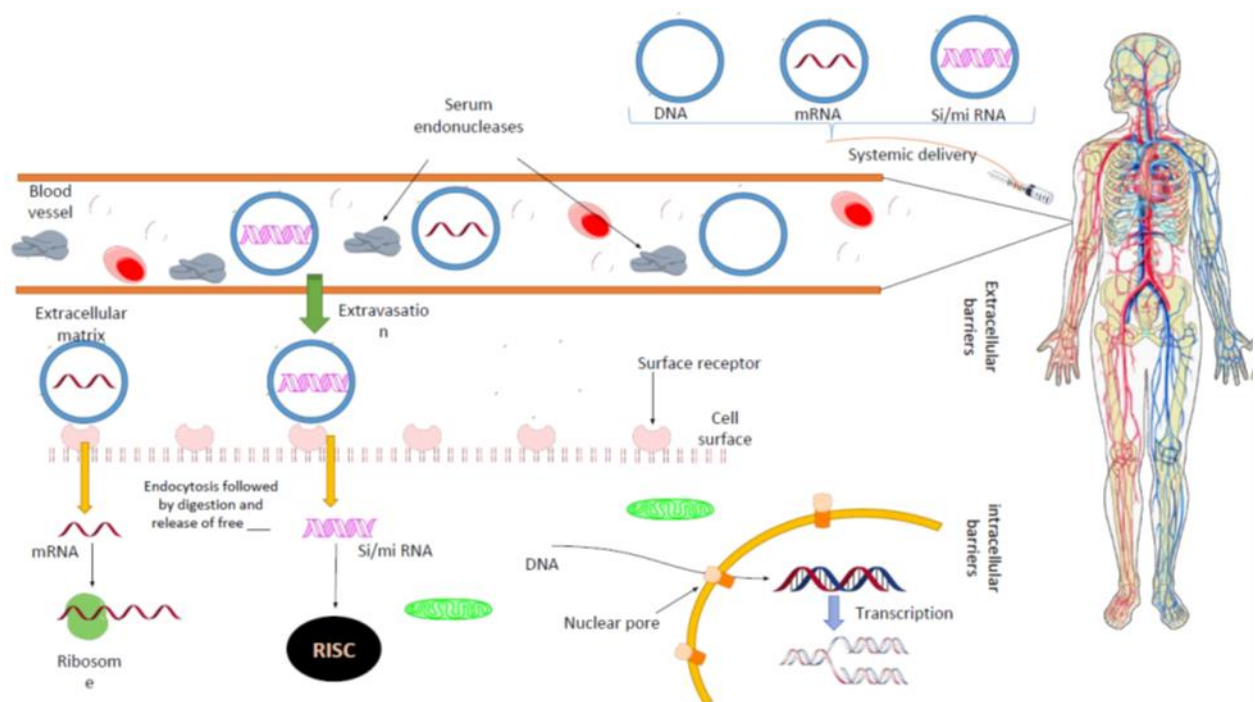


Figure 1.2 Barriers to successful delivery of nucleic acid using non-viral vectors. Non-viral vectors can be used to carry DNA, mRNA, and short double-stranded RNA. These vectors need to prevent rapid clearance and degradation by serum endonucleases. Also, they need to avoid aggregation and eventual clearance by RES. This can happen by using polyethylene glycol (PEG) or other compounds. These vectors are required to mediate cell entry and endosomal escape of the cargo³⁸. (Adapted from Reference 30)

1.2.3.2 Cationic Polymers

Cationic polymers bind DNA electrostatically to condense the genetic material to a few 10-100 nanometers in diameter. These complexes are often called polyplexes. Polymers can be off-shelf polymers or polymers designed specifically for gene delivery. These polymers are often comprised of DNA binding moieties; including primary, secondary, tertiary and quaternary amines. The polymers themselves can be either linear, branched, or dendritic in nature and due to the flexibility of polymers` chemistry, different functional groups can be introduced to improve gene delivery while maintaining biocompatibility and stability of the formulation.⁴⁴

1.2.3.2.1 Polylysine (PLL)

Polylysine is one of the off-shelf polymers that has been extensively used for gene delivery and helped to establish basic understanding of the mechanisms by which a polymer-DNA complex can be internalized, can escape the endosomal compartment, and can release the DNA from the polyplex. Polylysine itself showed very poor transfection results, both, *in vitro* and *in vivo*. When at physiological pH, PLL amine groups tend to be positively charged and therefore, they have low capacity for endosomal buffering and lysis.⁴⁵ Addition of an endosmolytic agent such as, chloroquine to polylysine gave moderate transfection results and conjugation of different ligands like asialo-orosomucoid glycoprotein to target the asialoglycoprotein receptor in mouse hepatocytes led to an increase in the transfection, as reported, in *in vivo* and *in vitro* studies⁴⁶.

1.2.3.2.2 Polyethylenimine (PEI)

PEI mediates gene delivery efficiently in the absence of an exogenous endosmolytic agent (lyses endosome). PEI-polyplexes have been used to target different cell types by ligand conjugation, using galactose⁴⁷, mannose⁴⁸, transferrin⁴⁹ and antibodies.⁵⁰ PEI has been successfully tested in gene delivery *in vivo* in different tissues including, the central nervous

system (CNS), the kidney⁵¹ and tumors.⁵² PEI is a highly efficient transfection agent due to its ability to efficiently escape from the endosome using the proton sponge mechanism.⁵³ The only drawback of the PEI is its relatively high toxicity.

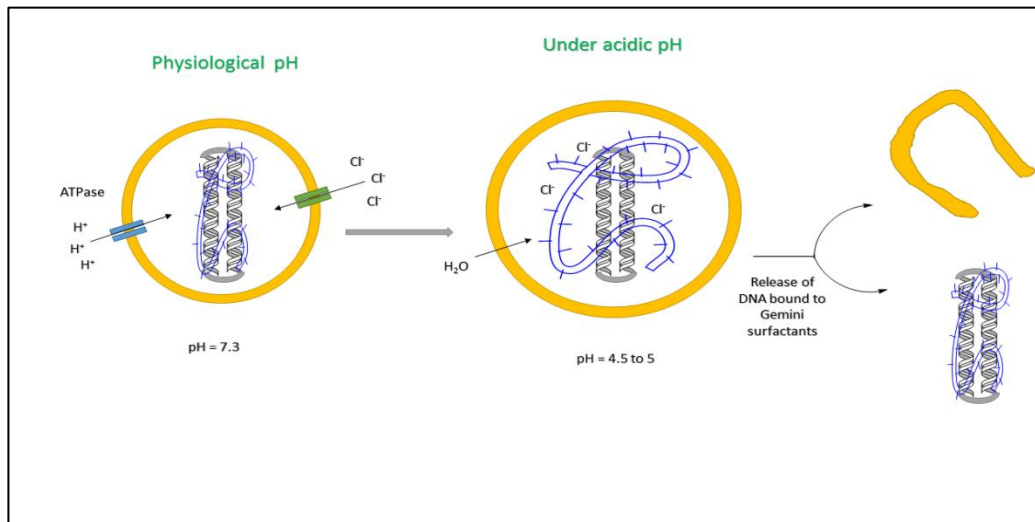


Figure 1.3 The proton sponge hypothesis. influx of H^+ and Cl^- ions into the endosome , which leads to swelling of the endosome, drop in its pH, and finally its rupture⁵³

The proton sponge mechanism (see Figure 1.3) can be described as follows: at physiological pH, amine groups within the cationic polymers, like PEI, are not fully charged, but are increasingly protonated in the endosome due to low pH. The low pH in the endosome is brought about by the ATPase enzyme which transports proton from the cytosol into the endosome. The accumulation of protons in the endosome is balanced by a high influx of chloride ions, which increases the osmotic pressure causing the rupture of the endosome. This process causes the release of the polyplex into the cytosol of the cell⁵⁴.

1.2.3.2.3 Membrane-disruptive peptides and Polymers

Endosomal escape is a crucial barrier to efficient gene delivery.³⁴ Some of the viruses have evolved specific acidic peptides in their protein coat, which can become protonated at acidic pHs, enabling them to fuse with the endosomal membrane and carry the cargo all the way to the

nucleus for gene translation, and protein expression. Isolating these peptides sequences from viruses and utilizing them for gene delivery is not plausible due to the potential for development of an immune response toward viral components.⁵⁵ This has led to increased interest in synthetic pH-responsive peptides. Stayton et al.⁵⁶ synthesized hydrophilic acid-responsive polymers that become hydrophobic once protonated within the acidic environment of the endosome. This change in the nature of the polymers causes these polymers to partition into, and ultimately disrupt, the endosomal membrane. Another approach to the design of pH-responsive membrane-disruptive polymers was successfully attempted by Murthy et al.⁵⁷, by introducing acid-degradable bonds, either in the polymer backbone or in the pendant groups. The research group used encrypted polymers (graft terpolymers), which consist of a hydrophobic membrane-disruptive backbone onto which hydrophilic polyethylene glycol (PEG) chains were grafted through an acetal linkage (acid-degradable linker). This polymer was used to deliver rhodamine-labelled oligonucleotides into the cytoplasm of hepatocytes. Two new polymer derivatives (polymers E2 and E3) were synthesized. E2 contained lactose moiety for targeting and PEG-FITC to increase half-life of the vector conjugated to it. On the other hand, E3 contained a pendant hexalysine moiety to complex the oligonucleotide. The fluorescence microscopy results showed that the polymers were able to directly escape the endosome and to efficiently deliver the oligonucleotides into the hepatic cytoplasm.

1.2.3.2.4 Cyclodextrin-containing polymers

Cyclodextrins (CDs) are cup-shaped molecules comprised of six, seven, or eight units of glucose, called α , β , or γ cyclodextrins, respectively. Due to the orientation of the glucose rings, the exterior of the cup is hydrophilic and the interior is hydrophobic, giving rise to the ability to form inclusion complexes with small, hydrophobic guest molecules. CDs are water soluble, biocompatible, and FDA approved compounds.⁴⁴ A linear cationic β -cyclodextrin-based

polymers (β CDPs) were synthesized by the condensation of a diamino cyclodextrin monomer with a diimidate comonomer. The resulting polymers were complexed with DNA to form polyplexes, which were able to transfect baby hamster kidney cells (BHK-21). The addition of β -cyclodextrin to the polymer backbone significantly lowered the toxicity associated with the polymer while retaining the efficiency of the polymer as a non-viral gene delivery vector, making CDPs a promising agent for *in vitro* and possibly for *in vivo* studies.⁵⁸

1.2.3.2.5 Chitosan

Chitosan is a natural, biodegradable polycationic polysaccharide with low toxicity. These properties make it an attractive gene and drug carrier due to its high positive charge density.⁵⁹ Chitosan is obtained by an alkaline deacetylation of chitin. Chitin is a polysaccharide found in the exoskeleton of crustaceans and insects⁶⁰, and is a copolymer of *N*-acetyl-D-glucosamine and D-glucosamine. It enhances the transport of drugs across the cell membranes due to its cationic nature, which provides strong electrostatic interactions with mucus, negatively charged mucosal surfaces, and macromolecules such as DNA.^{61,62} When binding DNA, chitosan forms spherical structures with a mean size of 100 nm. The smaller the size of the produced nanoparticle, the easier its passage across the cell membrane through either endocytosis or pinocytosis. This can ultimately increase the transfection efficiency.⁶³ Chitosan is easily modified in order to increase cell specificity in *in vitro* studies. Examples of these modifications are listed in sections 1.2.3.2.4.1 to 3, below:

1.2.3.2.5.1 Lactosylation

Chitosan was chemically modified by coupling lactose in order to target cells expressing a galactose-binding membrane lectin. Lactosylation did not improve the transfection in Human epithelial adenocarcinoma cell line (HeLa cells) and did not transfect Human hepatocarcinoma (Hep G₂) nor mouse liver epithelial cells (BNL CL₂ cells), either in the presence or absence of

chloroquine. This was attributed to decreased zeta potential of the polyplexes after the lactosylation⁶⁴. However, Hashimoto, et al. showed that 8% lac- substitution on chitosan as a non-viral gene delivery vector improved transfection efficiency in hepatocytes expressing asialoglycoprotein receptors.⁶⁵

1.2.3.2.5.2 Galactosylation

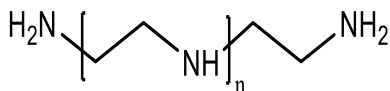
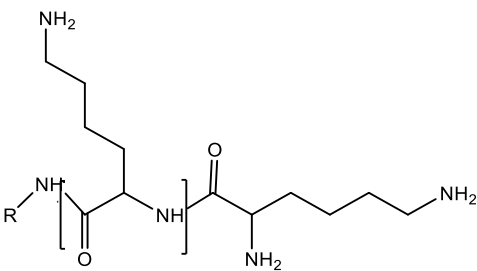
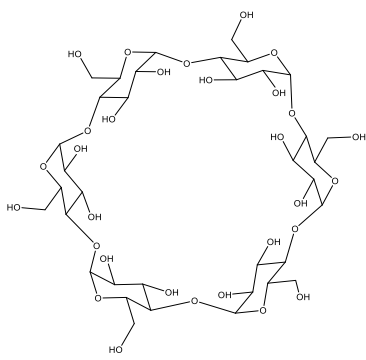
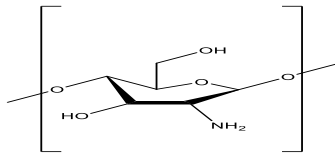
Chitosan was modified by galactosylation and polyethanol glycol (PEG) was grafted on the chitosan to generate GCP chitosan then was complexed with DNA and was used as a non-viral vector in the Hep G₂ cell line. However, the transfection efficiency of GCP/DNA complex was very low despite the small particle sizes produced at various charge ratios (N⁺/P⁻). The charge ratio is detrimental to the complexation and compaction process, as well as to the internalization process. An overall positive net charge is required to interact with the cell membranes. This mainly was the result of the interaction of the polyplexes with plasma proteins, which lead to the dissociation of the complexes⁶⁶.

1.2.3.2.5.3 Quaternization of oligomeric chitosan

To increase the transfection rate of chitosan as a vector, chitosan oligomers were quaternized by trimethylation, producing trimethylated chitosan oligomers (TMO). This process is based on reductive methylation using methyl iodide in an alkaline environment⁶⁷. The TMO polycations were complexed with DNA and tested for transfection efficiency in two cell lines: COS-1 (a green African monkey cells that resemble fibroblasts in humans), and Caco-2 (Colorectal adenocarcinoma cells). The transfection efficiency of the chitoplex was comparable to the positive standard in this study; DOTAP (1,2-dioleoyl-3trimethylammonium-propane) (see Table 1.1) in COS-1 in the absence of fetal calf serum (FCS). In the presence of FCS, the chitoplex's transfection results remained the same, whereas the DOTAP-DNA decreased. In Caco-2 cells, both DOTAP-DNA and the chitoplex had lower transfection efficiencies compared to those

observed with the COS-1 cell line, however, the chitoplex was superior in transfecting Caco-2 as compared to DOTAP-DNA.

Table 1.1 Structure of common studied cationic polymers

Generic name	Chemical name	Chemical structure
PEI	Polyethylenimine	
PLL	Poly(L-lysine)	
CD	Cyclodextrin	
Chitosan		

1.2.4 Cationic Lipids

Cationic lipids are amphiphilic molecules that consist of a hydrophilic head group, which may be cationic quaternary ammonium, amine, amino acids or peptides, guanidium, or heterocyclic functional groups⁶⁸, attached via a linker region (which can be any number of functional groups) to typically two hydrocarbon chains or cholesterol derivatives, which makes up the hydrophobic component of the amphiphilic lipids. Like any amphiphile in solution, lipids form various structural phases, including micellar, lamellar, cubic and inverted hexagonal phases.⁶⁹ A liposome is a minute spherical sac of phospholipid molecules enclosing a water droplet, to carry drugs or other substances into the tissues, and it has been investigated for over 20 years as a DNA vectors for gene therapy purposes, however the mechanisms by which they transfect cells are not fully understood. It is generally known that the success or failure of a liposomal based vector can depend on various physiochemical characteristics of the liposome/DNA complex.⁷⁰ These properties include the size of the lipoplex, the structure it can take in suspension, fusogenicity⁷¹, and the charge can play a role in transfection efficiency. One of the earliest seminal works on the use of liposomal based vectors was conducted by Felgner and coworkers⁷² in 1987. They demonstrated the ability of a cationic liposome with a glycerol backbone lipid called 1,2-di-O-octadecenyl-3-trimethylammonium propane (DOTMA) to deliver DNA in mouse L cells. As the knowledge surrounding liposomal based vectors advanced, endocytosis has been identified as the leading pathway into internalization of the non-viral vector. The limiting factor for gene delivery is the eventual formation fusion with a lysosome, however, different structural modifications to the already existing compounds have been applied, most successful of which is pH –dependent gene delivery systems. The pH-sensitive delivery vectors function by acceleration of the acidification of the endosomal compartment by introducing acid-sensitive linkage like the one in DC-Cholesterol.⁷³ The acidic medium of the endosome/lysosome, helped to cleave PEGylated-lipids, which were initially used to extend the

half-life of a drug or a gene delivery. At neutral pH, PEG carries out its function, and once it is exposed to mild acidic pH, it is cleaved in order to avoid its clustering through the interaction with serum proteins.⁷⁴

Cationic lipids are usually employed as a non-viral vector as part of a liposome. The negatively charged DNA is neutralized by an excess of positively charged cationic lipids in order to complex and compact the DNA to ensure the protection of the cargo from the endonucleases degradation. Liposomes have been associated with increased toxicity and this is caused by the high positive charge on the liposome.⁷⁵ The most commonly used charge ratios are 2:1, 5:1, and 10:1; however, there still does not appear to be any correlations between charge ratio and transfection efficiency that would apply across all cationic systems. Instead, the optimal charge ratio, while always greater than 1:1, is dependent on the chemical structure of the cationic component in the vector system.⁷⁶ The higher the charge ratio, the more toxic the liposome. Additionally, high charge ratio (giving rise to high surface charge) may lead to increased interaction with serum proteins resulting in neutralization of the vector. This process leads to increases in the particle size and precipitation of the whole complex, causing toxicity.⁷⁷ This toxicity can be monitored or controlled either by reducing the charge ratio or utilizing the toxicity to be cell-specific. These liposomes can be used alone and in conjunction with other component to increase the stability of the non-viral vector together with increase of the transfection, and at the same time, reduce the toxicity or render the toxicity cell-specific. Cationic lipids can be categorized according to their hydrophobic tails, their head groups and the nature of the linker, and the impact of variations in these groups will be reviewed, below:

1.2.4.1 Hydrophobic chains

There are two major classes of functional groups that form the hydrophobic region of the cationic lipids, namely, aliphatic and cholesterol derivatives.⁷⁸ Single-tailed aliphatic cationic lipids are

more toxic and less efficient carriers than their double-tailed counterparts as reported by Pinnaduwege et al. ⁷⁹ They tested and compared cetyl triethylammonium bromide (CTAB) in L929 mouse fibroblasts and reported higher toxicity and less efficiency than that of 1, 2-di-O-octadecenyl-3-trimethylammonium propane (DOTMA). However, Tang et al. ⁸⁰ synthesized a new cationic single-tail lipids-oleoyl ornithinate (OLON), and 6-lauroylhexyl ornithinate (LHON) by introducing a biodegradable ester linkage to the OLON. The cytotoxicity of LHON was lower than that of 1, 2-dioleoyl-3-trimethyl ammonium propane (DOTAP) or OLON. The transfection efficiency of the liposome composed of OLON/DOPE with DNA was 10 times higher than that of double-tailed 1',2'-dioleoyl-sn-glycero-3'-succinyl-1, 6-hexanediol ornithine conjugate (DOGSHDO) with an ornithine head group, DOTAP with an amine head group, and CTAB with quaternary head group and single tail. Cationic amphiphile with steroid backbones are more potent protein kinase C (PKC) inhibitors than the aliphatic chain analogues. Changing the structure from sterol to alkyl chain affects the pK_a of the amine group, regardless of whether it is tertiary or quaternary, and this renders the compound uncharged in the PKC assay, which is a safe, reliable method to measure the phosphorylated form of this enzyme (inhibited state). However, with the steroid derivatives, the toxicity is higher. ⁸¹

1.2.4.2 Hydrophilic head groups

The cytotoxicity of a cationic vector stems from its hydrophilic group, which usually consists of a primary, secondary, or tertiary amine, or quaternary ammonium group. ⁸² Guanidino and imidazole groups have also been tested. ⁸³ Ilies et al. ⁸⁴ synthesized pyridinium based compounds, with the primary compound named 1-(2,3-dioleoyloxypropyl)-2, 4, 6-trimethyl pyridinium lipid having a pyridinium group as its head group instead of amine or quaternary ammonium groups. These compounds were tested and compared to DOTAP as the standard transfection agent in different cancer cell lines. These compounds were mixed with different helper lipids, including

cholesterol, and the findings are that at 1:1 ratio with cholesterol, these pyridinium compounds showed superior transfection than that of DOTAP, specifically in the human lung adenocarcinoma (NCI-H23). Yingyong et al⁸⁵. synthesized three libraries of guanidinium-based transfecting agents and found that the library with two head groups and one tail were the most effective having less toxicity in comparison to the common detergents with quaternary ammonium head groups.

1.2.4.3 Linker bonds

Most of the linker bonds in synthesized lipids are ether, ester or amide bond. Compounds with ether linker have better transfection efficiency, but are too stable to biodegraded thus, causing toxicity. Cationic lipids such as DOTAP with ester bonds in the linker region are biodegradable and showed less cytotoxicity in cultured cells; however, they are also liable to decompose in the circulation system.⁸⁶ Recently, carbamate-linked lipids have been synthesized, and these have shown lower toxicity and most likely due to the nature of the carbamate linker being labile to acid hydrolysis in a mild acidic medium and stable in a neutral pH. This assists a fast and safe release of the DNA cargo from the non-viral vector in the late endosome/lysosome compartment.⁸⁷

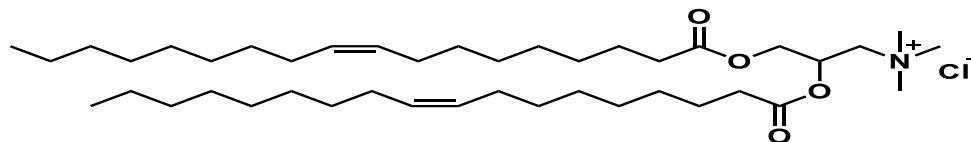
1.2.4.4 Helper Lipids

Neutral lipids have often been added as a component of cationic liposomes used for DNA transfection. These are usually added to modify liposome properties in order to increase the transfection. Three neutral lipids have been repeatedly mentioned in the literature and they have been extensively incorporated in various liposome systems. These are 1,2-dioleoylphosphatidylethanolamine (DOPE), 1,2-dioleoylphosphatidylcholine (DOPC) and cholesterol.⁷⁸ DOPE is by far the most efficient helper lipid for *in vitro* gene transfection.⁸⁸ It has been postulated, based on *in vitro* studies, that DOPE may facilitate cytoplasmic delivery via

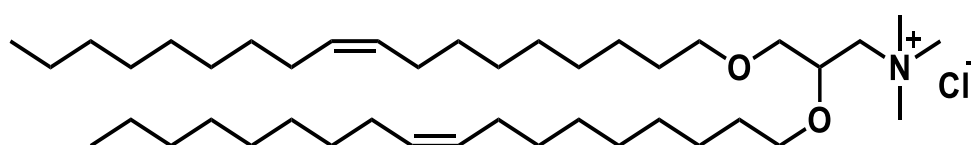
membrane fusion once positively charged DNA-liposome complexes are bound to the cell membrane.⁸⁹ DOPE helps to stabilize cationic liposomes and induce morphology transitions (from vesicle to inverted hexagonal or cubic structures), and this transition is speculated to facilitate the release of the lipoplexes from the late endosome/lysosome compartment through either fusion or destabilization of the endosomal membrane.⁹⁰ Contrary to this, Friend et al⁹¹. did not obtain any evidence that supports⁹² the fusion theory when they used DOTMA/DOPE liposome to transfer DNA segment.⁹¹ Hong et al. intravenously injected two different formulations of liposomes using dimethyldioctadecylammonium bromide (DDAB) as the cationic lipid, once with luciferase and DOPE and, once with Luciferase and cholesterol. In their study, cholesterol sustained the transfection efficiency and not DOPE. On the contrary, when cholesterol was replaced by DOPE, DOPE attenuated the *in vivo* transfection. Despite these two studies, we cannot preclude the role of DOPE in non-viral gene delivery. In an *in vivo* mouse study, Cholesterol and DOPE were used in formulations as helper lipids together with different lipids, specifically DDAB, DOTAP, and 1,2-di-O-octadecenyl-3-trimethylammonium propane (DOTMA), complexed plasmid DNA. DOTAP-Chol formulations showed 50 times greater expression in mice lungs as compared to DDAB system. The DOTMA-DOPE formulation showed an additional 50 times greater expression than the DOTAP-Chol formulation (Table 1.2 structures of common cationic and helper lipids in gene therapy).⁹³

Table 1.2 Structure of common cationic and helper lipids used in gene delivery

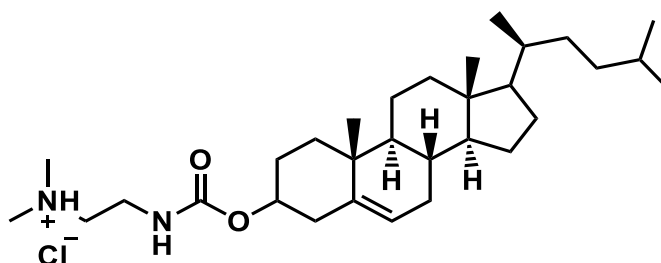
DOTAP



DOTMA



Cholesterol-DC



1.3 Gemini surfactants

Gemini surfactants are bis-surfactants that have attracted increasing attention in both industry and academia due to their unique "twin" or dimeric structure which gives rise to some very advantageous surfactant properties. Similar to any surfactant, they can be utilized in multiple applications including in soil remediation, soap and pigments industry, drug entrapment, and

recently, in gene delivery.³⁴ Menger⁹⁴ was the first person to use the term Gemini to describe this group of amphiphilic compounds in 1991. These unique compounds are usually composed of two monomeric surfactant units that linked by a spacer, at or near, the head group area (see Figure 1.4). The spacer can be short, made up of two or three methylene units, or can be long, made up of ten or more methylene units. Also, spacers can be either hydrophilic or hydrophobic (depending upon chemical structure) and they can contain functional groups (added for specific and controlled purposes), i.e. pH- sensitive amine groups that trigger changes in the aggregate properties.⁹⁵ The application of cationic gemini surfactants to gene delivery is the focus of this project, replacing cationic lipids as a non-viral vector in gene delivery and gene therapy studies.

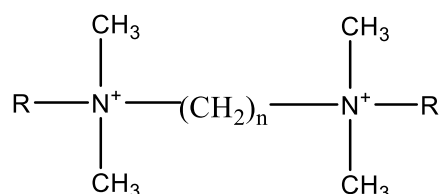


Figure 1.4 Chemical structure of N,N'-bis (dimethylalkyl)-alkane-diammonium-bromide (m-s-m) gemini surfactants. In this example R=C_mH_{2m+1} the alkyl tails connected to the quaternary ammonium head groups, which themselves are connected by spacer group of s methylene units in length

Some of the unique properties of gemini surfactants possess include: their ability to form aggregates of various morphologies in aqueous solutions, which makes them effective tool for drug entrapment and gene delivery applications.⁹⁶ Their low critical micelle concentrations (CMCs), is generally two to three- fold lower than the conventional surfactants⁹⁷, in particular, both of these properties are important to the application for gene delivery⁹⁸, where differences in aggregate morphology are known to impact DNA delivery and low CMC values correspond to lower surfactant concentration in a given formulation, potentially decreasing any toxic effects.³⁴

1.3.1 Structural variations in Gemini surfactants

As introduced above, gemini surfactants are synthetic amphiphilic compounds made up of two monovalent surfactants. This molecular structure contributes to GSs peculiar physicochemical properties including their low CMC, or their diverse aggregate morphologies in solutions. The covalent constraint of the spacer between the head groups is partially responsible for these unusual surfactant properties, which can in effect be tuned by varying the length, flexibility and extent of hydrophobicity/hydrophilicity of the spacer.⁹⁹ In addition to the variations within the spacer group, variations in the length and the nature of the alkyl tails of the surfactants are also easily made, allowing the formulator impact a variety of possible applications including: producing biocompatible and biodegradable surfactants for gene delivery and/or drug delivery applications, or increasing the wetting ability, or promoting emulsification of oil in water, or enhancing the dispersion of solids, or increasing the solubilisation power of dyes by controlling the structural properties.¹⁰⁰ The impact of various structural changes in the gemini surfactant structure are briefly reviewed in the sections below:

1.3.1.1 Variations in the alkyl tail

The physicochemical properties of gemini surfactants can be manipulated by changing the nature and the length of the alkyl tails. As for conventional surfactants, the CMC values for gemini surfactants decrease with an increase in the alkyl tail length⁹⁶, with the magnitude of decrease in the CMC values in gemini surfactants being greater than the corresponding monomeric ones.^{101,102} Gemini surfactants can induce various biological activities, including; the inhibition of bacterial activity¹⁰³, and drug and gene delivery.¹⁰⁴

The most well- studied family of GSs are the *N,N*-bis[(dimethyl alkyl)- α,ω -alkanediammonium dibromide], known as *m-s-m* gemini surfactants, where *m* is the carbon chain of the alkyl tails and *s* is the number of carbon atoms in the polymethylene spacer.⁹⁶ Asymmetry and branching

were also introduced in gemini surfactants at the tail level. Wang et al.¹⁰⁵ synthesized phytanyl-3-n and phytanyl-7NH-n gemini surfactants (see Figure 1.5) to evaluate the effect of branching in the alkyl tail (specifically an increase in hydrophobicity) on the transfection efficiency. *In vitro* studies showed superior transfection efficiency for phytanyl substituted surfactants compared to that of the symmetrical counterpart (16-3-16). The increased transfection efficiency was attributed to higher degrees of micellization (α) of the phytanyl surfactants and their ability to form vesicles in the absence of DNA, and transition into inverted hexagonal structures in the presence of DNA (Inverted hexagonal structure was associated with DOPE in the literature, enabling the fusion with the endosomal membrane, resulting in the escape of the complex from the endosomal compartment).¹⁰⁶ The inverted hexagonal structure was confirmed by SAX studies. The latter structure has been related to better transfection data in several studies.¹⁰⁶ The same inverted hexagonal morphology was tied to DOPE in earlier gemini surfactants/DNA/DOPE formulation in gene delivery studies.¹⁰⁷ Higher (α) values are associated with greater dissociation of counter-ions from the micelles, which would promote the interaction of the micelle with DNA, forming stronger polyplexes, and therefore enhancing transfection efficiency.¹⁰⁸

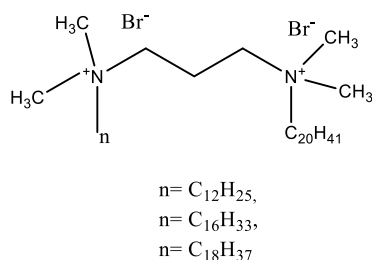


Figure 1.5 Chemical structure of phytanyl-3-n. Where n =1-bromododecane, 1-bromohexadecane, or 1-bromooctadecane

Dissymmetric gemini surfactants where hexylpyrene replaces one of the typical alkyl tails were synthesized with varying polymethylene spacer length groups, specifically propyl ($s = 3$), and hexyl ($s = 6$).¹⁰⁹ The incorporation of the bulky pyrene moiety in these surfactants significantly impacted the micellization properties. CMC values of pyrenyl surfactants were significantly lower than their symmetric counterparts (m-s-m), and these surfactants were prone to form not only micellar aggregates, but also pre-micellar aggregates. The presence of these aggregates was favored in pyr-6-12. These compounds have the ability to serve as emissive components in DNA-gemini lipoplex/polypoplex in DNA trafficking, in gene delivery and gene therapy applications.¹⁰⁹ This potential can help identify the key parameters to help overcome the barriers in non-viral gene delivery methods. One of the means is to track the pyrene moiety in *in vitro* study using fluorescence techniques.

The nature of the tail groups within gemini surfactants can have several effects on the physical-chemical behavior of the compounds. An important effect is the introduction of different degrees of unsaturation, which brings about gel-liquid crystalline transition within vesicles formed in these compounds. In a bilayer-forming phospholipids, the longer the tail the higher the transition temperature, when the saturated tails are replaced with unsaturated tails (oleyl tails C18:1 as an example), the transition temperature decreases considerably. The presence of the oleyl tail can induce the formation of different favorable aggregates at lower temperatures.¹¹⁰

In a study by Cardoso et al.,¹¹¹ they investigated the ability of different bis-quaternary ammonium gemini surfactants with different alkyl chain lengths to transfect human epithelial cervical carcinoma cell line (HeLa cells) with two different system: binary system with only DNA/GS, and ternary one with DNA/GS/DOPE/Chol (2:1 mol). Different charge ratios of N^+/P^- were investigated with a fixed ratio of helper lipids.¹¹¹ The physio-chemical properties of these two systems at different charge ratios were investigated and showed the presence of diverse

aggregate sizes ranging from 140-3000nm in the absence of the helper lipids, and 170-2100nm in the presence of helper lipids. However, the polydispersity and contained more than one aggregates, which made the particle size range very wide. This might have stemmed from the nature of the GS-DOPE antagonistic interaction in solution, which drives the gemini surfactant to interact with the DNA, and the DOPE not to interact with the nanoparticle, shielding it. This shielding effect might cause the appearance of one peak representing the DOPE average size¹¹². However, do to the hydrodynamic nature of the solution, sometimes, two peaks can be recognized, which ultimately gives the average size of the nanoparticle. These aggregates ranged from giant vesicles to small size vesicles and irregular shape aggregates. The *in vitro* studies showed that complexes with larger sizes are often better in transfection than smaller ones, attributed to the tendency of larger particles to sediment over the adherent cultured cells, thus increasing the contact area between the complexes and the cellular surfaces, hence, facilitating internalization. Larger complexes are also able to carry more DNA, which together with the presence of helper lipids contributes to higher transfection levels. The ability of gemini surfactants to adopt different morphologies in solution has been linked to improved transfection in non-viral gene delivery systems, specifically with certain aggregate structures, such as, inverted hexagonal and cubic structures.¹⁰⁷ In the current study by Cardoso et al., gemini surfactants with longer alkyl tails, 14-2-14, and 16-2-16 exhibited richer phase behavior irrelevant of the concentration range utilized, this phase behavior was not witnessed in 12-2-12 surfactant in the video-enhanced light microscopy (VELM) micrographs. This provides support for the lower transfection efficiency observed when using the binary system of 12-2-12/DNA. In the absence of helper lipids, the above system displayed a low transfection efficiency of 6.6% of cells transfected. This transfection efficiency of the 12-2-12 surfactant increased dramatically upon the addition of the helper lipid up to 45.7%, this efficient transfection might have been caused by the induction of higher morphology structures induced by DOPE and the reduction of

serum interactions due to the presence of cholesterol in the helper lipid system. 14-2-14 and 16-2-16 displayed 14.4% and 31.1% transfection efficiency in the absence of helper lipid, and 44.2%, and 53.9% in its presence, respectively. In the case of 16-2-16/DNA/helper lipid system, according to the VELM micrographs, there are two distinctive phases formed; lamellar and hexagonal, and both were compacted in a multi lamellar sandwich structure, giving rise to superior transfection efficiency.¹¹³ These suggest a strong influence of the alkyl tail length on transfection efficiency, with general observation that the longer the alkyl tail, the better the transfection.

In summary, the literature reviews demonstrates that complexes containing gemini surfactants with longer alkyl tail lengths ($m \geq 14, 16, 18$), or with unsaturation (oleyl), or branching (phytanyl) exhibit increased *in vitro* transfection relative to those with shorter tail lengths ($m \leq 10, 12$).

1.3.1.2 Variations in the head groups

The density and nature of the head group has been shown to influence gene transfection efficiency.¹¹⁴ The simplicity of varying the structure of these gemini surfactants led organic chemists to synthesize different surfactants by introducing biodegradable and biocompatible head groups, such as; sugars. Quaternary ammoniums were replaced by reduced sugars, such as glucose, and mannose connected to tertiary amines or amides with a polymethylene spacer.¹¹⁵ The presence of either glucose or mannose¹¹⁶ in the head group area provides a biocompatible vector, which will extend the half-life of the vehicle in the circulation in Chinese hamster ovarian cells (CHO).¹¹⁶ These sugars in the head group can lead to different hydration degrees and result in the formation of different aggregates (This impacts the head group area, and as a consequence, results in different morphologies).¹¹⁷ Also, the presence of the tertiary amines can lead to a pH-dependent aggregation behavior as a result of the protonation of the amines. At a lower pH, the

presence of the amine and the amide can assist in the escape of the vector from the late endosomal/lysosomal compartment and the possible release of the DNA cargo.¹¹⁵ The protonation effect is not a possibility with the amide linkage.

Amino acids are also employed in the structure of the gemini surfactants to increase the biocompatibility. Cardoso et al.¹¹⁸ investigated the ability of six members of a new family of serine- derived GSs (Figure 1.6) to safely mediate gene delivery and gene transfection. They conducted a comparative study based on: i) the influence of the length of the alkyl tail in three different series depending on the spacer linker: amine, amide; and ester, and ii) the effect of the nature of the linker spacer on the transfection. The effect of both the alkyl tail and the spacer were evaluated in a plain surfactant/DNA complexes, and on surfactant/DNA/ helper lipid systems with DOPE/Cholesterol (2:1) as the helper lipid system. All the serine surfactants having amine linkers mediated gene transfection, however, no trend with respect to the length of the alkyl tail on transfection was observed. (16Ser)₂N5 was the least efficient, which contrasts the already existing findings in the bis-quaternary ammonium gemini surfactants with hexadecyl tail, which showed the highest transfection efficiency.¹¹¹ In addition, the presence of serine in the alkyl tail adds to the complexity of the gemini surfactants and can impact the physio-chemical parameters quite differently, and hence, affect the transfection (The size of the complexes ranged from 163nm to 3µm, with an increase in the size promoted by the addition of the helper lipid at different charge ratios. The zeta potential was also impacted by the addition of the DNA to the GS and with longer alkyl tails, the overall charge remained positive even in the presence of the DNA). The lowest toxicity in the amine series was observed at an (8:1) charge ratio, following the sequence (18Ser)₂N5 > (14Ser)₂N5 > (16Ser)₂N5. (16Ser)₂N5 was shown to exert the highest toxicity and lowest efficiency in the transfection study. The helper lipid system employed in this study increased the transfection efficiency throughout the amine series. DOPE confers on the system the ability to escape lysosomal degradation through the formation of different aggregates,

and the cholesterol due to its biocompatibility. In addition, it is less prone to interact with serum proteins.¹¹⁹ However, helper lipids induced cytotoxicity in the case of complexes prepared with (18Ser)₂N5.

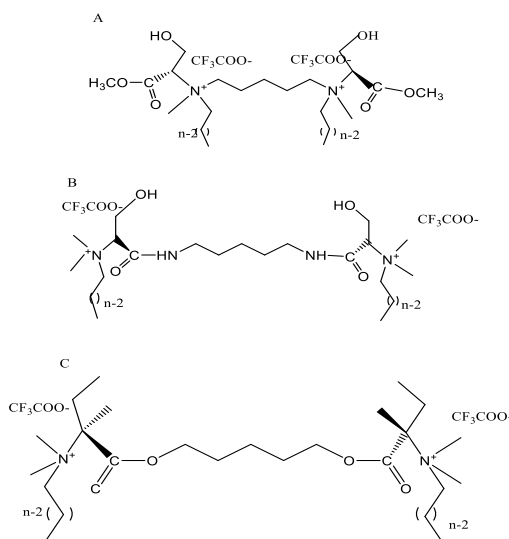


Figure. 1.6 Serine derived gemini surfactants, A) amine series designated as (nSer)₂Nm, B) amide series (12Ser)₂CON₅, and C) ester series (12Ser)₂COO⁻

One of the best available commercial transfection agent is lipofectamine[™] 2000 (Invitrogen) and it is a cationic lipid 2,3-dioleoyloxy-*N*-[2-(spermine carboxamide) ethyl]-*n,n*-dimethyl-1-propyl ammonium chloride (DOSPA) with five quaternary ammonium head groups.¹²⁰

Head group area plays a huge role in the condensation of DNA, and thus, in protecting it from the effect of endonucleases once internalized.

1.3. 1.3 Variations in the spacer group

Properties of dimeric surfactants can differ greatly from those of conventional surfactants. This has been related to the distribution of distances between head groups in micelles formed by these two types of surfactants.⁹⁹ For conventional surfactants, this distribution goes through a maximum at a thermodynamic equilibrium distance $d_T \approx 0.7\text{--}0.9$ nm, for dimeric surfactants the

distribution is bimodal, with a first maximum at a thermodynamic distance d_T and another narrower maximum at a distance d_s which corresponds to the length of the spacer.¹²¹ This length is determined by the bond lengths and bond angles between the atoms in the spacer group. The bimodal distribution of head group distances and the effect of the chemical link between head groups on the packing of surfactant alkyl tails in the micelle core are strongly affects the curvature of the surfactants and thus the micelle shape and properties of the solution. The effect of the changes in the spacer group was investigated by transmission electronic microscopy at cryogenic temperatures (cryo-TEM) for 12-s-12 dimeric surfactants with different spacer length ($4 \leq s \leq 12$).¹²² This study showed that 12-2-12 formed thread-like micelles at 2wt%, and 12-3-12 showed spheroidal micelles at 7wt% in solution. DTAB, a monomeric form of both 12-2-12, and 12-3-12, showed only spherical micelles irrelevant of the concentration and the ionic strength. The solution of 12-4-12, 12-8-12, and 12-12-12 exhibited densely packed spheroidal micelles at 5-7wt% and vesicles were formed in solutions of 12-16-12 and 12-20-12.⁹⁹ This demonstrates the effect of the s and the role it plays in determining the structure of the micelles formed.

The shape of aggregates formed by a gemini surfactant is influenced by its molecular structure. A theory used to predict the shape of micellar aggregates is that of the packing parameter (also known as the surfactant parameter, S , or the critical parameter, CPP), defined as:¹²³

$$P = v/la_0 \quad (1.1)$$

where v is the volume of the alkyl tails, l is the length of alkyl chains, and a_0 is the surface area occupied by the head group. The types of aggregate shapes predicted for certain ranges of P values are summarized in Table 1.3. As can be seen by the equation above, the packing parameter is impacted directly by the length and the volume of the alkyl tails and the head group area; although for traditional surfactants the head group area remains essentially constant. In dimeric surfactants, the spacer contributes significantly to the packing parameter, primarily by changing

the head group area. The effect of the spacer is difficult to generalize in simple terms. A large hydrophobic spacer will mainly contribute to the value of ν and on the other hand, a small rigid spacer directly contributes to the effective head group area, allowing smaller head groups for the same effects and in both cases allow for spherical micelles to form. Since the number of different possible gemini surfactants is large, all types of association structures can form and they have to be investigated individually.¹²⁴

Table 1.3 Packing parameter and expected aggregates structures¹²⁵

P	Aggregates` shapes	General surfactant type
<0.33	Spherical micelles	Single-chain surfactants with relatively large head groups
0.33-0.5	Cylindrical or rod-shaped micelles	Surfactants with relatively small head group
0.5-1.0	Vesicles or flexible bilayer structure	Double-chain surfactants with large head groups and flexible chains
1.0	Planar bilayer structures	Double-chain surfactants with small head groups or rigid chains
>1.0	Inverted micelles	Double-chain surfactants with small head groups, very bulky chains

The effect of the length of the spacer on the ability of the gemini surfactant to compact DNA was investigated by Karlsson et al.¹²⁴ in the 12-s-12 series. In their study, shorter spacers ($s = 2,3$)

showed the most efficient compaction of DNA and this is likely due to the spacing between the positive charges, which is small and keeps the surfactant acting like a divalent cation, thus interacts preferably with the negatively charged phosphate backbone. Larger values of s represent a more flexible spacer that can change its conformation to reduce the hydrocarbon-H₂O interaction; however, this will restrict the surfactant conformation and will result in entropy loss that has to be compensated for in order to compact the DNA. This happens through the association of the spacer within the hydrophobic core, thus reducing the coil- coexistence border. This happens only if the spacer is large enough to self-associate with the tails ($s \geq 10$). Intermediate spacers will be the least efficient in compacting DNA because it is not flexible enough to self-associate into the core. Despite the different effects of the spacer on the compaction of the DNA, the presence of coil-globular coexistence continue to persist regardless of the concentration.

This implies that the nature and/ or the length of the spacer group in the head group area of a gemini surfactant has been shown to play a significant role in gene delivery and transfection. Wettig et al.¹²⁶ investigated the introduction of tertiary (N-CH₃), and secondary (-NH) amine groups in the spacer group of the gemini surfactant and the impact these modifications had on transfection activity. When these gemini surfactants were complexed with DNA alone, they showed little to no transfection, with the exception of the secondary amine substituted 12-7NH-12 (1,9-bis(dodecyl)-1,1,9,9-tetramethyl-5-imino-1,9-nonanediammonium dibromide) which showed little transfection activity. The addition of DOPE resulted in a significant increase in transfection efficiency, in agreement with the previous studies of incorporating DOPE as part of non-viral delivery systems. DOPE helps to stabilize the cationic liposome and it also induces morphology transitions. These transitions are speculated to facilitate the release of DNA from the complex through either fusion or destabilization of the endosomal membrane.^{127,127b} This study, gemini surfactants containing substitution, with either tertiary (N-CH₃) or secondary

amine (-NH) in the spacer resulted in an increase in transfection efficiency. The highest level of transfection in COS-7 cells was achieved for the system containing the 12-7NH-12 gemini surfactants with an efficiency of 6.7 ± 0.5 ng luciferase/ 2×10^4 cells, comparable to the positive control (Lipofectamine plus®). Also, cell viability of the tertiary gemini surfactants 1,5-bis(dodecyl)-1,1,3,5,5-pentamethyl-3-aza-1,5-pentanediammonium dibromide (12-5N-12), 1,9-bis(dodecyl)-1,15,9,9-pentamethyl-5-aza-1,9 nonanediammonium dibromide (12-7N-12), 1,10-bis(dodecyl)-1,1,4,7,10,10 hexamethyl-5-diaza-1,1-dodacanediammonium dibromide (12-8N-12) were comparable to that of lipofectamine plus® (80%) and lower cell viability was reported for the secondary amine gemini surfactants with cell viability of 70%. 12-7N-12, and 12-8N-12 exhibited the highest and the lowest transfection efficiencies, respectively. This probably resulted from an increase in the steric hindrance presented in the 12-8N-12, which compromised its ability to bind to the DNA and to form aggregates. The equilibrium distance between the nitrogen centers were compared to the distance between the phosphate groups in the DNA, which is equivalent to 6.5 Å and 7.1 Å.¹²⁸ It has been estimated from a polyamine-DNA study that a spacing of 4.9 Å¹²⁹ between two nitrogen centres was calculated, which is equivalent to three methylene spacer between the nitrogens, is the ideal spacing to interacting with the DNA.¹³⁰ This spacing was found only in 12-7N-12 and 12-7NH-12 with 5.1 Å between the two quaternary ammoniums, calculated from molecular modelling studies. The 12-7NH-12 showed superior transfection to that of 12-7N-12, which was rationalized based upon the pH dependent nature of the secondary amine group in the 12-7NH-12 surfactant. This surfactant, upon protonation of the secondary amine group (forming a 3rd quaternary ammonium in the head group) undergoes a vesicle to micelle transition, resulting in either fusion or a destabilization of the endosomal membrane leading to its rupture and the release of the complex from the endosome.

In another study, a homologous series of hexyl pyridinium gemini surfactants with pyridinium rings replacing the quaternary ammonium groups and with different spacer lengths ($s = 4, 8,$ and

12) connecting the pyridinium head groups were synthesized (see Figure 1.7). These were employed as a non-viral gene delivery of plasmid vector in human rhabdomyosarcoma cell lines (RD-4) with or without DOPE as the helper lipid. Only bispyridinium with hexadecyl tails (P16) was chosen for gene transfection studies with three different lengths of the methylene spacer. All the three surfactants were able to compact the plasmid DNA, however, 1,1'-dihexadecyl-2,2'-tetramethylene bispyridinium dichloride (P16-4) were able to transfect DNA with P16-4 having the highest efficiency. This was attributed to a stacking behavior of the surfactant. Its ability to function like molecular tongs that are able to grip aromatic bases of the DNA and the phosphate groups. The phosphate groups can substitute the counter-ions between the aromatic rings, reducing the electrostatic repulsion existing between the head groups. Then, the hydrophobic interactions between the chains are capable of fully compacting the DNA and assembling into nanoparticles. When the length of the spacer increases, this arrangement becomes more difficult because the pyridinium rings are interacting with DNA sites that are far from each other. This resulted in little to no transfection being observed with 1,1'-dihexadecyl-2,2'-octamethylene bispyridinium dichloride (P16-8), and 1,1'-dihexadecyl-dodecamethylene bispyridinium dichloride (P16-12), respectively. From molecular modelling, the latter may adopt an extended conformation in solution due to the association of the long spacer into the hydrophobic core, resulting in the interaction of the head groups with the DNA sites that are far apart, which hinders the penetration through the cellular membrane. This reduces the intensity of the compaction and the ability of the nanoparticle to interact cellular membranes. However, in this study, the presence or absence of DOPE did not have any impact on the transfection efficiency.¹³¹

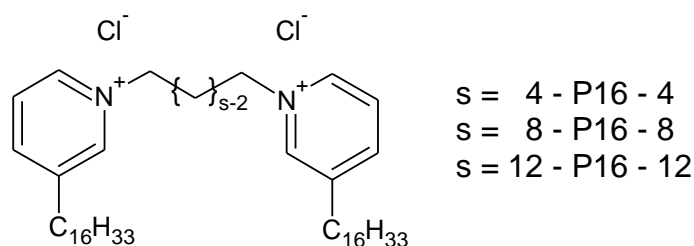


Figure 1.7 Structure of the bispyridinium gemini surfactants with different polymethylene spacer lengths

Cationic gemini surfactants with cholesterol moieties as their alkyl tails and two different spacer groups, hydroxyl ethyl ($\text{CH}_2\text{CH}_2\text{OH}$), and oligooxyethylene $(\text{CH}_2\text{CH}_2\text{O})_n$, as well as alkyl ($-\text{CH}_3$) and/or hydroxyethyl ($-\text{CH}_2\text{CH}_2\text{OH}$) moieties attached at the quaternary ammonium groups were synthesized and evaluated for their transfection ability by Misra et al.¹³² These molecules (shown in Figures 1.8A and 1.8B) are made of cholesterol skeletons attached via a linker to the cationic head groups, both the linker and the nature of the cationic head groups are of great importance to determine the efficiency of the transfection and the level of cytotoxicity. Formulations of DOPE/Cholesterol GS at a molar ratio of 1:1 enhanced the same level of transfection activity in the presence of serum in HeLa cells. As the spacer length of the oligooxyethylene was increased from 1 EO unit to 4, the transfection efficiency decreased. The introduction of a hydroxyethyl moiety in the spacer led to a further decrease in the transfection activity. Enhanced transfection efficiency was observed for the oligo-oxyethylene with $n = 1$. (CholHG-1ox) exhibiting ~65% GFP expression in the absence of serum, and increasing to approximately 90% GFP expressing cells in the presence of serum. The gemini with a hydroxyethyl spacer showed approximately 75% GFP expression in the presence of serum and the same level of transfection was observed for other oligo-oxyethylene substituted compounds, with $n = 2, 3$ and 4 in the presence of serum. The zeta potential of the lipoplex containing

CholHG-1ox was ~18 mV at an N+/P- charge ratio of 0.5 compared to that of CholHG-3ox (~12 mV at an N+/P- charge ratio of 0.5) in the presence of serum. A DNA release study using ethidium bromide re-intercalation assay with the same serum condition for the lipoplexes revealed that CholHG-1ox managed to release approximately 50% DNA, whereas the other gemini surfactants released only 30%. Dynamic light scattering data showed aggregates of an average size of approximately 137nm for CholHG-1ox, whereas CholHG-3ox displayed larger aggregates of approximately 220 nm. While the reason(s) for the enhanced transfection activity of the CholHG-1ox gemini surfactant is not clear, it was hypothesized that a shorter oxymethylene spacer group in addition to the presence of the cholesterol moiety in the tail group may play a crucial role in the DNA compaction in these lipoplexes. Cholesterol is known to form domains in the presence of serum proteins that can interact with cellular membranes through a lipid raft/membrane mechanism.¹³³ This can enhance the transfection efficiency. The presence of the hydroxyl groups in the spacer of the CholHG-1ox interacted with serum proteins found in the fetal bovine serum (FBS), and enhanced lipoplex association in the presence of serum. A DNase stability assay revealed that CholHG-1ox based lipoplexes displayed higher stability against DNase I in comparison to CholHG-3ox in presence of serum, which also may have accounted for some of the observed increases in transfection efficiency.

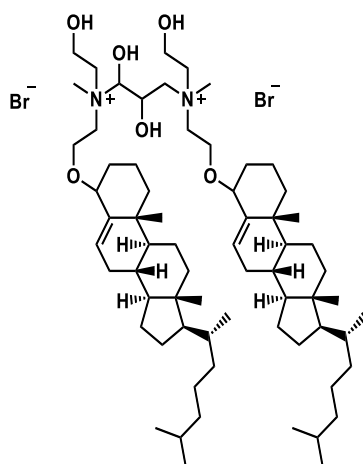


Figure 1.8 A Molecular structure of cholesterol-based gemini surfactants with hydroxyl spacer

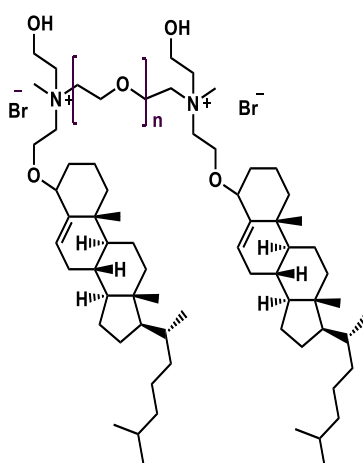


Figure 1.8.B Molecular structures of cholesterol-based cationic gemini surfactants with oligoxyethylene spacer¹³²

The literature review indicates that gemini surfactants with shorter spacer lengths ($s \leq 4$) or longer spacer lengths ($s > 10$) exhibited better transfection efficiency than those with the intermediate spacer length ($s = 5, 6$ methylene units). This can be attributed to the fact that these surfactant may be able to induce favorable morphologies with preferred packing parameters for the complexes; either gemini-DNA or gemini-DNA-helper lipids. An example of these morphologies include lamellar, inverted hexagonal or cubic. Another important aspect is the introduction of specific functional groups within the spacer and/or head group region may add

advantage to the complexes, such as; the presence of acid-labile functional groups. Also, the presence of cholesterol, spermine, pH-sensitive amide group (NH), guanidiniums, cardiolipin analogues, nucleolipids, and pyridinium, could impact compaction and condensation with negatively charged DNA molecules.

1.3.2 Transfection efficiency *in vitro* and *in vivo*

A promising tool to treat broad spectrum diseases, such as Alzheimer, and cancer, is gene therapy as in theory, it provides a specific cell with the necessary missing DNA or RNA to produce therapeutic proteins and either correct or add an old malfunction gene/ or a new gene. Due to major obstacles facing gene delivery, many vectors have been exploited and gemini surfactants are one of these vectors.¹³⁴ A review of literature revealed that so many gemini surfactants have been synthesized and characterized in recent years, with a number of these compounds have been examined for applications of gene therapy.³⁴ This section will review some of the recent examples; however, readers are referred to recent reviews for a more comprehensive reviews of gemini surfactants that have been applied to gene delivery.^{135,136}

McCregor et al. synthesized biocompatible peptide-based gemini surfactants (PGSs).¹³⁷ These surfactants were generated by varying the composition of the head groups, which contained the peptides, and the length of the tail (saturated, or unsaturated, but not branched), with two cysteine residues joined in the spacer by a thioether linkage (Figure 1.9) to increase the stability of the compounds, which could not be conferred when a thiol linkage was used. The capability of these PGSs to mediate transfection of a Chinese hamster ovary (CHO-DG44) cells, either alone or in the presence of DOPE in the formulation as a helper lipid was compared to a positive non-viral transfecting control. Gene transfection in these PGSs was dependent on the hydrophobic tails as well as the nature of the amide linkage between the three lysines in the head group area. Gene expression of PGS1 was superior to the rest and this possibly was because of the presence of

three lysines linked through their ϵ -amino group and the nature of the alkyl tails, which was unsaturated oleyl tail.¹³⁷

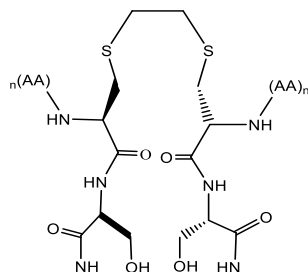


Figure 1.9 Peptide-based gemini surfactants with thioether linkage (PSG) with AA: lys- α -lys- α -lys-, lys- α -lys- ϵ -lys-, or (lys)₂lys-, and R= C₁₆, C₁₈ and C₁₂¹³⁷

Alqawlaq et al. developed and characterized non-viral gene delivery nanoparticles, composed of 12-7NH-12 gemini surfactant as the cationic moiety with pH- sensitive functional -NH- group within the spacer linker, *pCMV-tdtomato* as the plasmid, and two helper lipid systems; DOPE, and DOPE:DPPC at different N⁺-P⁻ ratio (5:1, 7.5:1, 10:1, 12.5:1, 15:1) were added to the nanoparticles.¹³⁸ The ability of these systems to treat glaucoma was tested *in vitro* and *in vivo*. PGL_{DOPE} nanoparticles showed the highest transfection efficiency in a model retinal cell line (RGC-5). This system also showed ability for binding and permeation across the corneal epithelium at a 10:1 charge ratio. After intravitreal administration of the gemini-DOPE-DNA, nanoparticles were localized in the nerve fiber layer of the retina. When the topical administration was tested, it was less effective with the nanoparticles being localized within the limbus, iris and conjunctiva. The presence of the helper lipids was reported to produce coexisting lamellar and inverted hexagonal phases at lower pH (endosome or lysosome), and this may have induced better transfection efficiencies in the formulations that contained DOPE. These features are important for better gene transfection and release of DNA into the cytosol.¹³⁸

Many of the gemini surfactants currently employed in gene therapy applications are symmetrical ones with either quaternary ammonium, carbohydrates, aminoacids, or pyridinium head groups and hydrocarbons alkyl tails with various length. More interest is growing in using gemini surfactants with different structures and dissymmetrical ones; Oda et al. synthesized these surfactants with dimethylene spacers¹³⁹, and Wang et al. synthesized asymmetrical gemini surfactants with six methylene units in the spacer, and two different hydrocarbon groups as the alkyl tails, with a total of $m+n=24$.¹⁴⁰ Dissymmetric gemini surfactants have been synthesized and their physiochemical properties have been characterized, but only few of these surfactants have been actually employed as non-viral gene delivery vectors. One of these few studies is the utilization of phytanyl gemini surfactants with DNA- helper lipid in gene delivery in OVCAR-3 cell-lines, which showed improved transfection when phytanyl-3-16 was used instead of 16-3-16, which has higher transfection efficiency than other surfactants that have been employed for such purposes.¹⁴¹

1.3.3 Gemini surfactants-DNA lipoplex and the interaction with cell membranes

Transfection efficiency of gemini surfactants-DNA has been investigated numerous times by many research scholars, and several of those have noticed partial, or transient, or complete improvement in transfection efficiency when helper lipids, whether its DOPE or a mixture of DOPE and other helper lipids, are added to the mixture forming a lipid-based vector.¹³⁵ Javid Akbar et al. showed that a non-ideal mixing behaviour is exhibited when DOPE is added to the gemini surfactants,¹¹² however, the interaction mechanisms between the helper lipid with the Gemini-DNA complex has not been yet identified. Various approaches and techniques have been utilized to study the modes of interaction(s) between these components of a non-viral vector and between these components and the lipid membranes; whether it is the cellular membrane or the endosomal membrane. Some of the techniques that have been utilized to examine these

interactions are: particle size and zeta potential, isothermal titration calorimetry,¹¹² atomic force microscopy,¹⁴² small X-ray scattering (SAXS),¹⁰⁵ and recently Langmuir Blodgett monolayer studies.¹⁴³ These studies aim to shed light on the interactions of the cationic surfactants with the DNA and the effect of their condensation and compaction of DNA on the ability of the nanoparticles to interact with lipid membranes. The Langmuir Blodgett technique is an approach used to increase the understanding of the interactions between the DNA/gemini surfactant complexes as part of the bulk water (sub-phase) in the presence of an amphiphile (gemini surfactants) with its ability to adsorb at the interphase due to its dual nature; and its possible interaction with the insoluble monolayer, which is deposited at the air/water interface, with its hydrophilic part facing the water sub-phase and its hydrophobic moiety toward the air. In this thesis, this approach was applied in order to mimic cellular membranes, to understand how the GS-DNA vector interacts with the membrane, how it may be endocytosed, and more importantly how the components of the delivery vector (i.e. gemini surfactants and helper lipids) disrupts or become incorporated into cellular membranes. It is anticipated that such studies can improve our understanding of some of the mechanisms involved in the transfection process when a non-viral vector is being used.

1.4 Langmuir-Blodgett (LB) monolayer studies and Brewster Angle Microscopy technique (BAM)

Investigation of the interactions of DNA with cationic moieties in the presence of model membranes resembling biological membranes is of great importance. This kind of study can clarify the role of these interactions and the effect of them on the delivery of a desired segment of the DNA into the cells by means of a non-viral vectors.¹⁴⁴ The LB method is a technique that allows the preparation of model membranes in a two dimensional system by spreading

phospholipids at the air-water interface¹⁴⁵ and it also offers a unique opportunity to investigate the nature and possible interactions between these monolayers and different molecules.¹⁴⁶ A molecular-level understanding of these interactions is necessary because depending on the lipid composition of cell membranes and tissues, biophysical interactions are altered, and this can be beneficial in developing target-specific drugs and drug delivery systems. So far, single or double component model membranes have been employed in such studies, and while these differ from the multicomponent biological systems, they offer a unique method to understand the mechanism by which exogenous molecules interact with lipid membranes.¹⁴⁷ The Langmuir trough, used to prepare Langmuir monolayer is often coupled to Brewster Angle Microscope (BAM), which allows direct visualization and determination of domains in the monolayer and the phases at which these domains exist at the air/water interface, thus allowing real-time observation and recording of film structure.

The Brewster Angle method is based on the fact that if a *p*-polarized light beam hits a surface, a reflection of that light occurs. However, if the surface is hit at the Brewster angle at 53° or near it, no reflection occurs. When the monolayer is spread at the air/water interface, the refractive index of the surface changes accordingly and some reflection occurs, allowing for images (based upon the differences in the refractive index) to be taken using a CCD camera.¹⁴⁸ In order to determine the surface pressure and the molecular areas associated with the components of the monolayer, a monolayer is spread on the water surface and the barriers found at each end of the trough are compressed at a constant speed. This process provides an isotherm of the surface pressure as a function of mean molecular area (Π -A) for the monolayer. The surface pressure of a monolayer can be calculated from the difference of the surface pressure of pure water at 20°C (72 mN/m) and the new recorded surface pressure of the monolayer.¹⁴⁸ In an ideal isotherm generated from a Langmuir monolayer, four principal phases can be observed; a gaseous phase

(G), liquid expanded phase (Le or L₁), liquid condensed phase (Lc or L₂), and solid or solid-like phase (S). These phases and the transitions are illustrated in Figure 1.10.

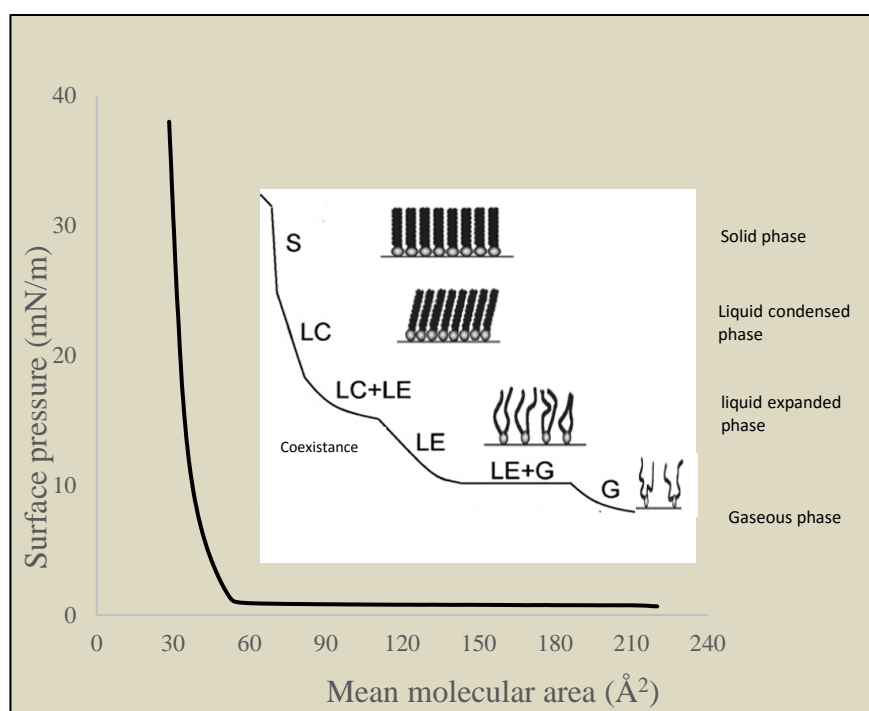


Figure 1.10 π -A isotherm obtained by compressing an insoluble lipid monolayer formed at an air-water interface. Adapted from reference^{149,148}

In the gaseous phase, surfactant molecules remain far apart and disoriented as can be seen in Figure 1.10. As the surface pressure increases (brought about by bringing the barriers on the Langmuir trough closer together), the surface area available to the molecules of the monolayer decreases, resulting in the formation of the liquid expanded, then liquid condensed, and finally the so-called solid phase. Additionally, there is the possibility of co-existence regions, where more than one phase exists (i.e. a liquid expanded – liquid condensed phase; L_E – L_C). Further compression of the monolayer results in the collapse of the monolayer; the monolayer may be squeezed into either the water or air phase, possibly into bi- or multilayer phases. Certain parameters of importance can be obtained from the Langmuir monolayer; as an example, the

minimum sectional area (A°) can be obtained from by extrapolating the isotherm at the steepest slope prior to collapse back to zero surface pressure.¹⁴³

For a Langmuir monolayer, surface tension changes as the compressibility of the monolayer increases, and this change is denoted as interfacial elasticity¹⁵⁰. This compressibility is defined as

$$C = -1/A(dA/d\pi)_T \quad (1.2)$$

Where A is the molecular area, and π is the surface pressure. The reciprocal of compressibility is denoted as compressibility modulus (C_s^{-1}). C_s^{-1} provides information on the phase transition(s) of a Langmuir monolayer, for instance, the more sharp the phase transition, the higher is the differential $d\pi/dA$ and stiffer the monolayer^{150b}

$$C_s^{-1} = 1/C = -A(dP/dA)_T \quad (1.3)$$

1.4.1 Lipid membrane composition

Lipids within the body have three different functions.¹⁵¹ First, lipids are used for energy storage, mainly as triacylglycerol and steryl esters, in lipid droplets. These reserves serve as caches of fatty acid and sterol components that are needed for membrane biogenesis. Second, cellular membranes are composed of polar lipids, which consist of a hydrophobic and a hydrophilic portion. The hydrophobic moieties have the propensity to self-associate and assemble into different morphologies (driven by the surrounding water). This fundamental principle of amphipathic lipids is a chemical property that enabled the first cells to segregate their internal constituents from the external environment.¹⁵² And this same principle assisted in the formation of discrete organelles within the cells. This function of lipids enables segregation of specific chemical reactions for the purposes of increased biochemical efficiency and restricted dissemination of reaction products. In addition to the barrier function, lipids provide membranes

with the potential for budding, characteristics that are essential for cell division, biological reproduction and intracellular membrane trafficking.¹⁵¹ The function of interest to our current study is the assembly of polar lipids into cell membranes and how in particular, molecules of foreign origins to the body can interact with the components of these membrane and be able to fuse or disrupt the homogeneity of these membranes. Lipids in cellular membranes are mainly glycerophospholipids (9600 species), sphingolipids (more than 100,000 species), and mono-, di-, or triglycerides variants.¹⁵³ Fatty-acid and sterol-based structures are also highly abundant. Cellular membrane lipids are divided into three distinct groups: phospholipids (glycerol-based lipids, 40-60 mol % of the total lipid fraction, ceramide-based sphingolipids, and sterols. Phospholipids are further subdivided into several groups according to their hydrophilic head groups; phosphatidylcholine (PC), phosphatidylethanolamine (PE), phosphatidylserine, phosphatidylinositol, and cardiolipin. The first three mentioned lipids are the principle lipids in cellular membranes. Sphingolipids possess sphingoid base as a backbone; and are responsible for the hydrophobicity of the core of the cellular membrane bilayer. cholesterol (30-50 mol % of the total lipid fraction) is responsible for the fluidity and packing of the lipid membrane.¹⁴³ Figure 1.11 illustrates how glycerophospholipids can be very diverse based on the linkages, degree of saturation, the length of the fatty acids, and the moiety of the head group area

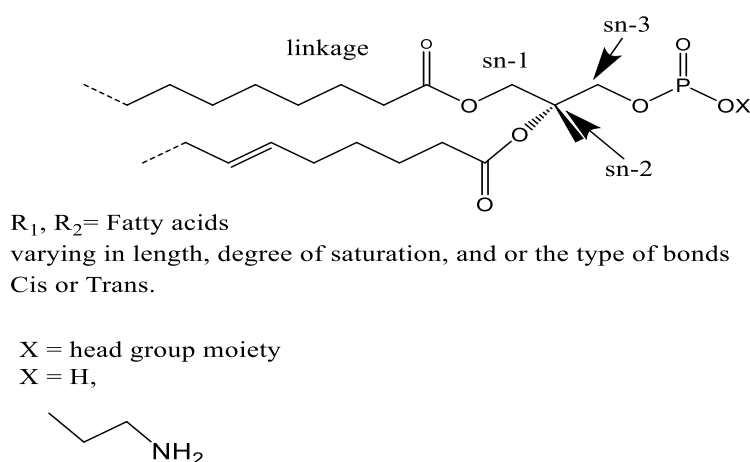


Figure 1.11 Glycerophospholipid structure and their diversity, depicted from Reference¹⁵³

1.4.2 Model membranes

Mammalian cell membranes consist of a lipid bilayer, which is composed mainly of phospholipids and cholesterol. Proteins of important cellular functions, such as, receptors, enzymes, and transporters are embedded in the lipid bilayer.¹⁵⁴ Depending on the function of the cell, the cellular membranes lipid composition may vary and different ratios of phospholipids, cholesterol, and sphingolipids become more or less abundant accordingly. Cellular membranes act as a barrier to many compounds and molecules and these membranes allow selective permeability through the interactions of certain compounds with these membranes or by the interactions of the compounds with certain receptors or transporters in order to grant them passage through cellular membranes and access to the cellular matrix. A method that can be employed to better understand the interactions between a drug and the cellular membranes, and to elucidate a mechanism of action through which a drug, or a compound can access the selective permeable membranes is the use of model membranes. Model cell membranes are systems in which their lipid organization mimics the arrangement of lipids in natural cell membranes.¹⁴⁵ A mixture of different lipids like cholesterol, dipalmitoyl phosphatidylcholine (DPPC), dioleoyl phosphatidylcholine (DOPC) and 1-palmitoyl-2-oleoylphosphatidylcholine (POPC) are used to make up model membranes that will be studied in this work. Depending on the cell type, the composition and the ratio of these lipids will vary.¹⁵⁵ Beside the cellular membrane and its importance in understanding the mechanism of how non-viral gene delivery vehicle can gain access to the cell, the endosomal membrane is of great importance as well. As mentioned earlier, lipid composition in the cellular membranes vary from one organelles or tissue to the other, and also it varies from the cellular membrane to the endoplasmic membrane. Mammalian cells maintain large differences in the sterol: phospholipid ratio in different organelles.¹⁵⁶ The main constituents of these membranes in general are the phospholipids (phosphatidylcholines), both

saturated and unsaturated.¹⁵⁷ Some of these membranes are composed of 30% cholesterol, however; the levels of cholesterol vary greatly among different cellular organelles. As reported in the literature, cholesterol comprises 30% of the lipid molecules in the plasma membrane (PM).¹⁵⁸ This level varies in the endoplasmic reticulum (ER), which is the site of cholesterol synthesis, only 1–10% of the lipid molecules are cholesterol.^{159,160} In the endocytic recycling compartment (ERC), the major intracellular sterol pool is found and cholesterol comprises up to 35% of the lipid composition within the ERC.¹⁶¹ In mammalian liver, the plasma membrane, lysosomal membranes and nuclear membrane contains cholesterol at around 19.5%, 14% and 10% of total lipids, respectively.¹⁶²

Van Meer et al. have suggested that the early and late endosomes may have a cholesterol content of lower than 30 % or ~25-30%.¹⁶³ In some of the recent Langmuir studies, a 30% composition of cholesterol was used and the rest of the lipid composition was usually 70%.¹⁶⁴ In this current study, in both of the normal model membrane and the malignant model membrane, a composition of 25% cholesterol and 75% DPPC (normal) or POPC (malignant) is used in order to mimic the endosomal membrane.

1.4.2.1 Types of model membranes

As previously mentioned, to gain insight into the mechanisms of physiological activities of biomolecules and their interactions with other molecules at the cellular membrane level, researchers can study either the natural membranes themselves, whether isolated or not, or a simplistic model membranes.^{150b} Many model membranes have emerged. Some examples of these methods are; Langmuir monolayers, liposomes and vesicles, and supported lipid membranes.

1.4.2.1.1 Langmuir monolayers

A Langmuir monolayer is formed by spreading amphiphilic molecules on a sub-phase of water or different buffer systems using a Langmuir trough. In this technique, temperature, surface pressure and sub-phase composition is controlled to mimic a biological membrane.¹⁶⁵ Surface pressure of biological cell membrane has been reported in the literature to range from 30-35 mN/m.¹⁶⁶ This range of surface pressure is readily accessible using the Langmuir method. The advantage of this technique arises from its simplicity in the preparation.¹⁶⁷ The preparation of Langmuir monolayers will be discussed in detail in section 4.2.

1.4.2.1.2 Liposomes / Lipid vesicles

Lipids usually form lamellar bilayer structures over the majority of their phase diagram.¹⁶⁸ In dilute solutions they form vesicles (liposomes). Liposomal model membrane systems have been extensively used as model membranes and these liposomes come in three types, uni-lammellar system such as; small unilammellar vesicle (SUV, 20-50 nm), large unilammellar vesicle (LUV, 50-100 nm), or giant unilammellar vesicle (GUV, 10-100 μm).¹⁴⁵

1.4.2.1.3 Supported lipid membranes

Due to the difficulty of working with lipid bilayers and membrane proteins, supported lipid bilayers are created by the self-assembly of lipids into bilayers on solid supports; usually mica, silicon, or glass.¹⁶⁹ These systems allow for an easier way to investigate biological processes at the cellular level, and provide insight and information about; ligand-receptor interactions, drugs and gene delivery via the interactions with lipid bilayer membranes,¹⁷⁰ viral attack,¹⁷¹ and cellular signaling events.¹⁷² A key finding is that the lipid molecules in supported membranes retain the lateral fluidity associated with lipid membranes in vesicles and in living cells.¹⁷³

Furthermore, living cells recognize components displayed on the surface of supported membranes; thus, if the appropriate components are present, the supported membrane can mimic cellular membranes. These lipid bilayer assemble on the supported surface by orienting the polar head groups toward the surface and the hydrophobic tails toward the other lipid. These supported cell membranes have been characterized by NMR, neutron and X-ray scattering techniques, as well as AFM.¹⁷⁴

Castano et al. synthesized a cholesterol derivative with guanidinium head groups (bis(guanidinium)-tris(2-aminoethyl)amine-cholesterol, BGTC). Guanidinium head groups are inherently positive in charge due to the presence of arginine residues, which stay positively charged over a wide range of pH due to the high pKa value¹⁷⁵. This cationic lipid's monolayer was examined with DNA in the aqueous sub-phase, and with mixture of BGTC/DOPE monolayer with DNA in the water sub-phase to investigate the interactions between these component to understand the efficient gene transfection results obtained with this cationic lipid's liposomes, both in vitro and in vivo. At a surface pressure of 20mN/m, and beyond the collapse surface pressure of >46mN/m, and at a charge ratio of BGTC:DNA of 1:5, with DNA excess, and at BGTC:DOPE molar ratio of 3:2, DNA was shown to interact with the BGTC:DOPE mixed monolayer, with BGTC interacting with DNA in the sub-phase through its polar head groups (facing the aqueous phase), and in contrast to that behaviour, DOPE acts with its polar head groups facing the air and the alkyl tail resides toward the aqueous sub-phase. When the pressure goes beyond the collapse pressure, DOPE forms a top layer, and DNA adsorbs under the BGTC monolayer, and manages to stabilize the BGTC molecules within the monolayer, which prevents it from flip-flopping like DOPE does. This behaviour is illustrated in Figures 1.12A, and 1.12B.

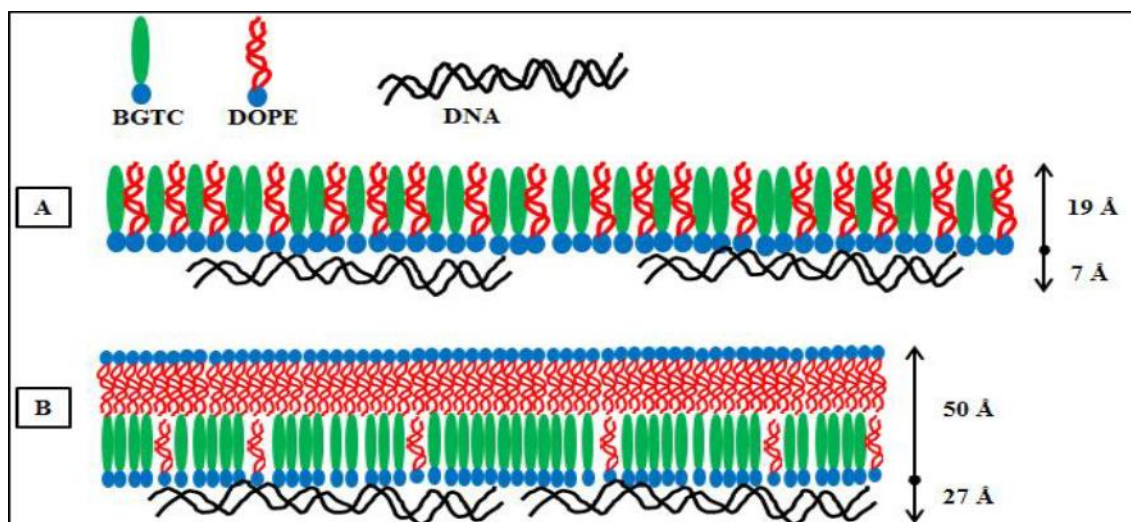


Figure 1.12 Scheme representing the interactions of DNA with BGTC and DOPE at two surface pressures. Scheme representing the interactions of DNA (~200bp) with BGTC and DOPE at two surface pressures. A) At 20mN/m, formation of an incomplete DNA monolayer at (+/-) charge ratio of low DNA with a layer thickness of 7Å below the BGTC/DOPE monolayer (thickness of ~19Å). B) Beyond the collapse pressure, DOPE forms a flip-flop layer on top of the BGTC with its head groups toward the air and its alkyl tail toward the BGTC layer with a thickness of 50Å, and the BGTC interacting with adsorbed organized layer of DNA with a thickness of 27Å.[Adapted from reference ^{175, 143}].

In another study by Matti et al., cationic gemini surfactants, 2, 3-dimethoxy-1,4- bis(*N*-hexadecyl-*N,N*-dimethyl-ammonium)-butane dibromide (SS-1) was synthesized and a monolayer of SS-1 together with 1-palmitoyl-2-oleoyl-*sn*-glycero—3-phosphate (POPC) were studied by Langmuir balance. A Langmuir monolayer study of the mixed system was conducted and surface pressure-area isotherms were measured at different X_{SS-1} concentration and the compressibility moduli (C_S^{-1}) were calculated. The mixed monolayers showed the same smooth isotherm of POPC alone, reflecting a liquid expanded phase, with no phase transition observed. However, a condensation effect was observed even at low surfactants concentration, i.e. $X_{SS-1} < 0.05$ with a reduction in the mean molecular area from 92Å^2 – 78Å^2 . In the presence of the DNA in the sub-phase, the SS-1-POPC monolayer was oriented differently; with the phosphate – ammonium (P^+/N^-) charge ratio and the lipid stoichiometry being the leading factors contributing to the changes happening in the monolayer and consequently the isotherm. As the DNA

concentration (in base-pair) increases, the monolayer was condensed from 92\AA^2 to 80\AA^2 . This condensation effect remains up to $X_{SS-1} < 0.5$, which corresponds to DNA/SS-1 charge ratio of 1.25. Expansion occurs after that due to the increased available molecules of DNA. However, as the DNA concentration exceeds that of SS-1, the condensation effect of the monolayer remain intact, irrelevant of the SS-1 concentration.¹⁷⁶ These changes in the isotherm can be observed in Figure 1.13.

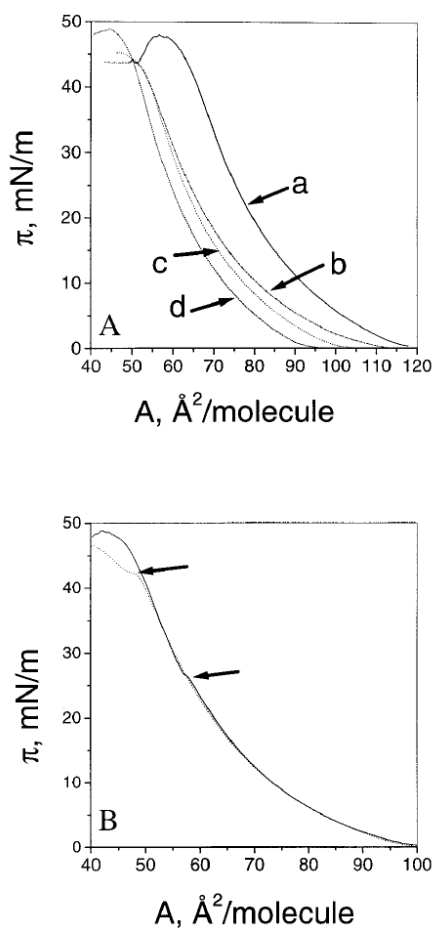


Figure 1.13 Surface pressure of POPC with SS-1 and DNA. A) Surface pressure isotherm of POPC (a), SS-1(b), and their mixed monolayers on a sub-phase of 5mM HEPES, 0.1mM EDTA, and pH=7.4., $X_{SS-1}=0.05$ (c), and $X_{SS-1}=0.13$ (d). B) Surface pressure-area isotherms of POPC/ X_{SS-1} at $X_{SS-1}=0.05$ (with straight line) and around surface pressure 27mN/m, discontinuity was observed, and DNA/ X_{SS-1} isotherm at a charge ratio of 1.25 is shown in the discontinuous line¹⁷⁶.

This literature review extensively described the synthesis of numerous novel gemini surfactants, their behavior alone and with other components of transfection, and the interaction with DNA in lipoplexes (liposomes) or polyplexes, with and without helper lipids (DOPE). This chapter also identified the different morphologies adopted by the gemini surfactants in solution and how different micelle structures can factor into the complexation, condensation of DNA, and transfection. Understanding the nature of the barriers that stand against the success of the non-viral gene delivery in transfection into an actual cell, and how to scale up from a cell into an organ or into an animal requires the employment of several techniques that can provide insight into how these lipoplexes components interact with each other. Moreover, understanding the condensation and the de-condensation of the DNA and its subsequent release from the delivery vehicle can bring into light the various factors that contribute essentially in the fundamental processes that govern transfection, and can minimize the concentration of other components, or even avoid the addition of other components that can reduce the possibility of aggregation.

This chapter also focused on understanding membrane fusion/disruption events, and how the interaction(s) between the transfection complex and the cell membrane is a critical step into gaining access to the inside of the cell. Next generation gene transfection vectors can include gemini surfactant coupled with surface modification of the liposome for targeting, additional environmentally responsive stimulus, or the formation of other “smart” vectors to deliver the DNA cargo to the nucleus. These modifications can reduce the toxicity caused by the vector or cause selective toxicity, which is favored in case of cancer cells.

Chapter 2: Hypothesis and objectives

2.1 Rational design of gemini surfactants and the focus of this research

Gemini surfactants are unique compounds that can be functionalized with different functional groups to yield diverse libraries of compounds that can be utilized for a variety of purposes. The focus of this work is to synthesize novel gemini surfactants that can serve for non-viral gene delivery systems and can improve transfection efficiency in *in vitro* studies and at the same time exert minimal or no toxicity on the biological hosts. For that new surfactants with specific functionality is required. The rational design of these surfactants can be done based on the observation of what has been reported in the literature. First, the presence of unsaturation can transform the micelles from simple structure; such as; worm-like micelles and cylindrical micelles¹⁷⁷ to more highly ordered structures; such as; inverted hexagonal structure, bilayers, and cubic micelles.¹⁰⁰ These latter morphologies have been reported to improve the transfection efficiency and many hypotheses on their mode of actions have been postulated, but little is known.

Second, the presence of bulky hydrocarbon chains also resulted in structural flexibility and the ability to induce phase transition and form more diverse structures when complexed with DNA. This has been observed in small-angle scattering technique (SAXS) in phytanyl-DNA complexes. Inverted hexagonal and cubic structures were related to the superior transfection efficiency observed in phy-3-16.¹⁷⁸ A bulky pyrenyl moiety was introduced as a hydrocarbon tail in the synthesis of asymmetrical gemini surfactants. Two of these surfactants were synthesized; pyr-3-12 and pyr-6-12, with both demonstrating peculiar thermodynamic behavior when they were complexed with the DNA. Instead of showing the complex behavior observed with symmetric gemini surfactants (12-s-12) through the demonstration of three different phases in their enthalpograms as the concentration of the DNA increases, these unique surfactants

showed only one large peak¹⁰⁹. The presence of a pyrenyl group in the structure of the gemini surfactant resulted in substantial changes in the binding interactions with DNA, disrupting and/or eliminating the flocculation observed with the 12-s-12 surfactants. This is possibly caused by strong intercalation of the pyrenyl group between DNA base pairs, that possibly forces the surfactant to adopt an orientation with the dodecyl tails oriented away from the complex, leading to a steric stabilization against flocculation.¹⁷⁹

Lipids form the majority of membranes in living organisms and depending on the lipids composition, the functions of the cellular membranes are altered. Also, certain lipids are abundant in different conditions; such as; unsaturated lipids in tumor tissues¹⁸⁰ and lipid raft domains in endocytosis.¹⁸¹ Lipid rafts (sizes ~10-200 nm) are composed of cholesterol, long-chain saturated sphingolipids and phosphatidylcholine (PC) and specific proteins. These microdomains are associated with the cell signaling, membrane trafficking, drug targeting and endocytosis.¹⁸² They also server as organizing centers for the assembly of signaling molecules It has been reported that sphingolipid/sterol assembly in lipid rafts can be modulated by glycosylphosphatidylinositol (GPI)-anchored proteins, certain transmembrane proteins, acylated cytosolic effectors, and cortical actin.¹⁸³ Lipid based formulations (lipoplexes) might influence the lipid rafts of cellular membranes, which in turn results in better endocytosis and endosomal escape of the lipoplex, which is why we are interested in model membrane to better understand the interactions of the lipoplex or the nanoparticle with these membranes.

However, the lack of understanding of how the DNA influences the arrangement of the vector components in a non-viral gene delivery vector once it is complexed; as well as how the vector components interact with biological membranes.

2.2 Hypothesis

It is hypothesized that the introduction of dissymmetry (either in the form of two alkyl tails of unequal length, or one alkyl tail and one bulky pyrene substituted tail) in the structure of gemini surfactants will improve their ability to function as transfection vectors by increasing membrane disruption.

2.3 Objectives

Short-term objectives:

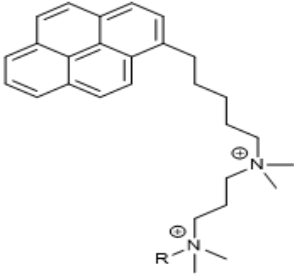
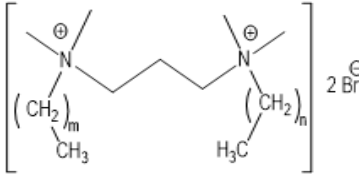
1. Synthesize and characterize the dissymmetric pyrene-based, and 12-3-n gemini surfactants, and
2. Determine their micellization properties.

Long-term objectives:

- 1) Characterize the complexes of the synthesized gemini surfactants with DNA by measuring their particle size and zeta potential.
- 2) Characterization the interaction(s) of gemini surfactant based complexes on model biological membranes:
 - a) DPPC-Cholesterol, and POPC-Cholesterol model membranes.
 - b) DPPC-Cholesterol, and POPC-Cholesterol model membranes with gemini surfactants.
 - c) DPPC-Cholesterol, and POPC-Cholesterol model membranes with Gemini surfactants, and DNA.
- 3) Determine In vitro transfection efficiencies for the pyrenyl and 12-3-n gemini surfactants in two cell lines; HEK-293, and MG-63.

The results and discussion regarding the short-term goal will be detailed in Chapter 3. Chapter 4 outlines the results and discussion about the long-term goals.

Table 2.1 Gemini surfactants synthesized and used in this study

Code name	Chemical structure
Pyrenyl-3-m	
m = 8, 12, 14, 16, and 18	
12-3-n	
n = 14, 16, and 18	

Chapter 3: Synthesis and characterization of dissymmetric Gemini surfactants

3.1 Introduction

The focus of this study is to rationally design and synthesize a novel dissymmetrical gemini surfactants and characterize them for future applications as non-viral gene delivery vehicle. The spacer linker has been shown to impact the critical micelle concentration (CMC), affect micelle structures in solution; as well as assist in the stabilization of nanoparticles or liposomes when the gemini surfactant is complexed with polyelectrolytes such as DNA.¹⁸⁴ Moreover, the spacer facilitates binding of the positively charged ammonium groups of gemini surfactants with the negatively charged phosphate backbone to help folding and compacting the DNA, to avoid its degradation by various nucleases; either in the endosome or the cytoplasm. Its effect has been studied and explored extensively and it has been shown to influence the gene transfection efficiencies.¹¹⁰ However, little work has been published that focus on the effect of the nature and the length of the alkyl tails. The length and volume of the alkyl tails impact the packing parameter which is directly linked to the morphologies displayed by the gemini surfactants in solution. These morphologies, especially inverted hexagonal/ cubic phases are linked to efficient transfection vectors⁷¹. For that, eight different dissymmetric gemini surfactants were synthesized and characterized, each of which can be categorized into two groups as indicated below:

Surfactant categories	Members
m-s-n (m-3-n)	Pyrene-3-8, pyrene-3-12, pyrene-3-14, pyrene-3-16 & pyrene-3-18 12-3-14, 12-3-16 , 12-3-18

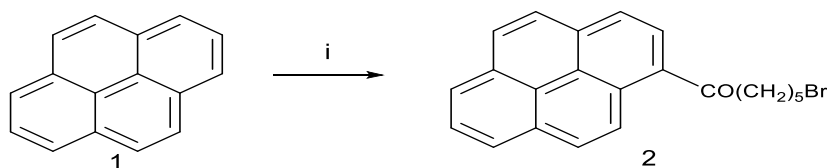
Pyrene has been widely used as a labelling molecule because of its nature as a chromophore. Pyrene absorbs and emits strongly due to its high molar absorbance coefficient in the near UV region.¹⁸⁵ The pyrene monomer fluorescence is characterized by several sharp peaks at wavelengths between 370 and 420 nm. The presence of sharp peaks in the fluorescence emission spectrum indicates the presence of discrete vibration levels in the pyrene monomer ground-state. In addition to the fluorescence of the pyrene monomer in the blue wavelength region, an excited pyrene has the ability to complex with a ground-state pyrene to form an excimer. The excimer fluoresces in the blue to green wavelength region with a broad structure less emission spectra centered at 460 to 480nm.¹⁸⁶ A relative indicator of the degree of association of the pyrene labels of macromolecules can be obtained by measuring the ratio of the fluorescence intensities of the excimer I_E , integrated from 500 to 530 nm, to the monomer I_M , integrated from 372 to 378 nm.¹⁸⁷ Due to these characteristic peaks, pyrene has been widely used to characterize micelles in solutions and a means to determine the CMC through the relative intensities in its fluorescence spectrum. Also, it is used to determine the polarity of microenvironments, such as; micelles¹⁸⁸. Due to the low solubility of pyrene in pure water, the efficiency of excimer formation is low at surfactant concentrations below the CMC. However, with concentrations higher than the CMC, pyrene molecules will be crowded into the micelles, which will give higher excimer peak formation.¹⁸⁹ In this current study, pyrenyl derivative (hexyl pyrene) is in the structure of the asymmetrical gemini surfactants. Its hydrophobicity and its ability to intercalate between the DNA strands will be integrated into a gemini surfactants micellization system in order to focus on the unique properties of these surfactants and the effect of the pyrene on these properties.

3.2 Methods and Materials

The synthesis of the gemini surfactants that were utilized in this project took place in our laboratory following the method of Wang et al. .¹⁹⁰

3.2.1.1 Synthesis of 5-bromohexane-1-pyrenyl ketone

5-Bromohexyl-1-pyrenyl ketone was the first intermediate in the functionalization step of pyrene to synthesize 6-(1-pyrenebromohexane), which represents the first tail. The synthesis pathway is in scheme 3.1. The first step was to dissolve pyrene (Aldrich, 10.0 g, 49.4mmol) and AlCl₃ (Aldrich, 8g, 60mmol) in 80 mL of CH₂Cl₂ that had been cooled to -78°C. Then, another 80 mL of CH₂Cl₂ that contained 6-bromohexanoyl chloride (Aldrich, 97%, 3.7mL, 24.7mmol) was added dropwise to the mixture, allowing the reaction to continue for 3h at -78°C. The reaction was quenched with 1M HCl, and then neutralized using a saturated aqueous NaCl solution, to separate the organic layer and let it dry with Na₂SO₄, overnight. Excess solvent was removed via rotary evaporation to yield a yellow paste that was further purified by soxhlet extraction (pentane 100%) to produce a yield of 11g with purity of 86-90%. ¹H NMR data is given in Appendix A.

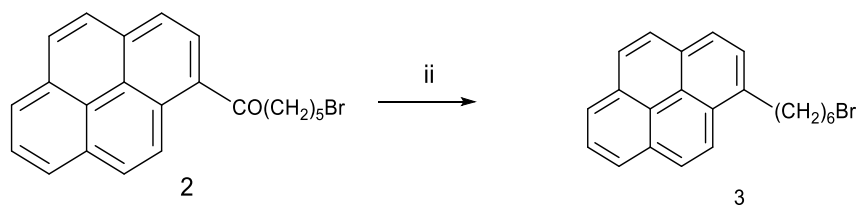


Scheme 3. 1 Synthesis of 5-bromohexane-1-pyrene ketone .i: AlCl₃, CH₂Cl₂, 6-bromohexanoyl chloride, the reaction was run at -78°C for 3h.

3.2.1.2 Synthesis of 6-(1-pyrenylbromohexane)¹⁹¹

Trifluoroacetic acid (15ml) and 2.3g of 5-bromohexyl-1-pyrenyl ketone (6mmol) were dissolved in 65 mL of CH₂Cl₂ and cooled to 0°C. 2.7 mL of triethylsilane (Aldrich, 99%) was added,

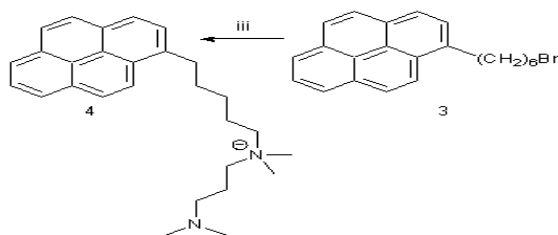
dropwise to the mixture and stirred for three days under an argon (Ar) atmosphere at room temperature. Then, the reaction was neutralized with saturated aqueous NaHCO₃ (Sigma), and the oil layer was separated and dried over Na₂SO₄ overnight (Scheme 3.2.). The crude oil was further purified using soxhlet extraction with pentane to give yield of 92-100%. ¹H NMR data is given in Appendix A.



Scheme 3.2. Synthesis of 6-(1-pyrenyl)hexyl bromide ii. TFA, triethylsilane, with CH₂Cl₂ under Argon for 3 days at room temperature

3.2.1.3 Synthesis of *pyr-3(N-(3-dimethylaminopropyl)-N, N-dimethyl-6-(pyren-6-yl)-hexan-1-ammonium bromide)*

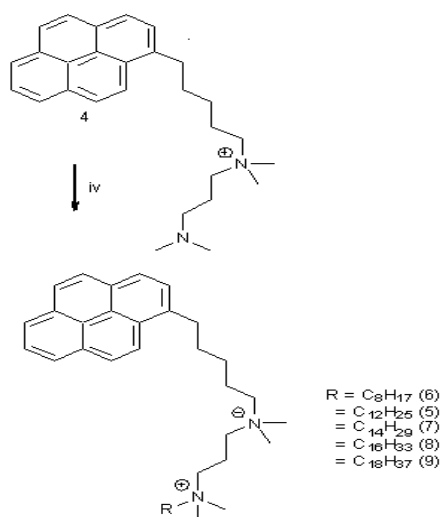
6-(1-Pyrenyl)bromohexane (1.58 g, 4.33 mmol) and *N,N,N',N'*-tetramethylpropane diamine (Aldrich, 99%, 0.92 mL, 5.5 mmol) were added to 40 mL of anhydrous acetonitrile. The mixture was stirred at 45°C for three days (Scheme 3.3). The solvent was reduced to ~10 mL using a rotary evaporation, leaving a light yellowish precipitate. This crude product was further recrystallized from hot acetonitrile and diethyl ether to yield an off-white solid with a yield of 100%. ¹H NMR data is given in Appendix 3.1A.



Scheme 3.3 Synthesis of pyr-3. iii. *N,N,N',N'*- tetramethylpropanediamine with CH₃CN reflux for 3 days at 45°C in CH₃CN

3.2.1.4 Synthesis of *pyr-3-m* (m = 8, 12, 14, 16 & 18)

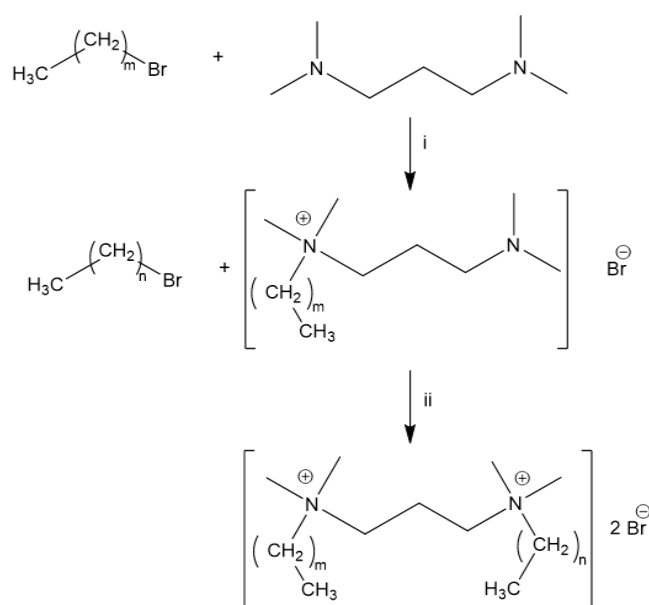
Pyr-3(2.0 g, 4 mmol) and 1-bromododecane (2.7 mL, 9.0 mmol) or 1-bromotetradecane (3.32 mL, 4 mmol), or 1-bromohexadecane (1.22 mL, 4 mmol), or 1-bromooctane (0.69 mL, 4 mmol) were added to 40 mL of anhydrous acetonitrile (Scheme 3.4). The mixture was stirred at 45°C for two days. The solvent was removed using rotary evaporation. The product was recrystallized from a mixture of acetone and ethyl acetate and dried overnight with a yield of 46-60%. ¹H NMR data is given in Appendix A.



Scheme 3.4 Synthesis of *pyr-3-n*. iv. 1-bromooctane, 1-bromododecane, 1-bromotetradecane, 1-bromohexadecane, and 1-bromooctadecane with CH₃CN reflux for 2 days at 45°C

3.1.2 Synthesis of m-3-n surfactants

Synthesis of the dissymmetric gemini surfactants with the general formula of m-3-n, where $m \neq n$, $m = 12$ and $n = 14, 16$, and 18 followed the general scheme described by Menger and Littau.¹⁹² All of the gemini surfactants were synthesized by reflux of 1-bromododecane (Sigma Aldrich, Canada) with one molar equivalent of *N,N,N',N'*-tetramethylpropane diamine (Aldrich, Canada) in HPLC grade of acetonitrile for 24 h. The reaction was then stopped, cooled down in ice bath before applying filtration. Recrystallization in hot acetonitrile was applied. The purity of the intermediate is then tested by ¹H NMR before the reaction was allowed to continue by refluxing it with either 1-bromotetradecane, 1-bromohexadecane, or 1-bromooctadecane (Sigma Aldrich, Canada) in acetonitrile for another 24 h. Then, filtration of the cooled product was done for the final product, which was further dried in the vacuum oven before it was recrystallized from a mixture of acetonitrile and ethyl acetate. The purity of the final gemini surfactants was confirmed with ¹H NMR. A representative scheme of the synthesis is given below (Scheme 3.5) and ¹H NMR data can be found in Appendix A.



Scheme 3.5 General scheme for the synthesis of 12-3-n, where n =1-bromotetradecane, 1-bromohexadecane, and 1-bromooctadecane

3.1.3 Determination of the Krafft temperatures

Cationic gemini surfactants` solubility increases when subjecting the solutions to increasing temperature. At a certain temperature value for each specific surfactant, there is a characteristic sharp increase in the solubility and this is referred to as the Krafft temperature (T_K). We can determine this temperature by means of specific conductivity as reported in the literature.¹⁹³

To measure the Krafft temperature, a clear-saturated aqueous solution of the surfactants should be prepared (the concentrations of the solutions are 5 times more than the known or speculated critical micelle concentration (CMC)). Then, the solutions are refrigerated overnight until precipitation is observed. The solution is then placed in a temperature-controlled vessel that is connected to a circulating water bath Model RE304 (Lauda, Germany). The initial temperature was set at $10.00^\circ\text{C} \pm 0.01$ and it was incrementally increased. The conductivity solution was measured as a function of temperature using a SevenEasyTMS30 conductivity meter (Mettler Toledo, Switzerland) and double-walled glass titration cell (Fisher Scientific, USA), with a cell constant of 0.475 cm^{-1} . Two break points are observed in the temperature-conductivity plot; one representing the Krafft temperature (T_K) and the other break point representing what might be a transition point.

3.1.4 Surface tension measurement

Surface tension was measured using a TE3 automated tensiometer (Lauda, Germany), applying the Du Nuoy ring method and all of the surfactants surface tension values were corrected using the method of Harkins and Jordan.¹⁹⁴ The surface tension was measured after each titration of a surfactant solution in Milli-Q water to a 40 mL of Milli-Q water at 25°C . Triplicate readings were taken automatically in each experiment and each experiment is run twice. The critical micelle concentration is determined from the plot of the surface tension and the logarithm

concentration of the surfactants¹⁹⁴. Surface tensions were measured until the variability between measurements was less than 0.1mN/m.

3.1.5 Specific conductivity

The specific conductivities were measured using a SevenEasyTMS30 conductivity meter (Mettler Toledo, Switzerland) and double-walled glass titration cell (Fisher Scientific, USA), with a cell constant of 0.475cm⁻¹ at 25C°. Temperatures were controlled using RE304 circulating water bath purchased from Lauda (Germany). Specific conductivities were measured after each addition of a concentrated solution of the gemini surfactant to a 30 mL of pure water after calibrating the meter using KCl solution (at 1413µS.cm⁻¹).¹⁹⁵ The CMC is determined at three different temperatures (25°C, 30°C, and 35°C). The CMC values can be determined from the abscissa of the inter-section of the trend lines connecting the experimental points before and after the CMC (hypothesized) in a surface tension vs. log concentration plot or fit from the conductivity points according to Carpena et using this equation (1)¹⁹⁶:

$$K = \kappa_0 + A_1 c + d(A_2 - A_1) \frac{\ln(1 + e^{(c - c_{mc})/d})}{(1 - e^{-(c - c_{mc})/d})}$$

The degree of micelle ionization (α) is calculated by the ration of the slopes of the two areas in the graph.

3.1.6 Fluorescence studies

Fluorescence emission spectra of pyrenyl gemini surfactants in aqueous solutions and pyrene in methanol have been recorded using Spectra max M5 microplate reader (molecular devices, USA) at excitation wavelength 363nm after scanning the excitation spectrum of pyrene in methanol. These samples were measured in transparent disposable cuvettes (ZEN0118) (Malvern instruments, UK). The excitation and emission slit-widths were set at 1 nm. An average of 40–50 scans was recorded.

3.1.7 Docking studies

Molecular docking studies for pyrene based surfactants were performed to give additional information on how pyrenyl surfactants interact with each other (either via self and/or intermolecular aggregation) when present in the aqueous phase. This study was conducted through a collaboration study with Dr. Praveen Nekkar Rao's lab. Discovery studio (DS) Structure-based-design software (version 4.5, BIOVIA/Accelrys, San Diego, USA) was used for the docking studies. Briefly, 3D models of the pyrene based surfactants surrounded with water molecules were designed using the Build fragment tool. Energy minimization was performed using the steepest descent and conjugate gradient minimizations for 1000 interactions. The distance dependent dielectric model was used as the implicit solvent model for the energy minimization step. The CDOCKER algorithm was used to dock a surfactant monomer with another monomer after defining a 25Å sphere radius around the surfactant molecule. The CHARMM force field was used for the docking studies using 25 top hits and random conformations and full potential as true value. The most stable interaction conformation between the pyrene based surfactants was evaluated based on CDOCKER energy and CDOCKER interaction energy in Kcal/mol. The type of interaction occurring between the self- aggregating pyrene surfactants (i.e. self or intermolecular) were also visualized using the docked molecules.

3.2 Results and Discussion

3.2.1 Krafft temperature

Below the Krafft temperature (T_K), the solution was not homogenous. Once the Krafft temperature is hit, micelle formation begins and the solubility is increased. This sharp increase in solubility represents the Krafft temperature, which is the temperature when the CMC is reached and aggregates formation becomes spontaneous. This sharp increase in temperature is signaled also by rapid increase in conductivity. Several factors affect the Krafft temperature's

increase in surfactants; such as, in the presence of unsaturation, branching and substitution of either the alkyl tails, or the counter ions, or the head groups.¹⁹⁷ All of the pyrenyl gemini surfactants showed precipitation after 24-48h of refrigeration and after that, the solutions were left at room temperature to thaw in order to run the experiments. Pyr-3-8 T_K was $<20^\circ\text{C}$ and as the alkyl tail of the pyr-GSs increases from octyl to octadecyl the Krafft temperature increase, and this shows a linear correlation. The 12-3-n gemini surfactants behaved in the same manner of the pyrenyl surfactants, but with a less significant increase between 12-3-14 and 12-3-16 and significant increase for 12-3-18. T_K of 12-3-14 = 33°C , 12-3-16 = 35°C , and T_K of 12-3-18 = 60°C . However, at higher temperatures there was a second break point and we believe it indicates a phase transition and the beginning of the formation of higher and more complicated morphologies. This break point was witnessed in both of the pyrene-3-m surfactants and the 12-3-n surfactants. The values of Krafft temperatures and the transition temperatures of the eight surfactants were obtained from the plots of the temperature-specific conductance and are presented in Figure 3. 1 and Figure 3.2.

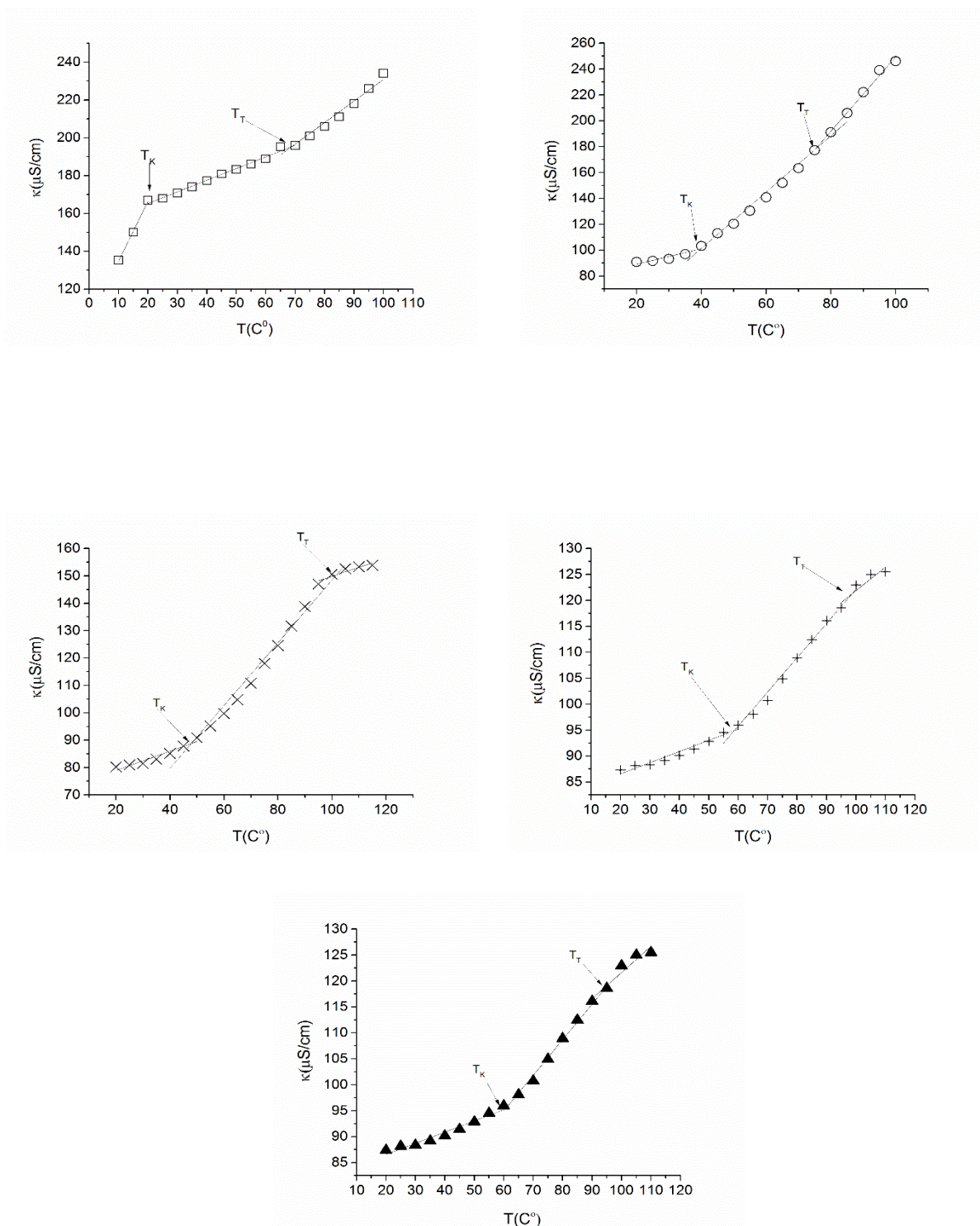


Figure 3.1 Krafft temperatures and transition temperatures of pyrenyl gemini surfactants of pyr-3-8 (\square), pyr-3-12 (\circ), pyr-3-14 (\times), pyr-3-16($+$), pyr-3-18 (\blacktriangle), The arrows indicate both T_K and T_T , respectively.

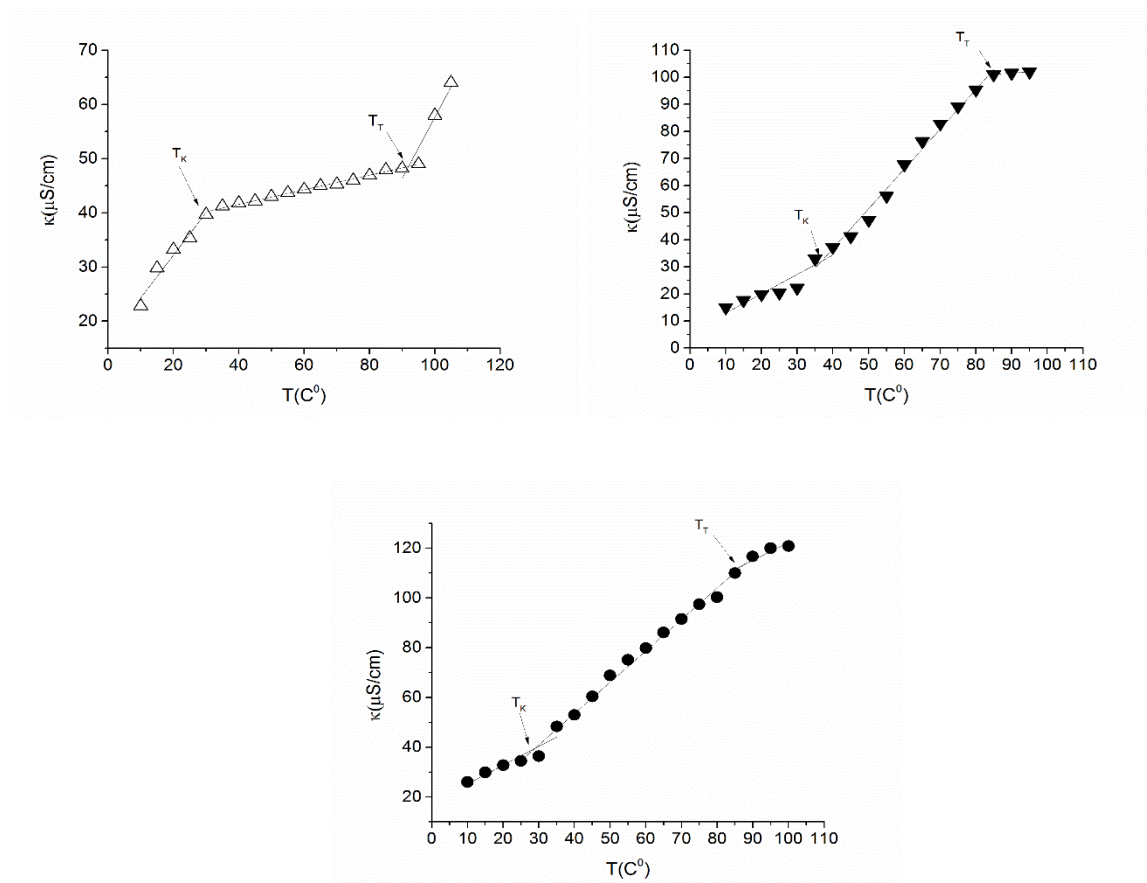


Figure 3.2 Krafft temperatures and Krafft temperatures of 12-3-14 (Δ), 12-3-16 (\blacktriangledown), 12-3-18 (\bullet)

The results of the Krafft temperatures in both of the groups followed the trend that was observed for symmetrical gemini surfactants of m-3-m category, where m=12, 16, and 18. The longer the alkyl tail, the higher the hydrophobicity and the higher the Krafft temperature.¹⁰⁰ The same observation was noticed in a previous study on phytanyl dissymmetric gemini surfactants conducted by Wang and Wettig in 2011.¹⁰⁵ Below the T_K , the increase in both the temperature and the conductivity was slow for all the dissymmetric surfactants, however, once the T_K is reached and its onset represents the beginning of micellization, a rapid incline in both of the temperatures and the conductivity can be noticed. The Krafft temperatures of all of the synthesized surfactants are summarized in Table 3.1.

Table 3.1. Krafft temperatures (T_K) and the transition temperatures (T_T) of the dissymmetric gemmini surfactants

Gemini surfactant	T_K	T_T
Pyr-3-8	<20	72
Pyr-3-12	42	75
Pyr-3-14	45	90
Pyr-3-16	60	95
Pyr-3-18	<60	<95
12-3-14	33	85
12-3-16	35	85
12-3-18	60	90
12-3-12	-	12.7
14-3-14	-	RT

3.2.2 Surface tension analysis and favored interactions

Plots of surface tension as a function of the logarithm concentration of the pyrenyl gemini surfactants in aqueous solutions are shown in Figure. 3.3 and Table 3.2 with the CMC gradually decreasing with the increase in the alkyl tail length from octyl to octadecyl. In a plot of surface tension as a function of the logarithm of surfactant concentration, the CMC can be determined from the intersection of two lines, which represents the area below and above the CMC. The first line shows a linear decline, and the other one represents the plateau area (minimal surface tension). In a logarithmic plot of the CMC as a function of the hydrocarbon tail, shown in Fig.3.4 the symmetrical m-3-m gemini surfactants show a linear pattern with the exception of (18-3-18) .^{105, 198} When the CMCs of the pyrenyl surfactants are plotted in this manner, they show a slight decrease from pyr-3-12 (0.21mM) to pyr-3-14 (0.15mM) then pyr-3-16 (0.113m M), followed by a greater decrease between pyr-3-16 and pyr-3-18 (0.024mM). Most of the pyrenyl gemini

surfactants show a clear break point at the CMC. However, that of pyr-3-18 was poorly defined, suggesting the presence of pre-micellar aggregation and this kind of behavior was reported before in gemini surfactants with longer alkyl tails, $m < 18$, in 12-s-12; where $s = 12, 14$, and 16 .⁹⁸ The same behavior was reported in dissymmetric gemini surfactants with bulky unsaturated tails, such as, phytanyl-3-16.¹⁰⁵ As seen in Fig. 3.4, the CMC of 12-3-14 was dramatically smaller than that of 12-3-12 (0.32mM versus 0.98mM, respectively).⁹⁶ The CMC values decrease gradually for both of 12-3-16 (0.22mM), and 12-3-18 (0.17mM). Although the CMC of these gemini surfactants are dramatically lower than their symmetrical counterparts, the onset of micellization required higher concentrations for it to occur, especially for 12-3-14 and this can be noticed in the surface tension results (γ_{cmc} for 12-3-14 = 26.22mN/m, 12-3-16 = 32.21mN/m, and 12-3-18 = 40.24mN/m). The longer the tail, the higher the hydrophobicity and the easier for surfactant monomers to aggregate. For the pyrene-based surfactants, the onset of micellization occurred earlier than the corresponding m-3-m surfactants. This may be caused by the presence of pyrene ring within the surfactants, which adds to the hydrophobicity of the gemini surfactant through the pyrene stacking, leading to enhanced hydrophobic interactions. The contribution of additional methylene unit to the CMC value in both groups of surfactants was more like that of a single-tail surfactant.¹⁹⁹ This may be attributed to the increased intermolecular hydrophobic interactions between tails of same length between the monomers within the micelles. Similar to the symmetric gemini surfactants, γ_{cmc} decreases with the increase in the gemini surfactant's concentration, which indicates the formation of a monolayer at the air/water interface, thus reduces the surface tension of water. In pyrenyl surfactants, γ_{cmc} values are relatively higher than the corresponding m-3-m as well as those of m-3-n surfactants, suggesting an earlier onset of micellization (with the exception of pyr-3-8). Pyrene-3-8 has a short tail, rendering the surfactant more hydrophilic and increasing its solubility in water, favoring the bulk over the surface. The low value for γ_{cmc} (27.61mN/m) is consistent with this interpretation.

Table 3.2 Critical micelle concentration (CMC), head group area (a_o), packing parameter (P), and surface excess concentrations (Γ_i) of Pyrene-based and 12-3-n surfactants

Surfactant	CMC (mM) ^a	γ (mN/m)	Γ_i (mol/nm ²)*10 ⁻⁶	a_o (nm ² /mol)	P
Pyrene-3-8	0.178 ±0.02	27.6	9.47x10 ⁻⁷	0.35	<1
Pyrene-3-12	0.21±0.02	43.14	2.97	0.56	1
Pyrene-3-14	0.15±0.03	41.2	1.47	1.13	0.46
Pyrene-3-16	0.14±0.03	43.58	3.16	0.526	0.91
Pyrene-3-18	0.024±0.07	40	2.38	0.7	0.65
12-3-14	0.32±0.014	26.22	5.74	0.3	<1
12-3-16	0.22±0.014	32.21	8.07	0.21	<1
12-3-18	0.17±0.02	40.24	8.68	0.19	<1
12-3-12	0.98±0.04			1.11	0.38

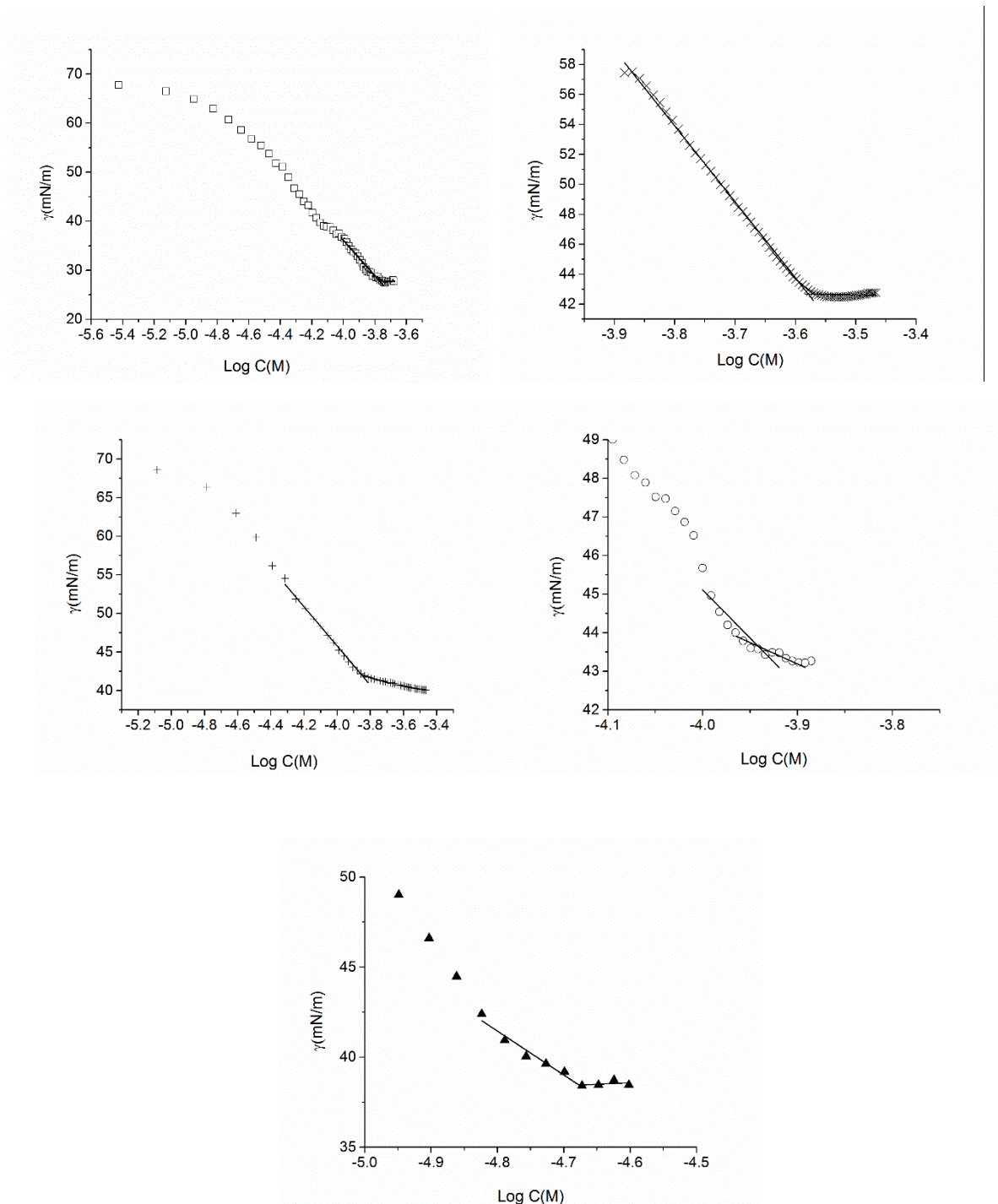


Figure 3.3 Surface tension of pyrene-based gemini surfactants of pyr-3-8 (■), pyr-3-12(x), pyr-3-14 (+), pyr-3-16(○), and pyr-3-18 (▲). Linear fits are indicated by lines and CMC values are calculated from the intersection of these two lines. Plots values are in Appendix A

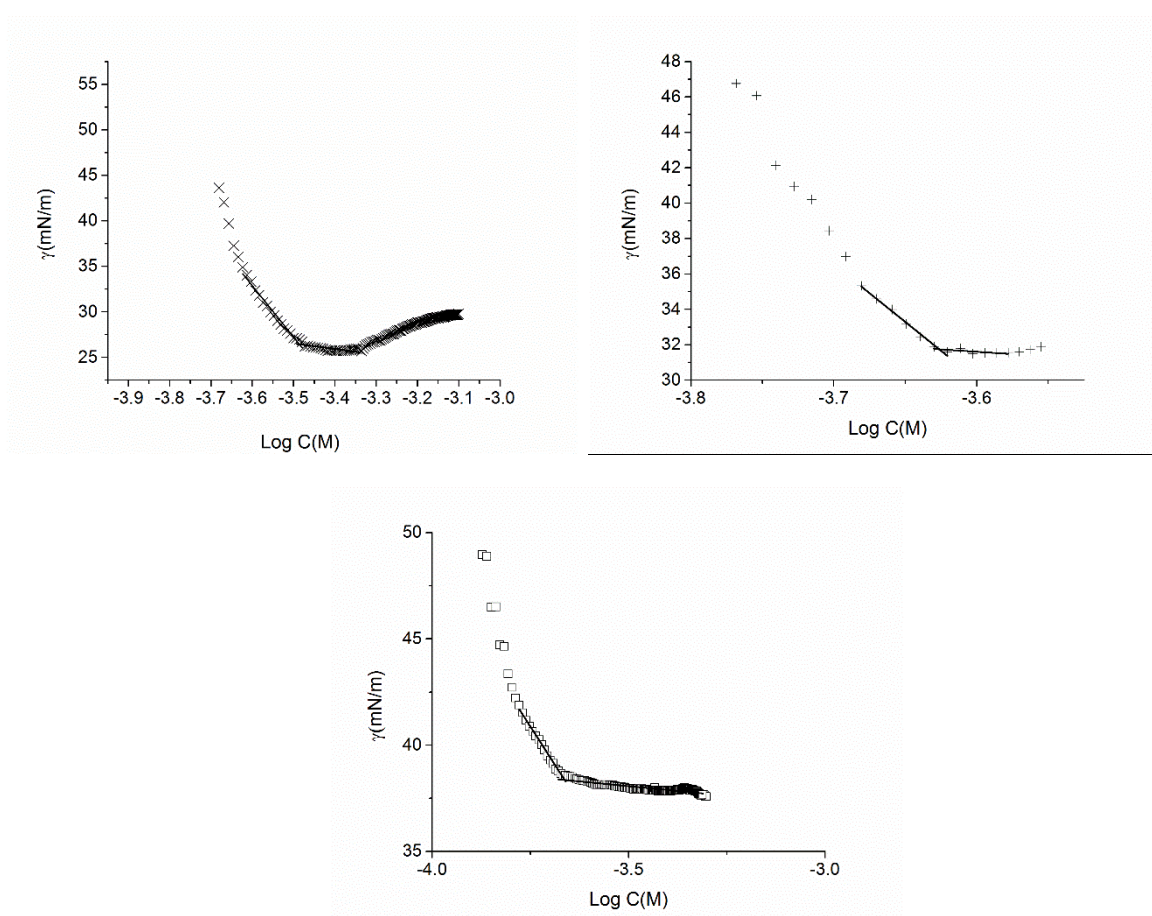


Figure 3.4 Surface tension plots of asymmetric gemini surfactants; 12-3-14 (x), 12-3-16(+), and 12-3-18(□). Linear fits are indicated by lines and CMC values are calculated from the intersections. Plots values are in Appendix A

A plot of the logarithm of the CMC as a function of hydrocarbon tail length for the pyrenyl and the 12-3-n surfactants are plotted in Figures.3.3 and 3.4. The symmetrical gemini surfactants showed linear decrease with the increase in the alkyl tail length with the exception of 18-3-18, which skewed from the linear behavior.¹⁰⁵ Pyrene based surfactants followed the linear trend with barely observed decrease from pyr-3-14 to pyr-3-16, followed by larger decrease for pyr-3-18. However, pyr-3-12 did not follow the same decreasing trend. 12-3-n surfactants followed the same behavior observed in the pyrenyl surfactants.

Pyrene has been widely used as a fluorescent probe to characterize micro-heterogeneous systems, such as; micelles.²⁰⁰ This is largely due to the significant sensitivity to the polarity of the solvent

being used. Based on that, pyrene shows characteristic vibronic bands around 370-420nm in its fluorescence spectrum. The absolute and relative intensity, width and position of this band depends highly on the polarity of the microenvironment.²⁰¹ Due to the low solubility of pyrene in pure water, the efficiency of excimer formation is low at surfactant concentrations below the CMC. However, with concentrations higher than the CMC, pyrene molecules will be crowded into the micelles, which will give higher excimer peak formation.²⁰² This is not the case when pyrene is existing within the structure of the surfactants. The excimer may be formed in all the concentrations whether below or above the CMC and this is due to the high abundance of pyrene molecules. However, with concentrations below the CMC, formation of pre-micellar aggregates may trigger the appearance of excimer signal. Pineiro et al. showed that pyrene molecules interact with the surfactant molecules far below the CMC, which confirms our results.²⁰³ The emission spectra of all of the pyrenyl surfactants in water showed more or less the same pattern of the pyrene spectrum in methanol with the monomer fluorescence maximum at 390 nm and the spectra are well resolved and different from the red-shifted broad peak in the fluorescence band at 460 nm for pyrene and pyr-3-8 spectra which indicates the formation of the excimer. However, the peak shifted more toward the red for the rest of the pyrenyl surfactants. This small red shift is most likely the effect of increased hydrophobicity of the medium and this is caused by the formation of the micelles and with the increase in the alkyl tail length, the onset of micellization occurs earlier, which contributes to the hydrophobicity. As mentioned earlier, post and below the CMC concentrations of these gemini showed the presence of the excimer formation at around 480-490nm with weaker intensity. This reflects the abundance of the pyrene surfactants within the hydrophilic region before the micellization and in the hydrophobic micelles after the CMC. However, the presence of the dimer peak around 480 nm, indicates the formation of the excimer. Also, this is an evidence of the formation of pre-micellar aggregates that might be caused by the pi-pi stacking, highlighting the importance of these weak interactions

between surfactants in solution. However, pyrene-3-12 with concentration lower than the CMC showed very little evidence of dimer formation in its fluorescence spectrum. This can be attributed to the length of the hexyl pyrenyl tail which is equal to 11-11.5 bonds and this makes pyr-3-12 acts as symmetrical gemini surfactants below the CMC, thus minimize the effect of the intermolecular hydrophobic interactions, limiting the pi-pi stacking and enhancing the interactions with the dodecyl tail (Figure 3.5). Pyrene stacking in pyrene-based gemini surfactants can be seen in Figure 3.6.

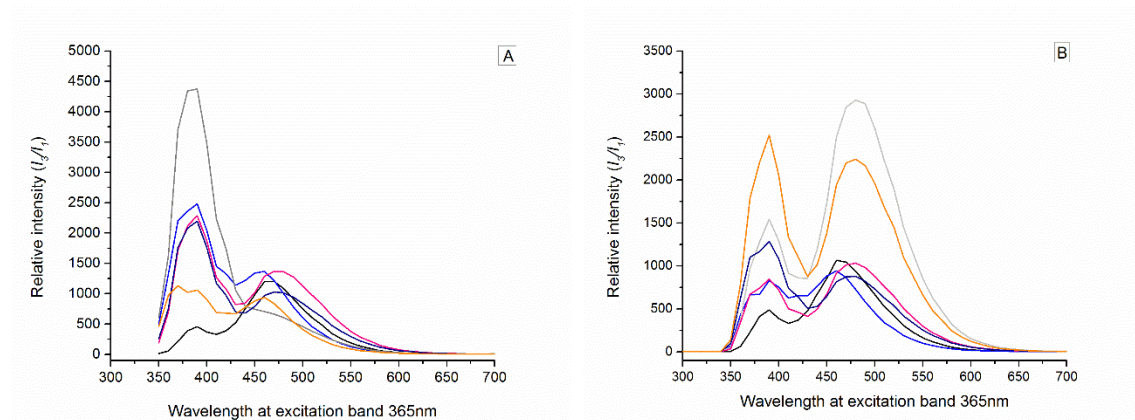


Figure 3.5 Fluorescence spectra of pyrenyl gemini surfactants: a) before the CMC, b) After the CMC (pyrene black, pyr-3-8 blue, pyr-3-12 grey, pyr-3-14 pink, pyr-3-16 navy, and pyr-3-18 orange). The intensity of the excimer peak in pre-CMC solution is lower than the intensity of the peak after the CMC, which indicates the presence of the pyrene within the hydrophobic micelles. Relative intensity has been used to determine the CMC values based on the excited state and the ground state of the pyrene molecules.

To further explore the nature of the interaction(s) between the tail groups of the py-3-n surfactants, docking simulations were carried out in a collaboration project with Dr. Praveen Nekkar Rao and his Msc. Student, Sarabjeet Singh. The docked poses obtained were ranked based on CDOCKER energy and CDOCKER interaction energies in Kcal mol⁻¹ and the type of polar and nonpolar interactions observed between adjacent surfactants were analyzed. The results of the studies indicate that pi-pi stacking interactions between pyrene rings on adjacent

py-3-8 surfactant molecules was the most favored type interaction occurring between the molecules (Figure 3.6A). It was also observed that pi-pi cation and pi-sigma stacking interactions occurred (Figure 3.6B) and these interactions gave the most stable biomolecular complex. Similar results were obtained for each of the py-3-n surfactants, although the tendency for self-aggregation within a single surfactant molecule increases as the alkyl chain length increases as can be seen in the case of Py-3-18, where cation-pi and pi-sigma interactions were observed in Figure 3.7.

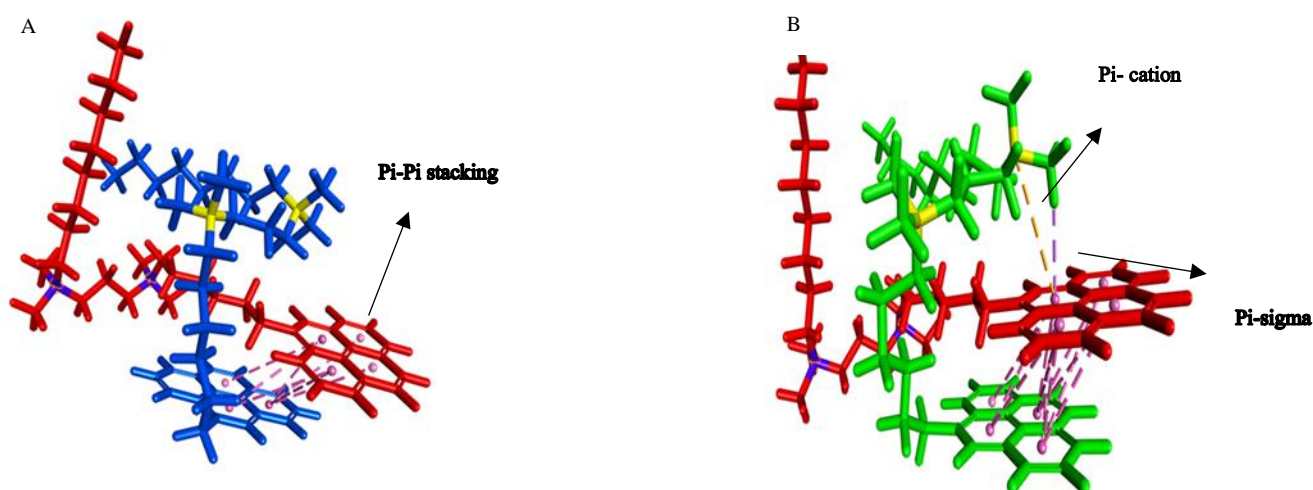


Figure 3.6 Docking studies of interactions between two pyr-3-8 monomers. A) Pi-Pi interactions between two pyrene rings in tow monomers of pyr-3-8 surfactants. B) Pi-cation (yellow line) and Pi-sigma (purple) are other means of interactions

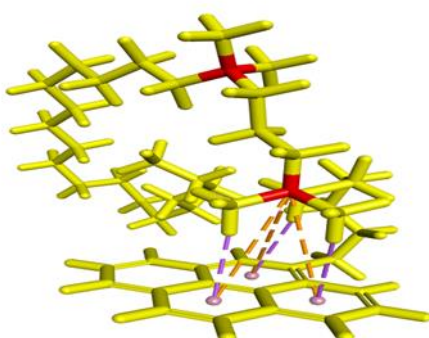


Figure 3.7 Self-aggregation behavior of Pyr-3-18 in the presence of water

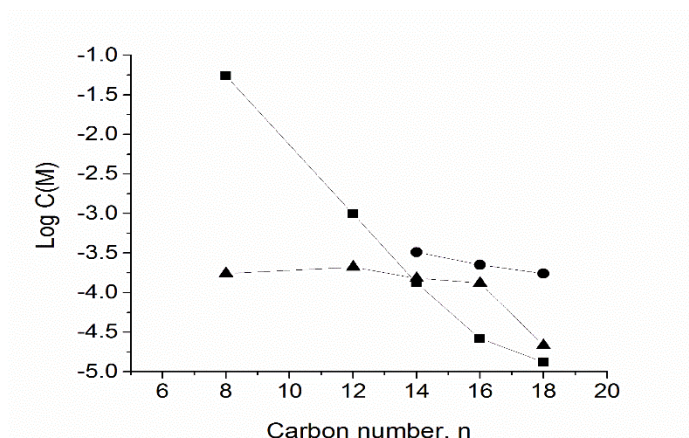


Figure 3.8 Variation of the logarithmic CMC as a function of alkyl tail length (determined by tensiometry), m3-m. (■), pyr-3-n (▲), 12-3-n (●)

The minimum head group areas for the pyrenyl surfactants are also reported in Table. 3.2. The head group area can be calculated from the surface excess concentration according to equation 2 below:

$$a_o = (N_A \Gamma)^{-1} \quad (3.2)$$

N_A is Avogadro number 6.022×10^{23} , and Γ_i is the surface excess concentration calculated from the Gibb's adsorption equation:

$$\Gamma_i = (-1)/2.303nRT (d\gamma/d\log C)_T \quad (3.3)$$

In equation (3), R is the gas constant, T is the absolute temperature in Kelvin, γ is the surface tension in mN.m^{-1} , $(d\gamma/d\log C)$ is the slope of the linear part of the γ -logC plot and n is 3 for gemini surfactants, accounting for one dimeric ion and two monomeric counter ions. The head group areas (a_o) for the pyrenyl gemini surfactants are all smaller than that of their symmetrical counterparts.¹⁹⁰ Increased asymmetry, enhances the hydrophobic intermolecular interactions, leading to lower CMC values and higher aggregation ability.¹⁹⁰ Also, with longer hydrocarbon

tails, a_o values decrease due to higher packing density at the air/water interface in comparison to their symmetrical counterparts. For pyr-3-18, although a_o is higher than the previous surfactant pyr-3-16, it is still lower than that of its symmetrical counterpart 18-3-18¹⁹⁸, similarly, the a_o of pyr-3-14 is lower than that of 14-3-14.²⁰⁴ The non-existence of a trend to follow in the minimum head group area for the pyrene based surfactants with the increase in the alkyl tail stems from the presence of the pyrene rings in one of the alkyl tail, which hinders and limits the interaction with the other alkyl tail, depending on its length. These results contradict the reported data that indicates that a higher degree of asymmetry results in stronger interactions, leading to smaller head group areas, especially with small spacer as in our case; $s = 3$. The variations in head group areas of m-3-n surfactants, result from the packing of the hydrophobic tails at the air/water interface. The a_o values decreased for the dissymmetric gemini surfactants in our studies, whether for pyr-3-n or for m-3-n surfactants compared to their symmetrical counterparts (m-3-m), which suggests the higher packing at the air/water interface due to greater dissymmetry of the tails. A trend was established for 12-3-n surfactants.

For 12-3-14, 12-3-16, and 12-3-18, a_o values are smaller than the a_o values of their symmetrical counterpart. As the hydrophobicity of the 12-3-n surfactants increase, the CMC values decrease, and the surfactants monomers favors adsorption at the air/water interface. This leads to higher degree of intermolecular interactions between the alkyl tails, resulting in smaller mean molecular area. However, the discrepancy found in the pyrenyl gemini surfactants was reported in other surfactants, such: phytanyl-3-m by Wang et al.¹⁰⁵ The head group areas for both of phy-3-12, and phy-2-16 surfactants were smaller than those of 12-3-12, and 16-3-16 surfactants, respectively.^{105, 178} However, phy-3-18 was approximately 1.5 times that of 18-3-18.¹⁴¹ The same trend of increasing a_o despite the increase in the asymmetry was reported by Wang et al. when they tested the effect of dissymmetry of gemini surfactants in a non-aqueous solution; protic ionic liquid (EAN). For m-2-n surfactants, 16-2-8 minimum head group area was 67.6 \AA^2

and 14-2-10 was 80.5 Å², respectively. Both of these surfactants a_o values are lower than their symmetrical counterpart 12-2-12¹⁹⁹.

Table 3.3 Values of symmetric and dissymmetric gemini surfactants head group areas (a_o) as reported in the literature

Gemini surfactant	Head group area (a _o) (nm ² /mol)
14-3-14	1.35
18-3-18	1.28
12-2-12	1.2
Phy-3-12	0.78
Phy-2-16	0.91
Phy-3-18	1.92
16-2-8	0.67
14-2-10	0.81

The shape of the micelles formed in solution plays a key role in determining the properties of gemini surfactants and how these GSs can be utilized in different industries. The packing parameter "P" of a surfactant describes the shape of the aggregates formed by a surfactant in aqueous solution, and can be calculated from:

$$P=v/a_o l \quad (3.4)$$

where v is the hydrophobic volume of a surfactant molecule calculated from Tanford's equation and l is the length of the hydrocarbon tails (also calculated from Tanford's equations)²⁰⁵

$$V=0.0274+0.0269n \quad (3.5)$$

$$l=0.154+0.1265n \quad (3.6)$$

The calculated values of the volume, length, and the packing parameter for the py-3-n are reported in Table 3.3 in Appendix A. The total volume of the hydrophobic tails is given by (v₁ + v₂) and the length of the hydrophobic group will be equal to the length of the longest tail. As seen in Table 3.3, as well as in the literature, aggregates formed by m-3-m gemini surfactants

tend to form cylindrical micelles with a P value of approximately 0.35 depending upon the alkyl tail length. The replacement of one of the tail group by a pyrenyl ring dramatically impacts the hydrophobic volume due to the bulkiness of the fused rings without impacting the overall length of the hydrophobic group except for the py-3-8 surfactant. This restricts the geometry of the system such that cylindrical, lamellar and inverted micelles are now the predicted favorable geometry. These different packing values are affected by the head group area as well. The head group areas of the pyrenyl surfactants showed no consistency whatsoever in the data obtained from the surface tension. In equations 3.5 and 3.6, n is the number of carbon atoms in the hydrocarbon tails of the surfactant. The packing parameter for the pyrene-3- n gemini surfactants is dramatically impacted by the presence of the bulky pyrenyl ring in the molecule. The aggregates shapes predicted by equation 3.4 are cylindrical (pyr-3-14), vesicles (pyr-3-16), inverted micelles (pyr-3-8), or lamellar (pyr-3-12 and pyr-3-18). This may be due to the presence of the bulky pyrene ring which adds to the hydrophobic volume, but not to the length of the tail.¹⁰⁵ For 12-3- n surfactants, inverted micelles were formed. This is largely due to the small head group areas that were caused by tight packing at the air/water interface due to increased intermolecular hydrophobic interactions.

3.2.3 Conductivity measurements

The graphs of specific conductivity versus concentration of the pyrene-based gemini surfactants are plotted in Figures.3.9 (a, b, and c) and those of 12-3- n in Figures 3.10(a, b, and c). The CMCs for pyr-3-8 pyr-3-12, pyr-3-14, and pyr-3-16 obtained from the conductivity studies are in agreement with those obtained from tensiometry, and from the literature for pyr-3-12 at 25°C.¹⁰⁹ However, less agreement between those methods was obtained for pyr-3-18 with CMC=0.024mM in surface tension and 0.06mM in conductivity studies, which is common when comparing the results using different techniques to measure different properties in self-assembly

.¹⁰⁵ CMCs for 12-3-14, 12-3-16, and 12-3-18 are in good agreement with those obtained from the surface tension measurements. Also, conductivity measurements of all of the surfactants were investigated at two different temperatures (303.15-308.15K). In conductivity studies, κ increases as C increases; however, the rate of increase in κ , relative to C, is different below and above the CMC. At low concentrations, surfactant molecules are completely ionized and above the CMC, only some of the counterions are bound to micelles, which causes a reduction in the effective charge of the micelle.¹⁴⁰ Thus, the slope of κ vs C above the CMC is smaller than that below the CMC. This came in agreement for all of the dissymmetric surfactants in the current study. The degree of micelle ionization parameter is defined as a fraction of an ionic surfactant's counter ions that are dissociated from micelles, leaving the micelles charged.²⁰⁶ This parameter can be obtained from the ratio of A_2/A_1 . Counterion binding increases with increasing alkyl tail length for an ionic surfactant,²⁰⁷ which means α decreases with the increased tail length for ionic surfactants. The trend has been attributed to the increased in micelle surface charge density on increasing tail length. However, the degrees of micelle ionization are higher for pyrenyl surfactants compared to m-3-m surfactants, despite having low CMC values. Higher α values correspond to greater degree of dissociation of the counter ions from the surface of the micelles. Why these dissymmetric gemini surfactants behave differently from what is generally reported in the literature is still unknown. With higher α , the repulsive forces between the partially charged micelles will play greater role in the aggregate structures within the micelles. The pyrenyl surfactants also exhibit a strong upward curvature in the plot of κ vs. C in the region of the CMC, which is an indication of the presence of pre-micellar aggregates formation¹⁰⁸. Similar behavior was observed for 12-3-n surfactants. The same behavior was reported in phytanyl-3-n gemini surfactants. Phy-3-16 α value was 0.67 and phy-3-12 was 0.46¹⁰⁵.

Wang et al. synthesized a series of dissymmetric gemini surfactants, designated as $C_mC_6C_n$ ($m+n=24$). They found that CMC decreases with the increase in the asymmetry and α values

decrease as a result of higher packing of the head groups and the higher charge density at the micelle/solution interface.¹⁴⁰ In a series of 12-*s*-12 with *s* = 2, 3, and 4, Menger et al. concluded that α values increase with the increase in the spacer length and this is probably due to increase in the space between the head groups, which leads to an increase in the degree of micelle ionization and the binding of Br⁻ to the micelle in solution.²⁰⁸ The CMC values decreased with the increase of the alkyl tail length, and the increase in the temperature as can be seen in Figures 3.9 and Figure 3.10. The decrease in the CMC with the increase in the temperature is a consequence of the decreased hydrophilicity of the surfactants molecules and reduction of hydration, which favors micellization. Also, the increase in temperature breaks down the structured water surrounding the hydrophobic groups,²⁰⁹ which means that the process of removing an alkyl tail from the water is endothermic²¹⁰. With the increase in the temperature, the dissociation of the bound counterions increases, and α values increase. In pyrene-based surfactants, the highest α values were reported at 30°C, then for some of the surfactants, the values either decrease or increase. This inconsistency may be attributed to the arrangement of the pyrene within the surfactants in the micelles. Pyrene bulky structure affects the assembly of the surfactant monomers into the micelle, and according to the length of the alkyl tail, the interaction can be either tight or loose, which can impact the structure of the micelle, and the binding of the counter-ions. Pyr-3-8 α values increased with the increase in the temperature ($\alpha_{25^\circ\text{C}} = 0.42 \pm 0.01$, $\alpha_{30^\circ\text{C}} = 0.72 \pm 0.007$, and $\alpha_{35^\circ\text{C}} = 0.74$), but pyr-3-14 α values decreased (0.67 at 25°C to 0.54, and 0.56 at 30°C, and 35°C, respectively). The same trend was observed for 12-3-*n* gemini surfactants with the highest α values at 30°C. The increase in the temperature favors micellization as can be noticed from the CMC values for all of the surfactants. Data of both CMC and α values are reported in Table 3.4.

Table 3.4 Critical micelle concentration (CMC), and the degree of micelle ionization values (α) obtained from the conductivity measurements at three different temperatures (25°C, 30°C, and 35°C)

Temperature (°C)	Surfactant	CMC(mM)	α
25°C	Pyr-3-8	0.13 ± 0.007	0.42 ± 0.01
	Pyr-3-12	0.16 ± 0.007	0.61 ± 0.00
	Pyr-3-14	0.16 ± 0.028	0.67 ± 0.02
	Pyr-3-16	0.13 ± 0.002	0.61 ± 0.02
	Pyr-3-18	0.06 ± 0.014	0.57 ± 0.01
	12-3-14	0.34 ± 0.070	0.28 ± 0.00
	12-3-16	0.18 ± 0.020	0.39 ± 0.02
	12-3-18	0.18 ± 0.020	0.44 ± 0.02
	30°C	Pyr-3-8	0.12 ± 0.002
Pyr-3-12		0.16 ± 0.007	0.78 ± 0.00
Pyr-3-14		0.08 ± 0.007	0.54 ± 0.04
Pyr-3-16		0.12 ± 0.001	0.79 ± 0.01
Pyr-3-18		0.04 ± 0.007	0.53 ± 0.04
12-3-14		0.25 ± 0.141	0.38 ± 0.00
12-3-16		0.18 ± 0.007	0.49 ± 0.141
12-3-18		0.18 ± 0.002	0.49 ± 0.00
35°C		Pyr-3-8	0.10 ± 0.000
	Pyr-3-12	0.12 ± 0.000	0.73 ± 0.00
	Pyr-3-14	0.05 ± 0.000	0.56 ± 0.00
	Pyr-3-16	0.09 ± 0.000	0.6 ± 0.00
	Pyr-3-18	0.04 ± 0.000	0.66 ± 0.00
	12-3-14	0.23 ± 0.000	0.23 ± 0.03
	12-3-16	0.17 ± 0.000	0.44 ± 0.00
	12-3-18	0.16 ± 0.000	0.46 ± 0.00

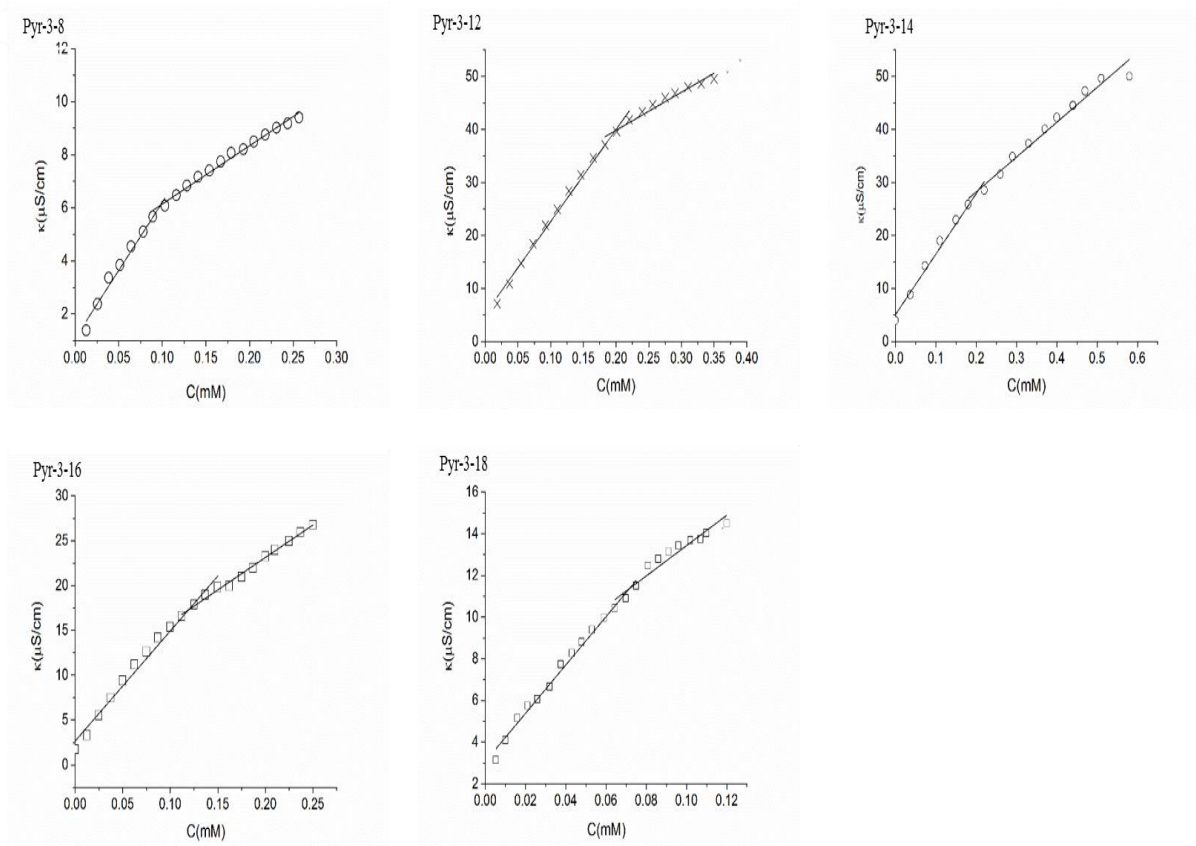


Figure 3.9.A Specific conductivity (κ) –concentration (C) studies for pyrene-based gemini surfactants at 25°C. The CMC is represented by the intersection of two lines below and above the CMC. The experimental data is listed in Appendix B

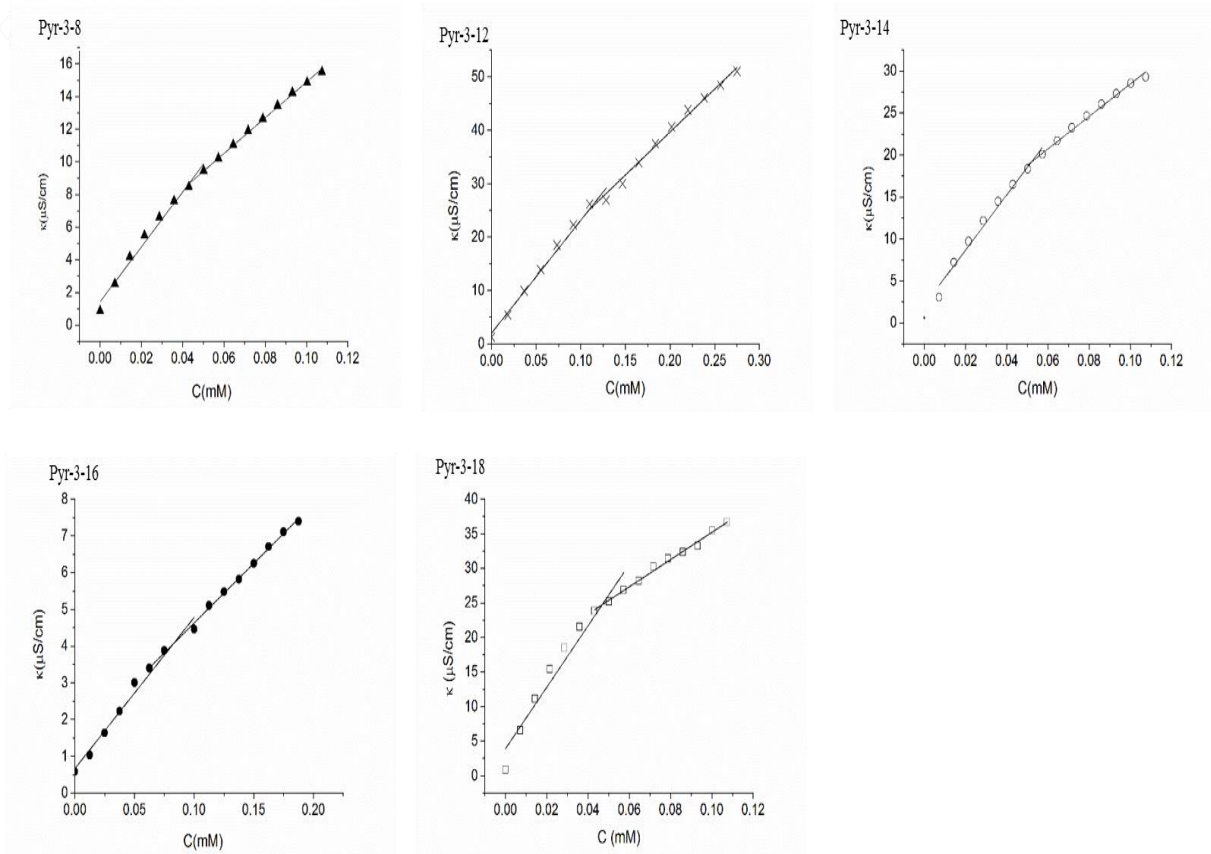


Figure 3.9B Specific conductivity (κ) –concentration (C) studies of pyrene-based gemini surfactants at 30°C . The CMC is represented by the intersection of two lines below and above the CMC

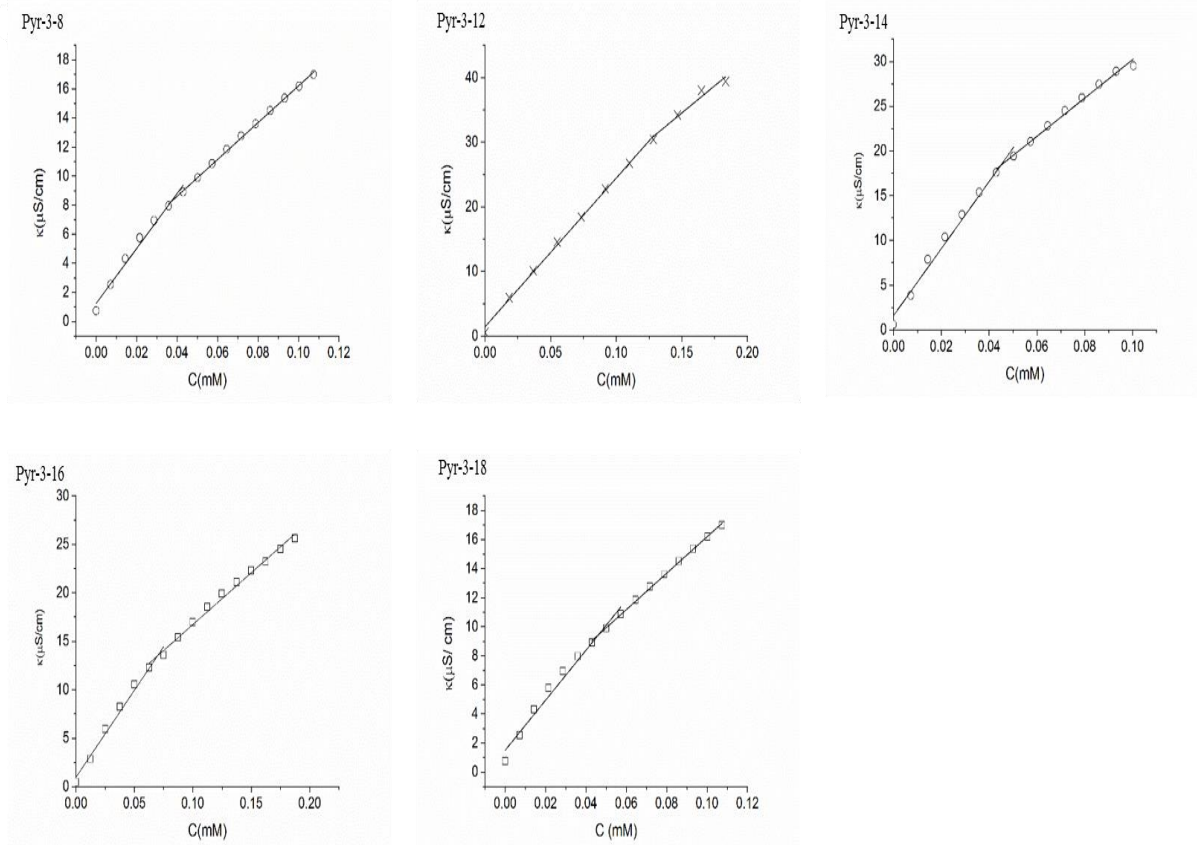


Figure 3.9C Specific conductivity (κ) –concentration (C) studies for pyrene-based gemini surfactants at 35°C . The CMC is represented by the intersection of two lines below and above the CMC

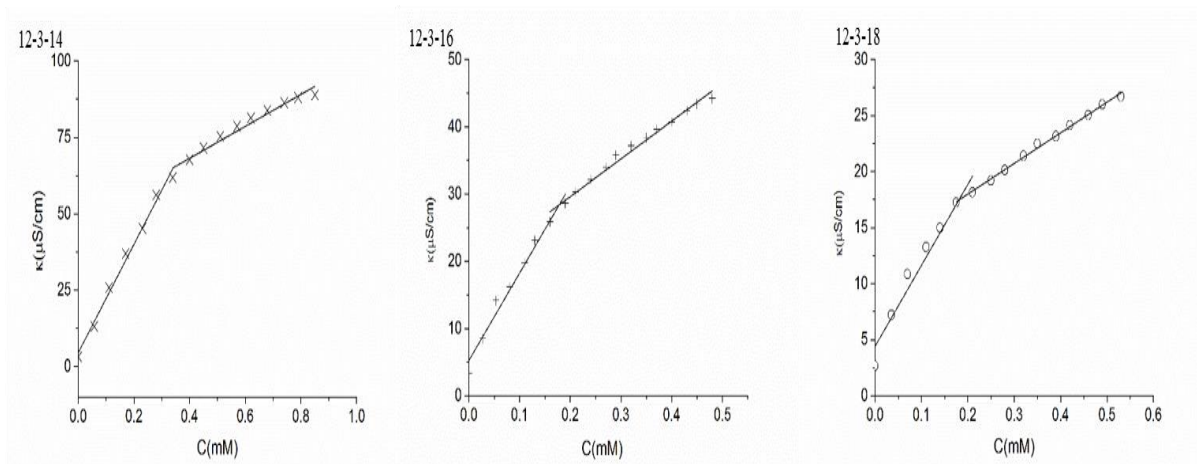


Figure 3.10A Specific conductivity (κ) -concentration (C) studies of 12-3- n gemini surfactants at 25°C . The CMC is represented by the intersection of two lines below and above the CMC

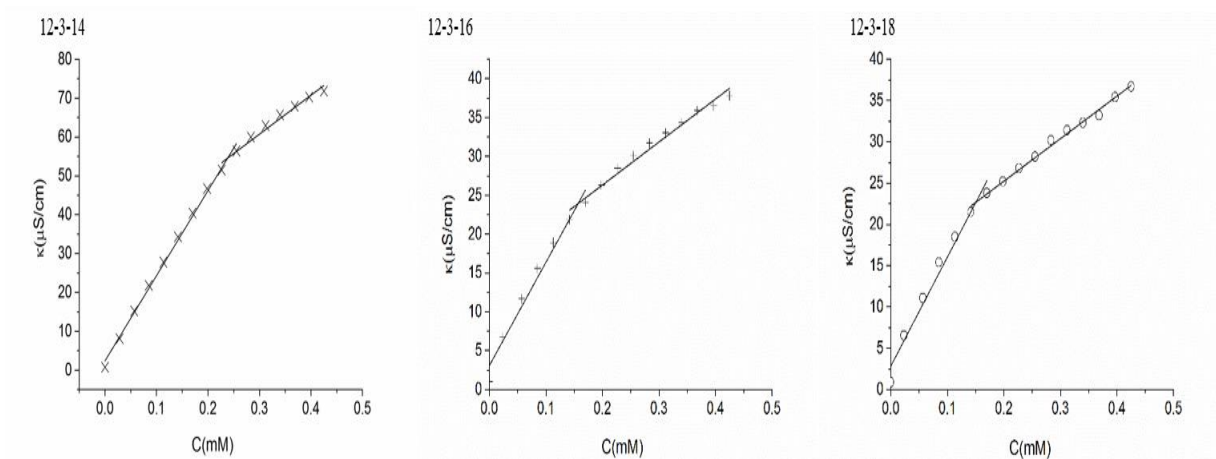


Figure 3.10B Specific conductivity (κ) –concentration (C) studies of 12-3-n gemini surfactants at 30°C. The CMC is represented by the intersection of two lines below and above the CMC

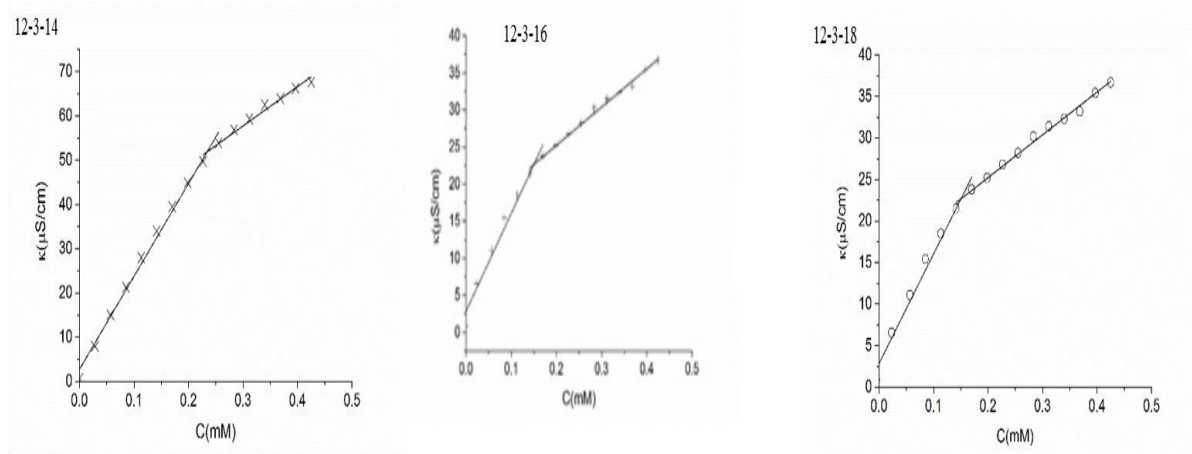


Figure 3.10C Specific conductivity (κ) -concentration (C) studies of 12-3-n gemini surfactants at 35°C. The CMC is represented by the intersection of two lines below and above the CMC

The thermodynamic parameters of the micellization process of the pyrene-based surfactants and the 12-3-n gemini surfactants were calculated by applying the pseudo-phase separation model for ionic surfactants according to:

$$\Delta G_m^\circ = 2(1-\alpha)RT \ln X_{cmc} \quad (3.7)$$

where α is the degree of micelle ionization, which was obtained from the ratio of the two slopes of the two regions in the conductivity-concentration plot, and X_{cmc} is the molar fraction at the CMC, $X_{cmc} = CMC/55.4$, 55.4M+ CMC moles of water/L at 25°C. Table 3.4 presents all the thermodynamic parameters of micellization of the dissymmetric gemini surfactants at different temperatures. For the pyrenyl surfactants, the results show that at a certain temperature, as the m/n ratio increases, ΔG_m° values become more negative and this implies the spontaneity of the aggregation process, also ΔG_m° increases for the same surfactant at different temperatures, which lead to lower CMC. The higher the temperature, the lower the CMC with the increased hydrophobicity as a result of increased alkyl tail length. However, the process of micellization is entropy driven as ΔH_m° is positive throughout the pyrenyl and the asymmetrical surfactants as well and this means that the removal of a surfactant tail from the water into the core is endothermic.

In the asymmetric gemini surfactants, ΔG_m° values were decreasing from 12-3-14 to 12-3-18 at a specific temperature, which suggests that the addition of one methylene unit to one tail requires energy. This might be attributed to the increase in the disorder of the solution, leading to a decrease in ΔG_m° . This was confirmed by the plot of the variation of $(\Delta G_m^\circ (\text{CH}_2))$ with the degree of dissymmetry m/n, which shows the relationship between the Gibbs free energy per mole of CH_2 ($\Delta G_m^\circ (\text{CH}_2)$) with the degree of the dissymmetry (see Figure 3.11) In the pyrenyl surfactants, as the m/n increases, the ΔG_m° becomes more negative, which favors the aggregation led by the hydrophobic interactions. Values of $|T\Delta S_m^\circ|$ for all of the asymmetric gemini surfactants in this study were higher than those of $|\Delta H_m^\circ|$, which again suggests that the aggregation process of these surfactants is entropy-driven.¹⁴⁰ However, when comparing the dissymmetric gemini surfactants to the pyrenyl surfactants, we notice that ΔG_m° of 12-3-14 > pyr-3-14, 12-3-16 > pyr-3-16, and 12-3-18 > pyr-3-18 at the same temperature, although the

latter's difference is not that significant as those of 12-3-14 and 12-3-16. This suggests that substituting an alkyl tail with hexyl pyrene requires more energy due to the geometric restraints created by the aromatic pyrene. The values of the thermodynamic parameters at different temperatures is enlisted in Table 3.5.

Table 3.5 Gibbs free energy of micellization (ΔG_m°), enthalpy of micellization (ΔH_m°), and the entropy of micellization (ΔS_m°) of pyrene-based gemini surfactants and 12-3-n surfactants at different temperatures

Temperature	Surfactant	ΔG_m° (KJ.mol ⁻¹)	ΔH_m° (KJ.mol ⁻¹)	ΔS_m° (KJ.K ⁻¹ .mol ⁻¹)	T ΔS
298.15K	Pyr-3-8	-49.24	34.72	0.28	83.96
	Pyr-3-12	-56.27	17.00	0.25	73.27
	Pyr-3-14	-52.64	81.26	0.45	133.90
	Pyr-3-16	-57.11	27.50	0.28	84.61
	Pyr-3-18	-64.00	31.80	0.32	95.80
	12-3-14	-72.55	28.81	0.34	101.36
	12-3-16	-69.57	3.47	0.24	73.04
	12-3-18	-66.39	8.35	0.25	74.74
	12-3-12	-70.00			
14-3-14	-78.32				
303.15k	Pyr-3-8	-51.10	35.89	0.29	86.99
	Pyr-3-12	-46.36	17.56	0.21	64.00
	Pyr-3-14	-65.25	84.00	0.49	149.26
	Pyr-3-16	-46.86	28.41	0.25	75.27
	Pyr-3-18	-68.91	32.91	0.33	101.82
	12-3-14	-69.50	29.78	0.32	99.28
	12-3-16	-64.88	3.74	0.23	68.62
	12-3-18	-64.31	8.63	0.24	72.94
	Pyr-3-8	-51.50	37.10	0.29	88.59
	Pyr-3-12	-51.23	18.15	0.23	69.40
	Pyr-3-14	-67.013	86.80	0.5	153.80
	Pyr-3-16	-61.00	29.35	0.29	90.35
	Pyr-3-18	-61.10	34.00	0.31	95.10
	12-3-14	-66.63	30.77	0.31	97.40
	12-3-16	-68.85	3.70	0.24	72.56
	12-3-18	-67.91	8.92	0.25	76.83

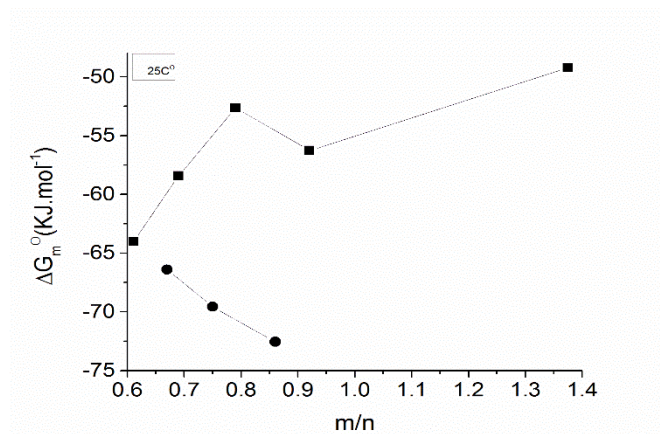


Figure 3.11 The variation of the free of micellization ($\Delta G_m^0(\text{CH}_2)$) with the degree of dissymmetry m/n from the conductivity studies of Pyr-3- n (▲), and 12-3- n (●)

3.3 Conclusion

The pyrene-based gemini surfactants, pyr-3- n , ($n=8, 12, 14, 16$, and 18), and the dissymmetric gemini surfactants, 12-3- n , $n= (14, 16, 18)$ were synthesized, The aggregation properties of these surfactants were characterized. The Krafft temperatures of pyrene-3- n and 12-3- n increased with the increase in the alkyl tail length. This finding follows the general observations with all other gemini surfactants.²¹² Pyr-3- n and 12-3- n showed much lower CMC values than those of their symmetrical counterparts. This is due to increased hydrophobicity of the pyrene-3- n surfactants, and due to the dissymmetry of the 12-3- n surfactants, which imparts unique properties on the gemini surfactants. The docking studies showed that the first interaction happening in the pyr-3- n surfactants is the pyrene-pyrene interactions, and this may cause the initiation of the micelle formation start at a very high surface pressure. The pyrene is included as a guest molecule into the micelle. The higher degrees of micellization were also observed in both of the groups, the pyrenyl surfactants and the dissymmetric ones. The higher the α , the easier the binding of the DNA as it replaces the counter ions to reduce the repulsive attraction forces between the two head groups. Head group areas are smaller in pyrene-based surfactants than those of the symmetrical counterparts, indicating enhanced intermolecular hydrophobic interaction, which results in smaller a_o . However, pyrene-3-14 has a relatively larger head group area. This may be

caused by the asymmetry effect appearing at this surfactant, because before that pyr-3-12 is close to symmetry and pyr-3-8 has very low surface tension due to their high solubility in aqueous phase. The packing parameter is calculated for the pyr-3-n and 12-3-n compounds are indicative of the formation of various morphologies, especially in the pyr-3-n surfactants. Pyr-3-8 form inverted micelles, whereas pyr-3-14 forms cylindrical micelles, pyr-3-16 forms vesicles and pyr-3-12 and pyr-3-18 form lamellar. Both vesicles and inverted micelles have been linked to better transfection results in the literature.

These key parameters such as low CMC values, small head group area (a_h), and high α values indicate that these surfactants, at lower concentrations, they can form micelles of various morphologies in solutions and they are capable of easily binding and electrostatically interacting with DNA in order to decrease the repulsive interactions between the head group area. These properties favors the complexation and formation of nanoparticles of relatively small size with DNA, which means a possibility for a better transfection vector and possibly yielding a better transfection efficiency.

Chapter 4 Characterization of the Gemini Surfactant-DNA complexes Langmuir-Blodgett (LB) and Brewster's Angle Microscopy (BAM)

4.1 Introduction

As previously mentioned in Chapter I, one of the most interesting applications of gemini surfactants is as non-viral gene delivery vectors.^{135,34} Transfection using a non-viral vector is not as efficient as the viral vectors, which also highly dependent on the type of cell line being transfected (for *in vitro* studies), the structure of the compounds used in the formulation of the vectors (more specifically the type(s) of modifications implemented in the structure of the vector component), the types of helper lipids used, the morphologies the resulting complexes adopt in solution, and the duration of post-transfection (time for transgene expression), which depends on the surfactant's structure as well as the cell-line used in the experiment. Moreover, transfection complex surface charge and size can play essential roles, it has been extensively discussed in the literature,^{213,214} although a specific correlation to surfactant structure has remained quite elusive.

In our study of gemini surfactant based non-viral transfection vectors, the impact of gemini surfactants, and the complete gemini surfactant transfection complex on model membranes of both healthy and cancerous cells are being investigated, prior to attempting *in vitro* transfection studies. The aim of this investigation is to better understand the mode of interaction between the molecules of the monolayer, usually zwitterionic lipids, and the gemini surfactants and the resulting transfection complexes, In addition, this study can give us insight into how the gemini surfactant-DNA complexes can escape the endosomal membrane. The Langmuir-Blodgett (LB) monolayer method is a technique that allows the preparation of monolayers (as model membranes) in a two dimensional system by spreading phospholipids (in our case either DPPC/Cholesterol or POPC/Cholesterol at a ratio of 75%_25% at the air-water interface).¹⁴⁵

Surface pressure – molecular area isotherms can be collected, and analyzed to determine the phase behaviour of the lipids within the monolayer as a function of surface pressure. This method also offers a unique opportunity to investigate the nature and possible interactions between these monolayers and different molecules¹⁴⁶ by combining the Langmuir trough with the Brewster Angle Microscope. The BAM instrumentation allows high resolution and real-time imaging of monolayers, and this allows a molecular-level understanding of the interactions between the components of the monolayer together with the components of the sub-phase. This is necessary because the lipid compositions of cell membranes and tissues vary based on the organ or the tissues of origin. The lipid compositions alter the biophysical interactions, this knowledge led to the development of target-specific drugs and drug delivery systems.¹⁴⁵

In the current study, the eight synthesized gemini surfactants` monolayers alone, with two different lipid systems; DPPC/Cholesterol, and POPC/Cholesterol at 75%_25% ratio, and with the DNA in the sub-phase was investigated and images of the topography formed at different surface pressure were taken by BAM with a CCD camera embedded in the system. Several projects within our lab are investigating the interactions between different cationic moieties with DNA employing Langmuir monolayer with the BAM technique as non-viral gene delivery vehicle to assess the interactions, and whether or not certain components can enhance transfection or not¹⁴³. Although transfection with gemini surfactants alone or with helper lipids have been investigated in numerous cell lines, model membranes have not been implemented to access the mode of interactions at the cell membrane level. However, drug targeting model membranes have been characterized using Langmuir monolayer in several studies. Wnetrzak et al. investigated the interaction of alkylphosphocholines (APCs), which are antineoplastic selective moiety, with three individual model membranes; cholesterol, DPPC, and POPC.^{150b} DPPC and POPC are the most abundant phospholipids, both in healthy and cancerous tissues

(Leukaemia), and cholesterol was chosen because of its crucial role in regulating membrane physicochemical properties in eukaryotic cells.²¹⁵

4.2 Materials and Methods

4.2.1 Materials

Gemini surfactants pyr-3-8, pyr-3-12, pyr-3-14, pyr-3-16, pyr-3-18, 12-3-14, 12-3-16, and 12-3-18 were synthesized and characterized as described in chapter 3 according to procedures previously reported in the literature.^{109,192} The degree of purity was determined by using ¹H NMR and surface tension measurements. 1, 2-dipalmitoyl-sn-glycero-3-phosphocholine (DPPC), 1-palmitoyl-2-oleoyl-sn-glycero-3-phosphate (POPC), and cholesterol was purchased from Avanti Polar Lipids (Alabaster, USA). Double-stranded salmon sperm DNA (Sigma-Aldrich, Oakville, Canada) was used without further purification. Chloroform was obtained from Sigma-Aldrich (Oakville, Canada).

4.2.2 Preparation of Langmuir monolayer

Surfactants, lipids, and mixtures were dissolved in chloroform at a concentration of 2.5 mmol/L. A salmon sperm DNA stock solution was prepared by dissolving DNA in Millipore-Q a concentration of 100 mg/L. The final concentration of DNA in all the monolayer experiments was 0.2 mg/mL. Monolayers were prepared on a large (14.5 cm by 53 cm) Langmuir trough (KSV Instruments, Helsinki, Finland), with surface pressure monitored using the Wilhelmy plate method. A volume of 20 µL of surfactant and/or lipid solution was carefully deposited onto the surface of the sub-phase using a micro-syringe (GASTIGHT®, Hamilton-Bonaduz, Schweiz, Switzerland) and the chloroform. For experiments that involved only water as the sub-phase, the monolayer was allowed to equilibrate for 10 minutes. For experiments involving aqueous DNA (0.2mg/mL) as a sub-phase, the sub-phase was given 30 minutes to equilibrate with DNA prior

to the addition of the surfactant or lipids, and an additional 30 minute equilibration time was allowed for the monolayer after deposition of the surfactant and/or lipids. After equilibration, compressions of the monolayers on the trough were carried out at a rate of 15 mm/min. and the surface pressure – mean molecular area isotherms were collected.¹⁴³ When DNA and the gemini surfactants (2.5 mM) were dissolved in the sub-phase, the DNA was added first with 30 minutes equilibration, followed by the addition of gemini surfactant and additional 10 minute equilibration to allow interactions between the DNA and the GS to occur. Isotherms and BAM images of monolayers prepared from the gemini surfactants (in the absence or presence of DNA), as well as for monolayers of DPPC/Chol or POPC/Chol (as model membranes) in the absence or presence of the gemini surfactants or the gemini surfactant/DNA complexes.

4.2.3 Brewster`s Angle Microscopy (BAM)

The Langmuir trough is equipped with a Brewster angle microscope (BAM) (KSV Instruments, Helsinki, Finland). The BAM consists of a standard He-Ne laser used as a light source with a power of 50 mW, wave length of 658 nm and a spatial resolution of the device was 2 μm . Briefly the p-polarized light is reflected at the air/water interface, and monitored at the Brewster angle ($\sim 53.1^\circ$) using a CCD camera that can capture either images or real-time video of the monolayer.

4.3 Analysis of Surface pressure-Area isotherms (π -A)

The surface pressure-area isotherms obtained for the Langmuir monolayers were used, along with the compressibility modulus (C_S^{-1}), to determine the phase behavior of the monolayer. The compressibility modulus is calculated from the following equation:

$$C_S^{-1} = -A(\delta\pi/\delta A)_T \quad 4.1$$

where A is the molecular area at a certain surface pressure π . Several parameters can be derived from the π -A isotherm, such as; the molecular area at collapse (A_C), the collapse pressure (π_C),

the lift-off area (A_L), and the limiting area or the minimum cross-sectional area (A_∞). The lift-off area (A_L) is the molecular area at which the isotherm starts rising above the baseline, and provides insight into the molecular orientation at the gas-liquid phase region.²¹⁶ The limiting area or the minimum cross-sectional area (A_∞) is the area occupied by the molecules within the monolayer, prior to collapse, can be calculated by extrapolation of the isotherm at the steepest slope prior to the collapse back to the zero surface pressure.¹⁴⁸

As mentioned earlier, the compressibility modulus provides information regarding the phase behavior of the monolayer. For values of $C_S^{-1} < 12.5 \text{ mN/m}$, the monolayer is in the gaseous phase, at a $C_S^{-1} = 12.5\text{-}50 \text{ mN/m}$, the monolayer is in the gas-liquid phase, and for $C_S^{-1} = 50\text{-}100 \text{ mN/m}$, the monolayer is in a liquid expanded phase, for values of $100\text{-}150 \text{ mN/m}$, the monolayer is in the liquid expanded-liquid condensed coexistence, for values of $> 150\text{-}250 \text{ mN/m}$, the monolayer is in the liquid condensed phase, and for values of C_S^{-1} above 250 mN/m , the monolayer is in the solid phase. As C_S^{-1} value becomes higher, this is an indication of the stability of the monolayer, corresponding to a less elastic membrane

4.4 Results and discussion

While the model membranes in this work are comprised of 75% DPPC or POPC and 25% cholesterol, in order to understand the isotherms of the mixed lipid monolayer, an examination of the isotherms of each component is of a great importance. Our group has previously characterized the behavior of monolayers prepared from pure cholesterol, DPPC, or POPC.¹⁴³ Pure cholesterol forms a typical condensed monolayer with liftoff areas of $\sim 43.2 \text{ \AA}^2$ with a collapse pressure of the monolayer of $\sim 45 \text{ mN/m}$, and the minimum cross sectional area for cholesterol in the monolayer is 34.4 \AA^2 /molecule.¹⁴³ All of the parameters determined in our lab for the cholesterol monolayers are consistent with the results described in the literature^{217,218} (See Appendix B). Cholesterol forms a condensed monolayer in which molecules arrange

themselves in a vertical position or slightly tilted towards the surface. DPPC exhibits a characteristic transition region (at $\pi = 5$ mN/m), corresponding to orientation changes of molecules upon compression, with a minimum cross-sectional area of 60.2 \AA^2 and collapses at a surface pressure of 53.3 mN/m (see Appendix B). POPC forms a liquid-expanded monolayer without any visible transition throughout the isotherm (see Appendix B), with a minimum cross-sectional area of 75 \AA^2 , with a lower collapse pressure (~ 40 mN/m) compared to the saturated phospholipid (DPPC).^{150b} When a small fraction of cholesterol is added to the DPPC or POPC monolayers, it profoundly alters the morphology of phospholipid monolayers. Cholesterol forms distinctive domains and lowers surface viscosity by orders of magnitude. Introducing cholesterol to DPPC monolayer can alter the rheology and isotherm, suggesting fundamentally different molecular organization.²¹⁹ Cholesterol increased the rigidity of the system once it was added to it and reduce permeability, however, in the DPPC/Cholesterol, at biological surface pressure (30-35mN/m), at pH = 7, the monolayer is found in the solid phase (S).¹⁴³

4.4.1 Langmuir isotherms of pyrene-based Gemini surfactants

The Langmuir monolayer studies of the pyrenyl and the 12-3-n gemini surfactants were carried out at room temperature in Millipore milli Q water. These isotherms are illustrated in Figures 4.1 to 4.8 and the parameters derived from the surface pressure-area isotherms are listed in Tables 4.1 and 4.2 for both types of model monolayers; DPPC-Cholesterol, and POPC-Cholesterol. To gain a better insight into the interactions, we have injected the surfactant systems into the sub-phase (with or without DNA), mixed them and subsequently spread the DPPC-Cholesterol, or POPC-Cholesterol model membrane monolayers on top of the sub-phase that now contains the complete gene delivery system. Many researchers have used the DPPC-cholesterol based system to evaluate drug-membrane interactions,²²⁰ and phospholipid-model membrane interactions.^{150b} Since the surface pressure of the actual cell membrane ranges from 30-35 mN/m,²¹⁸ we will be

focusing on this surface pressure range along with the detailed analyses of the isotherms presented below.

For pyrenyl gemini surfactants, the monolayers of these surfactants alone at the air/water interface, whether for pyrene-3-8 with the shortest tail, or for pyrene-3-18 with the longest tail, are enlisted in Table 4.1. All the pyrenyl gemini surfactants when spread as monolayers were soluble and they submerged in the sub-phase. None of these surfactants formed a monolayer that could be characterized by an isotherm (the π_c of pyr-3-8 was 0.25mN/m and the highest was that of pyr-3-18 with a collapse pressure of 1.7mN/m). This can be attributed to the very low CMC values of these surfactants, favoring micelle formation, and thus disillusion of these surfactants occurred in the bulk aqueous phase as micelles, rather than adsorbing to the interface. Similar results were reported for the 12-6-12 gemini surfactants, which showed no surface pressure change at the air/water interface despite the compression of a monolayer.²²¹

The π -A isotherms for the model membrane monolayers show that the addition of the pyrenyl gemini surfactants (either with or without DNA) has a dramatic effect on the monolayer properties. DPPC-Cholesterol monolayer's lift-off area is 56.48Å² (see Figure 4.1 and Table 4.1). After the addition of pyrene-3-8, the lift-off area increased up to 98 Å². This is indicative of high abundance of gemini surfactant molecules at the interface and strong attraction between the GS and the monolayer (hydrophobic interactions between the octyl tail and the DPPC alkyl tails, the hexyl tail of the hexyl pyrene with the DPPC, and may be electrostatic interactions between the positive charge of the ammonium head groups and the negative charge of the phosphate group). These molecules assemble in the spaces between the monolayers particles at a low surface pressure. This effect can also be observed in the compressibility modulus below surface pressure of 20mN/m (Figure 4.1B). As the compression increases, gemini surfactant molecules are squeezed out of the monolayer and back into the bulk, restoring the compressibility modulus to values comparable to those for DPPC-Chol monolayer alone (Figure 4.1B). Based

upon both the apparent slope/shape of the π -A isotherm (Figure 4.1A), the values obtained for the compressibility modulus (Figure 4.1B), the DPPC-Chol monolayer exhibited an LE phase, as opposed to the solid phase formed by DPPC-Chol alone in the presence of pyr-3-8 at a surface pressure ranging from approximately 20mN/m-40mN/m. At 40mN/m, the monolayer exhibits a phase transition from LE-LC phase with a compressibility modulus rising up to 150mN/m. The monolayer stayed in the LC phase until the collapse at a surface pressure (π_c) of 53.021 mN/m and with a collapse area (A_c) of 46.71Å² (see Table 4.1).

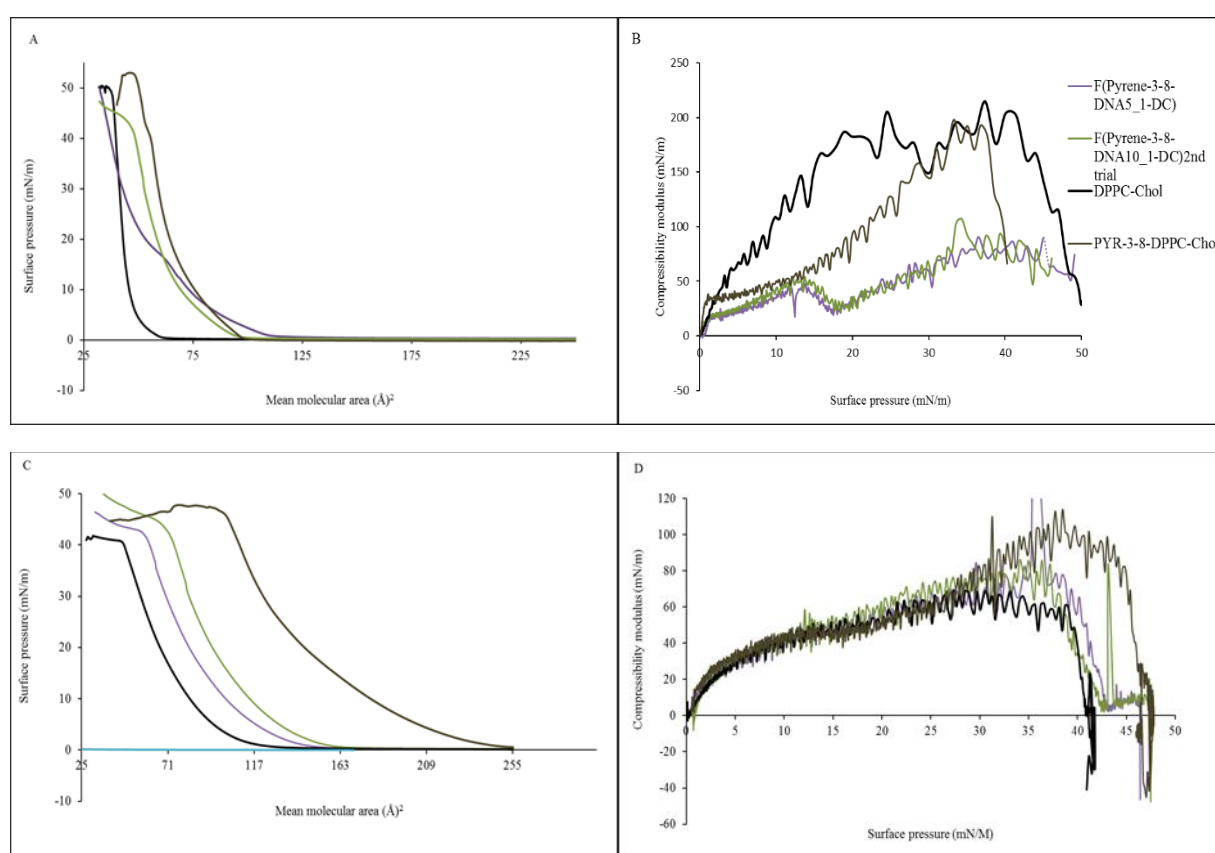


Figure 4.1: Compression isotherms (π -A) for A) DPPC/Cholesterol (75%/25%, black line) and C) POPC/Cholesterol (75%/25%, black line) monolayers treated with: pyrene-3-8 (grey), py-3-8:DNA at a 10:1 charge ratio (green), py3-8:DNA at a 5:1 charge ratio (Purple). Compressibility modulus (C_S^{-1}) as a function of surface pressure (π) for B) DPPC/Cholesterol and D) POPC/Cholesterol (75%/25%, black line) were calculated according to Equation 4.1; the line colors correspond to the same treatments described for A) and C).

Table 4.1 Monolayer properties for the DPPC/Chol (75/25) and POPC/Chol (75/25) monolayers at 20°C treated with py-3-m or py-3-m/DNA complexes

System	A_L (Å ²)	A_∞ (Å ²)	A_c (Å ²)	π_c (Å ²)	C_s^{-130} (mN/m)	C_s^{-135} (mN/m)
DPPC (75%)/Chol (25%)	61	44.0	36.7	50.7	255	275
POPC (75%)/Chol (25%)	121	70.0	47.2	40.6	58 ± 3	56 ± 3
<i>Pyrene-3-8</i>						
Py-3-8 - DPPC/Chol	98	75.0	46.7	53.0	146	192
10:1 Py-3-8:DNA - DPPC/Chol	100	74.0	45.3	43.2	63 ± 7	92
5:1 Py-3-8:DNA - DPPC/Chol	109	50.8	32.1	50.2	58	75
Py-3-8 - POPC/Chol	255	158	95.8	47.2	81 ± 5	89 ± 8
10:1 Py-3-8:DNA - POPC/Chol	167	115	68.2	43.9	76	86
5:1 Py-3-8:DNA - POPC/Chol	160	99.8	58.0	42.3	62	74
<i>Pyrene-3-12</i>						
Py-3-12 - DPPC/Chol	150	130	101	49.5	332	243
10:1 Py-3-12:DNA - DPPC/Chol	225	175	119	50.9	118	142
5:1 Py-3-12:DNA - DPPC/Chol	245	175	117	50.8	109	128
Py-3-12 - POPC/Chol	145	100	52.6	40.5	69	75
10:1 Py-3-12:DNA - POPC/Chol	200	110	55.1	39.6	52	41
5:1 Py-3-12:DNA - POPC/Chol	200	110	56.5	39.8	42	48
<i>Pyrene-3-14</i>						
Py-3-14 - DPPC/Chol	103	76.0	45.8	52.5	143	175
10:1 Py-3-14:DNA - DPPC/Chol	153	80.0	39.0	50.3	69	63
5:1 Py-3-14:DNA - DPPC/Chol	120	53.1	24.7	49.4	58	62
Py-3-14 - POPC/Chol	>255	180	119	47.1	90	108
10:1 Py-3-14:DNA - POPC/Chol	225	127	66.2	39.6	53	47
5:1 Py-3-14:DNA - POPC/Chol	250	135	68.4	39.4	49	50
<i>Pyrene-3-16</i>						
Py-3-16 - DPPC/Chol	69.1	57.0	32.1	45.6	78	128
10:1 Py-3-16:DNA - DPPC/Chol	124	66.0	34.6	51.1	89	90 ± 3
5:1 Py-3-16:DNA - DPPC/Chol	93.4	61.4	34.0	44.3	73 ± 2	77 ± 8
Py-3-16 - POPC/Chol	150	85.2	54.0	45.2	67	80
10:1 Py-3-16:DNA - POPC/Chol	162	119	58.1	44.2	46	54
5:1 Py-3-16:DNA - POPC/Chol	183	107	62.8	40.3	40	48
<i>Pyrene-3-18</i>						
Py-3-18 - DPPC/Chol	65.4	53.1	33.4	44.3	104	142
10:1 Py-3-18:DNA - DPPC/Chol	68.3	60.1	32.4	41.4	65 ± 3	83 ± 5
5:1 Py-3-18:DNA - DPPC/Chol	78.6	58.3	33.2	45.1	52 ± 5	69
Py-3-18 - POPC/Chol	176	132	63.6	48.6	74	95 ± 4
10:1 Py-3-18:DNA - POPC/Chol	177	127	47.5	43.6	60	64
5:1 Py-3-18:DNA - POPC/Chol	179	126	48.5	43.6	60	34

When DNA is added to the DPPC-Cholesterol and py-3-8 system, at a 5:1 surfactant: DNA charge ratio, distinct differences in the monolayer behaviour are observed. A new phase transition can be seen in both π -A isotherm and the compressibility modulus, which can be attributed to result from electrostatic interactions between the DNA phosphate groups and the GS's ammonium group. This transition is consistent with a G to LE transition, based upon the values observed for the compressibility modulus. As surface pressure continues to increase, a small plateau (or shoulder) is observed over a range of surface pressures from approximately 15 – 20 mN/m, corresponding to a decrease in the compressibility modulus, which corresponds to an LE – LC co-existence region. As surface pressure continues to increase, the LC phase is observed, over a broad range of surface pressures of from 30-45mN/m.

For the system containing DNA at a 10:1 gemini surfactant/DNA charge ratio, the sharp discontinuity observed in the π -A isotherm, corresponding to the onset of the LE – LC coexistence region, disappears; however, the compressibility modulus clearly shows similar phase behaviour. Different parameters, such as, A_L , A_∞ and A_C also help characterize the monolayer. The A_L values for DPPC/Chol monolayer in the presence of both py-3-8 and DNA at a charge ratio of 10:1 and 5:1 are 100\AA^2 and 109\AA^2 , respectively (Table 4.1), and do not appear to differ from that observed for the DPPC-Chol monolayer treated with py-3-8 alone (98.1\AA^2). The cross-sectional area (A_∞) for the DPPC-Cholesterol monolayer is 61.1\AA^2 in the absence of gemini surfactants or DNA, which increases to 75\AA^2 upon the addition of pyr-3-8. A slight decrease is observed for the addition of DNA at a 73.9\AA^2 at a charge ratio of 10:1. A much greater decrease in A_∞ value is seen with a further increase in the concentration of DNA at a charge ratio of 5:1 (50.8\AA^2). At this point, the limiting area is approximately equal to that for the monolayer in the absence of any added DNA and suggests the complete extraction of gemini surfactant from the monolayer, into DNA bound complexes.

However, if we compare the compressibility modulus for the monolayers treated with the GS:DNA at 10:1 and 5:1 ratios, the values of C_S^{-1} in the range of surface pressures from 30 – 40 mN/m are more or less the same, and for both ratios at 30 mN/m, and 35 mN/m, there is a substantial reduction in the compressibility modulus, to approximately 75 – 95 mN/m (Table 4.1), corresponding to an LE phase. This is indicative of very strong interactions and significant incorporation of either the GS alone or the GS-DNA complexes at higher surface pressures. The overall effect of pyrene-3-8 alone or with DNA is in fluidizing the monolayer, thus allowing molecules either to interact with the monolayer through hydrophobic interactions at the surface, or by incorporating the GS molecules within the monolayer. Several drugs have similarly been observed to have a fluidizing effect in the literature. Examples include paclitaxel,²²² and prazosin²²³ with DPPC-Cholesterol membranes, hexadecylphosphocholine and erucylphosphocholine with POPC-cholesterol membranes,^{150b} and toremifene with dipalmitoyl-phosphatidyl-glycerol (DPPG) membranes.²²⁴ In all cases, the presence of the drug molecule substantially reduced the compressibility modulus of the pure model membrane, which was considered to be a result of the fluidizing effect of drug to the model membrane.

In contrast to the very solid-like DPPC-Chol monolayer, the POPC-Cholesterol system is much more fluid with two distinctive phase transitions observed (Figure 4.1C); one at surface pressure of 0.8-25mN/m and the other at surface pressures ranging from 20-40mN/m. The first is a transition from a gaseous phase to a LE phase (with a compressibility modulus of 43 mN/m – 50 mN/m, see Figure 4.1D), the second phase transition is what appears to be from an LE to LE-LC coexistence phase ($C_S^{-1} = 98$ mN/m). Just prior to collapse, it appears that there is a shift back into an LE phase, followed by collapse; however it is more likely that the onset of this “LE” phase is actually the point of monolayer collapse. The compressibility modulus plots (Figure 4.1D) for the POPC-Chol system are much more informative for the identification of the phase behaviour of this monolayer, given the almost featureless shape of the π -A isotherm. When the

GS was added to the monolayer, the collapse surface pressure increased from 40mN/m to 47 mN/m, which is an indication of increased stability of the monolayer. When the GS was added to the monolayer, which is an indication of increased stability of the monolayer. When py-3-8 or the py-3-8:DNA complexes were added to the POPC/Chol monolayer, the isotherms were shifted to higher molecular area, but retained essentially the same shape, further confirmed by the similarity of the compressibility modulus curves. This indicates that while the addition of the surfactant or surfactant:DNA complexes did disrupt the monolayer, most likely due to some incorporation of these components into the monolayer (giving rise to the increase in molecular area), they did not have the same extent of disruptive impact as for the DPPC/Chol monolayers. Given the fact that the POPC/Chol monolayer is meant to be a model for a “diseased” cellular membrane, this has concerning implications for the effectiveness of these systems as delivery vectors.

BAM images of the mixed DPPC-Cholesterol system, at low surface pressure (~0.27 to 1.22 mN/m) where the monolayer is in the G-LE phase transition, show circular or ovoid domains.¹⁴³ Upon compressing the monolayer, the LE phase transitions into the LC phase transition where blurred images are observed (Figure 4.1E). As the monolayer is further compressed and transitions into an S phase, the domains merge together and form a solid film (shown by the uniform grey background, with bright dots that likely correspond to domains rich in cholesterol). The same types of domains are observed for the DPPC/Cholesterol monolayer treated with py-3-8 (Figure 4.2). At low surface pressures of 0.2-1.6 mN/m, when the monolayer is in the G phase, the ovoid domains of the DPPC-Chol monolayer are again observed. Upon compression, during the G-LE phase transition, a grey background containing small bright domains are observed. The bright domains likely correspond to areas that into which the gemini surfactant has been incorporated, possibly containing cholesterol, allowing a more homogenous monolayer to form overall, although given the compressibility modulus described above, one

that is more fluid in nature. The domains remained essentially unchanged, visually, during the remainder of the compression.

As the DNA is added (regardless of charge ratio) at low surface pressures ~ 0.1 - 0.2 mN/m, distinct differences in the BAM images are observed (Figures 4.2). The different domains that corresponded to either DPPC or cholesterol rich domains can no longer be observed, and a more heterogeneous, less differentiated grey background is observed. As the surface pressure is increased, and consistent with the isotherm data (above), the images become consistent with the LE-LC domain characterized by a uniform grey background with small bright domains distributed throughout. Interestingly, there is a clear linear pattern to the bright domains observed for the image of the DPPC-Chol monolayer treated with py-3-8 at a surface pressure of 20 mN/m (Figure 4.2). This could be a direct visualization of the DNA adsorbed at the interface; however it should be noted that this was not generally observed for all of our systems.

For the POPC-Cholesterol system treated with py-3-8, due to the pre-existing fluidity of the POPC-Cholesterol system, no clear distinctive domains are observed, although a somewhat uniform distribution of small bright domains is already evident even at low surface pressures (Figure 4.2C). As the compression increases, these small bright domains remain, and there are no further indications in the BAM images of any other phase transitions. The BAM images for the POPC-Cholesterol monolayer treated with py-3-8/DNA (Figure 4.2D) shows comparable behaviour to that for the POPC-Cholesterol monolayer treated with the same system; however the bright domains appear even smaller, and more uniformly distributed, which may indicate that the py-3-8 surfactant is able to bridge between the POPC and cholesterol molecules as compared to the DPPC and Cholesterol molecules, giving rise to a more uniform, and more fluid monolayer, also consistent with the isotherm data, above.

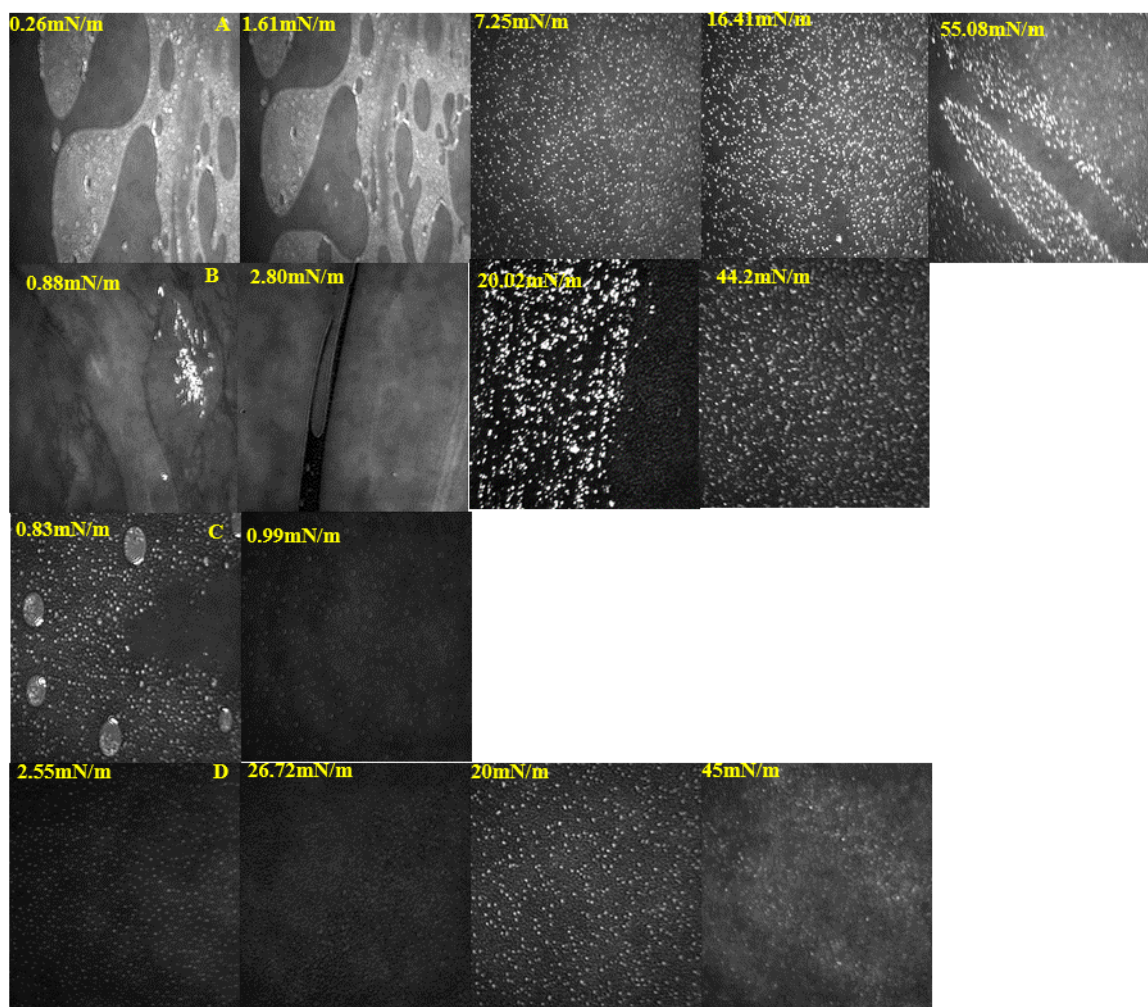


Figure 4.2 BAM images for DPPC/Cholesterol and POPC/Cholesterol monolayers treated with py-3-8 gemini surfactant or py-3-8/DNA complexes. A) DPPC/Cholesterol treated with py-3-8, B) DPPC/Cholesterol treated with py-3-8/DNA (5:1 charge ratio), C) POPC/Cholesterol treated with py-3-8, D) POPC/Cholesterol treated with py-3-8/DNA (5:1 charge ratio)

Pyrene-3-12 acts in the same way as pyrene-3-8 when it is spread on the surface of the trough, it cannot be compressed to form a monolayer (due to its solubility) and does not give an isotherm. When pyrene-3-12 was added to the sub-phase in the presence of DPPC-Cholesterol, the isotherm and compressibility modulus plots are very similar to that for the pure DPPC-Chol monolayer, although for the isotherm, it again has been shifted to much higher molecular areas (Figures 4.3A and B). The DPPC-Chol monolayer is predominantly found in the LC phase over most surface pressures, ranging from $\sim 10 - 40$ mN/m, as observed from the compressibility

modulus (Figure 4.3B). Interestingly, as noted above, when treated with py-3-12, the $\pi - A$ isotherm for the monolayer shifts to higher molecular areas, which suggests an expansion of the monolayer; however, the compressibility modulus over the same surface pressure range ($\sim 10 - 30$ mN/m) clearly indicates that the monolayer enters a solid phase in the presence of the py-3-12. The surfactant is clearly becoming incorporated into the DPPC/Cholesterol monolayer, and appears to enhance the rigidity of the monolayer, possibly by occupying gaps between DPPC and cholesterol. The C_s^{-1} value at 30 mN/m showed increase in the compressibility modulus from 255 mN/m for DPPC-Cholesterol alone to 332 mN/m when treated with pyr-3-12, and a slight decrease at 35 mN/m from 274.6 mN/m to 243.35 mN/m for pyrene-3-12/DPPC-Cholesterol system. This suggests that the system is becoming more rigid upon the addition of py-3-12 despite the increase in the lift-off area from 61.6 \AA^2 to 150 \AA^2 , which is higher than all of the DPPC-Cholesterol monolayers with pyrene-3-8 and DNA. The A_∞ value for this system is 130 \AA^2 (compared to 75 \AA^2 for the untreated DPPC/Chol monolayer), indicative of the monolayer becoming more elastic due to incorporation of the py-3-12 molecules into the monolayer. Despite the incorporation of the pyrene-3-12 molecules in the monolayer, due to the unique structure of this surfactant in particular, whether for its bulkiness (the presence of pyrene and the presence of the dodecyl tail), or for symmetrical behavior (as described previously in chapter III), it appears to fit much better into the DPPC-Chol monolayer as compared to pyr-3-8. Because of the larger area occupied by the py-3-12 at the interface (as compared to either DPPC or cholesterol, this would lead to the observed increase in the lift-off area and the limiting area, giving rise to a false indication of fluidity of the monolayer. It is much more likely that the increased rigidity indicated by the compressibility modulus more accurately reflects the structure of the DPPC-Chol monolayer upon treatment by py-3-12.

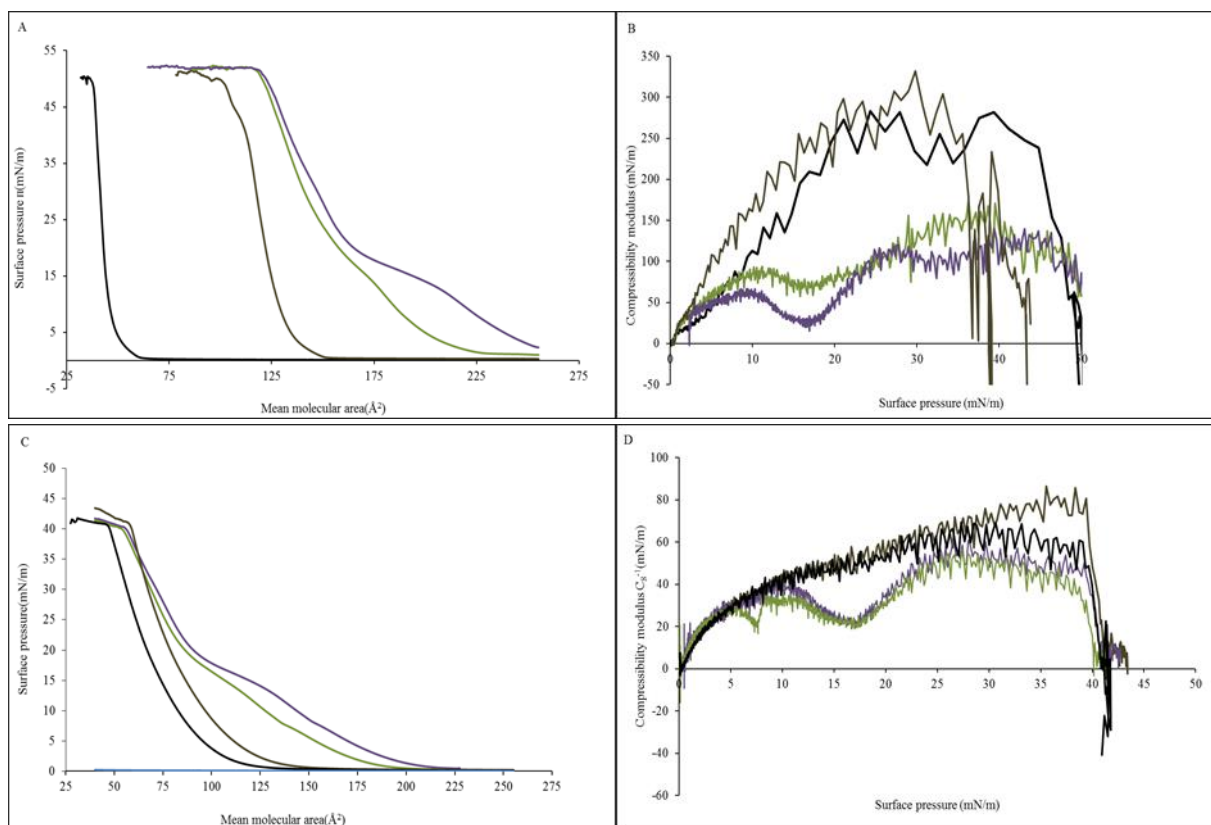


Figure 4.3 Compression isotherms (π -A) for A) DPPC/Cholesterol (75%/25%, black line) and C) POPC/Cholesterol (75%/25%, black line) monolayers treated with: pyrene-3-12 (grey), py-3-12:DNA at a 10:1 charge ratio (green), py3-12:DNA at a 5:1 charge ratio (Purple). Compressibility modulus (C_s^{-1}) as a function of surface pressure (π) for B) DPPC/Cholesterol and D) POPC/Cholesterol (75%/25%, black line) were calculated according to Equation 4.1; the line colors correspond to the same treatments described for A) and C).

Upon the addition of DNA to the sub-phase containing pyr-3-12, as observed for the py-3-8 systems, the presence of several new phases can be observed in the monolayer both in the π – A isotherms (Figure 4.4) and the compressibility modulus (Figure 4.2B). A key difference between the py-3-8 and py-3-12 systems is that for the py-3-8 systems, the addition of DNA had little effect on the observed lift off areas (98\AA^2 vs. 100\AA^2 or 108\AA^2). For the py-3-12 systems, the addition of DNA results in a much more dramatic shift of the isotherms, giving rise to correspondingly larger lift off areas, i.e. 225\AA^2 , and 245\AA^2 in the presence of DNA at 10:1 and 5:1 charge ratios, respectively, vs. 150\AA^2 in the absence of DNA. The phases formed for the py-3-12/DNA treated DPPC-Chol monolayers are similar to those for the py-3-8/DNA treated

monolayers; however, the transitions are much sharper, and much clearer evidence of the LE, LE-LC coexistence, and LC phase can be observed. Again, the impact of added DNA is much stronger for the 5:1 charge ratio, as compared to the 10:1 charge ratio, due to the increased concentration of DNA.

While the addition of py-3-12 had a much greater impact on the DPPC-Chol monolayer as compared to the POPC monolayer (Figure 4.3A vs 4.1A), the reverse is true for the POPC-Chol monolayers, where py-3-12 appears to have less of an effect on these membranes (Figure 4.3C vs 4.1C). The isotherm for the pyrene-3-12 treated POPC-Cholesterol monolayer is essentially the same shape as that for POPC-Cholesterol alone; with the exception of a small shift to higher molecular area, giving rise to a slightly larger lift off area (145\AA^2 vs 121\AA^2 , Table 4.1) (see Figures 4.3C and 4.3D). The similarity of the compressibility modulus plot confirms this observation (Figure 4.3D). As for the DPPC-Chol monolayer, the addition of DNA to py-3-12 again resulted in substantially more disruption to the POPC-Chol monolayer, as compared to the addition of py-3-12 alone. The same LE and LE-LC coexistence phases are observed; however, the compressibility modulus clearly indicates that the POPC-Chol monolayer (Figure 4.3D and Table 4.1) never enters a true LC phase. These results suggest the py-3-12 is more disruptive to the disease model (POPC-Chol) membranes and a much greater potential for the py-3-12 surfactant as a transfection vector.

From the BAM images (see Figure 4.4) for the DPPC/Chol monolayer in the presence of py-3-12, very different domains are observed compared to that seen for the py-3-8 surfactant, which likely arises from the decreased solubility of the py-3-12 surfactant in the bulk and an increased affinity for the interface. Circular and irregular bright domains are observed consistent with the transition from G to LE phase. As the surface pressure increases, the monolayer transitions from LE to the LE-LC and eventually the LC phase the monolayer becomes more compact as the domains become densely packed, and small bright domains are again observed.

As the monolayer finally transitions into the S phase no distinctive domains can be seen, which is suggestive of the homogeneity of the monolayer, and thus the increase of the rigidity of the system.

As the DNA is added to the sub-phase of the pyrene-3-12 full system, irregular bright domains are observed, and as the surface pressure increases, the net-work like domains of DPPC-Cholesterol are seen with bright circular (dots) domains found on top of these networks (within). The underlying structure of these domains could again be attributed to the adsorption of DNA at the interface, interacting with py-3-12 within the monolayer, although in this case, the linear structure seen for py-3-8/DNA and DPPC/Chol (Figure 4.2B at 20 mN/m) is not observed. As surface pressure continues to increase, these irregular structure persist, and suggest a much stronger interaction with DNA at the interface; however the nature of this interaction is still somewhat unclear. For the POPC/Cholesterol monolayers in the presence of py-3-12 or py-3-12/DNA, the BAM images were quite similar to those observed for POPC/Chol with py-3-8 or py-3-8/DNA (Figure 4.4C). A grey homogeneous background is generally observed, again with small bright domains distributed uniformly throughout. The irregular structure seen in the presence of py-3-12:DNA for the DPPC/Chol system is NOT observed with POPC/Chol, suggesting that the composition of the monolayer itself (namely DPPC) is important in defining the interaction(s) that occur at the interface, and that POPC, possibly due to its non-symmetric tails, is better able to accommodate the disruptive effect that the large DNA molecules have on the monolayer structure.

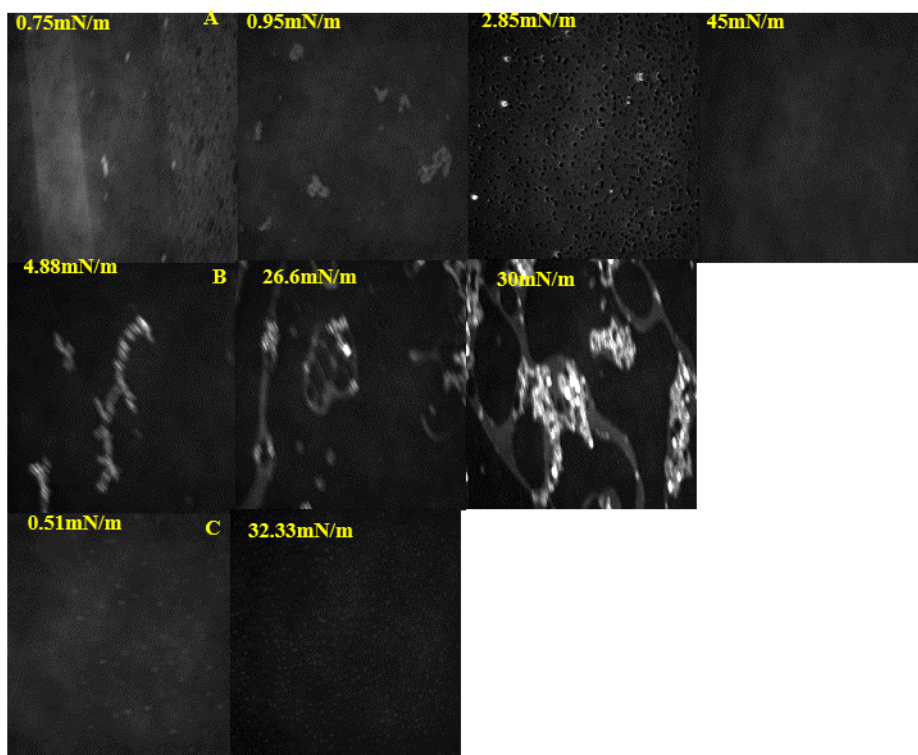


Figure 4.4 BAM images for DPPC/Cholesterol and POPC/Cholesterol monolayers treated with py-3-12 gemini surfactant or py-3-12/DNA complexes. A) DPPC/Cholesterol treated with py-3-12, B) DPPC/Cholesterol treated with py-3-12/DNA (5:1 charge ratio), C) POPC/Cholesterol treated with py-3-12, D) POPC/Cholesterol treated with py-3-12/DNA (5:1 charge ratio)

The π -A isotherm for the DPPC/Cholesterol monolayer in the presence of py-3-14 is shown in Figure 4.5A. As seen for the py-3-12 surfactant, the addition of py-3-14 shifts the isotherm to higher molecular areas, although not as high as for py-3-12, in fact the isotherms are more similar to those seen in the presence of py-3-8. The lift off area in the presence of py-3-14 is 103 \AA^2 compared to 150 \AA^2 observed in the presence of py-3-12 and the 98 \AA^2 seen in the presence of py-3-8, again suggesting that the effect of py3-14 is similar to that for py-3-8. The cross-sectional areas also show the same trend (Table 4.1). Three phases can be observed in the compressibility modulus plot; the LE phase seen at very low surface pressures (0 to 2 mN/m), a very long LE-LC phase at surface pressures up $\sim 15 - 20 \text{ mN/m}$ and finally an LC phase that extends up to the point of collapse at surface pressures above 20 mN/m. The compressibility modulus decreases from 255.2mN/m for DPPC-Cholesterol monolayer alone

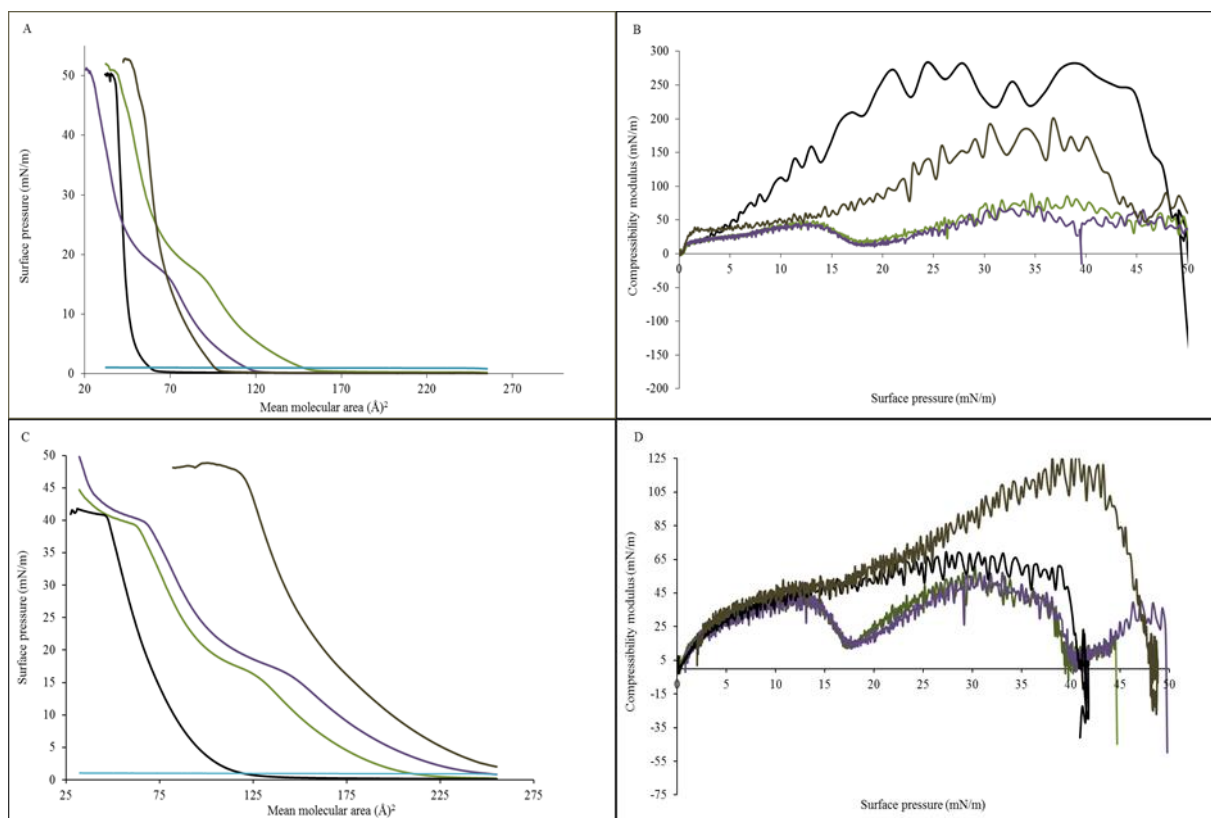


Figure 4.5 Compression isotherms (π -A) for A) DPPC/Cholesterol (75%/25%, black line) and C) POPC/Cholesterol (75%/25%, black line) monolayers treated with: pyrene-3-14 (grey), py-3-14:DNA at a 10:1 charge ratio (green), py3-14:DNA at a 5:1 charge ratio (Purple). Compressibility modulus (C_s^{-1}) as a function of surface pressure (π) for B) DPPC/Cholesterol and D) POPC/Cholesterol (75%/25%, black line) were calculated according to Equation 4.1; the line colors correspond to the same treatments described for A) and C).

to 143mN/m for pyrene-3-14/DPPC-Cholesterol monolayer around surface pressure of 30mN/m, and another decrease around surface pressure of 35mN/m (from 274.6mN/m to 174.96mN/m), again comparable to the effect of py-3-8. As for py-3-8, it would seem, based upon the isotherms alone, that py-3-14 also does not appear to strongly interact with the DPPC/Chol monolayer, and despite the apparent increase in hydrophobicity, py-3-14 prefers to form micelles rather than incorporate into the monolayer as py-3-12 does. The BAM images obtained for the DPPC/Chol monolayer treated with py-3-14 are consistent with this interpretation, although the size of the bright domains observed at a surface pressure of \sim 35 mN/m (Figure 4.6A) is increased relative to lower surface pressures, indicating some incorporation of py-3-14 into the monolayer.

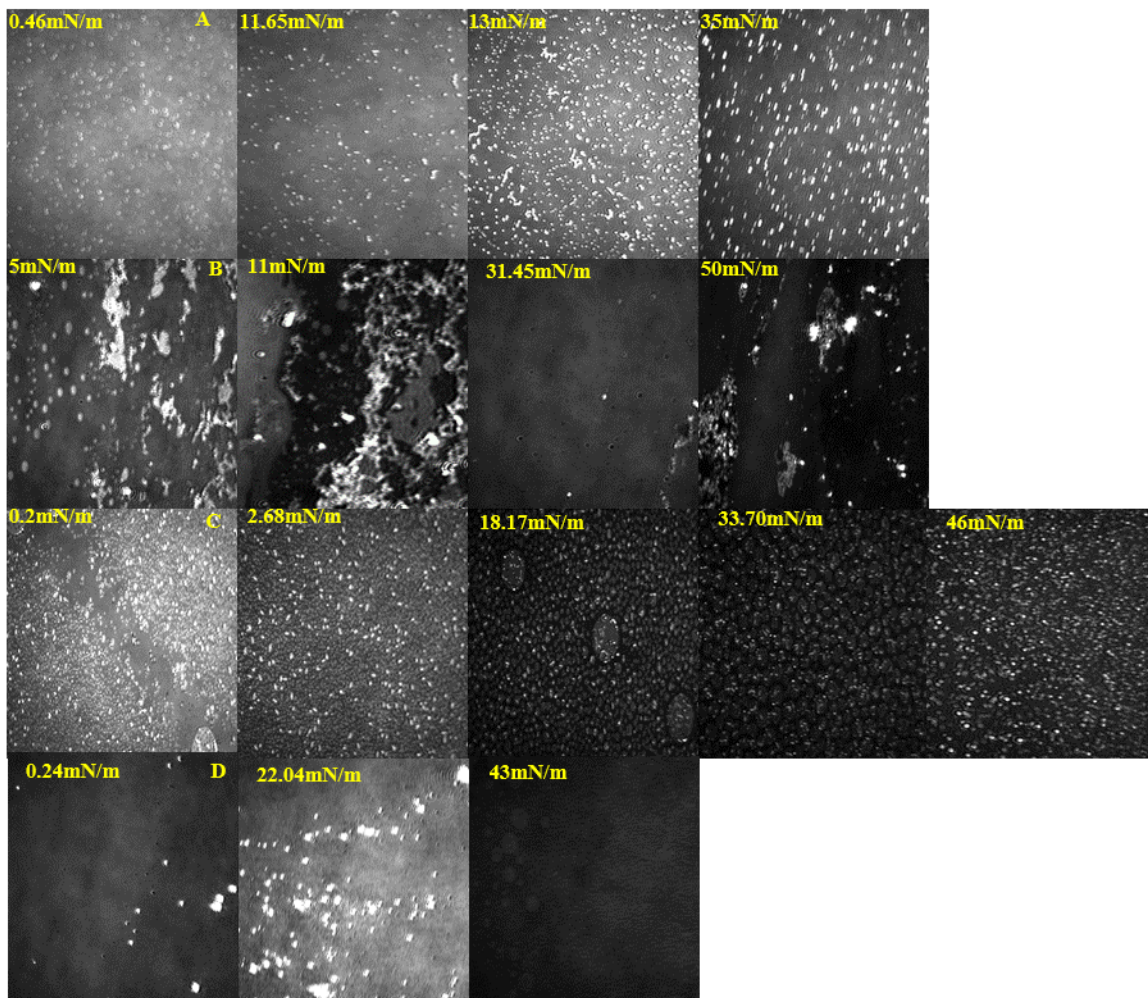


Figure 4.6 BAM images for DPPC/Cholesterol and POPC/Cholesterol monolayers treated with py-3-14 gemini surfactant or py-3-14/DNA complexes. A) DPPC/Cholesterol treated with py-3-14, B) DPPC/Cholesterol treated with py-3-14/DNA (5:1 charge ratio), C) POPC/Cholesterol treated with py-3-14, D) POPC/Cholesterol treated with py-3-14/DNA (5:1 charge ratio)

When DNA is with py-3-14 in the sub-phase, the LE, LE-LC coexistence and LC phase are again clearly observed in the DPPC/Chol monolayer (Figure 4.5A). The behaviour again appears to mirror that for the py-3-8, with small differences in the magnitudes of the molecular areas. The py-3-14/DNA has a substantial disruptive effect on the structure of the monolayer, confirmed by the low compressibility modulus values seen in Figure 4.5B and Table 4.1. This large disruptive effect is additionally confirmed from the BAM images for the monolayer treated

with py3-14:DNA. As shown in Figure 4.6B, regardless of surface pressure, large networks of aggregates are observed, the assembly of which is most likely due to the interaction of the py-3-14:DNA complexes at the interface. The monolayer appears to be somewhat more uniform at a surface pressure of ~ 31 mN/m; however networked aggregates are still observed (lower right corner of the image at 31 mN/m in Figure 4.6B) as are dark, pinhole defects that correspond to holes in the monolayer.

The presence of pyr-3-14 in the sub-phase of POPC/Cholesterol monolayer shifts the $\pi - A$ isotherm to higher molecular areas (Figure 4.5C), also shown by the increase in the various area properties derived from the isotherm (see Table 4.1), although the monolayer remains essentially featureless. The compressibility modulus shows that the monolayer remains in an LE phase over a wide range of surface pressures ($\sim 2 - 20$ mN/m); however it eventually enters and LC phase, with the py-3-14 increasing the compressibility modulus of the system, both at 30mN/m, and 35mN/m ($C_S^{-1}_{30} = 90$ mN/m, and $C_S^{-1}_{35} = 108$ mN/m), increasing the rigidity of the POPC/Chol monolayer, likely due to integration of py-3-14 into the monolayer as a result of the hydrophobicity of the surfactant. The BAM images (Figure 4.6 C) clearly show a change in the nature of the small bright domains with the monolayer becoming densely packed with a high abundance of the bright circular domains that seem to be growing in shape; this is consistent with incorporation of py-3-14 into the monolayer and the transition of the monolayer into the LC phase (Figure 4.6C, image at $\pi \sim 18$ mN/m). As the surface pressure continues to increase the small bright domains appear to be clustered on larger, grey circular domains that grow in size with further increases in π . This highly ordered monolayer is consistent with the above discussion where the py-3-14 appears to increase the rigidity of the POPC/Chol monolayer. Upon addition of DNA (regardless of charge ratio), a significant disruption of the monolayer is again observed, greater than that observed with the DPPC/Chol monolayer, described above (see Figure 4.5C and D, as well as Table 4.1). Multiple phases are observed in both the isotherm

(Figure 4.5C) and the compressibility modulus (Figure 4.5D); however all these were appearing in the LE or LE-LC coexistence region, again indicative of extensive disruption upon treatment with the py-3-14/DNA complexes. This can also be observed from the BAM images (Figure 4.6D), which still show small bright domains; however these are very randomly dispersed throughout the monolayer at low (0.24 mN/m) and intermediate (22 mN/m) surface pressures.

The addition of py-3-16 or py-3-18 to the DPPC/Chol monolayer has very similar effects. Small increases in A_L , A_∞ , and A_c are observed, with the increase being larger for py-3-16, compared to py-3-18 (Table 4.1). The shapes of the $\pi - A$ isotherms are also quite similar, with both suggesting a decrease in the order of the monolayer (Figures 4.7A and 4.8A) that the compressibility modulus indicates is an LE-LC transition phase (Figures 4.7B and 4.8B). Again, as observed for py-3-8, the isotherms do not suggest a strong interaction on their own; however the impact is much more evident by looking at the magnitude of the reduction in C_s^{-1} (or C_s^{-1}) from 250 mN/m for the DPPC/Chol monolayer to 78 mN/m for py-3-16 and 104 mN/m for py-3-18 (Table 4.1). BAM images of the DPPC/Chol monolayer treated with py-3-16 (Figure 4.9A) or py-3-18 (Figure 4.10A) are again consistent with this interpretation, with the same types of domains being observed (at surface pressures associated with a given phase) as previously described for py-3-14.

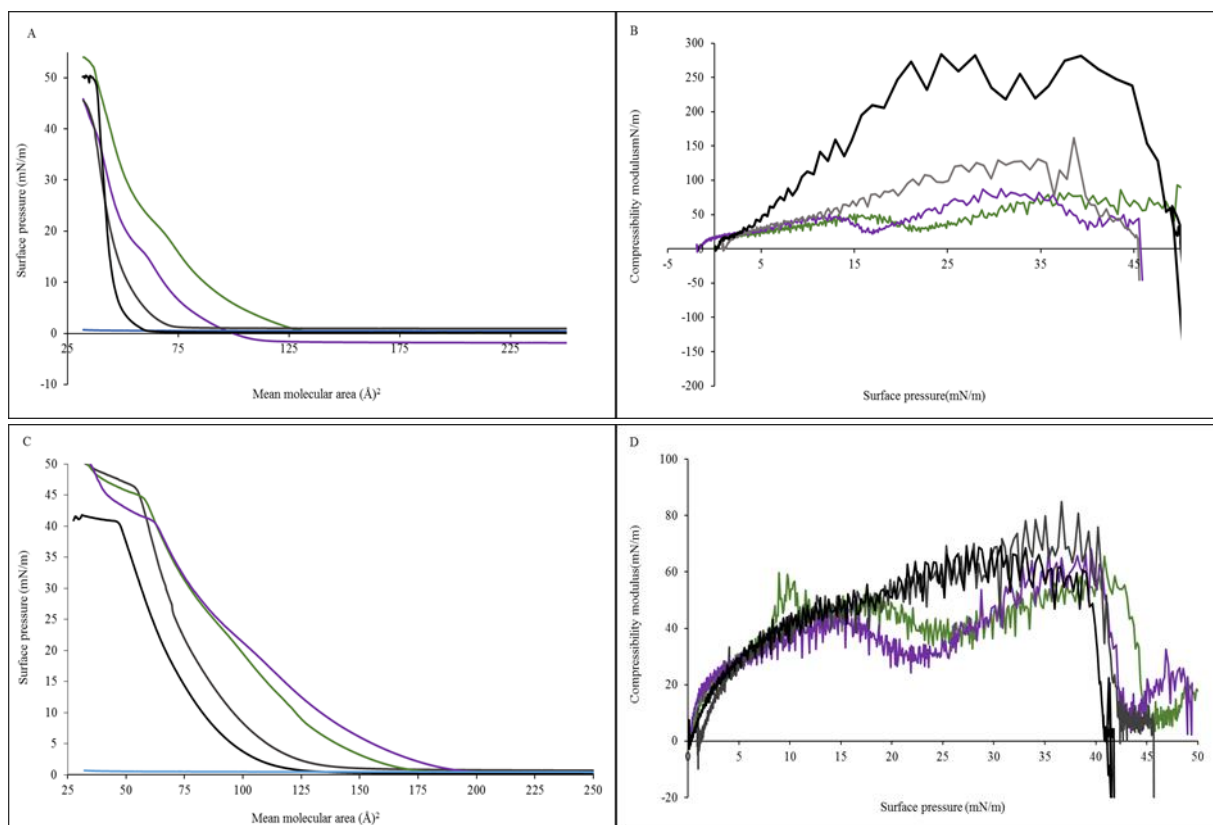


Figure 4.7 Compression isotherms (π -A) for A) DPPC/Cholesterol (75%/25%, black line) and C) POPC/Cholesterol (75%/25%, black line) monolayers treated with: pyrene-3-16 (grey), py-3-16:DNA at a 10:1 charge ratio (green), py3-16:DNA at a 5:1 charge ratio (Purple). Compressibility modulus (C_S^{-1}) as a function of surface pressure (π) for B) DPPC/Cholesterol and D) POPC/Cholesterol (75%/25%, black line) were calculated according to Equation 4.1; the line colors correspond to the same treatments described for A) and C).

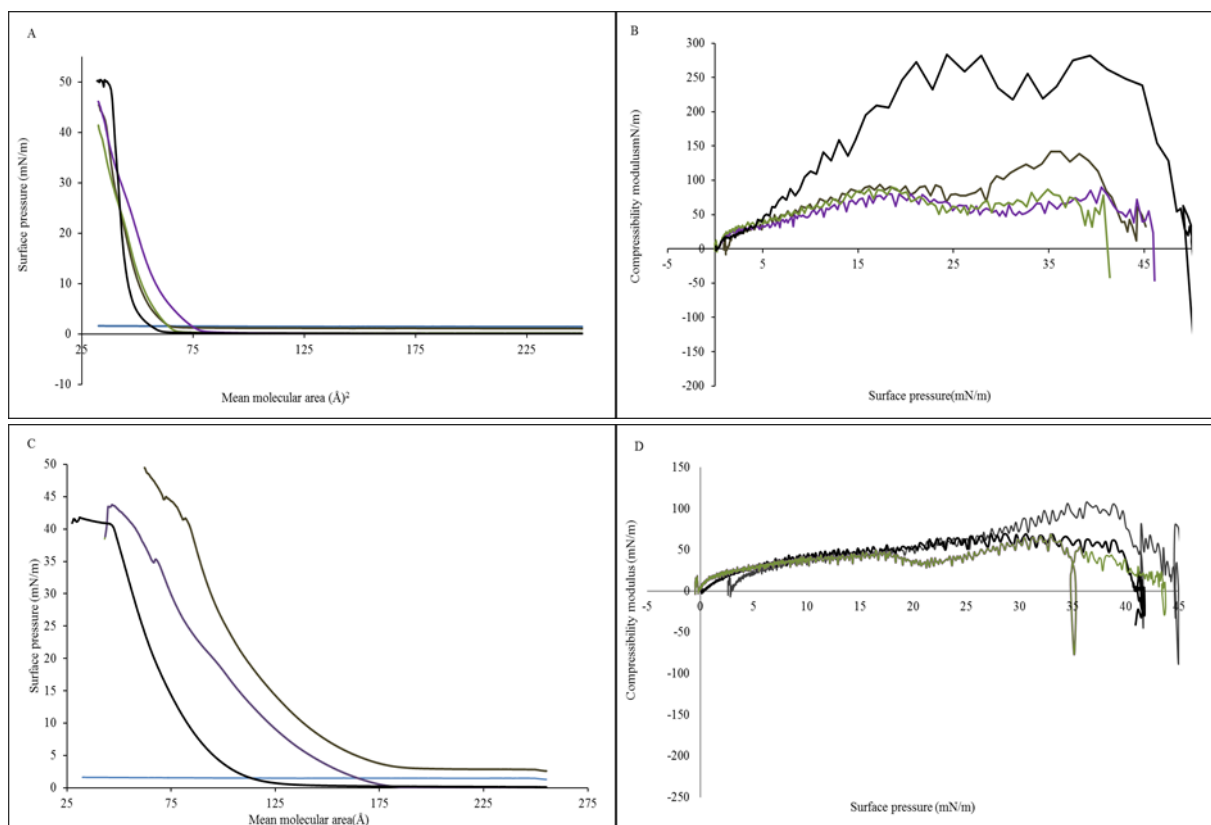


Figure 4.8 Compression isotherms (π -A) for A) DPPC/Cholesterol (75%/25%, black line) and C) POPC/Cholesterol (75%/25%, black line) monolayers treated with: pyrene-3-18 (grey), py-3-18:DNA at a 10:1 charge ratio (green), py3-18:DNA at a 5:1 charge ratio (Purple). Compressibility modulus (C_S^{-1}) as a function of surface pressure (π) for B) DPPC/Cholesterol and D) POPC/Cholesterol (75%/25%, black line) were calculated according to Equation 4.1; the line colors correspond to the same treatments described for A) and C)

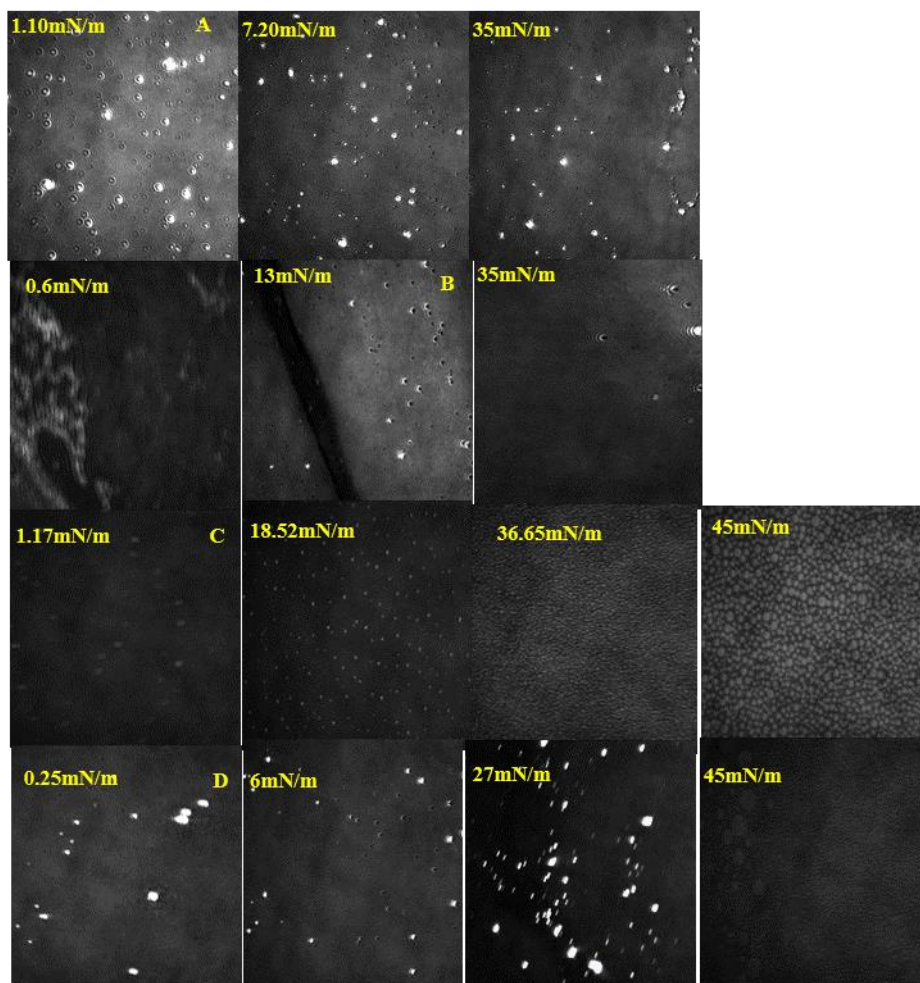


Figure 4.9 BAM images for DPPC/Cholesterol and POPC/Cholesterol monolayers treated with py-3-16 gemini surfactant or py-3-16/DNA complexes. A) DPPC/Cholesterol treated with py-3-16, B) DPPC/Cholesterol treated with py-3-16/DNA (5:1 charge ratio), C) POPC/Cholesterol treated with py-3-16, D) POPC/Cholesterol treated with py-3-16/DNA (5:1 charge ratio)

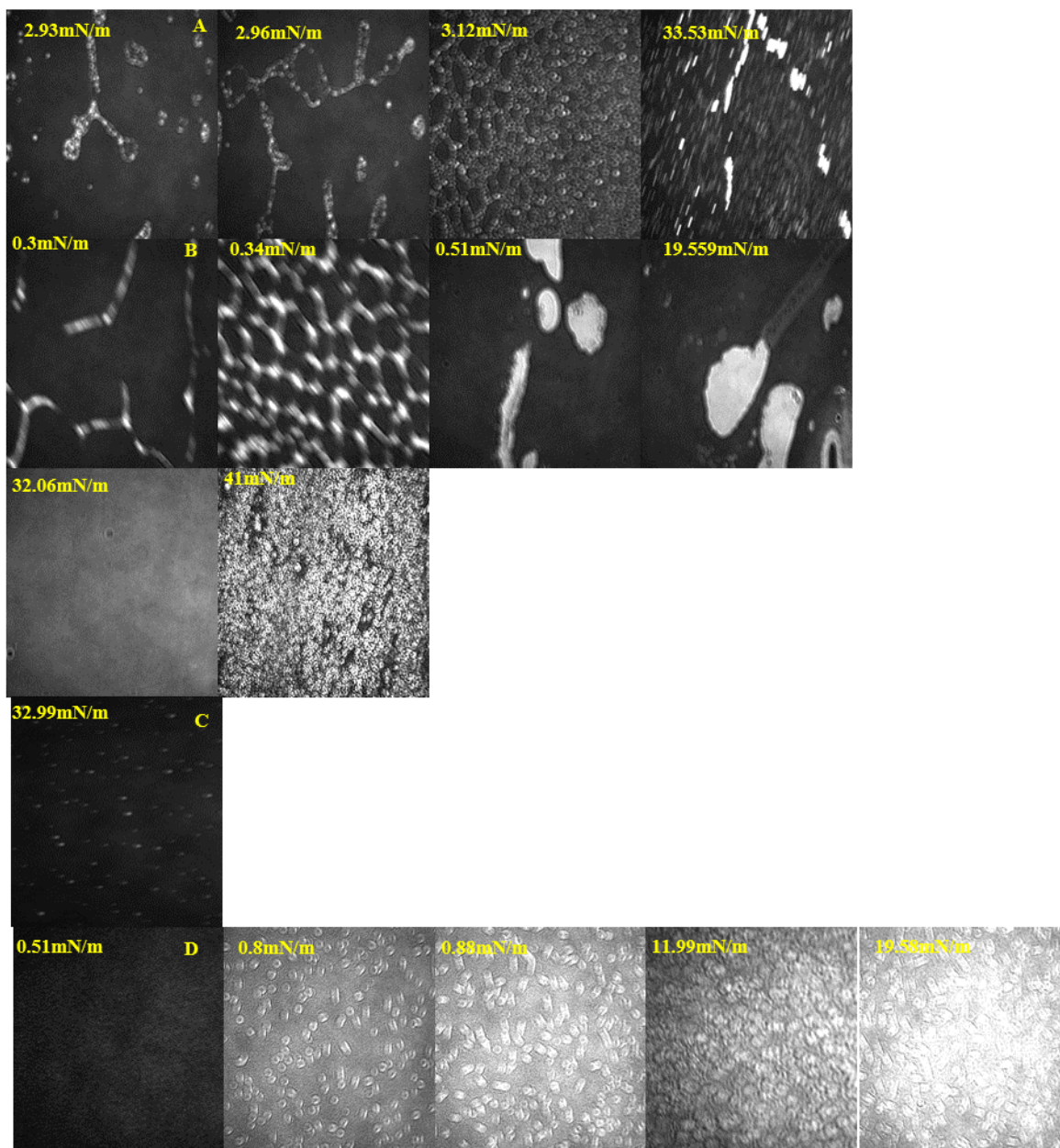


Figure 4.10 BAM images for DPPC/Cholesterol and POPC/Cholesterol monolayers treated with py-3-18 gemini surfactant or py-3-18/DNA complexes. A) DPPC/Cholesterol treated with py-3-18, B) DPPC/Cholesterol treated with py-3-18/DNA (5:1 charge ratio), C) POPC/Cholesterol treated with py-3-18, D) POPC/Cholesterol treated with py-3-18/DNA (5:1 charge ratio)

Upon the addition of DNA (regardless of charge ratio) to either pyr-3-16 or py-3-18, the effects on the DPPC/Chol monolayer are again very similar for the two surfactants. For both surfactant:DNA systems, the monolayer is predominantly in the LE phase, although the slight inflection observed in the $\pi - A$ isotherm (Figure 4.7A or 4.8A) and the valley observed in the

compressibility modulus (Figure 4.7B or 4.8B), clearly indicate a coexistence LE-LC phase at higher surface pressures (above 15 to 20 mN/m). In our studies, the surfactants having the highest transfection efficiency in OVCAR-3 cells were 16-3-16, which was previously shown by the group to be efficient not only in *in vitro* transfection, but also as an *in vivo* topical transfection vector in a mouse study;²²⁵ and phytanyl-3-16, which gave even greater transfection efficiency (*in vitro*) than 16-3-16.¹⁰⁵ This efficacy may have resulted from the ability of both 16-3-16 and phy-3-16 to form vesicle like micelles in the absence of DNA, and may trigger the formation of high order structures once the DNA is added to it, including inverted micelles, and cubic structures, which have been linked to improved transfection efficiency.⁷¹ When 16-3-16 was added to a DPPC/Cholesterol monolayer, it was not as efficient in reducing the compressibility modulus as pyr-3-16 was ($C_S^{-1}_{30} = 131$ mN/m and $C_S^{-1}_{35} = 105$ mN/m for the 16-3-16 surfactant; unpublished data). Based upon this observation, our monolayer study suggests that the presence of the bulky pyrenyl moiety impacts the structure of the monolayers, and possibly corresponding cellular membranes, to a greater extent than a second hexadecyl tail would; however, this will be examined with transfection studies for the py-3-m surfactants, in Chapter V of this thesis. The BAM images are again consistent with the above interpretation of the isotherms and compressibility modulus plots; interestingly at low surface pressures, the BAM images for py-3-18 show an extensive network of bright, almost linear domains, even in the absence of DNA (Figure 4.10A and 4.10B). Given the overall length of the alkyl hydrophobic tail for this surfactant in particular, it may be the case that it prefers to form threadlike aggregates, consistent with the threadlike micelles observed for long-chain symmetric gemini surfactants such as the 18-3-18 surfactant.¹⁰¹

For the POPC/Cholesterol monolayers, the addition of either py-3-16 OR py-3-18 to the sub-phase again (as seen for py-3-14) creates a more rigid monolayer, as evidenced by the increases seen in the compressibility modulus values (Table 4.1). Again consistent with the

previous discussion for py-3-14, this is in contrast to the increases in lift-off and cross-sectional areas, which both are observed to increase for the monolayer in the presence of either py-3-16 or py-3-18. The BAM images for the POPC/Chol monolayers treated by either py-3-16 (Figure 4.9C) or py-3-18 (Figure 4.10C) again show evidence of the incorporation of the surfactant into the monolayer structure (particularly in Figure 4.9C), consistent with the increase in rigidity. Based upon the results obtained for ALL of the py-3-m surfactants, the increases in the various area values (Table 4.1) for the POPC/Chol monolayers, are attributed to the greater area occupied by the py-3-m head groups at the air/water interface. As these area values represent an average value for monolayers comprised of more than one type of molecule, and given that the variations in the area values are only modest in going from py-3-14 to py-3-16 to py-3-18, this interpretation is quite consistent with our results. The differences seen for py-3-8 and py-3-12 again relate to their molecular structure; with a lower hydrophobicity, py-3-8 is less likely to prefer the bulk monolayer as opposed to the interface, resulting in these molecules occupying a greater area at the interface. Py-3-12, being almost symmetrical with respect to the length of the alky tails, also occupies a large area at the interface. As the hydrophobicity of the surfactant continues to increase, the tails become increasingly compatible with the POPC or cholesterol tails, effectively decreasing the area occupied by the surfactant at the interface.

As for py-3-14, the addition of py3-16:DNA or py-3-18:DNA (at either 5:1 or 10:1) charge ratio causes fluidization of the POPC/Chol monolayer, as shown by the inflections in the π -A isotherms (Figures 4.7C or 4.8C) and the low values for the compressibility modulus (Figures 4.7D or 4.8D and Table 4.1). These monolayers are again mostly found in an LE phase, with evidence of an LE-LC coexistence phase at higher surface pressures. The BAM images for these systems (Figure 4.9D or 4.10D) are again consistent with this observation.

To summarize the effect of the pyrenyl gemini surfactants on the two model membranes; these surfactants, on their own (i.e. in the absence of added DNA) generally fluidize the DPPC-

Chol monolayers (representative of the “normal” cell membrane) and increase the rigidity of the POPC-Chol monolayers (representative of a “diseased” membrane. For the DPPC-Chol monolayers, the longer the alkyl tail (m) in the py-3-m surfactant, the greater the apparent fluidization; with the exception of py-3-12 which acted in an opposite fashion compared to the other surfactants for both the DPPC/Chol and the POPC/Chol monolayers. This is attributed to peculiar structural properties of the surfactant, which makes it closely resemble the symmetrical surfactants more than the dissymmetrical ones (the pyrene moiety adds to the volume of the surfactants, but not to the length). DNA increased the fluidization effect of py-3-m surfactants on the DPPC-Cholesterol monolayer. Pyrenyl gemini surfactants increased the compressibility moduli of the POPC-Cholesterol monolayer, when added to the sub-phase. All of the pyrene-based surfactants integrated into the POPC-Cholesterol monolayer, irrelevant of the alkyl tail length. Addition of DNA to the py-3-m surfactants induces a fluidization of the POPC/chol monolayer, although possibly not to the same extent as seen for the DPPC/Chol monolayers where the addition of DNA resulted in extensive reorganization of the monolayer, as observed from the BAM images. Given that escape from endosomes is one of the critical stages of DNA transfection, the ability of the surfactant to incorporate into and/or fluidize these membranes is essential. Based upon our results, the py-3-m surfactants are clearly capable of doing so and hold excellent promise as DNA transfection vectors.

4.4.2 Langmuir monolayer studies of dissymmetric gemini surfactants (12-3-n)

When 12-3-14 gemini surfactant is spread on the sub-phase as a monolayer, it dissolves into the sub-phase with the surface pressure remaining constant, and an isotherm is never formed, as observed for the py-3-m surfactants. The 12-3-n surfactants are more soluble than the py-3-m surfactants and so compression again forces the molecules from the interface into micelles within the bulk aqueous phase. The situation again changes as the 12-3-14 is added to the sub-phase

with DPPC-Cholesterol as the monolayer. The isotherm rises with a lift-off area of 50 \AA^2 , and a cross sectional (A_∞) area similar to that of DPPC-Cholesterol system alone (44 \AA^2 vs 45 \AA^2 in the presence of 12-3-14; see Table 4.2 and Figure 4.11A). As the surface pressure increases, the compressibility modulus decreases from 250 mN/m to 127 mN/m at 30 mN/m , and from 274 mN/m to 121 mN/m at 35 mN/m , which is suggestive of strong interaction(s) between the 12-3-14 molecules and the monolayer, resulting in increasing fluidity of the monolayer. From the BAM images (Figure 4.12A) the addition of 12-3-14 results in a network of narrow, bright domains; however, these domains look different from those found in the DPPC-Cholesterol system alone, and suggest that some of the surfactant may be locating at domain boundaries. As the surface pressure is increased, the bright circular domains, and at higher pressures clusters of these domains, are observed, consistent with previous observations for the py-3-m surfactants described above. At 14 mN/m , all these distinct domains disappear and only a homogenous monolayer can be observed. This is an indication of higher compression and the transition from LE to LE-LC phase.

Once the DNA is added to 12-3-14, substantial disruption to the monolayer is evident from the $\pi - A$ isotherms, which show a clear LE phase between surface pressures of 0 to $\sim 17 \text{ mN/m}$, an LE-LC coexistence phase, and no evidence of the formation of either an LC or S phase. The strong interactions between the GS and the DNA resulted in a large increase in the lift-off area (139 \AA^2 , and 146 \AA^2 at a charge ratio of 10:1, and 5:1, respectively), suggesting extensive reorganization of the monolayer at the surface. The A_∞ for both charge ratios is 125 \AA^2 , which indicates that the monolayer is more fluid than that of DPPC-Cholesterol alone. In the compressibility modulus plot (Figure 4.11B), there is a shift from LE to LE-LC phase around 10 mN/m and it persists till the collapse. The compressibility modulus values at $\pi = 30 \text{ mN/m}$ dropped from 255 mN/m to $\sim 36 \text{ mN}$ for both charge ratios, with a similar drop for $\text{Cs}^{-1}35$ (see Table 4.2). This dramatic drop in the compressibility modulus values is indicative of the

Table 4.2 Monolayer properties for the DPPC/Chol (75/25) and POPC/Chol (75/25) monolayers at 20°C treated with 12-3-s or 12-3-s/DNA complexes.

System	A_L (\AA^2)	A_∞ (\AA^2)	A_C (\AA^2)	π_C (\AA^2)	C_S^{-130} (mN/m)	C_S^{-135} (mN/m)
DPPC (75%)-Cholesterol (25%)	61.1	44	36.7	50.7	255	275
POPC (75%)-Cholesterol (25%)	121	70.0	47	40.6	58±3	56±3
<i>12-3-14</i>						
12-3-14/DPPC-Chol	50.0	45.0	28.5	37.9	127	121
10:1 12-3-14-DNA/DPPC-Chol	139	125	29.8	49.5	36	78
5:1 12-3-14-DNA/DPPC-Chol	146	125	30	49	37	61
12-3-14/POPC-Chol	89.7	69	40.5	42.9	80	98
10:1 12-3-14-DNA/POPC-Chol	176	152	44.8	42.6	46	65
5:1 12-3-14-DNA/POPC-Chol	225	197	35.8	48	49	61
<i>12-3-16</i>						
12-3-16/DPPC-Chol	70.5	49.8	31	42.8	90	91
10:1 12-3-16-DNA /DPPC-Chol	165	157	38	45.0	11	28
5:1 12-3-16-DNA/DPPC-Chol	171	166	39.5	44	2	27
12-3-16/POPC-Chol	120	85	49.9	40.6	64	58
10:1 12-3-16-DNA/POPC-Chol	>225	125	35.8	48	2	42
5:1 12-3-16-DNA/POPC-Chol	>225	207.8	38	53	4	39
<i>12-3-18</i>						
12-3-18	93	93.6	52	25.0		
12-3-18/DPPC/Chol	62.9	58.3	31.7	44	59	55
10:1 12-3-18-DNA /DPPC-Chol	151	156	36.7	51	26	55
5:1 12-3-18-DNA/DPPC-Chol	151	136	46.8	45.6	35	79
12-3-18/POPC/Chol	255	250	49.9	56	63	71
10:1 12-3-18-DNA /POPC-Chol	>180	160	46.0	39	8	30
5:1 12-3-18-DNA /POPC-Chol	>180	134	47.7	39.9	19	42

fluidizing impact of the GS- DNA complex on the DPPC-Cholesterol monolayer. The BAM images (Figure 4.12B) confirm the extensive reorganization, with very disorganized domains being observed at all surface pressures. A previous study of 2,3-dimethoxy-1,4-bis(N-hexadecyl-N-N-dimethyl-ammonium)butane dibromide (SS-1; a symmetric methoxy-substituted analogue of the 16-4-16 surfactant, which we have not studied), demonstrated that the addition of DNA and SS1 condensed a pure POPC monolayer, irrelevant of the DNA/GS charge ratio.¹⁷⁶ It was noted that the impact on the monolayer structure was highly on the structure of the DNA (whether it is ss-DNA or ds-DNA), on the structure of the GS, and also on the composition of the monolayer.^{176, 226}

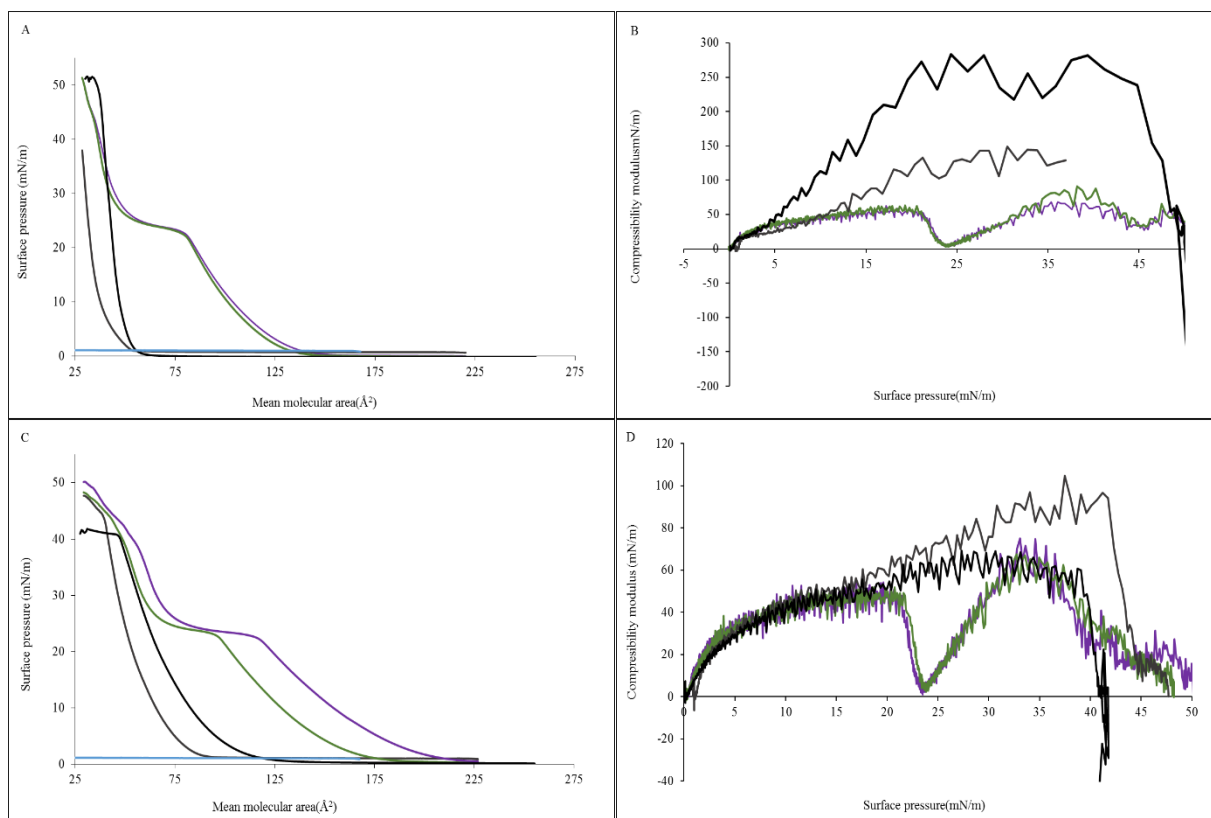


Figure 4.11 Compression isotherms (π -A) for A) DPPC/Cholesterol (75%/25%, black line) and C) POPC/Cholesterol (75%/25%, black line) monolayers treated with: 12-3-14 (grey), 12-3-14:DNA at a 10:1 charge ratio (green), 12-3-14:DNA at a 5:1 charge ratio (Purple). Compressibility modulus (C_s^{-1}) as a function of surface pressure (π) for B) DPPC/Cholesterol and D) POPC/Cholesterol (75%/25%, black line) were calculated according to Equation 4.1; the line colors correspond to the same treatments described for A) and C).

The 12-3-14 surfactant, when added to the POPC/Chol monolayer, behaves in the same way as seen for the addition of the pyrenyl surfactants to POPC/Chol monolayer, with a decrease in the lift-off area (89\AA^2), and the cross-sectional area remained more or less unchanged (69\AA^2), indicating that the GS is making the monolayer less fluid, also suggested by the shift in the isotherm to lower molecular areas (Figure 4.11C). This can also be observed from the rise in the compressibility modulus (Figure 4.11D), which at $\pi = 30\text{mN/m}$ increases from 58mN/m to 80mN/m , and at $\pi = 35\text{mN/m}$ from 55mN/m to 98mN/m . The BAM images are again consistent with this interpretation, with an increased ordering of the small bright domains seen formed within the monolayer as surface pressure is increased (Figure 4.12C). As soon as the DNA is added, the monolayer behaves quite differently, with higher lift-off areas

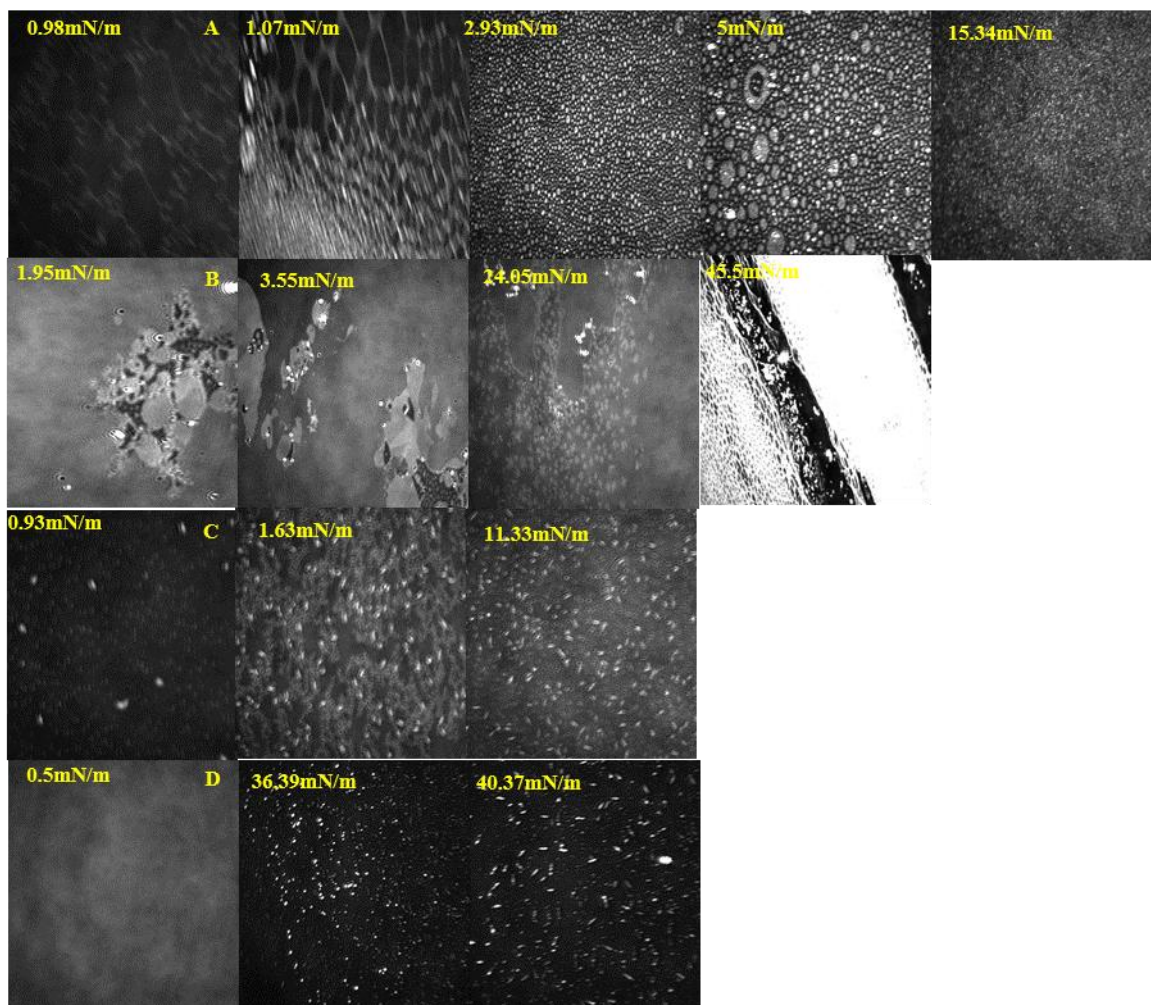


Figure 4.12 BAM images for DPPC/Cholesterol and POPC/Cholesterol monolayers treated with 12-3-14 gemini surfactant or 12-3-14/DNA complexes. A) DPPC/Cholesterol treated with 12-3-14, B) DPPC/Cholesterol treated with 12-3-14/DNA (5:1 charge ratio), C) POPC/Cholesterol treated with 12-3-14, D) POPC/Cholesterol treated with 12-3-14/DNA (5:1 charge ratio)

(from 121\AA^2 to 176\AA^2 and 255\AA^2 at 10:1 and 5:1 charge ratio, respectively), and higher cross sectional area (from 70.0\AA^2 to 152\AA^2 and 179\AA^2 at 10:1 and 5:1 charge ratio, respectively), which suggests increased fluidity of the monolayer. This fluidity confirms by the low compressibility modulus values (Figure 4.11D); C_S^{-1} drops from 58 mN/m to 46 mN/m and for the 10:1, and 5:1 charge ratios, respectively, indicating that the monolayer is in an LE phase at most surface pressures. No domains were observed at low surface pressure in the BAM images

(Figure 4.12D) and a mixture of network like domains and bright circular domains as well as the compression increases, similar to previous observations for the py-3-14 to py-3-18 surfactants.

The presence of 12-3-16 to the sub-phase for the DPPC/Chol monolayer shifts a part of the π -A isotherm to higher molecular area and part to lower molecular areas, such that it crosses over the isotherm for the pure monolayer (Figure 4.13). Effectively this means that the slope of the isotherm in the presence of 12-3-16 is less than for the absence of 12-3-16, which itself is evidence for fluidization of the monolayer by the surfactant. As the surface pressure increases, the large effect of the 12-3-16 surfactant can be observed, with a strong decrease in compressibility modulus (Figure 4.13B and Table 4.2). The compressibility modulus decreases from 255mN/m to 90mN/m at 30mN/m, and from 274mN/m to 91mN/m at 35mN/m, respectively, indicating the strong interactions between the monolayer and the GS molecules. At low surface pressure, BAM images (Figure 4.14A) show bright circular domains similar those described above, although not the network of narrow domains seen with the py-3-14 surfactant (Figure 4.12A). As the monolayer transitions into the LE phase, the BAM images show a mix of bright and dim circular domains, consistent with increased incorporation of the surfactant into the monolayer. As the surface increases further, a mixture of network like domains and circular domains are observed until a heterogeneous mix of different sized domains is observed, again consistent with increased fluidity.

As DNA is added to the DPPC-Chol monolayer in the presence of 12-3-16 in the sub-phase, extensive disruption of the monolayer occurs, clearly evident in both the isotherms (Figure 4.13A), which again show the characteristic shape indicating LE, LE-LC coexistence and LC phases, and the compressibility modulus (Figure 4.13B), which shows that instead of an LC phase, the phases seen more likely correspond to LE_A , $LE_A - LE_B$ coexistence, and LE_B phases, based on the very low compressibility modulus values observed. The interaction(s) between the DPPC/Chol monolayer and the 12-3-16:DNA complexes lead to a very large

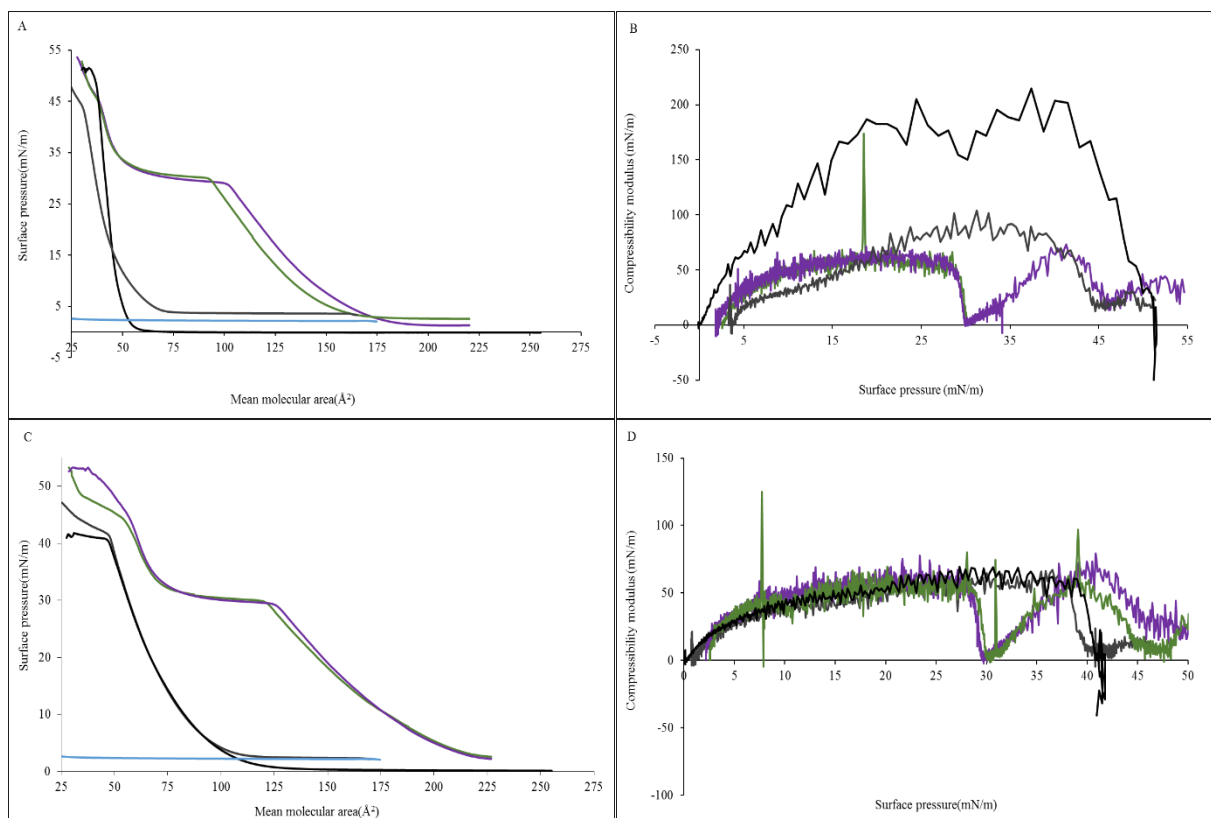


Figure 4.13 Compression isotherms (π -A) for A) DPPC/Cholesterol (75%/25%, black line) and C) POPC/Cholesterol (75%/25%, black line) monolayers treated with: 12-3-16 (grey), 12-3-16:DNA at a 10:1 charge ratio (green), 12-3-16:DNA at a 5:1 charge ratio (Purple). Compressibility modulus (C_s^{-1}) as a function of surface pressure (π) for B) DPPC/Cholesterol and D) POPC/Cholesterol (75%/25%, black line) were calculated according to Equation 4.1; the line colors correspond to the same treatments described for A) and C).

reduction in the $C_s^{-1}_{30}$ values from 255 mN/m to 11 mN/m and 2 mN/m for charge ratios of 10:1, and 5:1, respectively, and in the $C_s^{-1}_{35}$ values from 275 mN/m to 28 mN/m and 27 mN/m (Table 4.2). The deep minima observed in the compressibility modulus plots (Figure 4.13B) when the surfactant:DNA complexes are added to the system are somewhat misleading in that they result from the fact that the compressibility modulus is based upon the derivative of surface pressure as a function of molecular area (recall equation 4.1). As such, if the rate of change in the surface pressure as a function of a change in molecular area is zero, i.e. the surface pressure shows a plateau in the π - A isotherm (as we see in Figure 4.13A) then the compressibility modulus drops to zero as well. Two valleys are seen for the 12-3-16 systems

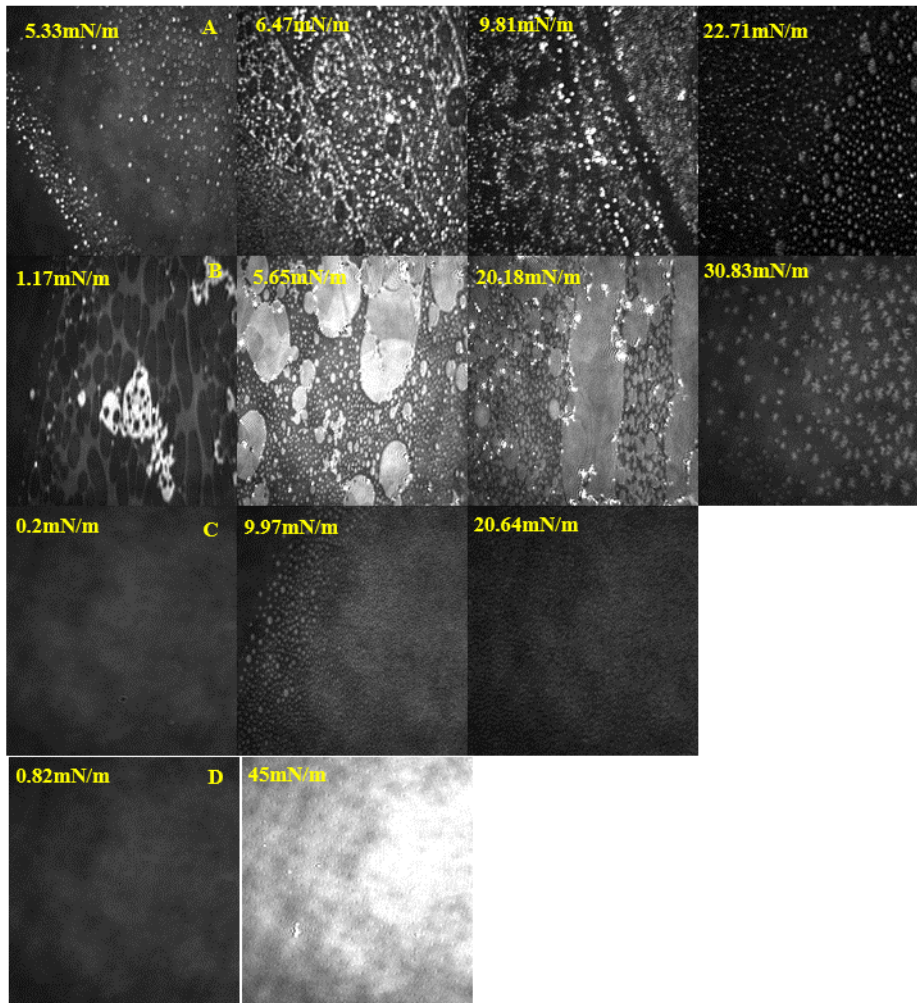


Figure 4.14 BAM images for DPPC/Cholesterol and POPC/Cholesterol monolayers treated with 12-3-16 gemini surfactant or 12-3-16/DNA complexes. A) DPPC/Cholesterol treated with 12-3-16, B) DPPC/Cholesterol treated with 12-3-16/DNA (5:1 charge ratio), C) POPC/Cholesterol treated with 12-3-16, D) POPC/Cholesterol treated with 12-3-16/DNA (5:1 charge ratio).

as a result of the large plateau at a surface pressure of ~ 30 mN/m and the small shoulder seen at ~ 45 mN/m in the isotherms for the 12-3-16:DNA systems. The BAM images of the monolayer in the presence of both 12-3-16 and DNA (Figure 4.14B) extensive disruption of the monolayer and clear evidence of multiple different phases. At a surface pressure of 30 mN/m, a mixture of both small circular, and larger “snowflake” domains can be seen, consistent with the coexistence of 2 different LE phases.

Both the π - A isotherm (Figure 4.13A) and compressibility modulus (Figure 4.14D) show that the POPC/chol monolayer appears to be unchanged by the addition of 12-3-16 to the system. A slight decrease in the lift-off area from 121\AA^2 to 120\AA^2 is seen (Table 4.2), while a slight increase in cross-sectional area from 70\AA^2 to 85\AA^2 is observed. This could suggest some minimal insertion of the 12-3-16 surfactant into the monolayer, but may also simply be within the experimental error of the system. The BAM images (Figure 4.14C) for POPC/Chol treated with 12-3-16 also show no evidence of reorganization within the monolayer, again suggesting little to no interaction.

POPC/Cholesterol monolayers treated with the 12-3-16:DNA complexes, at either 10:1 or 5:1 charge ratios, again resulted in extensive fluidization of the monolayer, as seen from both the isotherms (Figure 4.13C) and compressibility modulus (Figure 4.13C). As for the 12-3-14:DNA systems, multiple phases are observed for the 12-3-16:DNA complexes, that appear to be different LE phases based upon the low values seen for the compressibility modulus (Table 4.2). The BAM images obtained for these systems again show a relatively featureless monolayer at low surface pressures, and the same pattern of small bright domains at high surface pressures, again consistent with the phases inferred from the isotherms and compressibility modulus as described above.

In contrast to all of the surfactants previously discussed (i.e., 5 py-3-m surfactants plus 12-3-14 and 12-3-16) the 12-3-18 gemini surfactant is the only surfactant investigated that is able to form a monolayer at the air-water interface. When spread as a monolayer, it forms a monolayer that collapses at a relatively low surface pressure of ~ 25 mN/m, although it may be the case that this “collapse” actually represents a coexistence phase and that the true collapse occurs at a molecular area of 0, which is a clear indication that molecules are being forced from the monolayer into the bulk aqueous phase to form micelles (Figure 4.15A). Because of this, the molecular areas (Table 4.2) determined from the isotherm are somewhat artificial; however,

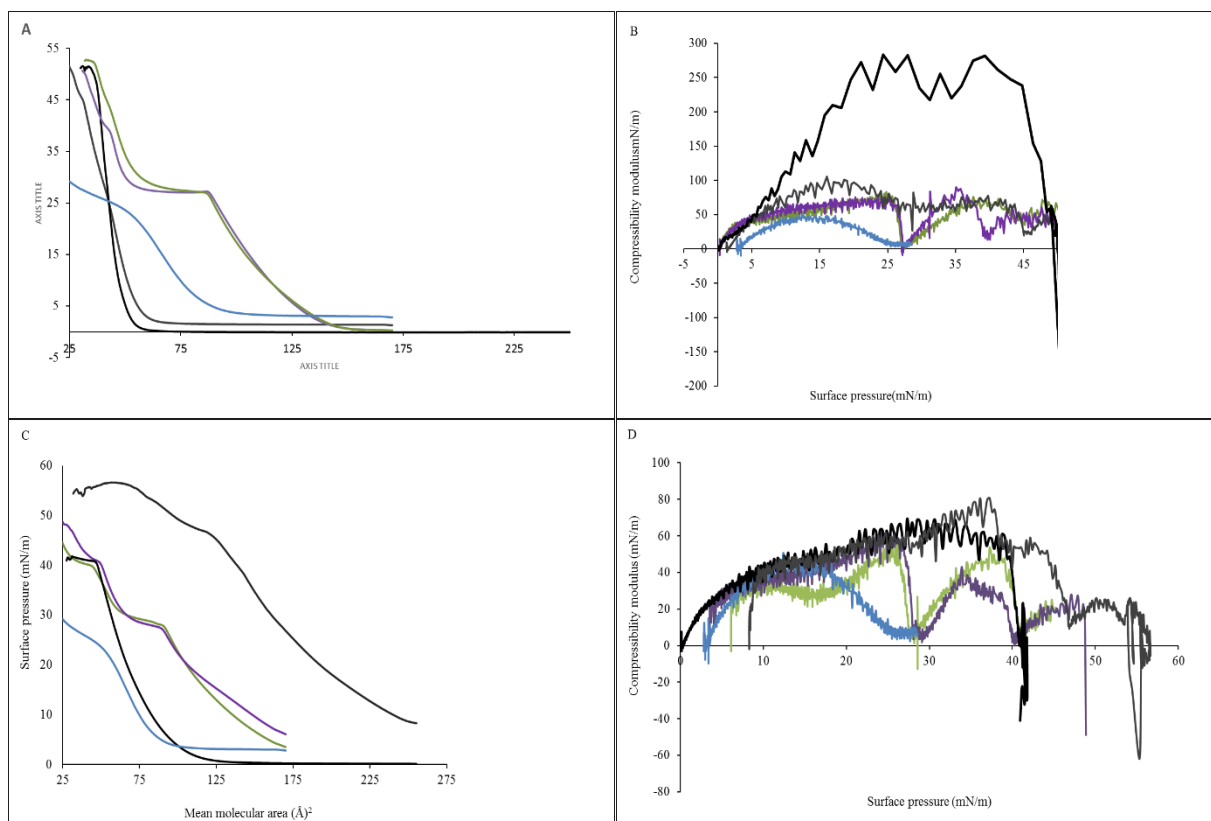


Figure 4.15 Compression isotherms (π -A) for A) DPPC/Cholesterol (75%/25%, black line) and C) POPC/Cholesterol (75%/25%, black line) monolayers treated with: 12-3-18 (grey), 12-3-18:DNA at a 10:1 charge ratio (green), 12-3-18:DNA at a 5:1 charge ratio (Purple). Compressibility modulus (C_s^{-1}) as a function of surface pressure (π) for B) DPPC/Cholesterol and D) POPC/Cholesterol (75%/25%, black line) were calculated according to Equation 4.1; the line colors correspond to the same treatments described for A) and C).

the cross-sectional area (A_∞) value of 93\AA^2 is quite consistent with head group areas reported in the literature for various m-3-m type gemini surfactants, although much larger than the head group area determined from our own surface tension measurements, described in Chapter III). The small lift-off area $\sim 93\text{\AA}^2$ in comparison to the lift-off area value for 16-7-16 (111.6\AA^2).¹⁴³ The compressibility modulus (Figure 4.15B) indicates that the monolayer formed is consistent with an LE phase, and exhibits circular domains in the BAM images.

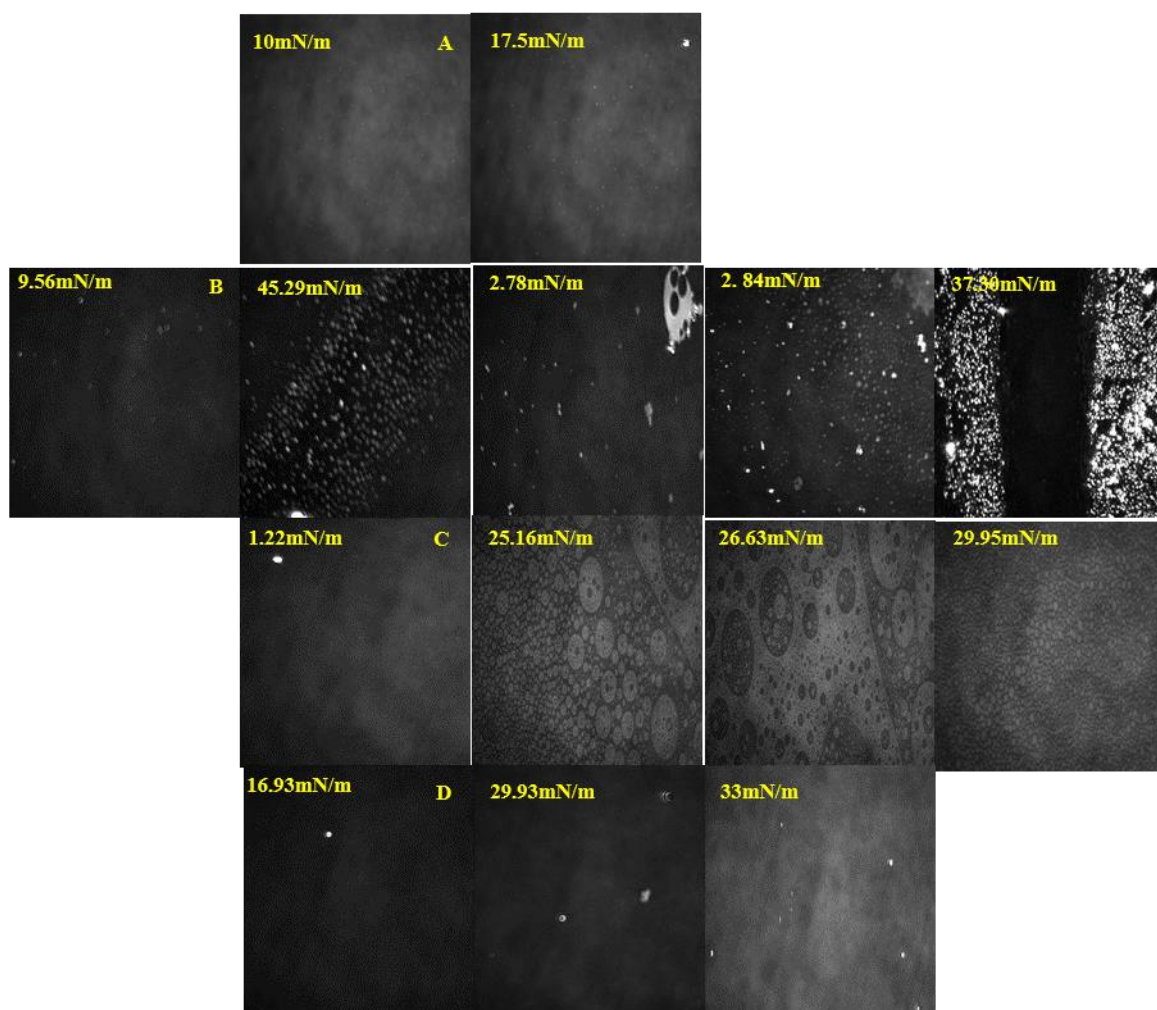


Figure 4.16 BAM images for DPPC-Cholesterol and POPC/Cholesterol monolayers treated with 12-3-18 gemini surfactant or 12-3-18/DNA complexes. A) 12-3-18 monolayer, B) DPPC-Cholesterol treated with 12-3-18, C) DPPC/Cholesterol treated with 12-3-18/DNA (5:1 charge ratio), D) POPC-Cholesterol treated with 12-3-18/DNA (5:1 charge ratio). POPC-Chol with 12-3-18:DNA showed no domains.

The addition of 12-3-18 to DPPC-Cholesterol monolayer resulted in an isotherm again similar to that for 12-3-16 (Figure 4.13A vs 4.15A) with similar increases in A_L and A_∞ (Table 4.1) as was also observed for 12-3-16. This, combined with the similarly low compressibility modulus values (Figure 4.15B), with $C_S^{-1}_{30}$ decreasing from 255 mN/m to 59 mN/m and $C_S^{-1}_{35}$ decreasing from 274mN/m to 55mN/m, is again consistent with a strong interaction of the surfactant with the monolayer, and the fluidization into an LE or LE-LC coexistence phase. BAM images of DPPC/Chol monolayer in the presence of 12-3-18 (Figure 4.16A) showed circular

domains of varying size randomly scattered over the image, consistent with a disordered LE-LC phase.

For DPPC/Chol monolayers treated with 12-3-18:DNA complexes (at either 5:1 or 10:1 charge ratios) again show clear indications of fluidization of the monolayer into multiple expanded phases (see Figure 4.15). The π -A isotherms shift to higher molecular areas as the monolayer becomes more fluid, with higher lift-off areas (151\AA^2 for both charge ratios) and higher minimum cross sectional areas of 156\AA^2 at 10:1 charge ratio, and 136\AA^2 at 5:1 charge ratio. The same LE_A , $LE_A - LE_B$ coexistence, and LE_B phases seen for the 12-3-16 surfactant, can again be seen here, although the compressibility modulus values (Figure 4.15B) suggest that the LE-LC and LC phases could also be a possibility. BAM images of this monolayer (Figure 4.16B) are featureless at low surface pressure, but at intermediate surface pressures, the multiple LE phases are clearly seen. At high surface pressure, the domains are more ordered, consistent with the possibility of an LC phase.

The addition of 12-3-18 to the sub-phase of POPC-Cholesterol monolayer has dramatic impact on the monolayer. Strong interactions cause high initial surface pressure values ($\sim 5\text{mN/m}$) in the absence of any compression (Figure 4.15C), and dramatically increase the lift-off area and the cross-sectional area to $A_L=255\text{\AA}^2$ and $A_\infty < 250\text{\AA}^2$. Overall the shape of the isotherm contains a number of small features at higher surface pressure, that suggest an extraordinarily complex mixture of phases, that based upon the compressibility modulus (Figure 4.15D, and Table 4.1) are again consistent with LE phases. Interestingly, the BAM images are remarkably boring given the extensive disruption indicated by the isotherm and compressibility modulus, and it is strongly recommended that these be repeated in future work.

The addition of DNA to 12-3-18 has the same type of effect on the POPC/cholesterol monolayer as the other 12-3-n surfactants, shifting the π -A isotherm to higher molecular areas;

although again a non-zero surface pressure is observed in the absence of compression due to apparently strong interactions. Lift-off and cross sectional areas are again dramatically increased (Table 4.1) and the low compressibility modulus values (Figure 4.15D and Table 4.2), indicates the fluidizing effect the 12-3-18-DNA complexes have on the POPC-Chol monolayer. BAM images of this system only displayed round domains throughout the entire compression, which is the characteristic of the POPC-Chol (showing no distinct domains).

In summary, the addition of the dissymmetric 12-3-n gemini surfactants generally fluidizes the DPPC/Chol and increases the rigidity of the POPC/Chol monolayer. For the most part, all three surfactants behaved similarly; although 12-3-16 acted differently when added to POPC-Chol as it did not increase the rigidity of the monolayer. In general, the disruptions resulted in the formation of LE, LE-LC coexistence, or LC phases; however as the tail length increased, the possibility of multiple LE phases in coexistence was also hypothesized. Addition of the DNA, regardless of the monolayer composition, and regardless of the alkyl tail length of the surfactant, resulted in the fluidization of the both types of monolayer again demonstrating the potential for transfection complexes comprised of these surfactants to be able to successfully disrupt endosomal membranes allowing for endosomal escape.

Overall, through our characterizations the DPPC/Chol and POPC/Chol monolayers using Langmuir monolayer studies combined with BAM, we have successfully characterized models of the endosomal membranes of normal cells (DPPC-cholesterol = 75:25 %), and of cancer cells (POPC-Cholesterol= 75%:25%). The mixed monolayer of DPPC-Cholesterol showed solid phase at a surface pressure from 30 to 35 mN/m, indicating the rigidity of the membrane. POPC/Cholesterol system found to be much more fluid at the same surface pressures, in the LE phase. Once the gemini surfactants were added to the DPPC-Cholesterol; whether those of pyrene-based surfactants, or the 12-3-n surfactants; with or without the DNA, the rigidity of the membrane was reduced substantially and fluidity was induced. In the absence of DNA this

appeared to be due to insertion of the surfactant molecules themselves into the monolayer structure, while in the presence of DNA appeared to result from interactions between the complexes and the monolayer at the air-water interface. The effect of the surfactants on the POPC/Chol system, whether the pyrenyl or the dissymmetric surfactants was to increase the rigidity of the monolayer in general, again due to insertion of the surfactant into the monolayer, however in this case, this may hinder the motion of the oleyl chain in the POPC molecules in the monolayer, giving rise to an increase in rigidity. The addition of DNA again resulted in increased fluidity of the monolayer, further suggesting that in the presence of DNA, the interactions are between the monolayer and the surfactant:DNA complexes at the air/water interface. It appears that the expected strong electrostatic interaction that occurs between the cationic head groups of the surfactant molecules and the phosphate ions in the DNA backbone is stronger than any driving force that would allow for incorporation of the surfactant into the monolayer. This may have implications for DNA transfection, which not only requires successful endosomal escape, which our results clearly indicate is a reasonable expectation for these systems, but also the release of the DNA from the transfection complex. If the interaction of the surfactants with DNA is strong enough to prevent incorporation of surfactant molecules into the monolayer, it is possible that DNA release could be impeded within the cells. The transfection activity of these surfactants will be studied in Chapter 4.

Chapter 5: Transfection and structural properties of dissymmetrical gemini surfactant based transfection complexes

5.1 Introduction

The lack of safe and efficient gene-delivery methods is a limiting obstacle to human gene therapy. Although synthetic gene-delivery vectors are safer than recombinant viruses, they generally possess low efficacy rates. In recent years, a variety of effective cationic compounds have been designed specifically for gene delivery (polymers, lipids and gemini surfactants).²¹⁴ A growing understanding of gemini surfactant`s gene-delivery mechanisms and the ability to manipulate the basic chemical structure of these unique molecules to cater to the growing need of a better transfection agent, it is possible that the gemini surfactants will be an important tool in gene therapy applications.⁵⁶ The gemini surfactants encountered in gene delivery are generally symmetric, with their head groups usually made of quaternary ammonium, or primary, secondary or tertiary amine groups.³⁴

The cationic groups are necessary for the neutralization and compaction of DNA. gemini lipids are interesting compounds and this is largely due to their biocompatibility and longer half-life in the body. Also, carbohydrates and peptides have been recently used as head groups or alkyl tails.³⁴ These have showed superior biocompatibility and in some cases gave better transfection results, depending on the cell line. Dissymmetric gemini surfactants have also been used in transfection. Phytanyl surfactants synthesized by Haitang Wang in Dr. Wettig`s lab, and the phy-3-n surfactants showed better transfection results in OVCAR-3- cell lines than 16-3-16 and 12-3-12 gemini surfactants.¹⁷⁸ To improve the transfection results many parameters have to be considered. Average particle size of the nanoparticle (lipoplex, or polyplex) is of great importance to assist in endocytosis. Also the flexibility of the nanoparticle to release the DNA is another important step. As mentioned earlier, the size of the nuclear pores in the nuclear

membrane is <50 nm, and the release of the DNA from the cationic portion of the complex is the only way to gain access to the nucleus. Another important parameter in gene delivery is the zeta potential of the complex. An overall positive charge is necessary to interact with negatively charged cell membranes and before that to complex and compact DNA. In this current project, physical characterization of the GS-DNA complex at different charge ratio is measured by means of particle size and zeta potential. Based on these results, charge ratios will be picked to test transfection in two cell lines, Human embryonic kidney cell line (HEK-293), and osteosarcoma cell line (MG-63). The first is an example of a healthy cell line and the second is an example of a diseased (cancer) cell line. Transfection efficiency and cell viability of the eight gemini surfactants was determined by flow cytometry technique. Also, Pyrene-based gemini surfactants was mixed with DNA (at charge ratios of 5:1, and 10:1), and DOPE lipid (3:2). These ratios were only determined after a process of testing and optimization. Protein expression was determined by means of ELISA in African green monkey fibroblasts cell line (COS-7) cell line (this experiment is done in collaboration with Dr. Ildiko Badea). One-way ANOVA statistical analysis was conducted to determine the significance of the results.

5.2 Materials and Methods

DOPE (1,2-dioleoyl-sn-glycero-3-phosphoethanolamine), and sodium bicarbonate were purchased from Sigma-Aldrich (Oakville, Ontario). The plasmid used in our transfection studies was *pGTINF* coding enhanced green fluorescence protein (EGFP) gene. A gift from Dr. Ildiko Badea (College of Pharmacy and Nutrition, Saskatchewan). The amplification of the plasmid took place in our laboratory. DOPE was prepared at 1 mM in PBS (pH9) and the preparation will be discussed in Chapter 4 section 4. LipofectamineTM 2000 was purchased from Invitrogen and used according to the manufacturer's protocol (Fisher scientific, Ottawa, Canada), HPLC grade ethanol (Sigma-Aldrich, Oakville, Canada), Dulbecco phosphate buffer saline (DPBS) (Fisher

scientific, Ottawa, Canada), NaOH (Sigma-Aldrich, Oakville, Canada), 0.25% 1X Trypsin(Fisher Scientific, Ottawa, Canada), Tryple™ Xpress (Fisher Scientific,Ottawa, Canada), Penicillin/Streptomycin antibiotics (Hyclone, Fisher Scientific, Ottawa, Canada), Fetal bovine serum (FBS) (GIBCO, Fisher Scientific, Ottawa, Canada), α -tocoferol (Sigma-Aldrich, Oakville, Canada), DMEM (ATCC, Cedarlane labs, Burlington, Canada), human osteosarcoma (MG-63) and human embryonic kidney cells (HEK-293) (Cedarlane labs, Burlington, Canada), EMEM™ (high glutamine)(Fisher scientific, Ottawa, Canada), 3-(4,5-dimethylthiazol-2-yl)-2,5-diphenyltetrazolium bromide (MTT) (Sigma-Aldrich, Oakville, Canada). Milli-Q water was used in the preparation of all solutions.

5.2.1 Particle size and Zeta potential

Particle size of eight gemini surfactants alone and with DNA at different charge ratios (+/-) was measured by dynamic light scattering at 25 °C using a Malvern Zetasizer Nano ZS instrument (Malvern instruments, UK). ZEN0118 (light scattering) and DS1070 (zeta potential) cuvettes were purchased from Malvern instruments (UK). The particle size distribution in water was obtained from the light scattered by particles illuminated with a laser beam (633 nm) at a scattering angle of $\theta = 173^\circ$. The particle size measurements are reported using a % volume distribution, and are repeated three times automatically in transparent disposable cuvettes (ZEN0118) (Malvern instruments, UK), with the average particle size being reported \pm standard deviation. The measurement of zeta potential of the complexes was performed by using electrophoretic light scattering with the same instrument. Zeta potentials were measured three times per sample and are expressed as the mean \pm standard deviation.

5.2.2 Plasmid DNA (*pTGINF-GFP*)

The recombinant plasmid DNA was amplified in *K-12* strains of *Escherichia coli* (a Gram negative, anaerobic, rod-shaped bacterium) (provided from Dr. Roderick Slavcev's lab at the

School of Pharmacy, University of Waterloo) in the generation of the recombinant cell constructs, extracted using centrifugation protocol of the E.Z.N.A.[®] Endo-Free Plasmid DNA Maxi Kit (OMEGA bio-tek, Georgia, USA), and treated with restriction enzymes followed by gel electrophoresis for sequence confirmation. Two restriction enzymes, xba-1 (Cat #R3104T, New England Biolabs, Whitby, Canada), and HINDIII-HF (Cat#R0145C, Biolabs, Canada) were used (in cut smart[™] buffer, Cat #B72045, Biolabs, Canada) to cut the DNA into specific fragments for identification in using gel electrophoresis (Agarose gel, Cat#BP1356, Fisher scientific, Canada, with ethidium iodide (B392-5). 0.5g of agarose was dissolved in 500mL of 6X TE buffer, which was heated in the microwave for 1min-1.5min with. This 1-1.5min heating was done in intervals of 30seconds to avoid bubbling and over flowing of the buffer (provided from Dr. Roderick Slavcev`s lab at the School of Pharmacy, University of Waterloo).

The protocol followed for agarose gel electrophoresis was as described by Lee et al.²²⁷ with minor modification. Prior to the sample preparation, the agarose gel is cast on the tray and left to dry for approximately an hour. The required volume (for ≥ 500 ng of plasmid) of the extracted plasmid sample, 1 μ L of the DNA-ladder standard (as control, 500 μ g / μ L, 1 kb size), and 6X Sample Loading Buffer/Dye solution (in glycerol) at a ratio of (Loading Buffer : Plasmid =) 1 : 5 was carefully pipetted, and separately mixed in appropriate combination (either Ladder + Dye or Samples + Dye). After adjusting the final volume of the individual mixture(s) by adding Milli Q water, 10 μ L of each mixture was separately pipetted into the designated wells before running the power. The electrophoresis power (potential difference of 100 volts, and 3 amperes of current) was allowed to run until the blue dye approaches the end of the gel (generally for >1.5 hr). As DNA diffuses within the gel over time, it becomes difficult to see the DNA bands, thus, UV imaging (provided in Figure 5.1) was done, shortly after the electrophoresis stopped, through an UV transilluminator at 302 nm.

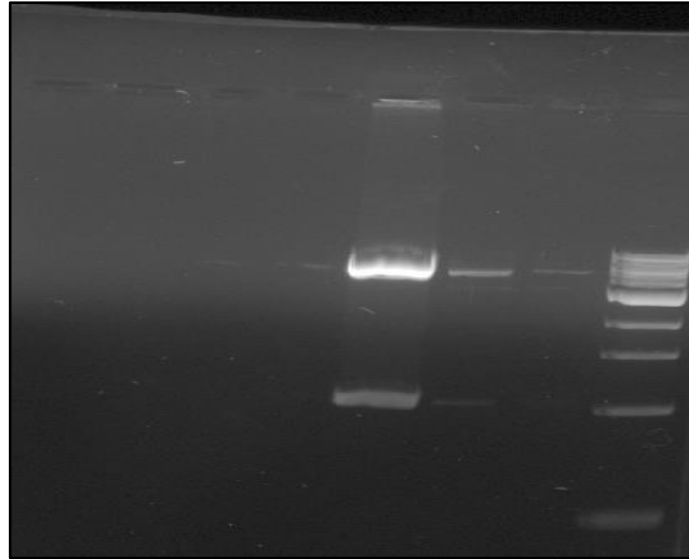


Figure 5.1 Gel electrophoresis of *pGTINF-GFP* plasmid extracted after the treatment with restriction enzymes (*xba-I* and *HINDIII-HF*). Three bands (751kb, 1095kb, and 3742kb) can be seen in the image

5.2.3 *In vitro* transfection

Transfection complexes were composed of the plasmid, gemini surfactants, and DOPE, or as a control of ONLY the plasmid with the gemini surfactants (no DOPE added). The media used was dependent upon the identity of the cell line used, DMEM, high glucose (GIBCO[®], Fisher scientific, Ottawa, Canada) was used for the HEK-293 cell line, and high glutamine EMEM (ATCC, Cedarlane, Canada) was used for the MG-63 cell-line. The plasmid *pGTINF-GFP* coding enhanced green fluorescence protein (EGFP) gene, obtained as a gift from Dr. Ildiko Badea (College of Pharmacy and Nutrition, University of Saskatchewan), was used at an amount of 0.2 μ g/well for the transfection. All the dissymmetric gemini surfactants and the symmetric 16-3-16 gemini surfactant (as a control) were prepared at concentration of 1.5mM, filtered through a 0.2 μ m syringe filter (Cat #09719A, Fischer scientific, Canada), and was used at a volume of 1.01 μ L/well to obtain a surfactant to plasmid charge ratio of 5:1. DOPE vesicles were prepared according to Wettig et al.¹²⁶ at concentration of 1mM in PBS (pH=9), filtered using a 0.45 μ m syringe filter (Fisher scientific, Ottawa, Canada), and used at a volume of 3.7 μ L/well.

The transfection complexes were prepared as follows: 0.2 μ g of the plasmid was mixed with 1.01 μ L of the gemini surfactant solution and incubated at room temperature for 15 minutes. After that, 3.7 μ L of the DOPE vesicle solution was added to the mixture and incubated for 30 minutes at room temperature. The complexes were then used to transfect cells as described below.

Transfection assays were carried out as reported in previous studies.^{228,225} One day prior to the transfection, HEK-293 and MG-63 cells were seeded onto a 96-well plate at a density of 2.5x10⁴ cells/mL and 1.5x10⁴ cells/ mL, respectively. The cells were incubated at 37 °C in a 5% CO₂ atmosphere for approximately 24 h to reach 85% confluency in 75-cm² tissue culture flasks in Dulbecco's modified Eagle's medium (DMEM) or (EMEM) obtained from Fisher scientific (Ottawa, Canada). These cells were supplemented with 10% (v/v) fetal bovine serum, 1% (v/v) antibiotic antimycotic agents on the day of transfection. One hour prior to transfection, cells media was removed and changed to medium prepared without fetal bovine serum (FBS) and antibiotics. Then the transfection complexes prepared as described above and added to the cells dropwise. The cells were then incubated at 37 °C in a 5% CO₂ atmosphere for 3h for both cell lines. Cells were also transfected using 16-3-16 (prepared as above for the dissymmetric gemini surfactants) and LipofectamineTM 2000 (Invitrogen, used according to the manufacturer's protocol) as the positive control, plasmid only, and dissymmetric gemini surfactant controls. After 3h incubation, the supernatant media was replaced by fresh media (DMEM or EMEM, depending on the cell type) with 20% FBS (without antibiotics) and the cells were again incubated in a 37 °C with 5% CO₂ atmosphere overnight to allow for EGFP expression. On the third day, cells were collected and resuspended in PBS mixed with propidium iodide. The samples were analyzed using a Guava easycyteTM 8HT benchtop flow cytometer (EMD Millipore, Etobicoke, Canada) which is a part of Dr. Spagnuolo's lab in the School of Pharmacy, University of Waterloo. 5,000 cells were analyzed for each sample. Transfection efficiency was

expressed in terms of the % of cells expressing the EGFP expression. Cell viabilities were expressed as the % cells that were dead (as determined by PI staining).

As there was some concern regarding possible contamination of the EGFP fluorescence by potential fluorescence from the pyrenyl groups in the structure of the py-3-m surfactants, transfection efficiencies were also obtained using an ELISA method, described below. All ELISA transfection and cell culture studies were carried out by the Badea group (Dr. Ildiko Badea) in the College of Pharmacy and Nutrition, University of Saskatchewan. For the ELISA measurements, COS-7 African green monkey kidney fibroblasts (ATCC, CRL-1651) were grown to 80% confluency in 75-cm² tissue culture flasks in Dulbecco's modified Eagle's medium (DMEM) obtained from ATCC (Manassas, VA USA). These cells were supplemented with 10% (v/v) fetal bovine serum, 1% (v/v) antibiotic antimycotic agents and incubated at 37°C in a 5% CO₂ atmosphere. A day prior to transfection, 96-well tissue culture plates were seeded at a cell density of 1×10^4 cells/well. The DMEM medium was changed one hour prior of the transfection with DMEM containing no FBS or antibiotics. Cells were transfected in the same manner described for the HEK-293 and MG-63 cells with the exception that 5 hrs incubation was allowed for transfection, rather than 3 hours. Lipofectamine Plus (Invitrogen Life Technologies) was used as a positive control according to the manufacturer's protocol. After the incubation period, the transfection mixtures were replaced with fresh DMEM containing 10% FBS. Supernatants were collected at 48 and 72h and replaced with fresh medium. The collected supernatants were stored at -20°C. The results presented are the average of three plates of quadruplicate wells.

5.2.4 Enzyme-Linked Immunosorbent Assay (ELISA)

ELISA was carried out to measure the level of interferon gamma using flat bottom 96-well plates according to the BD Pharmingen protocol.²²⁹ A standard IFN- γ curve was created using

recombinant mouse IFN- γ standard (BD Biosciences, Mississauga, ON, Canada) to calculate the concentration of the IFN- γ expressed by the cells after transfection. A 3-(4,5-dimethylthiazol-2-yl)-2,5-diphenyltetrazolium bromide (MTT) assay was used to determine the cytotoxicity of the pyrene-based gemini surfactants in the COS-7 cell-line, also at the University of Saskatchewan. For the MTT assay, three 96-well cell culture plates were seeded with cells at a density of 1×10^4 cells/well and treated with the complete complexes containing plasmid, GS, and DOPE (P/G/L) nanoparticles. These Plates were incubated for 5h at 37°C in a 5% CO₂ atmosphere before replacing the old media with fresh media as described above. Cell toxicity was evaluated at 48h and 72 hours post-transfection. Lipofectamine was again used as a positive control. A sterile solution of 5 mg/mL of MTT (Invitrogen, USA) in PBS was prepared, mixed with supplemented media and added to the cells. Then cells were incubated for 3h. The supplemented media was removed and the formed, purple formazan crystal was dissolved in dimethyl sulfoxide (spectroscopy grade, Sigma-Aldrich, ON, Canada). The plates incubated at 37 °C for 10 minutes and absorbance was measured at 550 nm using a microplate reader (BioTek® Microplate Synergy HT, Vermont, USA). The results are the average of three plates (treated with individually prepared formulations of quadruplicate wells) and the cytotoxicity was expressed as a percentage of the non-transfected control cells \pm standard deviation.

5.2.5 3-(4,5-Dimethylthiazol-2-yl)-2,5-diphenyltetrazolium bromide (MTT) assay

MTT assay was performed to examine the cytotoxicity of the pyrene-based gemini surfactants in the COS-7 cell-line. Three 96-well cell culture plates were seeded with cells at a density of 1×10^4 cells/well and treated with the GDP nanoparticles. Plates were incubated for 5 h at 37°C with 5% CO₂ before replacing the old media with fresh media as described in the transfection section. Cell toxicity was evaluated 48h after treatment. Lipofectamine, a commercial transfection agent, was used as a positive control. A sterile solution of 5 mg/mL of MTT (Fisher Scientific, Ottawa, Canada) in phosphate-buffered saline (PBS) was prepared, mixed with media

containing 10% FBS, then added to the cells and incubated for 3 h. The supplemented media was removed and the formed, purple formazan crystal was dissolved in dimethyl sulfoxide (spectroscopy grade, Sigma-Aldrich, Oakville, Canada) and the plates incubated at 37°C for 10 m. Absorbance was measured at 550 nm using a microplate reader (BioTek® Microplate Synergy HT, Vermont, USA). The results are the average of three plates (treated with individually prepared formulations of quadruplicate wells) and the cytotoxicity is expressed as a percentage of the non-transfected control cells ± standard deviation.

5.3 Results and Discussion

5.3.1 Particle size and zeta potential measurement

Physical characterization of the gemini surfactant- DNA complexes was conducted by measuring the particle size and zeta potential with Zetasizer Nano ZS (Malvern, UK). Average particle size of the gene transfection vector is of great importance and has been reported numerous times. Lipoplexes are used to protect the DNA from endonucleases from degradation, and they possess different morphologies ranging from, toroidal or spherical structures to inverted hexagonal and cubic²³⁰. Diameters of these particles range from about 10s of nanometers to several hundred nanometers. There is a general agreement that lipoplex size plays a significant role in determining the nature of the entry pathway of the lipoplexes into the cells. On one hand, larger polyplexes may result in more cell membrane contact and active phagocytosis²³¹. Although the main pathway of entry and access into cells happen through active endocytosis, clathrin-mediated and caveolin-mediated endocytosis have been reported to play a role in mediating entry into the cell, hence, transfection.²³² Qaddoumi and colleagues have shown that in primary cultures of rabbit conjunctival epithelial cells (RCEC), endocytosis of poly (DL-lactide-co-glycolide) (PLGA) NPs occurs mainly via clathrin- and caveolin-1-independent pathways.²³³

These authors suggested that nanoparticle uptake occurs by adsorptive endocytosis.²³⁴ These different entry pathways depend highly on the size of the nanoparticles (polyplex). 500nm or larger particles cannot gain access to cells via the clathrin pathway. A size-dependent mechanism has been proposed with clathrin-mediated pathway. Rejman et al.²³⁵ tested NPs in B16F10 (murine melanoma cell line) cells and showed a significant inhibition of internalization of nanoparticles with sizes between 200 and 50 nm, while the uptake of those with a size of 500 nm was unaltered or even slightly higher, which means large particles are internalized through a different pathway.

The size and zeta potential of the lipoplexes of dissymmetric gemini surfactants, and DNA were measured and tabulated in Appendix C (Tables 5.1, and 5.2). As can be seen in Figure 5.2 (py-3-m surfactants) and Figure 5.3 (12-3-n surfactants), at low charge ratios of 1:1, and 1:2 particles size was noticeably large with an overall negative zeta potential, indicating that complexation happens with the DNA, but the surfactants are unable to fully complex the DNA. As the charge ratio increases (5:1 and 10:1), all complexes have sizes less than 200nm with an overall positive net charge, except for pyrene-3-18. The reason for this remains unclear. Larger nanoparticles were also formed in the presence of 12-3-18, suggesting that the longer alkyl tails may result in less efficient compaction of the DNA, which could help explain the unusual negative charge for the py-3-18 complexes. For complexes containing pyrenyl gemini surfactants, the zeta potentials were above +30 mV at a charge ratio of 5:1 and greater, with the exception of pyr-3-8-DNA complex, indicating that the complexes are normally stable. For complexes containing asymmetric (12-3-n) surfactants, the zeta potential values were also above +30mV at higher charge ratios. In the current transfection experiments, only one charge ratio (5:1) was used for transfection studies, selected based upon

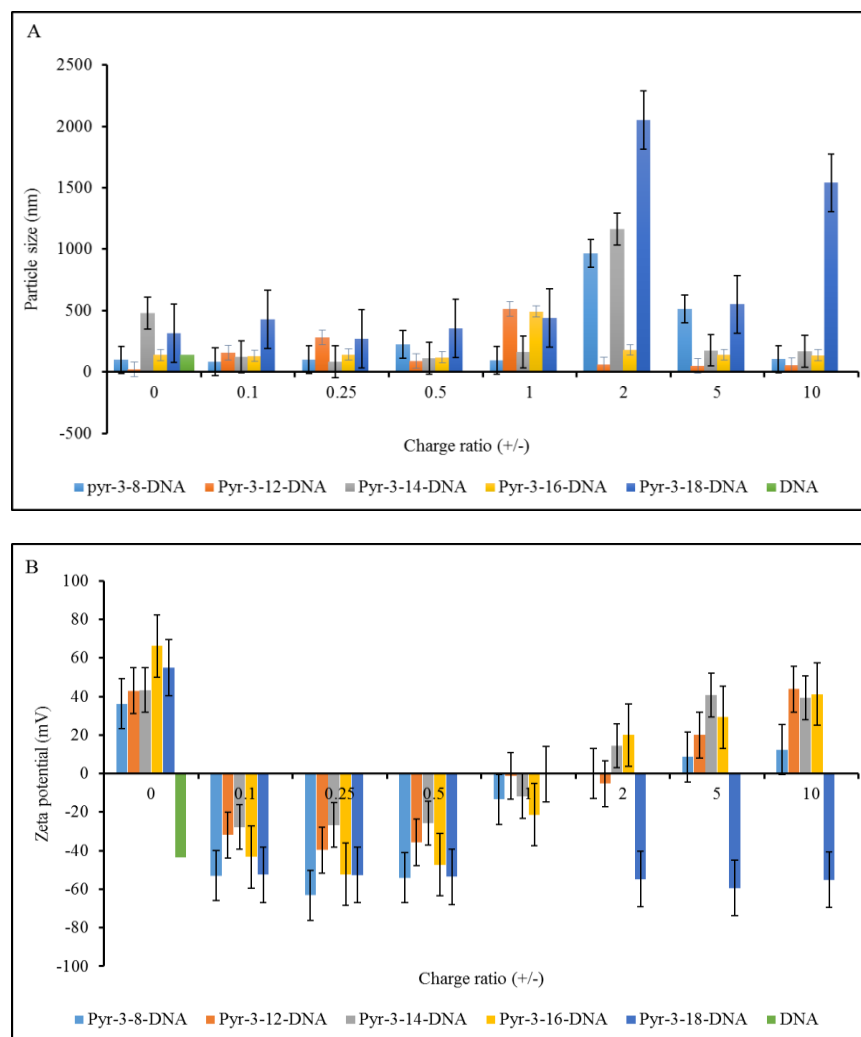


Figure 5.2 Physical characterization of nanoparticles, A) Particle size, B) Zeta potential of pyrene-based gemini surfactants (pyrene-3-8, pyrene-3-12, pyrene-3-14, pyrene-3-16, pyrene-3-18), with or without DNA.

the size and zeta potential results, and previous observations (for other surfactant systems) that the 5:1 ratio was correlated with better transfection in our lab.¹⁷⁸ We did not use a higher charge ratio due to concerns of increased toxicity associated with higher concentrations of quaternary ammonium surfactants.

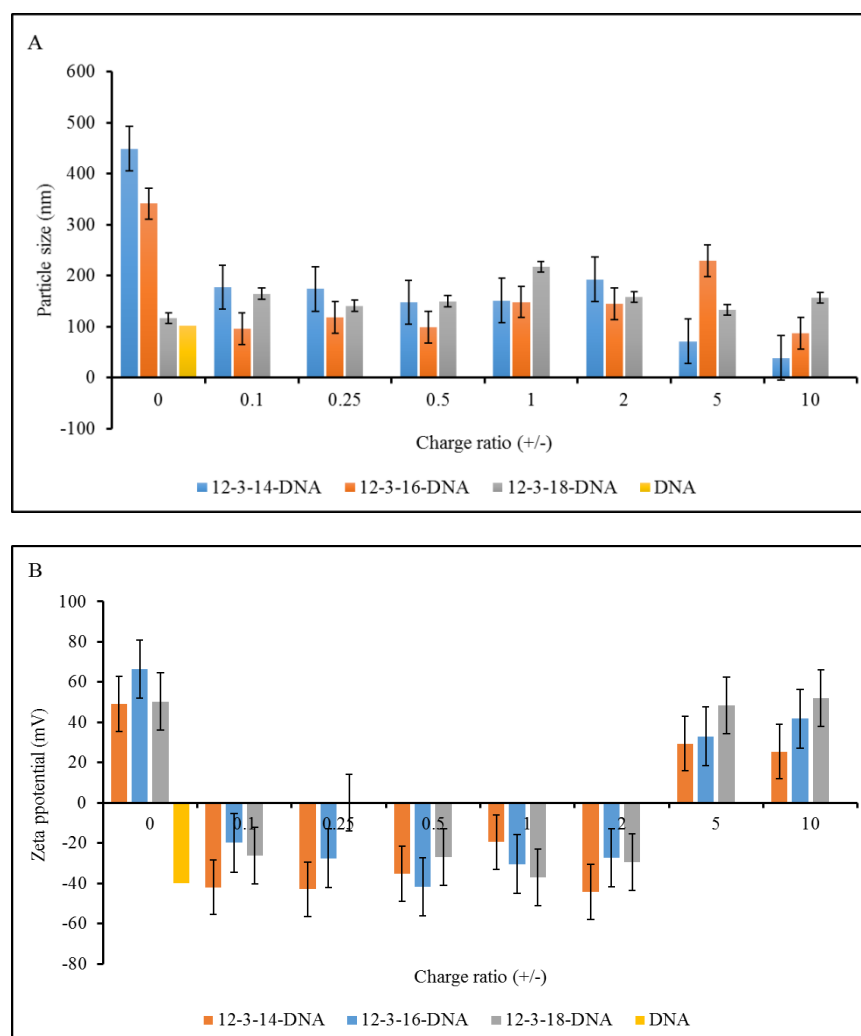


Figure 5.3 Physical characterization of the nanoparticles, A) Particle size, B) zeta potential of dissymmetric gemini surfactants 12-3-14, 12-3-16, 12-3-18, with and without DNA.

5.3.2 Evaluation of transfection efficiency *in vitro*

The dissymmetric gemini surfactants (12-3-n) in the MG-63 cell line were internalized and the DNA was being released, but the transfection efficiency was very low, especially for 12-3-14 (Figure 5.4A). This may be linked to cell viability as our cell viability results (Figure 5.4B) indicate these complexes are very toxic to the MG-63 cells. Cell viability after treatment with 12-3-14GPD (12-3-14 with DOPE at a DOPE:GS molar ratio of 3:2 and a GS:DNA charge ratio of 5.1) complexes is $8.1 \pm 0.4\%$, and for the 12-3-14:DNA complexes (with no added DOPE) the viability was even lower at $3 \pm 1\%$ (essentially 0!) Similar behavior was observed for the

12-3-18 complexes, although the transfection efficiencies and cell viabilities are much greater than those for 12-3-14. The transfection efficiencies for the 12-3-16 complexes efficiencies were 10.4 ± 0.8 and 11 ± 3 for complexes with (GDP) and without DOPE (GP), respectively,

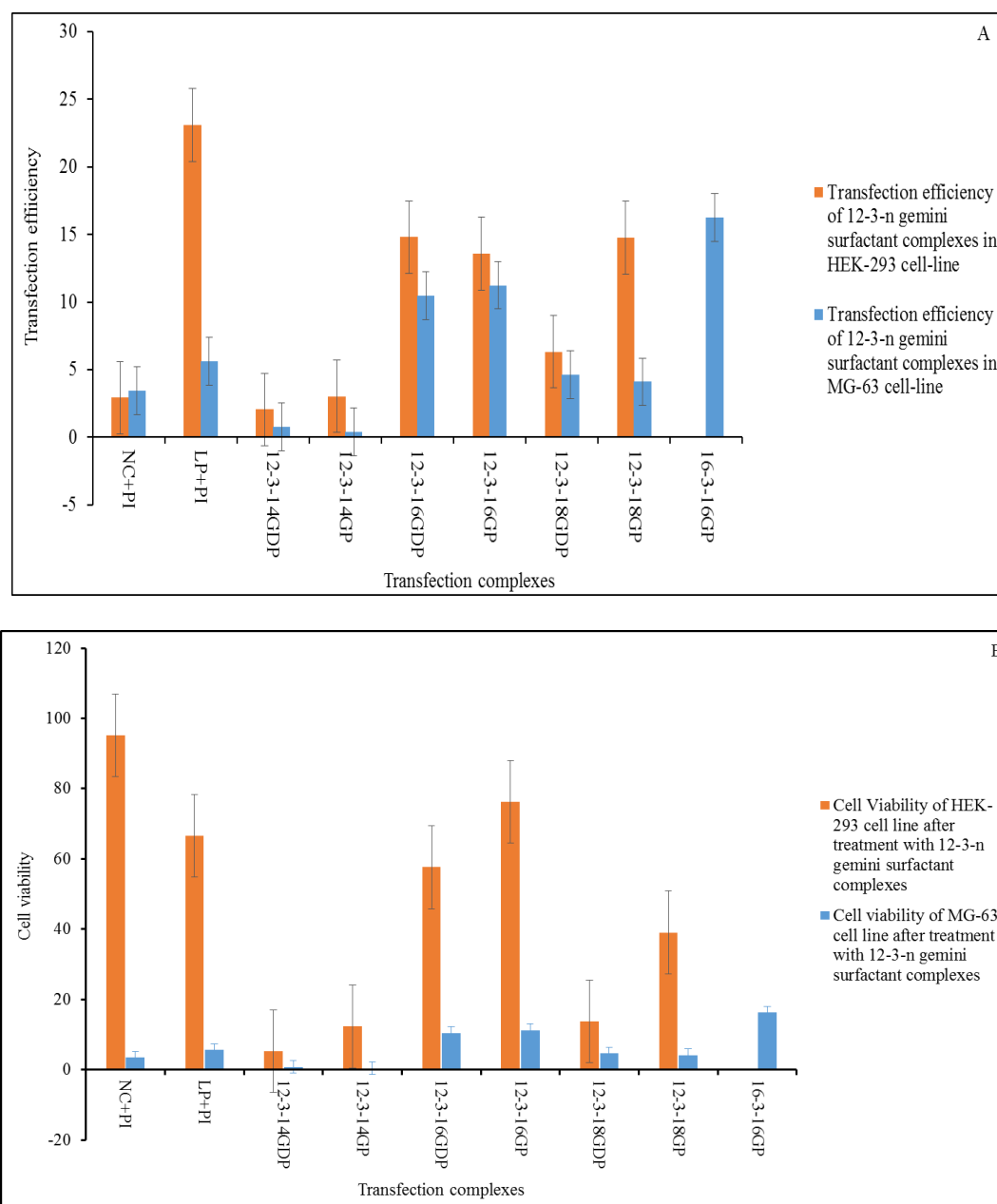


Figure 5.4 A) Transfection efficiency of 12-3-n gemini surfactant complexes in HEK-293 cell-line (orange), and in MG-63 cell-line (blue) and B) cell viability (violet) of dissymmetric (12-3-n) gemini surfactants complexes in MG-63 cell line

which are the highest among the dissymmetric surfactants. The 12-3-16 complexes also gave rise to the highest cell viabilities, $74 \pm 3\%$ and $76 \pm 12\%$ for the GDP and GP complexes, respectively. The same behaviour was observed previously in our group with a series of phytanyl substituted (phy-3-n) surfactants, where the phy-3-16 surfactant gave higher transfection than either phy-3-12 or phy-3-18 when complexed with DNA and DOPE in an OVCAR-3 cell line.¹⁷⁸ Similarly, for the symmetrical m-3-m surfactants, 16-3-16 gave higher transfection compared to 12-3-12 or 18-3-18, again when complexed with DNA and DOPE in PAM212 cell lines.¹²⁶ Unfortunately, possibly due to the low transfection efficiencies observed, the differences in the transfection efficiencies for the 12-3-n surfactants are not statistically significant, indicating that this initial, preliminary, transfection study will need to be repeated.

In the HEK-293 cell line, the 12-3-14 complexes again displayed low transfection ($\text{GDP} = 2 \pm 1\%$ and $\text{GP} = 3 \pm 2\%$; Figure 5.4), although the efficiency was higher in the HEK293 vs. the MG-63 cells. The viability of the 12-3-14 GP complexes ($12 \pm 6\%$) is higher than for the GDP system ($5 \pm 6\%$; again essentially 0), again consistent with the high toxicity observed in the MG-63 cells. The 12-3-16 complexes showed the highest level of transfection efficiency in the HEK293 cells, as well as the highest cell viability among the three surfactants. For all 3 surfactants, increased toxicity was seen upon addition of DOPE to the complexes; an observation that has been previously made in our group, however, this appears to be generally inconsistent with what has been reported in the literature.^{228,236,237} The 12-3-18 complexes showed better transfection in the absence of DOPE (12-3-18 $\text{GDP} = 6 \pm 2\%$, $\text{GP} = 14.8 \pm 0.8\%$). The transfection results for the three surfactant complexes without the DOPE come in agreement with the results obtained from the Langmuir monolayers.²¹³ The surfactant complexes increased the fluidity of the membranes, resulting in membrane fusing, and internalized. However, one of the major issues with these surfactants is their toxicity, which has been reported before.¹¹⁶

We attempted to examine the transfection efficiencies of the py-3-m surfactants using the same flow cytometry method as for the 12-3-n surfactants. Results for the transfection efficiencies and the cell viabilities for both cell lines for the five pyrene-based surfactants are found in Figure 5.5. At first glance, the problem with this data is immediately obvious; in the absence of ANY added plasmid or DOPE, the py-3-m surfactants show high (for the py-3-12 and py-3-14 surfactants very high) transfection was observed. This was observed in multiple experiments, and is of course impossible from a cell biology standpoint. Contamination was ruled out (by multiple experiments carried out with new samples, media, and reagents) meaning that an unknown cause was responsible. As pyrene is a fluorescent molecule it could potentially contribute to the overall fluorescence observed by the flow cytometer; however the normal pyrene fluorescence emission ranges from ~370 – 450 nm, well away from the emission wavelength for EGFP (509nm). What cannot be forgotten is that the pyrene moieties in our systems are bound to aggregating surfactants, forcing pyrene groups into close proximity with each other. Pyrene is of course well known for excimer formation, which red-shifts the fluorescence emission to higher wavelengths (~ 475 – 530 nm). Given this high molar ratio of surfactant:DNA base pairs (i.e. charge ratio), coupled with the low levels of transfection observed for the 12-3-n surfactants described above, we can conclude that the fluorescence from pyrene excimers is contaminating the signal from EGFP, rendering this assay useless for the py-3-m surfactants; the pyrene excimer emission was confirmed for the surfactants alone, for the GP and for the GDP complexes (data not shown). As such an alternative means of determining transfection efficiency for the py-3-m surfactants had to be used; an ELISA assay carried out in collaboration with Dr. Ildiko Badea from the College of Pharmacy at the University of Saskatchewan. The results of the ELISA assay will be discussed below.

The flow cytometry transfection results for the py-3-m surfactants were not useful, however, the cell viability assay used was still valid. Although it is based on fluorescent

emission, in this case the reporting chromophore is propidium iodide (PI), which has an emission maximum at 630nm, well resolved from the pyrene excimer (and EGFP) fluorescence. The pyrenyl surfactants showed greater cell viability compared to the positive control (Lipofectamine 2000,

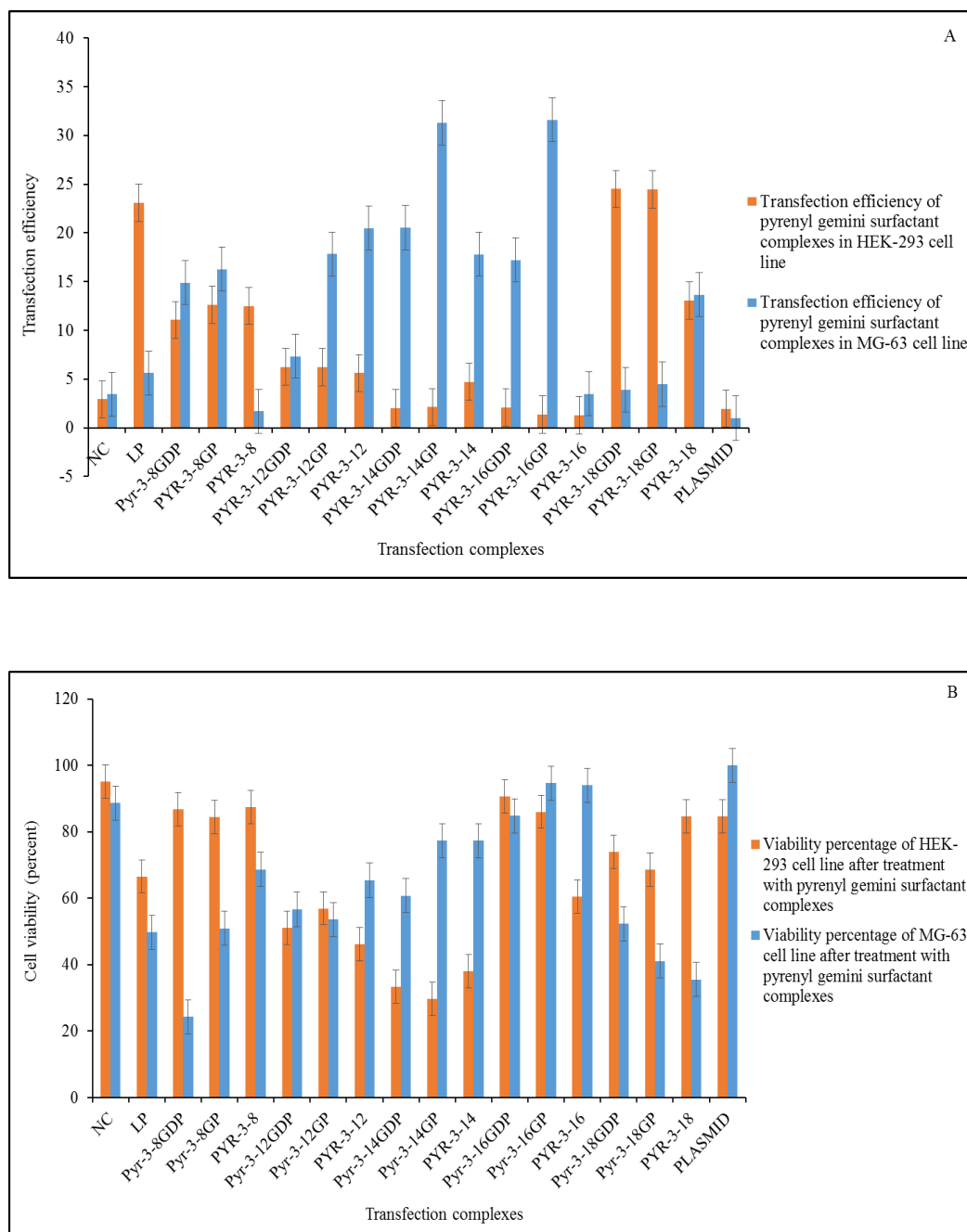


Figure 5.5 A) Transfection efficiency of pyrenyl gemini surfactant complexes in HEK-293 cell-line (orange) and in MG-63 cell-line (blue) and B) cell viability (same colors) with Lipofectamine 2000 as the positive control

cell viability = 50%; see Figure 5.5) with the exception of pyrene-3-8, which was observed to be quite toxic (24 % viable for the GDP system and 50% for the GP system). Similar results were observed in the HEK-293 cells.

The ELISA assay subsequently used to examine transfection efficiency for the py-3-m measures interferon-gamma protein (γ -IFN) expression directly and does not depend on fluorescence emission from EGFP. Very low transfection efficiencies (reported in terms of picogram/ 10^4 cells) were observed for the py-3-m surfactants (Figure 5.6), with the highest transfection observed for the py-3-8/DOPE/plasmid complexes at a 5:1 py-3-8:DNA charge ratio after 48h incubation (8600 ± 2600 pg/ 10^4 cells), and at a 10:1 charge ratio after 72h incubation (15000 ± 1500 pg/ 10^4 cells). It should be noted that these results are not directly comparable to the MG-63 or HEK-293 cells as a COS-7 cell line was used for transfection; however the COS-7 cells are known to be “easily transfectable” (Dr. Ildiko Badea, private communication). These results for pyr-3-8 complexes are higher than those of reported Lipofectamine plus in COS-7 cell line (INF- γ level of expression for Lipofectamine plus after 48 h = 2000pg/2000 cells, and <2500pg/2000 cells after 72 h).^{228, 238} The toxicity of the GDP nanoparticles prepared with the five gemini surfactants was evaluated in COS-7 cell line after 48 h of treatment. The cell viability of the pyrenyl surfactants in the COS-7 cell line were measured using an MTT-assay and are reported in Figure 5.7 (see also Table 5.9 in Appendix C). Cell viabilities are generally greater than 70% regardless of surfactant used; however both the ELISA assay and the cell viability assay lacked the Lipofectamine 2000 positive control and will need to be repeated in the future.

5.4 Conclusion

Overall, the 12-3-n and py-3-m surfactants were able to transfect DNA in multiple cell lines (for the 12-3-n surfactants); however the efficiencies observed were generally poor, and

certainly not at a level that could be suitable for any clinical application. Clearly extensive optimization of these systems would be required before any of the potential promise as a viable transfection vector (indicated by the results of our Langmuir monolayer and BAM studies) could be realized. The cell viabilities for the py-3-m surfactants was greater than that observed for the 12-3-n surfactants, with reasonable viabilities in MG-63 and HEK-293 cell lines, and good viabilities in the COS-7 cells. This suggests the py-3-m surfactants may have greater potential than the 12-3-n surfactants; however future studies are clearly required.

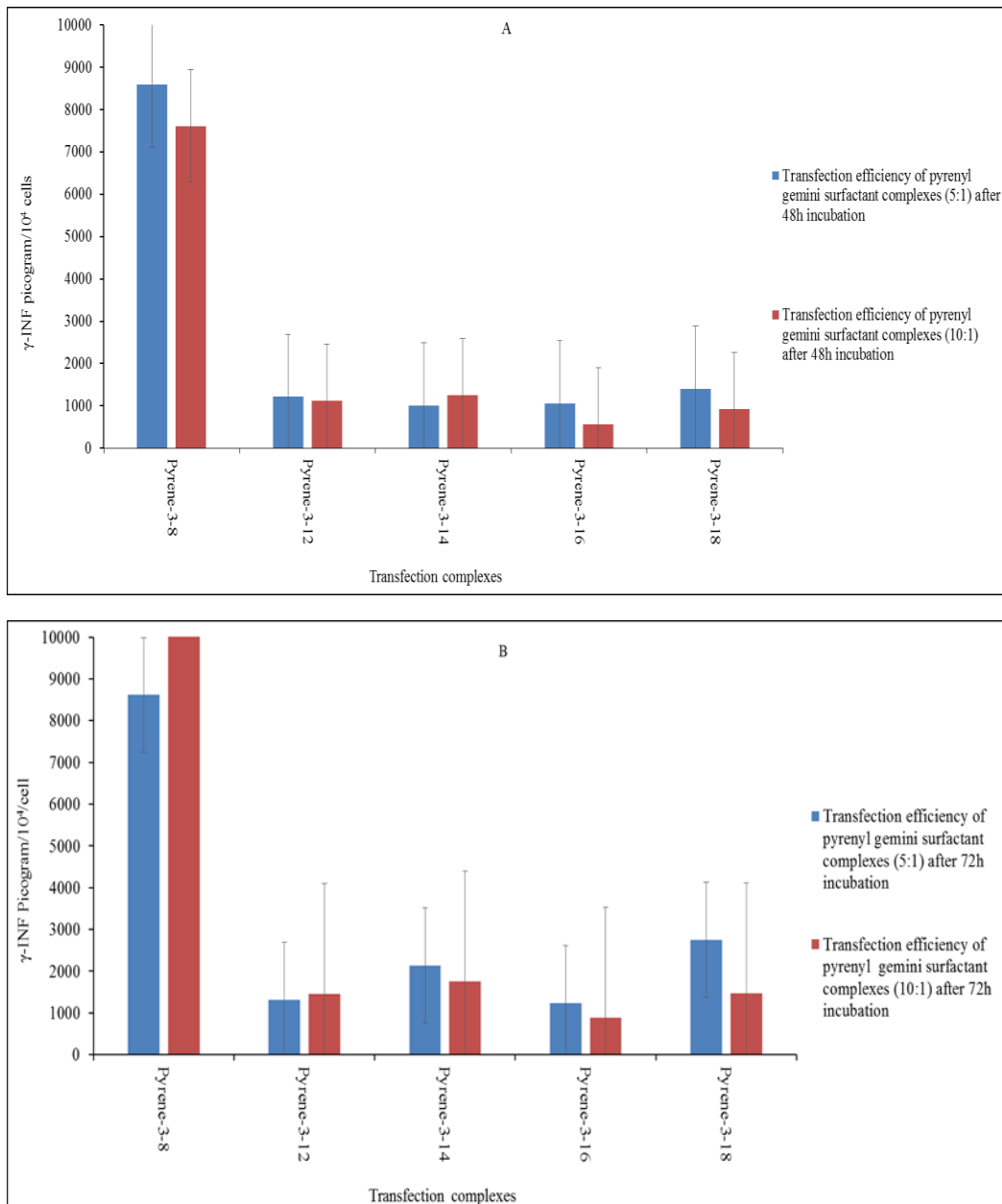


Figure 5.6 ELISA protein expression results of pyrene-based gemini surfactants complexes in COS-7 cell lines after two incubation times; A) 48h and B)72h with Lipofectamine plus as the positive control

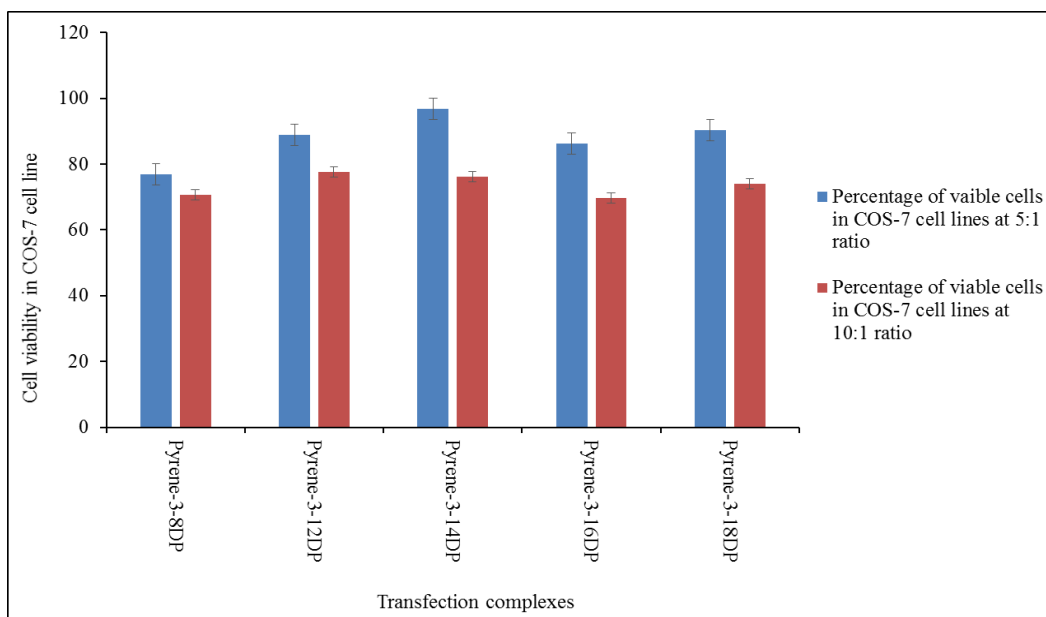


Figure 5.7 Cytotoxicity produced by pyrene-based gemini surfactant complexes in COS-7 cell line.

Chapter 6: Conclusion and future studies

We have successfully synthesized and characterized pyr-3-m and 12-3-n gemini surfactants. Pyrene-based gemini surfactants exhibited unique aggregation properties in solution with much lower CMC values than their symmetric counterparts with early onset of micellization. This is largely attributed to the presence of the pyrene moiety in the structure of the molecule, increasing the hydrophobicity of the surfactants, impacting the structure of the aggregates formed. These aggregates ranged from vesicular to lamellar and inverted structures. The 12-3-n gemini surfactants exhibited much lower CMC values compared to their symmetric counterparts, and this is possibly due to increased dissymmetry in the structure, enhancing the intermolecular hydrophobic interactions between the alkyl tails of the same length, favoring the micellization. Both of the pyrenyl and the dissymmetric gemini surfactants have higher degrees of micelle ionization compared to their symmetric counterparts, and this increases with the increase in the alkyl tail length. The higher the α , the greater the electrostatic repulsion between the two head groups, rendering the micelles partially charged, which enhances the interaction with the negatively charged phosphate groups of DNA to reduce the electrostatic repulsion between the head groups when used as a transfecting agent.

A study of the effect of these gemini surfactants alone or complexed with DNA on model membrane, mimicking the cellular membranes, using two model membranes (DPPC-Chol and POPC-Chol monolayers) was successfully determined in Chapter IV. We have successfully characterized models of the endosomal membranes of normal cells (DPPC-cholesterol = 75:25 %), and of cancer cells (POPC-Cholesterol= 75%:25%). The DPPC-Cholesterol monolayer showed solid phase at a surface pressure from 30 to 35 mN/m, indicating the rigidity of the membrane. Once the gemini surfactants were added to the DPPC-Cholesterol monolayer; whether those of pyrene-based surfactants, or the 12-3-n surfactants; with or without the DNA,

the rigidity of the membrane was substantially reduced and fluidity was induced. Pyrene-3-12 showed unique behavior that stood apart from the rest of the pyrenyl surfactants. When added to the monolayer, pyr-3-12 increased the compressibility modulus of the DPPC-Chol monolayer and this was attributed to its structure (closer to symmetry), which makes it fit better in between the gaps in the monolayer, making it more rigid. This behavior changes as soon as the DNA is added, the DNA reorients the pyr-3-12 structure, and changes its properties. This rearrangement induces fluidity of the monolayer, and this is applied to all of the pyrenyl gemini surfactants once the DNA is added. 12-3-n gemini surfactants showed to be dramatically disruptive to the DPPC-Chol, which was clear from the premature collapse induced by these surfactants. The POPC-Cholesterol system was found to be much more fluid at the same surface pressures, in the LE phase. All of the dissymmetric gemini surfactants (pyr-3-m and 12-3-n) increase the rigidity of the POPC-Chol monolayer due to insertion of the surfactant into the monolayer. However insertion of these surfactants between the molecules of POPC-Chol may hinder the motion of the oleyl chain in the POPC molecules in the monolayer, giving rise to an increase in rigidity. The addition of DNA resulted in increased fluidity of the monolayer as it was observed in the DPPC-Chol monolayer, further suggesting that in the presence of DNA, the interaction(s) are between the monolayer and the surfactant:DNA complexes at the air/water interface. Although our findings show that these gemini surfactants are expected to escape from the endosomal compartment, the strong interactions between the GS and the DNA may hinder the release of the DNA from the complex, which may result in its aggregation and clearance from the body instead of delivering the DNA into the nucleus. The Langmuir monolayer studies have proven the ability of the synthesized surfactants as part of GS-DNA complex to interact and be internalized into the membrane.

12-3-n and pyr-3-m gemini surfactants were able to transfect DNA in multiple celllines, however, the transfection results of 12-3-n were generally poor. Due to the spectral

contamination observed in the pyr-3-m transfection results, different method was used. ELISA assay for the transfection complexes in COS-7 were determined. In general, very little protein expression was observed for most of the pyrenyl surfactants, however, high protein expression (γ - INF) was recorded for pyr-3-8 complexes (whether after 48 h or 72 h incubation). Pyr-3-8 gave higher protein expression than the positive control (Lipofectamine plus), regardless the incubation time,²³⁹ proving to be a promising transfecting agent. These results might have been caused by the unique structure of the pyr-3-8, with short alkyl tail (octyl), which might have led to loose complexation to the DNA, possibly leading to easier release of the DNA from the complex. Pyr-3-m viability, whether determined by flow cytometry or MTT assay, proved that these surfactants are not as toxic as the 12-3-n or have higher cell viability than the positive control as observed for pyr-3-14 and pyr-3-16 complexes.

This project could be expanded by looking into these surfactants using Small-angle X-ray scattering (SAXS), which is a more accurate method to determine the presence of high-order morphologies. We can investigate dissymmetric surfactants using SAXS to observe changes of phase behavior to confirm the packing parameter results and the results observed in the Krafft temperature experiments, and whether or not the formation of inverted micelles is actually happening in the 12-3-n surfactants and in pyr-3-8 surfactant, and how adding the DNA can reorient the structures formed these surfactants in solution.^{240, 116} Moreover, differential scanning calorimetry (DSC) studies can be considered in order to observe the phase behavior (phase transition) as a function of temperature.

The effect of pluronics as co-surfactants that impart no toxicity and are biocompatible on model membranes, together with the GS-DNA complex can be investigated. Another area for further study is the effect of the pH on the monolayer. This was investigated by Taksim Ahmed in our lab with two different surfactants, 16-7N-16 and 16-7NH-16¹⁴³. The influence of pH on the interaction(s) of the vectors is very critical in the transfection experiments (*in vitro*). A better

understanding of the effect of pH can help us account for other possible factors that can hinder the passage of the vectors into the cell membrane, or even the passage through the cytosol without being cleared from the system. We can design the Langmuir monolayer with the temperature increased to 37°C to better mimic the conditions of the *in vitro* study instead of 20°C.

Another possibility is increasing the complexity of the model membranes to better mimic the real membranes. Additionally the late endosome is rich in lysobisphosphatidic acid (LBPA) or bis(monoacyl glycerol)phosphate (BMP) and a lysosome specific lipid which is not found elsewhere in the cells. Thus incorporating LBPA along with cholesterol could be a good model membrane study for the late endosome.

One of the strategies to improve transfection efficiency for gene therapy is to design new, more efficient vectors for transgene delivery. Transfection efficiencies of dissymmetric gemini surfactants were tested in two cell lines, MG-63 and HEK-293 and pyrenyl surfactant complexes were tested in COS-7 cell line as well. Data collected for pyrenyl surfactants showed very poor transfection results despite the observed disruptive actions of these surfactants in Chapter IV with both monolayers. 12-3-n gemini surfactant complexes showed low transfection as well, except for 12-3-16, which showed higher transfection (10% and 14% in both cell lines), which is still much lower than the lipofectamine 2000 in HEK-293 cells but not the MG-63. However, pyr-3-8 transfection results using ELISA has proven to be quite promising. More study and proper investigation of this surfactant in different cell lines is required to establish its efficiency as a transfecting agent. Moreover, optimization of the pyrenyl surfactant complexes with and without DOPE can be another strategy, because these surfactants proved to be not toxic or possess less toxicity compared to their symmetric or dissymmetric counterparts. Further investigation and more optimization should be considered before concluding their inefficiency as transfection agents.

Gene delivery abilities of these surfactants can be further investigated after applying structural modifications that can increase the transfection efficiency, such as, the introduction of tertiary or secondary amine into the spacer group. These modified pyr-7N-m and pyr-7NH-m can be tested in number of cell lines (PAM 212 and COS-7). Adding targeting moieties into the nanoparticle formulation (e.g. α - tocopherol or folic acid) to target a specific cell line can improve the transfection efficiencies. Folic acid receptors are over expressed in ovarian cancer and this can be a strategy to increase transfection efficiency.^{241, 242} Moreover, the effect of unsaturation can be investigated (C_{18:1}). The gene delivery assessment of these further-designed surfactants could be complemented by evaluation of their toxicological effects.

One of the options that can be explored, especially for pyr-3-8 complex, is the *in vivo* studies to see how well a non-viral vector would do when the complexity increases, and what optimization steps can be done to achieve a better transfection, and ultimately expression of the desired gene into a functioning protein. There are several *in vivo* studies that was done utilizing gemini surfactants as a non-viral vector with limited success, which means further testing and optimization are required to determine the full capability of gemini surfactants and other components of the vectors employed in each study.²²⁸ Intraperitoneal, intramuscular or subcutaneous methods were used for injecting the plasmid DNA or the lipoplex into animals in *in vivo* studies.²⁴³ In addition to those methods, topical DNA delivery where the formulation is applied to the skin with the aim of transfecting keratinocytes, dendritic cells or fibroblasts within the viable epidermis or dermis. Upon topical application, naked DNA or DNA encapsulated in a lipoplex system may be absorbed into the hair shaft and transfect the hair follicles, providing an opportunity for gene therapy of hair-growth disorders.²²⁸

References

1. Venter, J. C., Adams, M. D., Myers, E. W., Li, P. W., Mural, R. J., Sutton, G. G., Smith, H. O., Yandell, M., Evans, C. A., Holt, R. A. The sequence of the human genome. *Science* **2001**, *291*, 1304-1351.
2. Friedmann, T., Human gene therapy—an immature genie, but certainly out of the bottle. *Nat med* **1996**, *2*, 144-147.
3. Verma, I. M. Medicine. Gene therapy that works. *Science* **2013**, *341* (6148), 853-5.
4. Terheggen, H., Lowenthal, A., Lavinha, F., Colombo, J., Rogers, S. Unsuccessful trial of gene replacement in arginase deficiency. *Z. Kinderheilkde* **1975**, *119*, 1-3.
5. Sibbald, B. Death but one unintended consequence of gene-therapy trial. *Can. Med. Assoc. J.* **2001**, *164*, 1612-1612.
6. Giacca, M., Introduction to Gene Therapy. In *Gene Therapy*, Springer Milan: Milano, 2010; pp 1-7.
7. Giacca, M., Therapeutic Nucleic Acids. In *Gene therapy*, Springer-verlag Italia: 2010; Vol. 1, pp 9-45.
8. Butler, J., *Forensic DNA typing: Biology and technology behind STR markers*. Academic press: 2001.
9. Hyde, S. C., Gill, D. R., Higgins, C. F., Trezise, A. E., MacVinish, L. J., Cuthbert, A. W., Ratcliff, R., Evans, M. J., Colledge, W. H. Correction of the ion transport defect in cystic fibrosis transgenic mice by gene therapy. *Nature* **1993**, *362*, 250-255.
10. Templeton, N. A. E., *Gene and cell therapy: Therapeutic mechanisms and strategies [Revised and expanded]*. Marcel Dekker: New York, 2004.
11. Epstein, S. S. Environmental determinants of human cancer.[Hydrocarbons, Pesticides, Coal, Dyes, Rubber]. *Cancer Res.* **1974**, *34*, 1-37.
12. Wolff, J. A., Malone, R. W., Williams, P., Chong, W., Acsadi, G., Jani, A., Felgner, P. L. Direct gene transfer into mouse muscle in vivo. *Science* **1990**, *247*, 1465-8.
13. Liu, D., Satoh, E., Knapp, J.E., Naked DNA in Gene Therapy. *ELS* **2005**, 1-4.
14. Yang, N., Burkholder, J., Roberts, B., Martinell, B., McCabe, D. In vivo and in vitro gene transfer to mammalian somatic cells by particle bombardment. *Proc. Natl. Acad. Sci. U.S.A.* **1990**, *87*, 9568-9572.
15. Conwell, C. H. Molecules of Gene delivery: Recent progress in non-viral gene delivery. In *Non-viral gene therapy: Gene design and delivery.*, 1 ed.; Taira, K. K., K.; Niidomes, T., Ed. Springer-Verlag: Tokyo, Japan, 2005; Vol. 1, pp 4-8.
16. Wells, J. Li, L.H., Sen, A., Jahreis, G.P., Hui, S.W. Nonviral transfer technology: Electroporation enhanced gene delivery in mammary tumors. *Gene Ther* **2000**, *7*, 541-547.
17. Titomirov, A. V., Sukharev, S., Kistanova, E. In vivo electroporation and stable transformation of skin cells of newborn mice by plasmid DNA. *Biochim Biophys Acta* **1991**, *1088*, 131-4.
18. Hasson, E., Slovatzky, Y., Shimoni, Y., Falk, H., Panet, A., Mitrani, E. Solid tissues can be manipulated ex vivo and used as vehicles for gene therapy. *J Gene Med* **2005**, *7*, 926-35.
19. McMahan, J. M., Wells, D. J. Electroporation for gene transfer to skeletal muscles: current status. *BioDrugs* **2004**, *18*, 155-65.
20. Durieux, A. C., Bonnefoy, R., Busso, T., Freyssenet, D. In vivo gene electrotransfer into skeletal muscle: effects of plasmid DNA on the occurrence and extent of muscle damage. *J Gene Med* **2004**, *6*, 809-16.
21. Kamiya, H., Tsuchiya, H., Yamazaki, J., Harashima, H. Intracellular trafficking and transgene expression of viral and non-viral gene vectors. *Adv. Drug Deliv. Rev.* **2001**, *52*, 153-164.
22. Robbins, P. D. Chivizzani, S.C. Viral Vectors for gene therapy. *Pharmacol. Ther* **1998**, *80*.

23. Ginn, S. Alexander, IE., Edelstein, ML., Abedi, MR., Waxon, J., Gene therapy clinical trials world wide to 2012-an update. *J Gen Med* **2012**, *15*, 65-77.
24. Li, J., Pan, J., Zhu, X., Su, Y., Bao, L., Qiu, S., Zou, C., Cai, Y., Wu, J., Tham, I. W. K., Recombinant adenovirus-p53 (Gendicine) sensitizes a pancreatic carcinoma cell line to radiation. *Chin. J. Cancer Res.* **2013**, *25*, 715-721.
25. Guangyu, M., Shimada, H., Hiroshima, K., Tada, Y., Tagawa, M. Gene medicine for cancer treatment: Commercially available medicine and accumulated clinical data in China. *Drug Des. Dev. Ther* **2008**, *2*, 115-122.
26. Ginn, S. L., Alexander, I. E., Edelstein, M. L., Abedi, M. R., Wixon, J. Gene therapy clinical trials worldwide to 2012 - an update. *J Gene Med* **2013**, *15*, 65-77.
27. Blomer, U. Naldini, L., Verma, I M., Trono, D., Gage, FH. Applications of gene therapy to the CNS. *Hum.Mol.Genet* **1996**, *5*, 1397-1404.
28. Graham, F. P. L. Methods for construction of adenovirus vectors. *Mol.Biotechnol* **1995**, *3*, 207-220.
29. Yang, Wilson, J. M. Clearance of adenovirus-infected hepatocytes by MHC class I-restricted CD4⁺ CTL in vivo. *J.Immunol.* **1995**, *155*, 2564-2570.
30. Leopold, P. L., Ferris, B., Grinberg, I., Worgall, S., Hackett, N. R., Crystal, R. G. Fluorescent virions: dynamic tracking of the pathway of adenoviral gene transfer vectors in living cells. *Hum gene ther* **1998**, *9*, 367-378.
31. Luzio, J. P., Gray, S. R., Bright, N. A. Endosome-lysosome fusion. *Biochem.Soc. trans.* **2010**, *38*, 1413-6.
32. Sanlioglu, S., Benson, P. K., Yang, J., Atkinson, E. M., Reynolds, T., Engelhardt, J. F., Endocytosis and nuclear trafficking of adeno-associated virus type 2 are controlled by rac1 and phosphatidylinositol-3 kinase activation. *J. Virol* **2000**, *74*, 9184-9196.
33. Hacein-Bey-Abina, S. G., A., Wang, G P., Soulier, J., Lim, A., Morillon, E., Clappier, E., Caccavelli, L., Delabesse, E., Beldjord, K. Asnafi, V., MacIntyre, E., Dal Cortivo, L., Radford, I.; Brousse, N., Sigaux, F., Moshous, D., Hauer, J., Borkhardt, et al, Insertional oncogenesis in 4 patients after retrovirus-mediated gene therapy of SCID-X1. *J Clin Invest* **2008**, *118*, 3132.
34. Kirby, A. J., Camilleri, P., Engberts, J. B., Feiters, M. C., Nolte, R. J., Söderman, O., Bergsma, M., Bell, P. C., Fielden, M. L., García Rodríguez, C. L. Gemini surfactants: new synthetic vectors for gene transfection. *Angew.Chem.Int.Ed* **2003**, *42*, 1448-1457.
35. McCain, J., The Future of Gene Therapy. *Biotechnol HealthC* **2005**, *2*, 52-60.
36. Gao, X., Kim, K., Liu, D. Nonviral Gene Delivery: What We Know and What Is Next *AAPS J* **2007**, *9*, E92-E104.
37. Kostarelos, K. Miller, A.D. Synthetic, self-assembly ABCD nanoparticles; a structural paradigm for viable synthetic non-viral vectors. *Chem. Soc. Rev.* **2005**, *34*, 970-994.
38. Yin, H. Kanasty, R. L., Eltoukhy, AA., Vegas, A. J., Dorkin, J. R., Anderson, DG., Non-viral vectors for gene-based therapy. *Nat. Review.* **2014**, *15*, 541-555.
39. Thomas, M. Klibanov, A. M. Non-viral gene therapy: polycation-mediated DNA delivery. *Appl. Microbiol. Biotechnol.* **2003**, *62*, 27-34.
40. Morille, M., Passirani, C., Vonarbourg, A., Clavreul, A. , Benoit, J. P. Progress in developing cationic vectors for non-viral systemic gene therapy against cancer. *Biomaterials* **2008**, *29*, 3477-3496.
41. Wasungu, L. Hoekstra, D. Cationic lipids, lipoplexes and intracellular delivery of genes. *J. Control Release* **2006**, *116*, 255-264
42. Dinh, A.-T., Pangarkar, C., Theofanous, T., Mitragotri, S. Understanding intracellular transport processes pertinent to synthetic gene delivery via stochastic simulations and sensitivity analyses. *Biophys.l J* **2007**, *92*, 831-846.
43. Cooper, M. A. *The cell: A molecular approach*. Sinauer associates: 2000.

44. Pack, D. Hoffman, A.S., Pun, S.; Stayton, P.S., Design and Development of Polymers for gene delivery. *Nat. review. Drug delivery* **2005**, *4*, 581-593.
45. Mintzer, M A. Simanek, E. E. , Nonviral vectors for gene delivery. *Chem. Rev.* **2009**, *109* 259-302.
46. Wu, G. Y. Wu, C. H. , Receptor-mediated in vitro gene transformation by a soluble DNA carrier system. . *J. Biol. Chem.* **1987**, *264*, 4429-4432
47. Zanta, M. Boussif, O., Adib, A. , Behr, J.P. , In vitro gene delivery to hepatocytes with galactosylated polyethylenimine. *Bioconjugate Chem.* **1997**, *8*, 839-844.
48. Diebold, S. S. Kursa, M.; Wagner, E.; Cotten, M. ; Zenke, M. Mannose polyethylenimine conjugates for targeted DNA delivery into dendritic cells. *J. Biol. Chem.* **1999**, *274* , 19087-19094.
49. Kircheis, R., Blessing, R., Brunner, S., Wightman, L. , Wagner, E. , Tumor targeting with surface-shielded ligand-polycation DNA complexes. *J Control Release* (**2001**) , *72* , 165-170.
50. Wojda, U. Miller, J. L. Targeted transfer of polyethylenimine-avidin-DNA bioconjugates to hematopoietic cells using biotinylated monoclonal antibodies. *J. Pharm. Sci.* (**2000**), *89*, 674-681
51. Boletta, A. Benigni, A., Lutz, J. Remuzzi, G., Soria, M.R., Monaco, L., Nonviral gene delivery to the rat kidney with polyethylenimine. *Hum. Gene Ther.* **1997**, *8*, 1243-1251.
52. Coll, J. Collet, P., Brambilla, E., Desplanques, D., Behr, J. P., Favrot, M., In vivo delivery to tumors of DNA complexed with linear polyethylenimine. *Hum Gene Ther.* **1999**, *10*, 1659-66.
53. Behr, J. The proton sponge: a trick to enter cells the viruses did not exploit. *Chimia* **1997**, *51*, 34-36.
54. Nelson, N., Structure and pharmacology of the proton ATPase. *Trends. Pharmacol.Sci* **1991**, *12*, 71-75.
55. Plank, C. Oberhauser, B., Mechtler, K., Koch, C., Wagner, E. The influence of endosome-disruptive peptides on gene transfer using synthetic virus-like gene transfer systems. . *J. Biol. Chem.* **1994**, *269* , 12918-12924.
56. Pack, D. W.; Hoffman, A. S.; Pun, S.; Stayton, P. S., Design and development of polymers for gene delivery. *Nat. Rev. Drug Discov.* **2005**, *4*, 581-93.
57. Murthy, N.; Campbell, J.; Fausto, N.; Hoffman, A.; Stayton, P., Bioinspired polymeric carriers that enhance intracellular delivery of biomolecular therapeutics. *Bioconjugate Chem* **2003**, *14*, 412-419.
58. Hwang, S. Bellocq, N. C.; Davis, M. E., Effects of Structure of α -Cyclodextrin-Containing Polymers on Gene Delivery. *Bioconjugate Chem* **2001**, *12*, 280-290.
59. Kas, H., Chitosan: properties, preparations and applications to microparticulate systems. *J. Microencap* **1997**, *14*, 689-711.
60. Romøren, K.; Thu, B. J.; Evensen, Ø., Immersion delivery of plasmid DNA: II. A study of the potentials of a chitosan based delivery system in rainbow trout (*Oncorhynchus mykiss*) fry. *J Control Release.* **2002**, *85*, 215-225.
61. Hejazi, R. Amiji, M., Chitosan-based gastrointestinal delivery systems. *J. Controlled Release* **2003**, *89*, 151-165.
62. Fang, N. Chan, V., Mao, H.-Q., Leong, K.W. Interactions of phospholipid bilayer with chitosan: Effect of molecular weight and pH. *Biomacromolecules* **2001**, *12*, 1161-1168.
63. Corsi, K., Chellat, F., Yahia, L., Fernandes, J. C. Mesenchymal stem cells, MG63 and HEK293 transfection using chitosan-DNA nanoparticles. *Biomaterials* **2003**, *24*, 1255-1264.
64. Pouton, C., Seymour, L. W. Key issues in non-viral gene delivery. *Adv. Drug Del. Rev.* **1998**, *34*, 3-19.

65. Hashimoto, M.; Morimoto, M.; Saimoto, H.; Shigemasa, Y.; Sato, T., Lactosylated chitosan for DNA delivery into hepatocytes: the effect of lactosylation on the physicochemical properties and intracellular trafficking of pDNA/chitosan complexes. *Bioconjugate chem* **2006**, *17*, 309-16.
66. Thanou, M., Florea, B.I., Geldof, M., Junginger, H.E., Borchard, G. Quaternized chitosan oligomers as novel gene delivery vectors in epithelial cell lines. *Biomaterials* **2002**, *23*, 153-159.
67. Wasungu, L. Hokestra, D., Cationic lipids, Lipoplexes and intracellular delivery of gene. *J. Control Release* **2005**, *116*, 255-264.
68. Zhi, D., Zhang, S., Cui, S., Zhao, Y., Wang, Y., Zhao, D. The Headgroup Evolution of Cationic Lipids for Gene Delivery. *Bioconjug. Chem.* **2013**, *24*, 487-519.
69. Brgles, M., Santak, M., Halassy, B., Forcic, D., Tomasic, J. Influence of charge ratio of liposome/DNA complexes on their size after extrusion and transfection efficiency. *Int. J. Nanomed* **2012**, *12*, 393-401.
70. Almofti, M. R., Harashima, H., Shinohara, Y., Almofti, A., Baba, Y., Kiwada, H. Cationic liposome-mediated gene delivery: biophysical study and mechanism of internalization. *Arch Biochem biophys* **2003**, *410*, 246-253.
71. Safinya, C. R., Structures of lipid–DNA complexes: supramolecular assembly and gene delivery. *Cur. Opin Struct. Biol* **2001**, *11*, 440-448.
72. Felgner, P. L., Gadek, T. R., Holm, M., Roman, R., Chan, H. W., Wenz, M., Northrop, J. P., Ringold, G. M., Danielsen, M. Lipofection: a highly efficient, lipid-mediated DNA-transfection procedure. *Proc. Natl. Acad. Sci. U.S.A* **1987**, *84*, 7413-7417.
73. Hafez, I. M., Ansell, S., Cullis, P. R. Tunable pH-sensitive liposomes composed of mixtures of cationic and anionic lipids. *Biophys. J.* **2000**, *79*, 1438-1446.
74. Walker, G. F., Fella, C., Pelisek, J., Fahrmeir, J., Boeckle, S., Ogris, M., Wagner, E. Toward synthetic viruses: endosomal pH-triggered deshielding of targeted polyplexes greatly enhances gene transfer in vitro and in vivo. *Mol Ther* **2005**, *11*, 418-425.
75. Immordino, M. L., Dosio, F., Cattel, L. Stealth liposomes: review of the basic science, rationale, and clinical applications, existing and potential. *Int. J. Nanomed.* **2006**, *1*, 297-315.
76. Ewert, K. K., Samuel, C. E., Safinya, C. R. Lipid–DNA interactions: structure–function studies of nanomaterials for gene delivery. In *DNA interactions with polymers and surfactants*, Dias, R. L., B., Ed. John Wiley & Sons Nj, USA: 2008; Vol. 1, pp 377-404.
77. Dass, C. R., Vehicles for oligonucleotide delivery to tumours. *J. Pharm. Pharmacol.* **2002**, *54*, 3-27.
78. Lv, H., Zhang, S., Wang, B., Cui, S., Yan, J. Toxicity of cationic lipids and cationic polymers in gene delivery. *J. Control Release* **2006**, *114*, 100-109.
79. Pinnaduwege, P., Schmitt, L., Huang, L. Use of a quaternary ammonium detergent in liposome mediated DNA transfection of mouse L-cells. *Biochem Biophys acta* **1989**, *985*, 33-37.
80. Tang, F., Hughes, J. A. Synthesis of a single-tailed cationic lipid and investigation of its transfection. *J. Control Release.* **1999**, *62*, 345-358.
81. Bottega, R., Epan, R. M. Inhibition of protein kinase C by cationic amphiphiles. *Biochem* **1992**, *31*, 9025-9030.
82. Heyes, J. A., Niculescu-Duvaz, D., Cooper, R. G., Springer, C. J. Synthesis of novel cationic lipids: effect of structural modification on the efficiency of gene transfer. *J. Med. Chem* **2002**, *45*, 99-114.
83. Solodin, I., Brown, C. S., Bruno, M. S., Chow, C.-Y., Jang, E.-H., Debs, R. J., Heath, T. D. A novel series of amphiphilic imidazolium compounds for in vitro and in vivo gene delivery. *Biochemistry* **1995**, *34*, 13537-13544.
84. Iliès, M. A., Johnson, B. H., Makori, F., Miller, A., Seitz, W. A., Thompson, E. B., Balaban, A. T. Pyridinium cationic lipids in gene delivery: an in vitro and in vivo comparison of

transfection efficiency versus a tetraalkylammonium congener. *Arch Biochem Biophys* **2005**, *435*, 217-26.

85. Yingyongnarongkul, B. E., Howarth, M., Elliott, T., Bradley, M. Solid-Phase Synthesis of 89 Polyamine-Based Cationic Lipids for DNA Delivery to Mammalian Cells. *Chem. Eur. J.* **2004**, *10*, 463-473.

86. (a) Freedland, S. J., Malone, R. W., Borchers, H. M., Zadourian, Z., Malone, J. G., Bennett, M. J., Nantz, M. H., Li, J.-H., Gumerlock, P. H., Erickson, K. L. Toxicity of cationic lipid-ribozyme complexes in human prostate tumor cells can mimic ribozyme activity. *Biochem Mol Med* **1996**, *59*, 144-153; (b) Choi, J. S., Lee, E. J., Jang, H. S., Park, J. S., New cationic liposomes for gene transfer into mammalian cells with high efficiency and low toxicity. *Bioconjugate chem* **2001**, *12*, 108-113.

87. (a) Liu, D., Hu, J., Qiao, W., Li, Z., Zhang, S., Cheng, L. Synthesis of carbamate-linked lipids for gene delivery. *Bioorg. Med. Chem. Lett.* **2005**, *15*, 3147-3150; (b) Ren, T., Zhang, G., Liu, D. Synthesis of bifunctional cationic compound for gene delivery. *Tetrahedron Lett.* **2001**, *42*, 1007-1010.

88. Farhood, H., Serbina, N., Huang, L. The role of dioleoyl phosphatidylethanolamine in cationic liposome mediated gene transfer. *Biochim Biophys Acta* **1995**, *1235*, 289-295.

89. Zhou, X., Huang, L. DNA transfection mediated by cationic liposomes containing lipopolylysine: characterization and mechanism of action. *Biochim Biophys Acta* **1994**, *1189*, 195-203.

90. Hirsch-Lerner, D., Zhang, M., Eliyahu, H., Ferrari, M. E., Wheeler, C. J., Barenholz, Y. Effect of "helper lipid" on lipoplex electrostatics. *Biochim Biophys Acta* **2005**, *1714*, 71-84.

91. Friend, D. S., Papahadjopoulos, D., Debs, R. J. Endocytosis and intracellular processing accompanying transfection mediated by cationic liposomes. *Biochim Biophys Acta* **1996**, *1278*, 41-50.

92. Hong, K., Zheng, W., Baker, A., Papahadjopoulos, D. Stabilization of cationic liposome-plasmid DNA complexes by polyamines and poly(ethylene glycol)-phospholipid conjugates for efficient in vivo gene delivery. *FEBS Letters* **1997**, *400*, 233-237.

93. Templeton, N. S., Lasic, D. D., Frederik, P. M., Strey, H. H., Roberts, D. D., Pavlakis, G. N. Improved DNA: liposome complexes for increased systemic delivery and gene expression. *Nature Biotechnol.* **1997**, *15*, 647-652.

94. Menger, F. M., Littau, C. Gemini-surfactants: synthesis and properties. *J. Am. Chem. Soc.* **1991**, *113*, 1451-1452.

95. Iliés, M. A., Seitz, W. A., Johnson, B. H., Ezell, E. L., Miller, A. L., Thompson, E. B., Balaban, A. T. Lipophilic pyrylium salts in the synthesis of efficient pyridinium-based cationic lipids, gemini surfactants, and lipophilic oligomers for gene delivery. *J. Med. Chem.* **2006**, *49*, 3872-3887.

96. Wettig, S. D., Verrall, R. E., Foldvari, M. Gemini surfactants: a new family of building blocks for non-viral gene delivery systems. *Cur. Gene. Ther.* **2008**, *8*, 9-23.

97. Zana, R., Dimeric and oligomeric surfactants. Behavior at interfaces and in aqueous solution: a review. *Adv. Colloid Interface Sci.* **2002**, *97*, 205-253.

98. Song, L. D., Rosen, M. J. Surface properties, micellization, and premicellar aggregation of gemini surfactants with rigid and flexible spacers. *Langmuir* **1996**, *12*, 1149-1153.

99. Danino, D., Talmon, Y., Zana, R. Alkanediyl-. alpha.,. omega.-Bis (Dimethylalkylammonium Bromide) Surfactants (Dimeric Surfactants). 5. Aggregation and Microstructure in Aqueous Solutions. *Langmuir* **1995**, *11*, 1448-1456.

100. Zana, R., Xia, J. *Gemini surfactants: synthesis, interfacial and solution-phase behavior, and applications*. Crc Press: 2003; Vol. 117.

101. Zana, R., Benrraou, M., Rueff, R. Alkanediyl-. alpha.,. omega.-bis (dimethylalkylammonium bromide) surfactants. 1. Effect of the spacer chain length on the critical micelle concentration and micelle ionization degree. *Langmuir* **1991**, *7*, 1072-1075.
102. Rosen, M. J., Tracy, D. J. Gemini surfactants. *J. Surfactants Deterg.* **1998**, *1*, 547-554.
103. Kopecká-Leitmanová, A., Devinsky, F., Mlynarcik, D., Lacko, I. Interaction of amine oxides and quaternary ammonium salts with membrane and membrane-associated processes in E. coli cells: mode of action. *Drug Metabol Drug interact* **1989**, *7*, 29-52.
104. Bombelli, C., Giansanti, L., Luciani, P., Mancini, G. Gemini surfactant based carriers in gene and drug delivery. *Cur. Med. Chem.* **2009**, *16*, 171-183.
105. Wang, H., Wettig, S. D. Synthesis and aggregation properties of dissymmetric phytanyl-gemini surfactants for use as improved DNA transfection vectors. *Phys. Chem. Chem. Phys.* **2011**, *13*, 637-642.
106. Koltover, I., Salditt, T., Rädler, J. O., Safinya, C. R. An inverted hexagonal phase of cationic liposome-DNA complexes related to DNA release and delivery. *Science* **1998**, *281*, 78-81.
107. Foldvari, M., Badea, I., Wettig, S., Verrall, R., Bagonluri, M. Structural characterization of novel gemini non-viral DNA delivery systems for cutaneous gene therapy. *J. Exp.Nanosci.* **2006**, *1*, 165-176.
108. Li, X., Wettig, S. D., Wang, C., Foldvari, M., Verrall, R. E. Synthesis and solution properties of gemini surfactants containing oleyl chains. *Phys.Chem. Chem. Phys.* **2005**, *7*, 3172-3178.
109. Wang, C., Wettig, S. D., Foldvari, M., Verrall, R. E. Synthesis, characterization, and use of asymmetric pyrenyl-gemini surfactants as emissive components in DNA-lipoplex systems. *Langmuir* **2007**, *23*, 8995-9001.
110. Kirby, A. J., Camilleri, P., Engberts, J. B., Feiters, M. C., Nolte, R. J., Söderman, O., Bergsma, M., Bell, P. C., Fielden, M. L., García Rodríguez, C. L. Gemini surfactants: new synthetic vectors for gene transfection. *Angew Chemie Int Ed* **2003**, *42*, 1448-1457.
111. Cardoso, A. M., Morais, C. M., Silva, S. G., Marques, E. F., De Lima, M. C. P., Jurado, M. A. S. Bis-quaternary gemini surfactants as components of nonviral gene delivery systems: A comprehensive study from physicochemical properties to membrane interactions. *Int. J. Pharm.* **2014**, *474*, 57-69.
112. Akbar, J. R., Deubry, R., Marangoni, D. G., Wettig, S. D. Interactions between gemini and nonionic pharmaceutical surfactants. *Can. J. Chem.* **2010**, *88*, 1262-1270.
113. Muñoz-Úbeda, M. N., Misra, S. K., Barrán-Berdón, A. L., Datta, S., Aicart-Ramos, C., Castro-Hartmann, P., Kondaiah, P., Junquera, E., Bhattacharya, S., Aicart, E. How does the spacer length of cationic gemini lipids influence the lipoplex formation with plasmid DNA? Physicochemical and biochemical characterizations and their relevance in gene therapy. *Biomacromolecules* **2012**, *13*, 3926-3937.
114. Mintzer, M. A., Simanek, E. E., Nonviral vectors for gene delivery. *Chem. Rev.* **2008**, *109*, 259-302.
115. Johnsson, M., Engberts, J. B. Novel sugar-based gemini surfactants: aggregation properties in aqueous solution. *J.Phys. Org.Chemistry* **2004**, *17*, 934-944.
116. Wasungu, L., Scarzello, M., van Dam, G., Molema, G., Wagenaar, A., Engberts, J. B., Hoekstra, D. Transfection mediated by pH-sensitive sugar-based gemini surfactants; potential for in vivo gene therapy applications. *J. Mol. Med.* **2006**, *84*, 774-784.
117. Johnsson, M., Wagenaar, A., Stuart, M. C., Engberts, J. B. Sugar-based gemini surfactants with pH-dependent aggregation behavior: vesicle-to-micelle transition, critical micelle concentration, and vesicle surface charge reversal. *Langmuir* **2003**, *19*, 4609-4618.

118. Cardoso, A. M., Morais, C. M., Cruz, A. R., Silva, S. G., do Vale, M. L., Marques, E. F., de Lima, M. C. P.; Jurado, A. S., New serine-derived gemini surfactants as gene delivery systems. *Eur. J. Pharm. Biopharm.* **2015**, *89*, 347-356.
119. Faneca, H., Simões, S., Pedroso de Lima, M. C. Evaluation of lipid-based reagents to mediate intracellular gene delivery. *Biochim Biophys Acta* **2002**, *1567*, 23-33.
120. Yu, H., Chen, X., Lu, T., Sun, J., Tian, H., Hu, J., Wang, Y., Zhang, P., Jing, X. Poly (L-lysine)-graft-chitosan copolymers: synthesis, characterization, and gene transfection effect. *Biomacromolecules* **2007**, *8*, 1425-1435.
121. Alami, E., Beinert, G., Marie, P., Zana, R. Alkanediyl-. alpha.,. omega.-bis (dimethylalkylammonium bromide) surfactants. 3. Behavior at the air-water interface. *Langmuir* **1993**, *9*, 1465-1467.
122. Zana, R. Dimeric (gemini) surfactants: effect of the spacer group on the association behavior in aqueous solution. *J. Colloid Interface Sci.* **2002**, *248*, 203-220.
123. Israelachvili, J. N., Mitchell, D. J., Ninham, B. W. Theory of self-assembly of hydrocarbon amphiphiles into micelles and bilayers. *J. Chem. Soc. Faraday Trans* **1976**, *72*, 1525-1568.
124. Karlsson, L., van Eijk, M. C. P., Söderman, O. Compaction of DNA by Gemini Surfactants: Effects of Surfactant Architecture. *J. Colloid Interface Sci.* **2002**, *252*, 290-296.
125. Myers, D., *Surfactant science and technology*. John Wiley & Sons: 2005.
126. Wettig, S. D., Badea, I., Donkuru, M., Verrall, R. E., Foldvari, M. Structural and transfection properties of amine-substituted gemini surfactant-based nanoparticles. *J Gene Med* **2007**, *9*, 649-658.
127. (a) Chesnoy, S., Huang, L. Structure and function of lipid-DNA complexes for gene delivery. *Annu. Rev. Biophys. Biomol. struct.* **2000**, *29*, 27-47; (b) Dass, C. R. Biochemical and biophysical characteristics of lipoplexes pertinent to solid tumour gene therapy. *Int. J. pharm* **2002**, *241*, 1-25.
128. Egli, M., Saenger, W. *Principles of nucleic acid structure*. Springer Science & Business Media: 2013.
129. Ouameur, A. A., Tajmir-Riahi, H.-A. Structural analysis of DNA interactions with biogenic polyamines and cobalt (III) hexamine studied by Fourier transform infrared and capillary electrophoresis. *J. Biol.Chem.* **2004**, *279*, 42041-42054.
130. Ruiz-Chica, J., Medina, M., Sánchez-Jiménez, F., Ramirez, F. Fourier transform Raman study of the structural specificities on the interaction between DNA and biogenic polyamines. *Biophys. J.* **2001**, *80*, 443-454.
131. Fiscaro, E., Compari, C., Bacciottini, F., Contardi, L., Barbero, N., Viscardi, G., Quagliotto, P., Donofrio, G., Różycka-Roszak, B., Misiak, P., Woźniak, E., Sansone, F. Nonviral Gene Delivery: Gemini Bispyridinium Surfactant-Based DNA Nanoparticles. *J.Phys.Chem. B* **2014**, *118*, 13183-13191.
132. Misra, S. K., Biswas, J., Kondaiah, P., Bhattacharya, S. Gene transfection in high serum levels: case studies with new cholesterol based cationic gemini lipids. *PloS one* **2013**, *8*, e68305 (1-19).
133. Zhuang, L., Kim, J., Adam, R. M., Solomon, K. R., Freeman, M. R. Cholesterol targeting alters lipid raft composition and cell survival in prostate cancer cells and xenografts. *J. Clin. invest.* **2005**, *115*, 959-968.
134. De Lima, M. C. P., Simoes, S., Pires, P., Faneca, H., Düzgüneş, N. Cationic lipid-DNA complexes in gene delivery: from biophysics to biological applications. *Adv. Drug Deliv. Rev.* **2001**, *47*, 277-294.
135. Wettig, S. D., Verrall, R. E., Foldvari, M. Gemini surfactants: a new family of building blocks for non-viral gene delivery systems. *Curr. Gene ther.* **2008**, *8*, 9-23.

136. Bell, P. C., Bergsma, M., Dolbnya, I. P., Bras, W., Stuart, M. C., Rowan, A. E., Feiters, M. C., Engberts, J. B. Transfection mediated by gemini surfactants: engineered escape from the endosomal compartment. *J. Am. Chem. Soc.* **2003**, *125*, 1551-1558.
137. McGregor, C., Perrin, C., Monck, M., Camilleri, P., Kirby, A. J. Rational approaches to the design of cationic gemini surfactants for gene delivery. *J. Am. Chem. Soc.* **2001**, *123*, 6215-6220.
138. Alqawlaq, S., Sivak, J. M., Huzil, J. T., Ivanova, M. V., Flanagan, J. G., Beazely, M. A., Foldvari, M. Preclinical development and ocular biodistribution of gemini-DNA nanoparticles after intravitreal and topical administration: Towards non-invasive glaucoma gene therapy. *Nanomedicine: Nanotech Biol Med* **2014**, *10*, 1637-1647.
139. Oda, R., Candau, S. J., Huc, I. Gemini surfactants, the effect of hydrophobic chain length and dissymmetry. *Chem Commun* **1997**, *21*, 2105-2106.
140. Wang, X., Wang, J., Wang, Y., Ye, J., Yan, H., Thomas, R. K. Micellization of a series of dissymmetric gemini surfactants in aqueous solution. *J. Phys. Chem. B.* **2003**, *107*, 11428-11432.
141. Wang, H., Kaur, T., Tavakoli, N., Joseph, J., Wettig, S. Transfection and structural properties of phytanyl substituted gemini surfactant-based vectors for gene delivery. *Phys. Chem. Chem. Phys.* **2013**, *15*, 20510-20516.
142. Henderson, R. D. E. Nanoscale physics of surfactant gene delivery. 2016.
143. Ahmed, T. Langmuir-Blodgett Monolayer Studies of Mixed Gemini Surfactant-Phospholipid Monolayers system for Gene Therapy Applications. Waterloo, 2015.
144. Cristofolini, L., Berzina, T., Erokhina, S., Konovalov, O., Erokhin, V. Structural study of the DNA dipalmitoylphosphatidylcholine complex at the air-water interface. *Biomacromolecules* **2007**, *8*, 2270-2275.
145. Peetla, C., Stine, A., Labhasetwar, V. Biophysical interactions with model lipid membranes: applications in drug discovery and drug delivery. *Mol. pharm.* **2009**, *6*, 1264-1276.
146. Corvis, Y., Barzyk, W., Brezesinski, G., Mrabet, N., Badis, M., Hecht, S., Rogalska, E. Interactions of a fungistatic antibiotic, griseofulvin, with phospholipid monolayers used as models of biological membranes. *Langmuir* **2006**, *22*, 7701-7711.
147. Rubio-Magnieto, J., Luis, S. V., Orlof, M., Korchowiec, B., Sautrey, G., Rogalska, E. Effects of gemini amphiphilic pseudopeptides on model lipid membranes: A Langmuir monolayer study. *Colloids Surf B: Biointerfaces* **2013**, *102*, 659-666.
148. Barnes, G.; Gentle, I., *Interfacial science: an introduction*. Oxford University Press: 2011.
149. Moghaddam, B., Ali, M. H., Wilkhu, J., Kirby, D. J., Mohammed, A. R., Zheng, Q., Perrie, Y. The application of monolayer studies in the understanding of liposomal formulations. *Int. J. Pharm.* **2011**, *417*, 235-244.
150. (a) Vollhardt, D., Fainerman, V. Progress in characterization of Langmuir monolayers by consideration of compressibility. *Adv. Colloid Interface Sci.* **2006**, *127*, 83-97; (b) Wnętrzak, A., Łątka, K., Dynarowicz-Łątka, P. Interactions of alkylphosphocholines with model membranes—the langmuir monolayer study. *J. Membr. Biol.* **2013**, *246*, 453-466.
151. Van Meer, G., Voelker, D. R., Feigenson, G. W. Membrane lipids: where they are and how they behave. *Nat. Rev. Mol. Cell Biol.* **2008**, *9*, 112-124.
152. Lodish, H., Berk, A., Zipursky, S. L., Matsudaira, P., Baltimore, D., Darnell, J., *Mol. Cell. Biol.* WH Freeman New York: 2000; Vol. 4.
153. Yetukuri, L., Ekroos, K., Vidal-Puig, A., Orešič, M. Informatics and computational strategies for the study of lipids. *Mol. Biosyst.* **2008**, *4*, 121-127.
154. Singer, S. J., Nicolson, G. L. The fluid mosaic model of the structure of cell membranes. *Science* **1972**, *175*, 720-731.

155. Kenny, J. Mammalian cell membranes. The diversity of membranes. Robinson, G. J. a. D., Ed. Elsevir: Butterwoths, London and Boston, 1978; Vol. 2, p 364.
156. Ikonen, E., Roles of lipid rafts in membrane transport. *Cur Opin Cell Biol* **2001**, *13*, 470-477.
157. Guirr, M., James, A., Lipid Biochemistry. *University Press, Cambridge* **1980**.
158. Yeagle, P. L. Cholesterol and the cell membrane. *Biochim Biophys Acta*. **1985**, *822*, 267-287.
159. Maxfield, F. R., Wüstner, D. Intracellular cholesterol transport. *J.Clin. Invest.* **2002**, *110*, 891-898.
160. Lange, Y., Ye, J., Steck, T. L. How cholesterol homeostasis is regulated by plasma membrane cholesterol in excess of phospholipids. *Proc.Natl. Acad. Sci.U.S.A.* **2004**, *101*, 11664-11667.
161. Hao, M., Lin, S. X., Karylowski, O. J., Wüstner, D., McGraw, T. E., Maxfield, F. R. Vesicular and non-vesicular sterol transport in living cells The endocytic recycling compartment is a major sterol storage organelle. *J. Biol. Chem.* **2002**, *277*, 609-617.
162. Jamieson, G. A., Robinson, D. M., *Mammalian cell membranes: Volume 2: The diversity of membranes*. Elsevier: 2014.
163. Guha, S., Rajani, M., Padh, H. Identification and characterization of lipids from endosomes purified by electromagnetic chromatography. *Indian J. Biochem. Biophys.* **2007**, *44*, 443.
164. Marsh, M., McMahon, H. The structural era of endocytosis. *Science* **1999**, *285*, 215-220.
165. Feng, S.-S. Interpretation of mechanochemical properties of lipid bilayer vesicles from the equation of state or pressure-area measurement of the monolayer at the air-water or oil-water interface. *Langmuir* **1999**, *15*, 998-1010.
166. Nagle, J. Theory of lipid monolayer and bilayer phase transitions: effect of headgroup interactions. *J.Membr. Biol.* **1976**, *27*, 233-250.
167. Brezesinski, G., Möhwald, H. Langmuir monolayers to study interactions at model membrane surfaces. *Adv. Colloid Interface Sci.* **2003**, *100*, 563-584.
168. Janiak, M. J., Small, D. M., Shipley, G. G. Temperature and compositional dependence of the structure of hydrated dimyristoyl lecithin. *J. Biol.Chem.* **1979**, *254*, 6068-6078.
169. Boxer, S. G., Molecular transport and organization in supported lipid membranes. *Curr Opin Chem Biol* **2000**, *4*, 704-709.
170. Plant, A. L., Brighamburke, M., Petrella, E. C., Oshannessy, D. J. Phospholipid/alkanethiol bilayers for cell-surface receptor studies by surface plasmon resonance. *Anal. Biochem.* **1995**, *226*, 342-348.
171. Xu, L., Frederik, P., Pirollo, K. F., Tang, W.-H., Rait, A., Xiang, L.-M., Huang, W., Cruz, I., Yin, Y., Chang, E. H. Self-assembly of a virus-mimicking nanostructure system for efficient tumor-targeted gene delivery. *Hum Gene Ther* **2002**, *13*, 469-481.
172. Qi, S., Groves, J. T., Chakraborty, A. K. Synaptic pattern formation during cellular recognition. *Proc. Natl. Acad. Sci.U.S.A* **2001**, *98*, 6548-6553.
173. Johnson, S., Bayerl, T., McDermott, D., Adam, G., Rennie, A., Thomas, R., Sackmann, E. Structure of an adsorbed dimyristoylphosphatidylcholine bilayer measured with specular reflection of neutrons. *Biophys. J.* **1991**, *59*, 289-294.
174. Bayerl, T. M., Bloom, M. Physical properties of single phospholipid bilayers adsorbed to micro glass beads. A new vesicular model system studied by 2H-nuclear magnetic resonance. *Biophys. J.* **1990**, *58*, 357.
175. Castano, S., Delord, B., Février, A., Lehn, J.-M., Lehn, P., Desbat, B. Brewster angle microscopy and PMIRRAS study of DNA interactions with BGTC, a cationic lipid used for gene transfer. *Langmuir* **2008**, *24*, 9598-9606.

176. Matti, V., Säily, J., Ryhänen, S. J., Holopainen, J. M., Borocci, S., Mancini, G., Kinnunen, P. K. Characterization of mixed monolayers of phosphatidylcholine and a dicationic gemini surfactant SS-1 with a langmuir balance: effects of DNA. *Biophys. J.* **2001**, *81*, 2135-2143.
177. Raghavan, S. R., Kaler, E. W. Highly viscoelastic wormlike micellar solutions formed by cationic surfactants with long unsaturated tails. *Langmuir* **2001**, *17*, 300-306.
178. Wang, H. Phytanyl substituted asymmetric gemini surfactant-based transfection vectors for gene therapy. 2013.
179. Wettig, S. D., Deubry, R., Akbar, J., Kaur, T., Wang, H., Sheinin, T., Joseph, J. W., Slavcev, R. A., Thermodynamic investigation of the binding of dissymmetric pyrenyl-gemini surfactants to DNA. *Phys. Chem. Chem. Phys.* **2010**, *12*, 4821-4826.
180. Klock, J. C., Pieprzyk, J. K. Cholesterol, phospholipids, and fatty acids of normal immature neutrophils: comparison with acute myeloblastic leukemia cells and normal neutrophils. *J. lipid Res.* **1979**, *20*, 908-911.
181. El-Sayed, A., Harashima, H. Endocytosis of gene delivery vectors: from clathrin-dependent to lipid raft-mediated endocytosis. *Mol Ther* **2013**, *21*, 1118-1130.
182. Pike, L. J. Lipid rafts: bringing order to chaos. *J. Lipid Res.* **2003**, *44*, 655-67.
183. Vereb, G., Szollosi, J., Matko, J., Nagy, P., Farkas, T., Vigh, L., Matyus, L., Waldmann, T. A., Damjanovich, S. Dynamic, yet structured: The cell membrane three decades after the Singer-Nicolson model. *Proc. Natl. Acad. Sci. U. S. A.* **2003**, *100*, 8053-8.
184. Ahmed, T., Kamel, A. O., Wettig, S. D. Interactions between DNA and Gemini surfactant: impact on gene therapy: part I. *Nanomed* **2016**, *11*, 289-306.
185. Geschke, O., Klank, H., Telleman, P. *Microsystem Engineering of Lab-on-a-chip Devices*. Wiley Online Library: 2004; Vol. 258.
186. Birks, J. B., Photophysics of aromatic molecules. **1970**.
187. Cuniberti, C., Perico, A. Intramolecular excimer formation in polymers: Pyrene labelled polyvinylacetate. *Eur. Polym. J.* **1980**, *16*, 887-893.
188. Zheng, O., Zhao, J.-X. Solubilization of pyrene in aqueous micellar solutions of gemini surfactants C 12-s-C 12· 2Br. *J. Colloid Interface Sci.* **2006**, *300*, 749-754.
189. Sahoo, L., Sarangi, J., Misra, P. K. Organization of Amphiphiles. Part 1: Evidence in Favor of Pre-micellar Aggregates through Fluorescence Spectroscopy. *Bull. Chem. Soc. Jpn.* **2002**, *75*, 859-865.
190. Fan, Y., Li, Y., Cao, M., Wang, J., Wang, Y., Thomas, R. K. Micellization of dissymmetric cationic gemini surfactants and their interaction with dimyristoylphosphatidylcholine vesicles. *Langmuir* **2007**, *23* (23), 11458-11464.
191. Boal, A. K., Rotello, V. M. Radial control of recognition and redox processes with multivalent nanoparticle hosts. *J. Am. Chem. Soc.* **2002**, *124*, 5019-5024.
192. Menger, F. M., Littau, C. Gemini-surfactants: synthesis and properties. *J. Am. Chem. Soc.* **1991**, *113*, 1451-1452.
193. Zana, R., Alkanediyl- α,ω -bis(dimethylalkylammonium bromide) Surfactants: II. Krafft Temperature and Melting Temperature. *J. Colloid Interface Sci.* **2002**, *252*, 259-261.
194. Harkins, W. D., Jordan, H. F., A method for the determination of surface and interfacial tension from the maximum pull on a ring. *J. Am. Chem. Soc.* **1930**, *52*, 1751-1772.
195. Zhang, S., Yu, J., Wu, J., Tong, W., Lei, Q., Fang, W. Micellization Parameters of Six Gemini Quaternary Ammonium Surfactants from Measurements of Conductivity and Surface Tension. *J. Chem. Eng. Data.* **2014**, *59*, 2891-2900.
196. Carpena, P., Aguiar, J., Bernaola-Galván, P., Carnero Ruiz, C. Problems associated with the treatment of conductivity-concentration data in surfactant solutions: simulations and experiments. *Langmuir* **2002**, *18*, 6054-6058.

197. Shinoda, K., Hato, M., Hayashi, T. Physicochemical properties of aqueous solutions of fluorinated surfactants. *J. Phys. Chem.* **1972**, *76*, 909-914.
198. Chen, Q., Zhang, D., Li, R., Liu, H., Hu, Y. Effect of the spacer group on the behavior of the cationic gemini surfactant monolayer at the air/water interface. *Thin Solid Films* **2008**, *516*, 8782-8787.
199. Wang, X., Li, Q., Chen, X., Li, Z. Effects of structure dissymmetry on aggregation behaviors of quaternary ammonium gemini surfactants in a protic ionic liquid EAN. *Langmuir* **2012**, *28*, 16547-16554.
200. Förster, T., Selinger, B. Der Konzentrationsumschlag der Fluoreszenz aromatischer Kohlenwasserstoffe in Mizell-kolloidaler Lösung. *Z. Naturforsch.* **1964**, *19*, 38-41.
201. Kalyanasundaram, K. Thomas, J. Environmental effects on vibronic band intensities in pyrene monomer fluorescence and their application in studies of micellar systems. *J. Am. Chem. Soc.* **1977**, *99*, 2039-2044.
202. Sahoo, L., Sarangi, J., Misra, P. K. Organization of Amphiphiles. Part 1: Evidence in Favor of Pre-micellar Aggregates through Fluorescence Spectroscopy. *Bull. Chem. Soc. Jpn.* **2002**, *75*, 859-865.
203. Piñeiro, L., Novo, M., Al-Soufi, W. Fluorescence emission of pyrene in surfactant solutions. *Adv. Colloid Interface Sci.* **2015**, *215*, 1-12.
204. Han, L., Ye, Z., Chen, H., Luo, P., The interfacial tension between cationic gemini surfactant solution and crude oil. *J. surfactants. deterg.* **2009**, *12*, 185-190.
205. Nagarajan, R. Molecular packing parameter and surfactant self-assembly: the neglected role of the surfactant tail. *Langmuir* **2002**, *18*, 31-38.
206. Bales, B. L. A definition of the degree of ionization of a micelle based on its aggregation number. *J. Phys. Chem. B* **2001**, *105*, 6798-6804.
207. Zana, R. Ionization of cationic micelles: Effect of the detergent structure. *J. Colloid Interface Sci.* **1980**, *78*, 330-337.
208. Menger, F. M., Keiper, J. S., Mbadugha, B. N. A., Caran, K. L., Romsted, L. S. Interfacial Composition of Gemini Surfactant Micelles Determined by Chemical Trapping. *Langmuir* **2000**, *16*, 9095-9098.
209. Mahmood, E., Al-Koofee, D. A. Effect of temperature changes on critical micelle concentration for tween series surfactant. *GJSFR* **2013**, *13*, 1-7.
210. Espada, L., Jones, M. N., Pilcher, G. Enthalpy of micellization II. n-dodecyltrimethylammonium bromide. *J. Chem. Thermodyn* **1970**, *2*, 1-8.
211. Zana, R. Critical micellization concentration of surfactants in aqueous solution and free energy of micellization. *Langmuir* **1996**, *12*, 1208-1211.
212. Zana, R., Alkanediyl- α , ω -bis (dimethylalkylammonium bromide) surfactants: II. Krafft temperature and melting temperature. *J. Colloid Interface Scie.* **2002**, *252*, 259-261.
213. Wasungu, L. Hoekstra, D., Cationic lipids, lipoplexes and intracellular delivery of genes. *J. Control Release.* **2006**, *116*, 255-264.
214. Verma, I. M., Gene Therapy That Works. *Science* **2013**, *341*, 853-855.
215. Crane, J. M., Tamm, L. K. Role of Cholesterol in the Formation and Nature of Lipid Rafts in Planar and Spherical Model Membranes. *Biophys. J.* **2004**, *5*, 2965-2979.
216. Fahey, D., Small, D. M. Phase behavior of monolayers of 1, 2-dipalmitoyl-3-acyl-sn-glycerols. *Langmuir* **1988**, *4*, 589-594.
217. Lopes-Costa, T., Gámez, F., Lago, S., Pedrosa, J. M., Adsorption of DNA to octadecylamine monolayers at the air–water interface. *J. Colloid Interface Sci.* **2011**, *354*, 733-738.
218. Seoane, R., Minones, J., Conde, O., Minones, J., Casas, M., Iribarnegaray, E., Thermodynamic and Brewster angle microscopy studies of fatty acid/cholesterol mixtures at the air/water interface. *J. Phys. Chem. B* **2000**, *104*, 7735-7744.

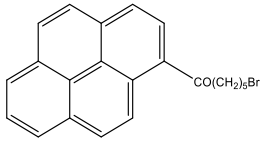
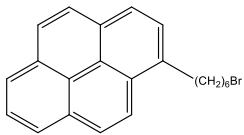
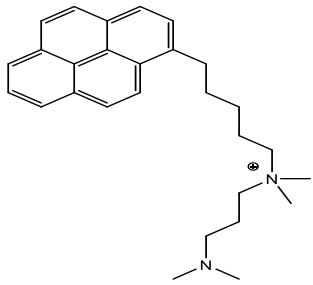
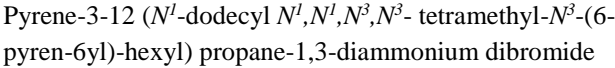
219. Kim, K., Choi, S. Q., Zell, Z. A., Squires, T. M., Zasadzinski, J. A. Effect of cholesterol nanodomains on monolayer morphology and dynamics. *Proc. Natl. Acad. Sci. U.S.A.* **2013**, *110*, E3054-E3060.
220. Arima, A. A., Pavinatto, F. J., Oliveira, O. N., Gonzales, E. R. The negligible effects of the antifungal natamycin on cholesterol-dipalmitoyl phosphatidylcholine monolayers may explain its low oral and topical toxicity for mammals. *Colloids Surf B Biointerfaces* **2014**, *122*, 202-208.
221. Chen, X., Wang, J., Shen, N., Luo, Y., Li, L., Liu, M., Thomas, R. K. Gemini surfactant/DNA complex monolayers at the air-water interface: Effect of surfactant structure on the assembly, stability, and topography of monolayers. *Langmuir* **2002**, *18*, 6222-6228.
222. Zhao, L., Feng, S.-S. Effects of cholesterol component on molecular interactions between paclitaxel and phospholipid within the lipid monolayer at the air-water interface. *J. Colloid Interface Sci.* **2006**, *300*, 314-326.
223. Gzyl-Malcher, B., Handzlik, J., Klekowska, E. Interaction of prazosin with model membranes—A Langmuir monolayer study. *Bioelectrochemistry* **2012**, *87*, 96-103.
224. Romão, R. I., Maçadas, E., Martinho, J. M. Da Silva, A. M. G. Interaction of toremifene with dipalmitoyl-phosphatidyl-glycerol in monolayers at the air-water interface followed by fluorescence microscopy in Langmuir-Blodgett films. *Thin Solid Films* **2013**, *534*, 584-590.
225. Badea, I., Wettig, S., Verrall, R., Foldvari, M. Topical non-invasive gene delivery using gemini nanoparticles in interferon- γ -deficient mice. *Eur. J. Pharm. Biopharm.* **2007**, *65*, 414-422.
226. Chen, Q., Kang, X., Li, R., Du, X., Shang, Y., Liu, H., Hu, Y. Structure of the complex monolayer of gemini surfactant and DNA at the air/water interface. *Langmuir* **2012**, *28*, 3429-3438.
227. Lee, P. Y., Costumbrado, J., Hsu, C.-Y., Kim, Y. H. Agarose gel electrophoresis for the separation of DNA fragments. *JOVE* **2011**, *62*, 9400-9405.
228. Badea, I., Verrall, R., Baca-Estrada, M., Tikoo, S., Rosenberg, A., Kumar, P., Foldvari, M. In vivo cutaneous interferon- γ gene delivery using novel dicationic (gemini) surfactant-plasmid complexes. *J Gene Med* **2005**, *7*, 1200-1214.
229. Al-Dulaymi, M. A., Chitanda, J. M., Mohammed-Saeid, W., Araghi, H. Y., Verrall, R. E., Grochulski, P., Badea, I. Di-Peptide-Modified Gemini Surfactants as Gene Delivery Vectors: Exploring the Role of the Alkyl Tail in Their Physicochemical Behavior and Biological Activity. *The AAPS J.* **2016**, 1-14.
230. Zhang, J.-S., SONG, L., Huang, L. Cationic liposome-protamine-DNA complexes for gene delivery. *Methods Enzymol.* **2003**, *373*, 332-342.
231. Prasad, T. K., Rangaraj, N., Rao, N. M. Quantitative aspects of endocytic activity in lipid-mediated transfections. *FEBS letters* **2005**, *579*, 2635-2642.
232. Pack, D. W., Hoffman, A. S., Pun, S., Stayton, P. S. Design and development of polymers for gene delivery. *Nat. Rev. Drug Discov.* **2005**, *4*, 581-593.
233. Qaddoumi, M. G., Gukasyan, H. J., Davda, J., Labhasetwar, V., Kim, K.-J., Lee, V. Clathrin and caveolin-1 expression in primary pigmented rabbit conjunctival epithelial cells: role in PLGA nanoparticle endocytosis. *Mol Vis* **2003**, *9*, 559-568.
234. Qaddoumi, M. G., Ueda, H., Yang, J., Davda, J., Labhasetwar, V., Lee, V. H. The characteristics and mechanisms of uptake of PLGA nanoparticles in rabbit conjunctival epithelial cell layers. *Pharm. Res* **2004**, *21*, 641-648.
235. Rejman, J., Oberle, V., Zuhorn, I. S., Hoekstra, D. Size-dependent internalization of particles via the pathways of clathrin- and caveolae-mediated endocytosis. *Biochem. J.* **2004**, *377*, 159-169.
236. Rosenzweig, H. S., Rakhmanova, V. A., MacDonald, R. C. Diquaternary ammonium compounds as transfection agents. *Bioconjugate Chem.* **2001**, *12*, 258-263.

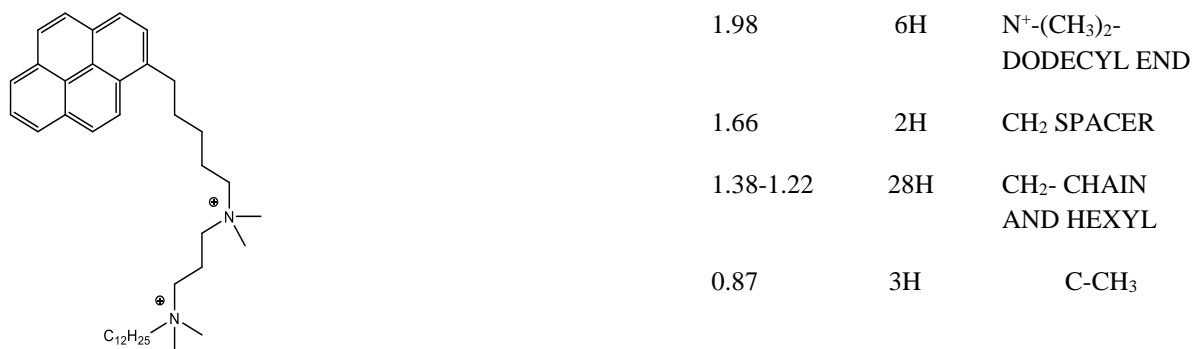
237. Felgner, J. H., Kumar, R., Sridhar, C., Wheeler, C. J., Tsai, Y. J., Border, R., Ramsey, P., Martin, M., Felgner, P. L. Enhanced gene delivery and mechanism studies with a novel series of cationic lipid formulations. *J. Biol. Chem.* **1994**, *269*, 2550-2561.
238. Yang, P., Singh, J., Wettig, S., Foldvari, M., Verrall, R. E., Badea, I. Enhanced gene expression in epithelial cells transfected with amino acid-substituted gemini nanoparticles. *Eur. J. Pharm. Biopharm.* **2010**, *75*, 311-320.
239. Acharya, D. P., Kunieda, H., Shiba, Y., Aratani, K.-i. Phase and rheological behavior of novel gemini-type surfactant systems. *J. Phys. Chem. B* **2004**, *108*, 1790-1797.
241. Sudimack, J., Lee, R. J. Targeted drug delivery via the folate receptor. *Adv. Drug. Deliv. Rev.* **2000**, *41*, 147-162.
242. Nishina, K., Unno, T., Uno, Y., Kubodera, T., Kanouchi, T., Mizusawa, H., Yokota, T. Efficient in vivo delivery of siRNA to the liver by conjugation of α -tocopherol. *Mol Ther* **2008**, *16*, 734-740.
243. Donkuru, M., Badea, I., Wettig, S., Verrall, R., Elsabahy, M., Foldvari, M. Advancing nonviral gene delivery: lipid-and surfactant-based nanoparticle design strategies. *Nanomed* **2010**, *5*, 1103-1127.

Appendices

Appendix A (Chapter III)

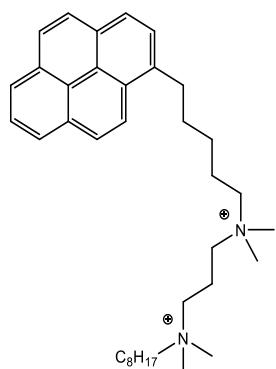
¹H NMR Spectra for the synthesized compounds

Compound	δ (ppm)	Number of protons	Group
5-Bromohexyl-1-pyrenyl ketone 	8.84	1H	PYR-C-H
	8.31-8.017	8H	PYR-H
	3.45	2H	CH ₂ -Br
	3.24	2H	α -CH ₂
	1.98-1.84	4H	β & δ -CH ₂
	1.65-1.55	2H	γ -CH ₂
	6-(1-Pyrenyl-bromohexane) 	8.27-7.83	9H
3.41-3.30		4H	α -CH ₂ & Pyr-CH ₂
1.90-1.81		4H	β & ϵ -CH ₂
1.51-1.48		4H	γ -CH ₂ & δ -CH ₂
Pyr-3(N-(3-dimethylaminopropyl)-N,N-dimethyl-6-(pyren-6-yl)-hexane-1-ammonium bromide) 	8.20-7.80	9H	PYR-H
	3.43	2H	N ⁺ -CH ₂
	3.40-3.16	4H	PYR-CH ₂ & CH ₂ -N ⁺
	3.05	6H	N ⁺ -(CH ₃) ₂
	2.36	2H	N-(CH ₃) ₂
	1.87-1.51	10H	(CH ₂) ₄ & β -CH ₂
Pyrene-3-12 (N ¹ -dodecyl N ¹ ,N ¹ ,N ³ ,N ³ - tetramethyl-N ³ -(6-pyren-6yl)-hexyl) propane-1,3-diammonium dibromide 	8.23-7.78	9H	PYR-H
	3.77-3.73	4H	N ⁺ -CH ₂
	3.33-3.31	6H	PYR-CH ₂ & CH ₂ -N ⁺ CHAIN
	3.2	6H	N ⁺ -(CH ₃) ₂ -PYRENE END



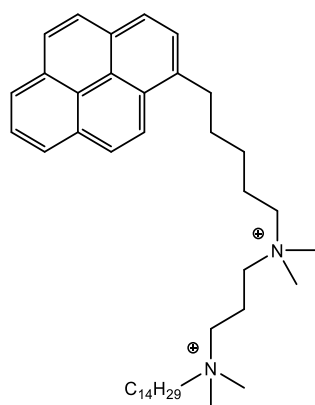
Pyrene-3-8 (*N*¹-Octyl *N*¹,*N*¹,*N*³,*N*³- tetramethyl-*N*³-(6-pyren-6yl)-hexyl) propane-1,3-diammonium dibromide

1.98	6H	N ⁺ -(CH ₃) ₂ - DODECYL END
1.66	2H	CH ₂ SPACER
1.38-1.22	28H	CH ₂ - CHAIN AND HEXYL
0.87	3H	C-CH ₃

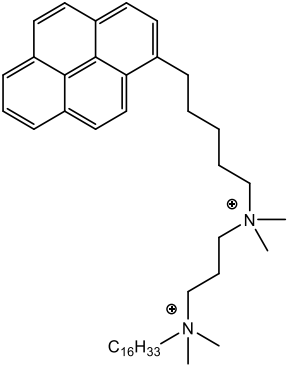
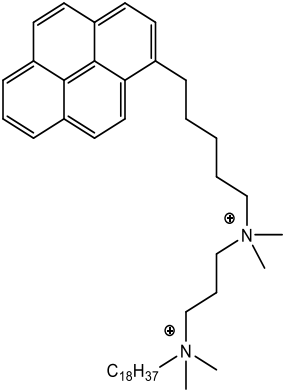
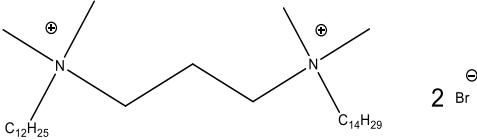


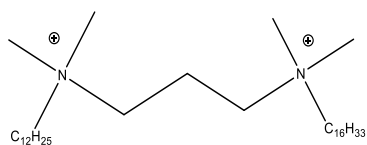
Pyrene-3-14 (*N*¹-tetradecyl *N*¹,*N*¹,*N*³,*N*³- tetramethyl-*N*³-(6-pyren-6yl)-hexyl) propane-1,3-diammonium dibromide

8.17-7.80	9H	PYR-H
3.77-3.73	4H	N ⁺ -CH ₂
3.61	6H	PYR-CH ₂ & CH ₂ - N ⁺ CHAIN
3.44	6H	N ⁺ -(CH ₃) ₂ - PYRENE END
2.73	6H	N ⁺ -(CH ₃) ₂ - OCTYL END
1.87	2H	CH ₂ SPACER
1.80-1.23	20H	CH ₂ - CHAIN AND HEXYL
0.87	3H	C-CH ₃

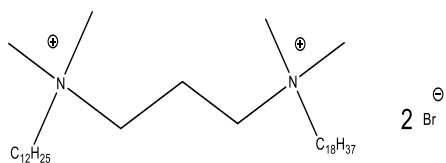


8.19-7.79	9H	PYR-H
3.72-3.57	4H	N ⁺ -CH ₂
3.31	6H	PYR-CH ₂ & CH ₂ - N ⁺ CHAIN
3.11	6H	N ⁺ -(CH ₃) ₂ - PYRENE END
2.55	6H	N ⁺ -(CH ₃) ₂ - TETRADECYL END
2.11	2H	CH ₂ SPACER
1.79-1.19	32H	CH ₂ - CHAIN AND HEXYL
0.87	3H	C-CH ₃
8.23-7.80	9H	PYR-H
3.59	4H	N ⁺ -CH ₂

Pyrene-3-16 (<i>N</i> ^l -hexadecyl <i>N</i> ^l , <i>N</i> ^l , <i>N</i> ³ , <i>N</i> ³ - tetramethyl- <i>N</i> ³ -(6-pyren-6yl)-hexyl) propane-1,3-diammonium dibromide	3.38-3.30	6H	PYR-CH ₂ & CH ₂ -N ⁺ CHAIN
	3.11	6H	N ⁺ -(CH ₃) ₂ -PYRENE END
	2.59	6H	N ⁺ -(CH ₃) ₂ -HEXADECYL END
	2.15	2H	CH ₂ SPACER
	1.83-1.21	36H	CH ₂ - CHAIN AND HEXYL
	0.87	3H	C-CH ₃
Pyrene-3-18 (<i>N</i> ^l -octadecyl <i>N</i> ^l , <i>N</i> ^l , <i>N</i> ³ , <i>N</i> ³ - tetramethyl- <i>N</i> ³ -(6-pyren-6yl)-hexyl) propane-1,3-diammonium dibromide	8.23-7.80	9H	PYR-H
	3.72	4H	N ⁺ -CH ₂
	3.41-3.22	6H	PYR-CH ₂ & CH ₂ -N ⁺ CHAIN
	3.18	6H	N ⁺ -(CH ₃) ₂ -PYRENE END
	2.7	6H	N ⁺ -(CH ₃) ₂ -OCTADECYL END
	2.11	2H	CH ₂ SPACER
	1.79-1.21	39H	CH ₂ - CHAIN AND HEXYL
	0.85	3H	C-CH ₃
12-3-14(<i>N</i> -dodecyl- <i>N</i> -tetradecyl-1, 3-propanediammonium dibromide)	3.88-3.83	2H	α-CH ₂ Spacer
	3.50-3.46	2H	γ-CH ₂ Spacer
	3.38	12H	N ⁺ -(CH ₃) ₄
	3.02-2.97	4H	(CH ₂) ₂
	1.82-1.78	4H	(CH ₂) ₂
	1.34-1.23	42H	(CH ₂) ₂₀ & β-CH ₂
	0.88-0.83	6H	(CH ₃) ₂
12-3-16(<i>N</i> -dodecyl- <i>N</i> -Hexadecyl-1, 3-propanediammonium dibromide)	3.88-3.83	2H	α-CH ₂ Spacer
	3.50-3.46	2H	γ-CH ₂ Spacer
	3.38	12H	N ⁺ -(CH ₃) ₄

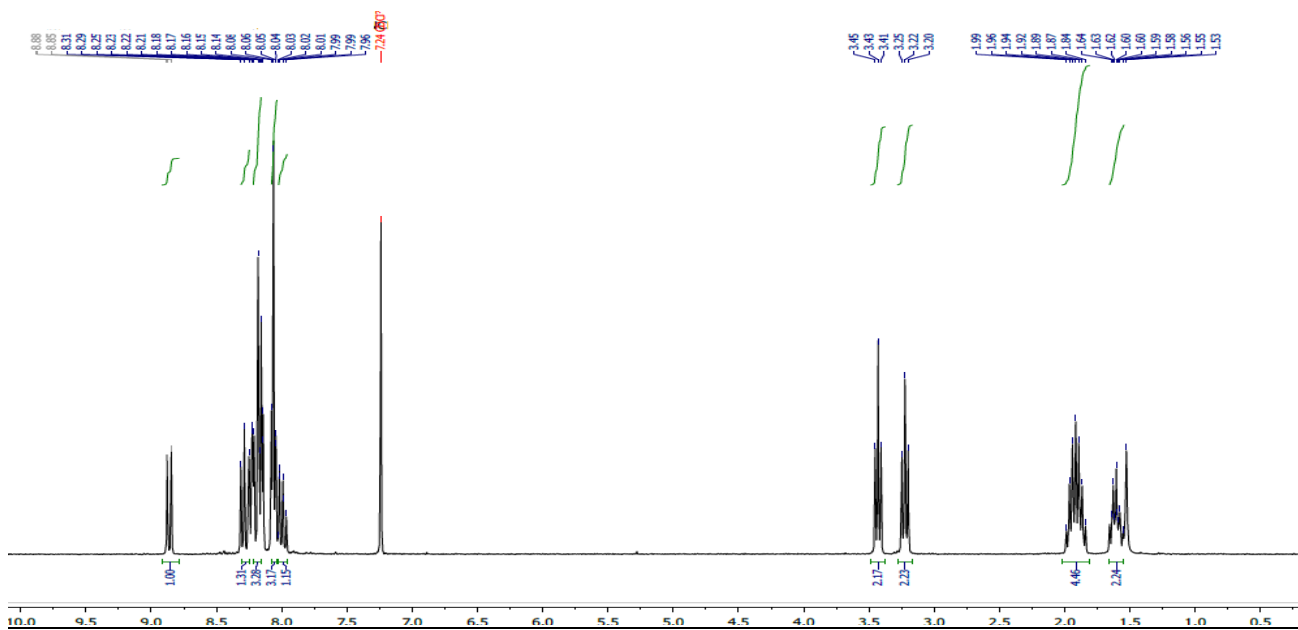


12-3-18(*N*-dodecyl-*N*-octadecyl-1,3-propanediammonium dibromide)

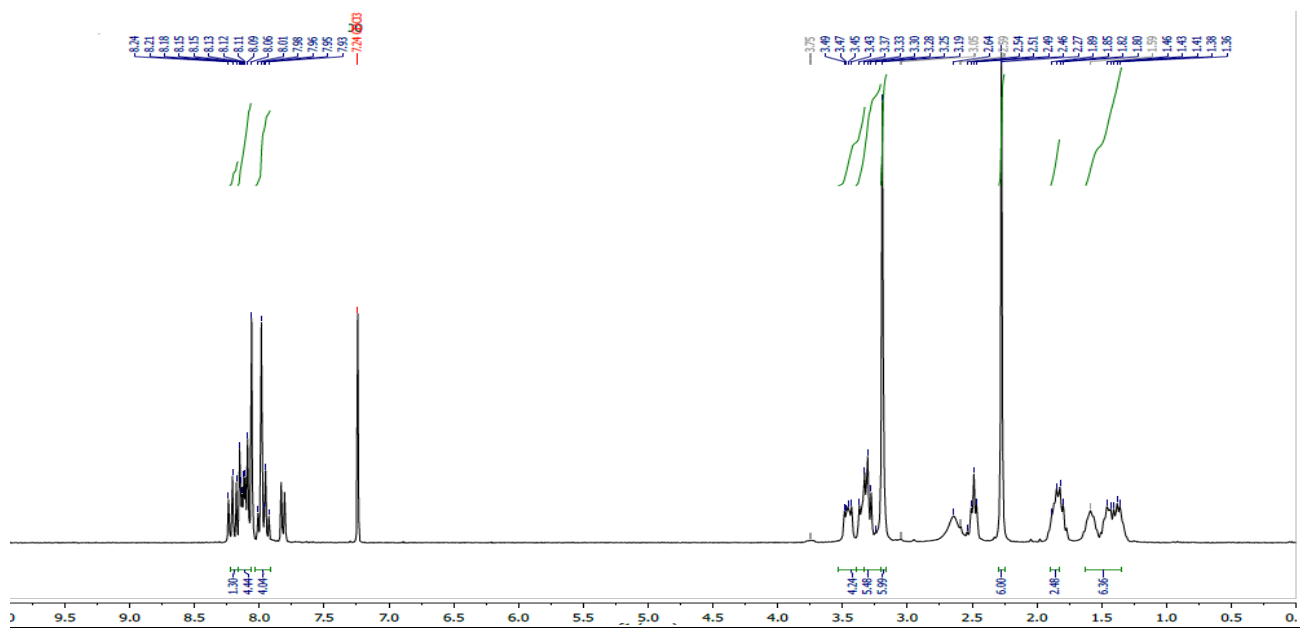


3.02-2.97	4H	(CH ₂) ₂
1.82-1.78	4H	(CH ₂) ₂
1.34-1.23	44H	(CH ₂) ₂₁ & β-CH ₂
0.88-0.83	6H	(CH ₃) ₂
3.88-3.83	2H	α-CH ₂ Spacer
3.50-3.46	2H	γ-CH ₂ Spacer
3.38	12H	N ⁺ -(CH ₃) ₄
3.02-2.97	4H	(CH ₂) ₂
1.82-1.78	4H	(CH ₂) ₂
1.34-1.23	46H	(CH ₂) ₂₂ & β-CH ₂
0.88-0.83	6H	(CH ₃) ₂

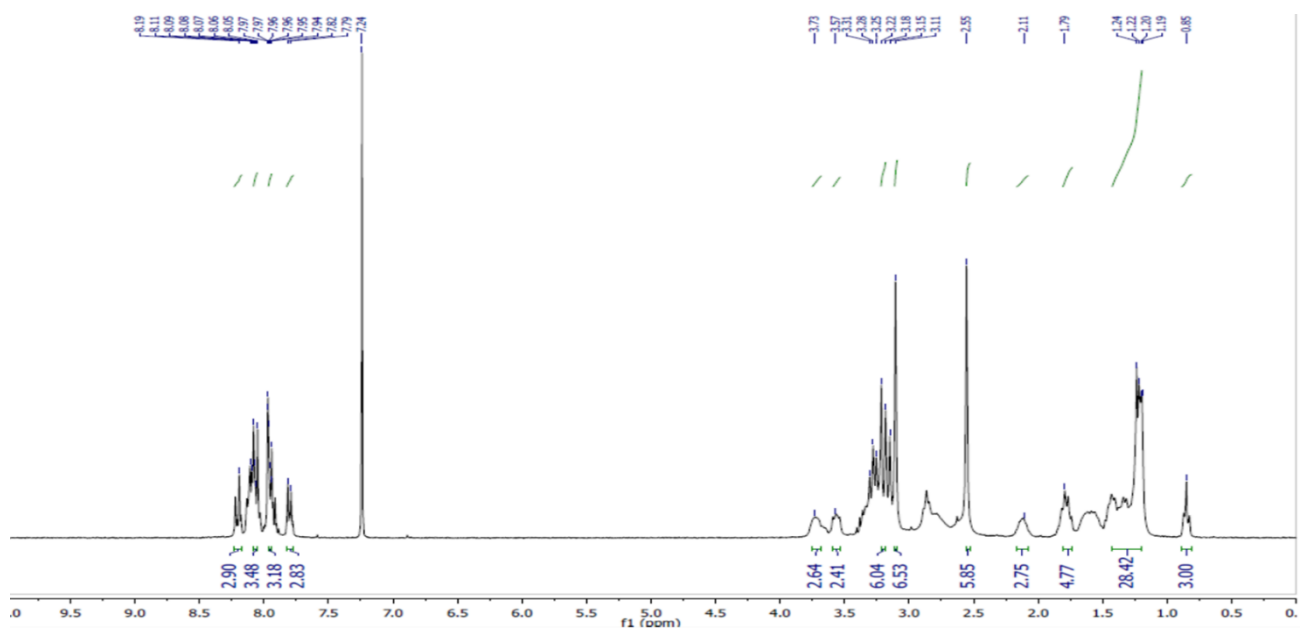
¹H NMR spectra for 5-Bromohexyl-1-pyrenyl ketone



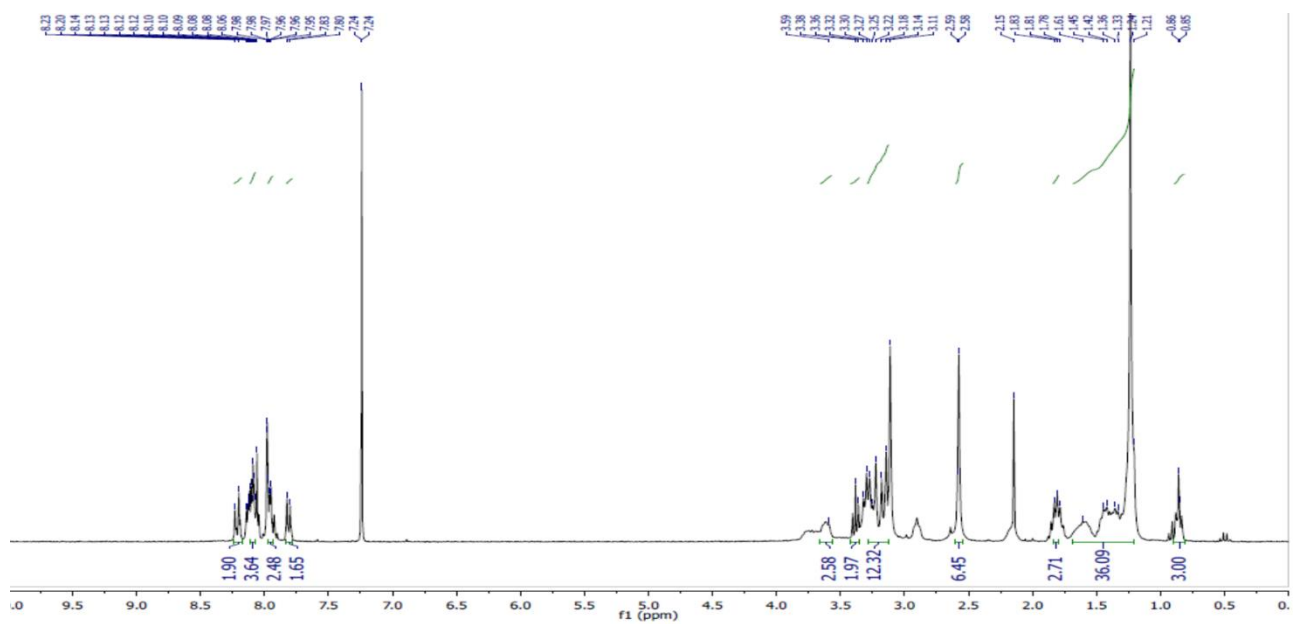
¹H NMR spectra for pyr-3



¹H NMR spectra for pyr-3-14



¹H NMR spectra for pyr-3-16



¹H NMR spectra for 12-3-14

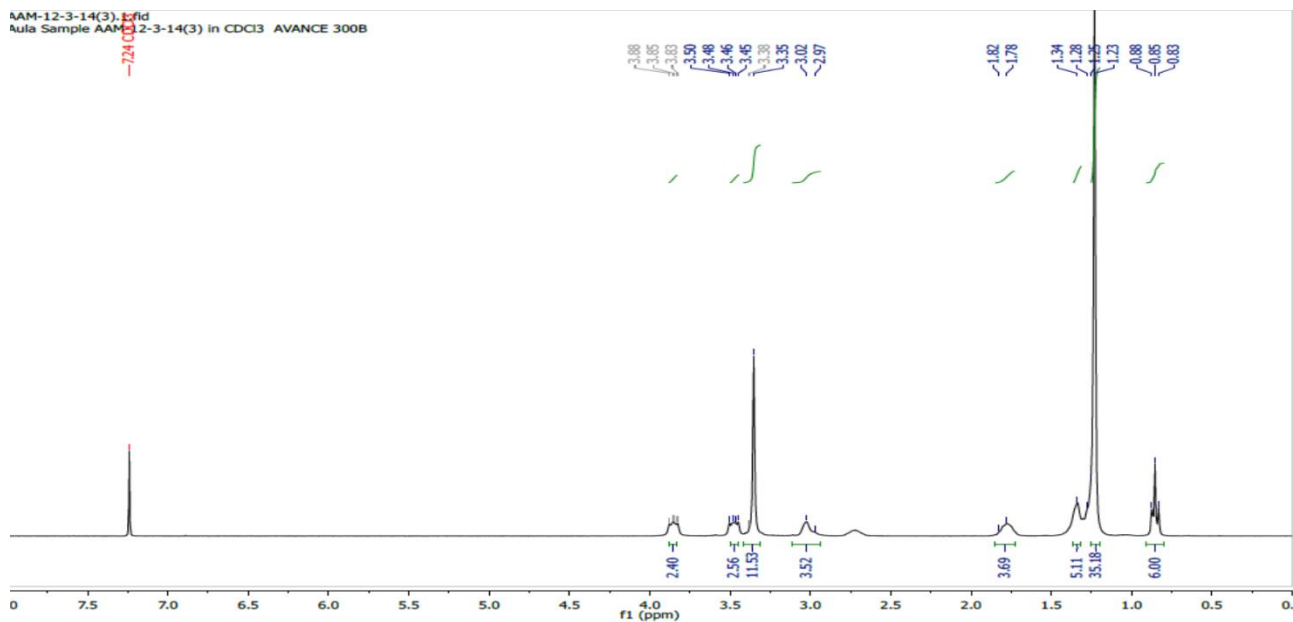


Table 3.1 Conductivity measurements of Pyrene-3-12

#	C(mM)	Conductivity. (uS/cm)	Average Conductivity	Std.
1	0	2.69	2.69	0.00
		2.70		
2	0.018	7.13	7.14	0.01
		7.15		
3	0.037	10.9	10.87	0.03
		10.9		
4	0.055	14.7	14.74	0.00
		14.7		
5	0.073	18.4	18.41	0.01
		18.4		
6	0.092	21.9	21.95	0.07
		22.0		
7	0.11	24.9	24.95	0.07
		25.0		
8	0.128	28.3	28.40	0.14
		28.5		
9	0.146	31.3	31.40	0.14
		31.5		
10	0.165	34.6	34.65	0.07
		34.7		
11	0.183	37.1	37.10	0.00
12	0.201	39.5	39.55	0.07
		39.6		
13	0.22	41.8	41.80	0.00
14	0.24	43.2	43.35	0.21
		43.5		
15	0.26	44.6	44.70	0.14
		44.8		
16	0.28	45.9	46.00	0.14
		46.1		
17	0.29	46.8	46.80	0.00
18	0.31	47.9	47.95	0.07
		48.0		
19	0.33	48.6	48.60	0.00
20	0.35	49.5	49.50	0.00

Table 3.2 Surface measurement of 12-3-16

Log C (M)	Surface tension (mN/m)
-5.14927	68.19
-4.85029	65.77
-4.67618	60.89
-4.55331	56.83
-4.45840	53.63
-4.38132	50.9
-4.31629	48.44
-4.26033	45.47
-4.21118	43.13
-4.16732	41.08
-4.12792	39.35
-4.09212	37.73
-4.05927	36.43
-4.02907	35.36
-4.00104	34.58
-3.97488	33.98
-3.9505	33.67
-3.92758	33.21
-3.90597	32.73
-3.88558	32.39
-3.86629	32.23
-3.84796	32.21
-3.83051	32.03
-3.81398	32.16
-3.79786	32.22
-3.7827	32.14
-3.76843	32.14
-3.75426	32.03
-3.74088	32.1
-3.72790	32.01
-3.71564	32.23
-3.70339	32.14
-3.69179	32.21
-3.68080	32.18
-3.67009	32.48
-3.65933	32.56
-3.64942	32.72
-3.63944	32.93
-3.62996	32.91
-3.62068	32.86
-3.61160	33.04
-3.60297	33.00

-3.59450	32.89
-3.58619	33.17
-3.57804	33.19
-3.57028	33.2
-3.56266	32.88
-3.55517	33.02
-3.54780	32.98
-3.54078	33.00
-3.53388	32.92
-3.52708	33.12
-3.52039	33.30
-3.51401	33.06
-3.50772	33.13
-3.50152	32.96
-3.49541	33.66
-3.48938	33.48
-3.48363	33.17
-3.47796	33.33
-3.47236	33.33
-3.46684	33.63
-3.46156	33.28
-3.45636	33.67
-3.45121	33.61
-3.44612	33.76
-3.44110	33.56
-3.43630	33.74
-3.43156	33.48
-3.42670	33.70
-3.42224	33.70
-3.41764	33.75
-3.41310	33.60
-3.40877	33.57
-3.40449	33.71
-3.40024	33.62
-3.39604	33.65
-3.39203	33.76
-3.38791	33.76
-3.38398	33.61
-3.38008	33.72
-3.37622	33.72
-3.37255	33.60
-3.36875	33.66
-3.36514	33.82
-3.36141	33.77

-3.35786	33.87
-3.35434	33.81
-3.35099	33.81
-3.34752	33.84
-3.34422	33.92
-3.34095	33.93
-3.33756	33.88
-3.33434	33.86
-3.33128	33.86
-3.32810	33.88
-3.32509	33.82
-3.32195	33.91
-3.31898	33.85
-3.31603	33.89
-3.31309	33.86
-3.31018	33.91
-3.30728	33.90
-3.30454	33.89
-3.30181	33.88
-3.29897	33.82
-3.29627	33.83
-3.29360	33.85
-3.29093	33.84
-3.28842	33.87
-3.28579	33.88
-3.28330	33.88
-3.28070	33.88
-3.27824	33.86
-3.27579	33.82
-3.27336	33.80
-3.27094	33.83
-3.26865	33.80
-3.26626	33.81
-3.26388	33.80
-3.26163	33.79
-3.25939	33.73
-3.25716	33.78
-3.25495	33.76
-3.25275	33.78
-3.25055	33.73
-3.24837	33.72
-3.24632	33.72
-3.24415	33.68
-3.24212	33.70

-3.24009	33.70
-3.23807	33.72
-3.23606	33.73
-3.23406	33.74
-3.23207	33.81
-3.23009	33.75
-3.22812	33.68
-3.22627	33.69
-3.22442	33.67
-3.22247	33.67
-3.22064	33.66
-3.21882	33.66
-3.21701	33.66
-3.21520	33.67
-3.21340	33.65
-3.21161	33.62
-3.20993	33.59
-3.20815	33.65
-3.20648	33.66
-3.20472	33.67
-3.20306	33.67
-3.20141	33.65
-3.19977	33.63
-3.19814	33.63
-3.19651	33.62
-3.19488	33.64
-3.19327	33.65
-3.19176	33.66
-3.19015	33.64
-3.18865	33.64
-3.18706	33.69
-3.18557	33.65
-3.18408	33.66
-3.18251	33.66
-3.18103	33.67
-3.17956	33.65
-3.17810	33.68
-3.17674	33.64
-3.17528	33.65
-3.17383	33.60
-3.17239	33.67
-3.17105	33.62
-3.16961	33.64
-3.16828	33.66

-3.16694	33.65
-3.16562	33.67
-3.16420	33.65
-3.16288	33.69
-3.16157	33.68
-3.16025	33.68
-3.15895	33.68
-3.15774	33.63
-3.15644	33.65
-3.15514	33.70
-3.15394	33.67
-3.15265	33.63
-3.15146	33.64
-3.15018	33.63
-3.14899	33.66
-3.14781	33.65
-3.14663	33.67
-3.14537	33.65
-3.14419	33.63
-3.14302	33.61
-3.14186	33.61
-3.14078	33.61
-3.13962	33.55
-3.13846	33.58
-3.13731	33.57

Table 3.3 Surface tension measurement of Pyrene-3-16

Log C (M)	Surface tension (mN/m)
-5.55246	69.74
-5.25308	69.76
-5.07864	69.77
-4.95531	69.47
-4.86012	69.44
-4.78258	69.37
-4.71709	69.38
-4.66069	69.37
-4.61100	69.39
-4.56682	69.38
-4.52709	69.37
-4.49085	69.36
-4.45757	69.20
-4.42694	67.82
-4.39860	67.21

-4.37213	66.01
-4.34730	65.04
-4.32404	64.14
-4.30207	62.81
-4.28127	61.47
-4.26161	59.09
-4.24290	57.68
-4.22514	56.33
-4.20809	55.01
-4.19193	53.99
-4.17635	53.13
-4.16146	52.36
-4.14715	51.46
-4.13337	50.86
-4.12008	50.19
-4.10732	49.56
-4.09500	49.00
-4.08308	48.48
-4.07155	48.08
-4.06037	47.89
-4.04960	47.52
-4.03915	47.47
-4.02900	47.15
-4.01914	46.87
-4.00955	46.52
-4.00023	45.68
-3.99121	44.96
-3.98237	44.54
-3.97376	44.20
-3.96541	44.00
-3.95727	43.79
-3.94929	43.6
-3.94154	43.58
-3.93397	43.43
-3.92658	43.49
-3.91936	43.48
-3.91225	43.34
-3.90535	43.27
-3.89873	43.23
-3.89191	43.22
-3.88561	43.27
-3.87900	43.19
-3.87288	43.28
-3.86685	43.19

-3.86091	43.08
-3.85504	43.03
-3.84925	43.03
-3.84354	43.17
-3.83827	43.10
-3.83270	43.30
-3.82757	43.19
-3.82213	43.14
-3.81712	43.15
-3.81217	43.20
-3.80692	43.31
-3.80208	43.41
-3.79729	43.33
-3.79255	43.71
-3.78820	43.29
-3.78357	43.37
-3.77898	43.23
-3.77444	43.38
-3.77026	43.23
-3.76613	43.18
-3.76172	43.09
-3.75766	43.15
-3.75365	42.97
-3.74967	42.89
-3.74542	43.02
-3.74151	43.07
-3.73794	43.04
-3.73410	42.86
-3.73029	42.74
-3.72652	42.72
-3.72307	42.7
-3.71936	42.64
-3.71596	42.57
-3.71231	42.41
-3.70897	42.33
-3.70565	42.42
-3.70208	42.39
-3.69882	42.35
-3.69558	42.83
-3.69236	42.44
-3.68917	42.39
-3.68600	42.29
-3.68285	42.28
-3.67998	42.31

-3.67688	42.24
-3.67380	42.27
-3.67099	42.25
-3.66795	42.25
-3.66518	42.26
-3.66243	42.19
-3.65945	42.15
-3.65674	42.16
-3.65404	42.21
-3.65136	42.22
-3.64869	42.18
-3.64604	42.20
-3.64341	42.20
-3.64079	42.16
-3.63819	42.29
-3.63561	42.21
-3.63303	42.14
-3.63071	42.20
-3.62817	42.25
-3.62564	42.15
-3.62336	42.23
-3.62086	42.37
-3.61860	42.94
-3.61635	43.04
-3.61389	43.08
-3.61167	43.16
-3.60946	42.86
-3.60725	42.95
-3.60506	43.07
-3.60289	43.02
-3.60072	43.22
-3.59856	43.25
-3.59641	43.15
-3.59428	42.9
-3.59215	42.87
-3.59004	42.87
-3.58814	42.91
-3.58604	42.99
-3.58396	43.07
-3.58209	43.21
-3.58002	43.16
-3.57817	43.23
-3.57612	43.33
-3.57429	43.30

-3.57246	43.20
-3.57044	43.22
-3.56862	43.25
-3.56682	43.27
-3.56502	43.07
-3.56323	42.96
-3.56145	42.65
-3.55948	43.10

Table 3.4 Krafft temperature measurement of Pyrene-3-16

Temp(C°)	Cond. (uS/cm)	Ave. Cond. (uS/cm)	Std.
10	83.2	83.20	0.00
15	85.8	85.90	0.14
	86.0		
20	87.3	87.35	0.07
	87.4		
25	88.1	88.15	0.07
	88.2		
30	88.3	88.35	0.07
	88.4		
35	89.1	89.15	0.07
	89.2		
40	90.1	90.15	0.07
	90.2		
45	91.3	91.40	0.14
	91.5		
50	92.8	92.85	0.07
	92.9		
55	94.4	94.50	0.14
	94.6		
60	95.9	95.95	0.07
	96.0		
65	98.0	98.05	0.07
	98.1		
70	100.7	100.75	0.07
	100.8		
75	104.8	104.90	0.14
	105.0		
80	108.8	108.90	0.14
	109.0		
85	112.5	112.45	0.07
	112.4		
90	116.0	116.10	0.14

	116.2		
95	118.6	118.60	0.00
100	122.9	122.95	0.07
	123.0		
105	125.0	125.00	0.00
110	125.5	125.50	0.00

Table 3.5 Packing parameter and the structure of the micelle

Surfactants	a_s (\AA^2)	V (\AA^3)	l (\AA)	P
Pyr-3-8	35	837	16.05	1.50
Pyr-3-12	56	945	16.68	1.00
Pyr-3-14	113	999	19.21	0.46
Pyr-3-16	52.6	1053	21.74	0.92
Pyr-3-18	70	1107	24.27	0.65
12-3-14	30	756	19.21	1.30
12-3-16	21	810	21.74	1.77
12-3-18	19	864	24.27	1.87

Appendix B (Chapter IV)

Graph 4.1 Pyrene-3-8 monolayer π -A

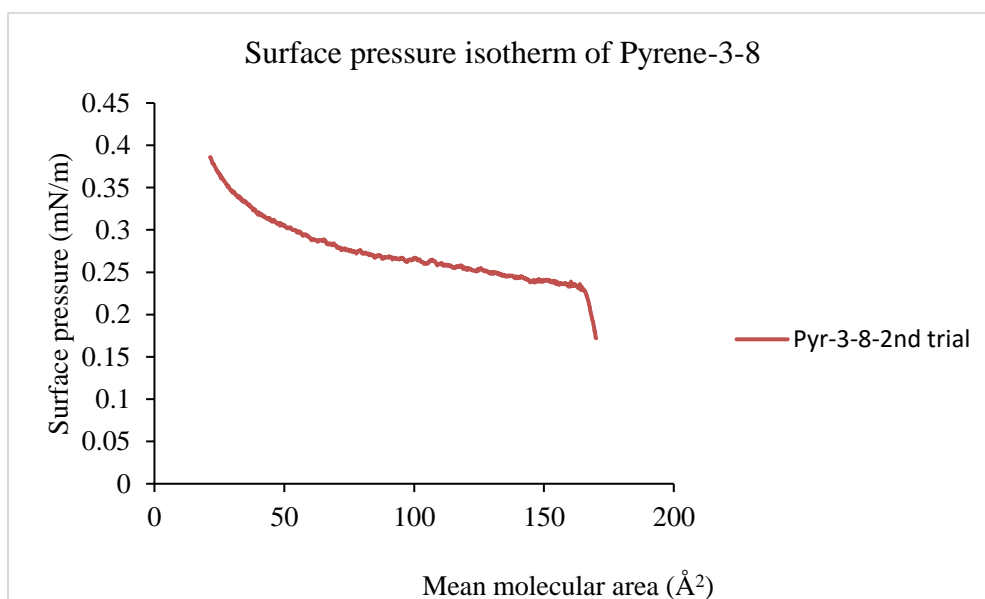


Figure 4.2 Compressibility modulus of Pyrene-3-8 monolayer

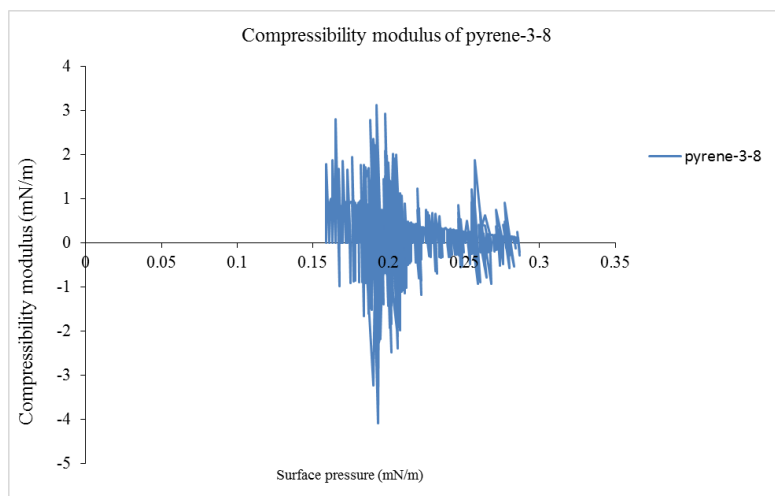


Figure 4.3 Surface pressure-area isotherm of Cholesterol monolayer

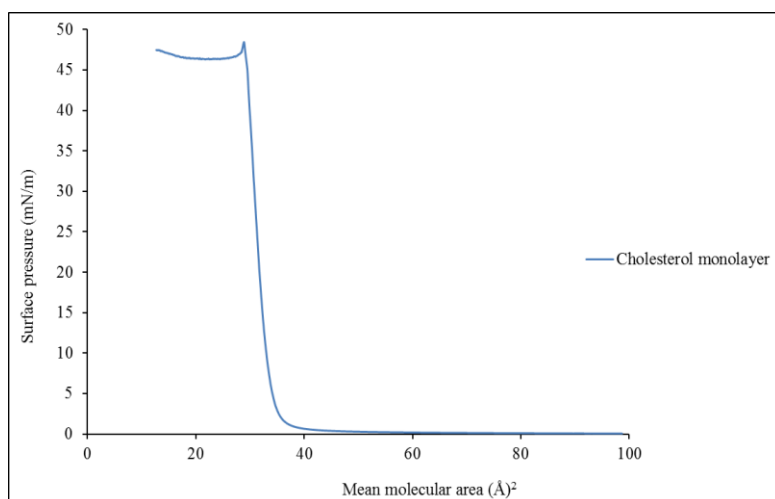


Figure 4.4 Surface pressure-area isotherm of DPPC monolayer

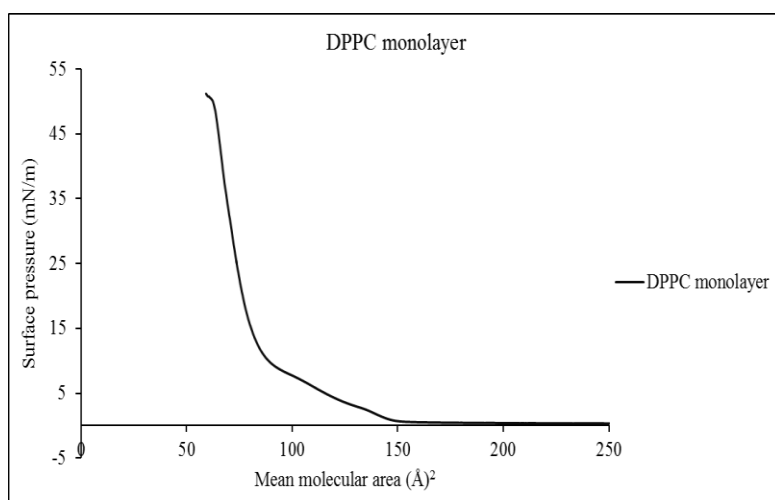
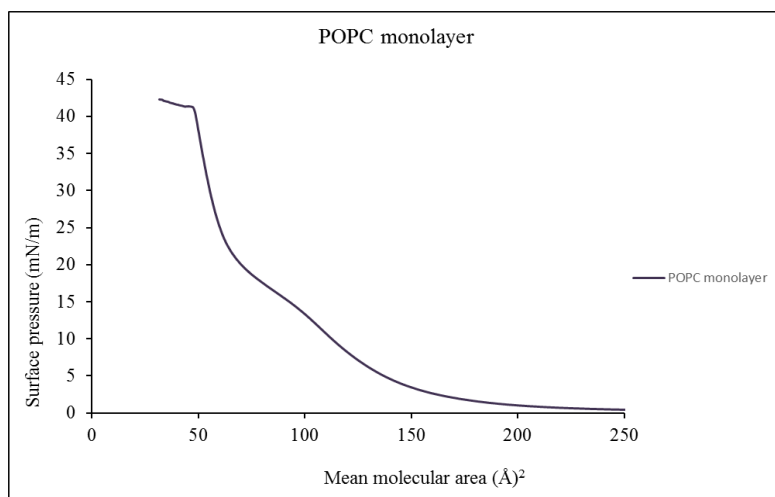


Figure 4.5 Surface pressure-area isotherm of POPC monolayer



Appendix C (Chapter V)

Table 5.1 Particle size of 12-3-14 and DNA nanoparticles at different charge ratio

C (mM)	Ratio	Ave. size(nm)	ST.D	Z-Ave	PDI
0.01	0	449.33	205.82	d.nm	
0.01	0.1	177.50	3.48	303.1	0.467
				360.2	0.385
				684.7	0.622
0.025	0.25	174.20	19.36	180.3	0.226
				173.6	0.224
				178.6	0.218
0.05	0.5	148.10	9.10	181.2	0.664
				178.7	0.429
				189.5	0.551
0.1	1	151.60	38.76	196.0	0.373
				159.0	0.567
				167.6	0.489
0.2	2	192.77	4.38	160.6	0.283
				153.8	0.249
				161.1	0.266
0.5	5	71.12	4.39	138.1	0.286
				150.3	0.301
				155.9	0.399
1	10	38.91	2.245	77.4	0.344
				78.7	0.347
0	0	119.17	16.94	84.3	0.375
				119.1	0.222
				141.2	0.252
				194.5	0.380
				79.3	1.000
				79.7	1.000
				134.0	0.447
				188.7	0.482
				197.4	0.503
				192.2	0.488
				56.3	1.000
				120.1	0.747
				57.3	1.000
				75.6	0.297
				70.7	0.252
				67.0	0.243
				174.0	0.497
				435.0	0.794
				298.7	0.809
				37.4	0.264

	37.8	0.266
	41.5	0.365
	135.4	0.232
	120.5	0.252
	101.6	0.465

Table 5.2 Zeta potential of 12-3-14

1	C (mM)	Ratio	ZP Ave.	ZP (mV)	ST.D	Mob
	0.01	0	49.10		2.26	$\mu\text{mcm/Vs}$
	0.01	0.1	-42.03	51.6	0.87	4.046
				47.2		3.697
				48.5		3.800
	0.025	0.25	-42.93	-41.8	7.57	-3.276
				-43.0		-3.371
				-41.3		-3.234
	0.05	0.5	-35.27	-44.5	0.83	-3.485
				-34.7		-2.720
				-49.6		-3.886
	0.1	1	-19.47	-34.6	0.49	-2.715
				-35.0		-2.743
				-36.2		-2.840
	0.2	2	-44.23	-18.9	0.31	-1.480
				-19.8		-1.551
				-19.7		-1.544
	0.5	5	29.40	-44.5	0.30	-3.488
				-43.9		-3.442
				-44.3		-3.469
	1	10	25.47	29.4	5.94	2.307
				29.7		2.327
	0	0	-53.73	29.1	1.80	2.280
				37.2		2.916
				15.4		1.211
				23.8		1.862
				-55.4		-4.346
				-51.8		-4.057
				-54		-4.235

Table 5.3 Transfection efficiency and cell viability of Pyrene-based and dissymmetric (12-3-n) gemini surfactants in MG-63 cell line.

Transfection complexes	Transfection efficiency	Cell viability
NC+PI	3.45 ± 2.14	88.65 ± 16.88
LP+PI	5.60 ± 1.72	49.77 ± 13.55
GDP-PY-12 ¹	17.35 ± 2.79	56.66 ± 0.73
GP-PY-12	20.53 ± 4.45	53.58 ± 8.07
PY-3-12	31.31 ± 1.29	65.40 ± 0.85
PLASMID	1.67 ± 0.45	100.00 ± 1.01
GDP-PY-14	17.79 ± 2.05	60.75 ± 6.80
GP-PY-14	17.23 ± 0.60	77.33 ± 9.50
PY-3-14	31.60 ± 2.38	53.65 ± 3.10
GDP-PY-16	3.48 ± 1.25	84.76 ± 17.21
GP-PY-16	3.91 ± 0.89	90.04 ± 3.35
PY-3-16	4.48 ± 0.91	94.63 ± 2.08
GDP-PY-18	13.67 ± 2.23	52.27 ± 6.51
GP-PY-18	14.89 ± 6.89	41.10 ± 0.38
Py-3-18	16.21 ± 2.14	30.94 ± 5.11
GDP-PY-8	7.34 ± 4.19	24.32 ± 3.10
GP-PY-8	17.83 ± 5.90	50.94 ± 3.50
PY-3-8	19.11 ± 1.54	67.85 ± 5.31
GDP-12-3-14	0.77 ± 0.21	8.11 ± 0.46
12-3-14P	0.38 ± 0.27	3.20 ± 1.19
GDP-12-3-16	10.46 ± 0.88	73.84 ± 2.74
12-3-16P	11.24 ± 3.37	76.36 ± 12.07
GDP-12-3-18	4.62 ± 0.69	42.56 ± 8.27
12-3-18P	4.10 ± 0.77	48.75 ± 5.30

PGD: Plasmid+GS+DOPE, P: Plasmid, and PY¹: Pyrene, LP: Lipofectamine 2000, and NC: negative control

Table 5.4 Transfection efficiency and cell viability values of pyrene-based, and 12-3-n gemini surfactants complexes in HEK-293 cell line

Complexes	Transfection efficiency	Cell viability
NC+PI	2.92 ± 1.04	95.15 ± 0.67
LP+PI	23.10 ± 7.30	66.58 ± 11.41
GDP-PY-12	6.25 ± 2.03	51.17 ± 9.70
GP-PYR-12	6.22 ± 1.74	56.96 ± 8.90
PYR-3-12	1.97 ± 0.70	46.23 ± 5.11
GDP-PY-14	2.00 ± 0.10	84.48 ± 21.27
GP-PYR-14	2.12 ± 0.32	33.43 ± 6.00
PYR-3-14	4.73 ± 0.71	29.69 ± 2.54
GDP-PYR-16	2.09 ± 0.90	38.029 ± 4.16
GP-PYR-16	1.36 ± 0.30	90.07 ± 1.41
PYR-3-16	1.29 ± 0.15	86.03 ± 3.32
GDP-PYR-18	24.50 ± 7.42	60.25 ± 23.98
GP-PYR-18	24.46 ± 0.87	74.05 ± 13.34
PYR-3-18	13.04 ± 6.64	84.63 ± 8.43
GDP-PYR-3-8	11.06 ± 6.29	86.71 ± 0.41
GP-PYR-3-8	12.56±0.86	84.42 ± 0.00
PYR-3-8	12.52 ± 4.74	12.52 ± 0.00
GDP-12-3-14	2.05 ± 1.37	5.27 ± 20
GP-12-3-14	3.03 ± 1.77	12.27 ± 5.90
GDP-12-3-16	14.8 ± 1.38	57.63 ± 6.38
GP-12-3-16	13.57 ± 5.18	76.27 ± 17.34
GDP-12-3-18	6.32 ± 1.61	13.76 ± 4.31
GP-12-3-18	14.77 ± 0.75	39.07 ± 6.61

Table 5.5 MTT assay for the pyrene-based gemini surfactants complexes

	1	2	3	4	5	6	7	8	9	10	11	12
A	1.718	2.202	3.014	2.425	2.976	2.526	2.682	2.132	2.765	2.351	3.911	3.473
B	2.782	2.254	2.802	2.59	2.775	2.528	2.801	2.206	2.744	2.362	4.037	3.969
C	2.782	2.321	2.873	2.568	2.757	2.479	2.835	2.298	3.061	2.352	3.9	3.715
D	2.642	2.357	2.778	2.443	3.979	2.309	2.819	2.355	3.087	2.492	3.762	3.518
E				3.504	3.993	3.864	3.703	3.736	3.889	3.767	3.286	3.349
F				3.971	3.8	3.8	3.716	3.942	2.583	3.888	2.286	3.331
G				3.53	3.921	3.81	3.633	3.709	3.674	3.202	3.503	3.163
H				3.455	3.875	3.49	2.992	3.873	2.286	3.254	3.503	2.004

Viability %

	Pyrene-3-8											
5	1.718	2.782	2.782	2.642		53.20533	86.1567	86.1567	81.821		76.83493	13.75691
10	2.202	2.254	2.321	2.357		68.19449	69.80489	71.87984	72.99474		70.71849	1.853056
	Pyrene-3-12											
5	3.014	2.802	2.873	2.778		93.34159	86.77609	88.97491	86.03283		88.78136	2.846432
10	2.425	2.59	2.568	2.443		75.10065	80.21059	79.52927	75.6581		77.62465	2.266746
	Pyrene-3-14											
5	2.976	2.775	2.757	3.979		92.16476	85.93992	85.38247	123.227		96.67854	15.55727
10	2.526	2.528	2.479	2.309		78.22855	78.29049	76.77299	71.50821		76.20006	2.776078
	Pyrene-3-16											
5	2.682	2.801	2.835	2.819		83.05977	86.74512	87.79808	87.30257		86.22639	1.865806
10	2.132	2.206	2.298	2.355		66.02663	68.31836	71.16754	72.9328		69.61133	2.644605
	Pyrene-3-18											
5	2.765	2.744	3.061	3.087		85.63023	84.97987	94.79715	95.60235		90.2524	4.960868
10	2.351	2.362	2.352	2.492		72.80892	73.14958	72.83989	77.1756		73.9935	1.842009

Table 5.6 Statistical analysis: one-way ANOVA test of the asymmetric 12-3-n gemini surfactants in MG-63 and HEK-293 cell lines

Cell line	Formulation	Mean transfection	Transfection SD	Transfection SE	Viability mean	Viability SD	P Value	F value	Independent Variable
MG-63	Asymmetric full	5.284089	4.265666	1.421889	25.54921	13.54451	0.985	0.008	Transfection
	Asymmetric plasmid	5.242229	5.084563	1.694854	22.83906	15.33754			
MG-63	Positive control	5.606289	1.451699	0.3748271	49.76729	11.45297	0.782	0.078	
	Treatment	5.263159	4.552939	1.0731381	24.19413	14.10591			
MG-63	Positive control	5.606289	1.451699	0.3748271	49.76729	11.45297	3.45E-06	31.78	Viability
	Asymmetric	5.263159	4.552939	1.0731381	24.19413	14.10591			
MG-63	Negative control	3.450393	1.810859	0.4675619	88.65382	14.27005	4.31E-14	169.1	
	Treatment	5.263159	4.552939	1.0731381	24.19413	14.10591			
HEK-293	Asymmetric full	7.724621	5.748258	1.916086	26.34086	24.26054	0.521	0.431	Transfection
	Asymmetric plasmid	9.522161	5.861673	1.953891	37.82408	27.21913			
HEK-293	Positive control	23.102105	6.178396	1.595255	66.57943	9.650446	7.60E-08	48.86	Transfection
	Treatment	8.623391	5.707341	1.345233	32.08247	25.700799			
HEK-293	Negative control	2.921962	0.881482	0.2275977	96.155	0.571	0.000599	14.6	Transfection
	Treatment	8.623391	5.707341	1.3452332	32.08247	25.70			
HEK-293	Negative control	0.921962	0.881482	0.2275977	96.155	0.571	7.87E-11	92.69	Viability
	Treatment	8.623391	5.707341	1.3452332	32.08247	25.7			

Table.5.7 ELISA test calculations for 48 h

Charge ratio	Protein expression			
	Pyrene-3-8			
5	1.299	1.276	2.195	1.96
10	0.904	1.655	1.554	1.898
	Pyrene-3-12			
5	0.312	0.23	0.417	0.326
10	0.202	0.41	0.374	0.231
	Pyrene-3-14			
5	0.403	0.361	0.267	0.105
10	0.345	0.367	0.218	0.388
	Pyrene-3-16			
5	0.267	0.306	0.318	0.277
10	0.187	0.192	0.268	0.163
	Pyrene-3-18			
5	0.594	0.279	0.312	0.245
10	0.195	0.183	0.241	0.459
Lipofectamine	3.79	3.408	3.502	3.102
NT	0.112	0.098	0.092	0.09

Table.5.8 ELISA test calculations for 72 h

Charge ratio	Protein expression			
	Pyrene-3-8			
5	0.993	0.86	1.66	1.492
10	1.983	1.86	2.334	2.038
	Pyrene-3-12			
5	0.353	0.187	0.259	0.293
10	0.273	0.382	0.303	0.207
	Pyrene-3-14			
5	0.425	0.597	0.409	0.099
10	0.24	0.234	0.273	0.582
	Pyrene-3-16			
5	0.239	0.353	0.242	0.218
10	0.171	0.242	0.301	0.15
	Pyrene-3-18			
5	0.485	0.428	0.56	0.387
10	0.195	0.202	0.246	0.536
lipofectamine	3.598	3.224	3.126	3.6
Non treated	0.099	0.097	0.096	0.094

Table 5.9 Protein expression of γ -INF-GFP after 48h and 72h incubation period for Pyrene-based gemini surfactants formulation (GDP)

48H	Protein expression average	
	5	10
Pyrene-3-8	8589.43 \pm 2527.13	7615.02 \pm 2301.03
Pyrene-3-12	1210.22 \pm 415.24	1118.06 \pm 558.72
Pyrene-3-14	1008.29 \pm 716.57	1254.94 \pm 414.04
Pyrene-3-16	1051.66 \pm 129.88	566.48 \pm 246.46
Pyrene-3-18	1406.73 \pm 867.46	929.69 \pm 689.12

72H	Protein expression average	
	5	10
Pyrene-3-8	8613.53 \pm 2874.87	14603.87 \pm 1501.19
Pyrene-3-12	1311.28 \pm 517.02	1447.51 \pm 541.80
Pyrene-3-14	2128.65 \pm 1547.24	1753.56 \pm 1249.43
Pyrene-3-16	1236.64 \pm 452.9	885.80 \pm 515.03
Pyrene-3-18	2744.48 \pm 559.9	1473.64 \pm 1212.32

Table 5.10 Toxicity of Pyrene-based gemini surfactants-DNA-DOPE complex in COS-7 cell line

Formulation	1:5 ratio	1:10 ratio
Pyrene-3-8DP	76.83 \pm 13.76	70.72 \pm 1.85
Pyrene-3-12DP	88.78 \pm 2.84	77.62 \pm 2.27
Pyrene-3-14DP	96.68 \pm 15.56	76.20 \pm 2.80
Pyrene-3-16DP	86.23 \pm 1.86	69.61 \pm 2.64
Pyrene-3-18DP	90.25 \pm 4.96	73.99 \pm 1.84

**ELSEVIER LICENSE
TERMS AND CONDITIONS**

Jun 01, 2016

This is a License Agreement between Aula Al Muslim ("You") and Elsevier ("Elsevier") provided by Copyright Clearance Center ("CCC"). The license consists of your order details, the terms and conditions provided by Elsevier, and the payment terms and conditions.

All payments must be made in full to CCC. For payment instructions, please see information listed at the bottom of this form.

Supplier	Elsevier Limited The Boulevard, Langford Lane Kidlington, Oxford, OX5 1GB, UK
Registered Company Number	1982084
Customer name	Aula Al Muslim
Customer address	90 Marshall st Kitchener, ON n2j 2t4
License number	3880400794251
License date	Jun 01, 2016
Licensed content publisher	Elsevier
Licensed content publication	Biophysical Journal
Licensed content title	Characterization of Mixed Monolayers of Phosphatidylcholine and a Dicationic Gemini Surfactant SS-1 with a Langmuir Balance: Effects Of DNA
Licensed content author	V. Matti, J. Säily, Samppa J. Ryhänen, Juha M. Holopainen, Stefano Borocci, Giovanna Mancini, Paavo K.J. Kinnunen
Licensed content date	October 2001
Licensed content volume number	81
Licensed content issue number	4
Number of pages	9
Start Page	2135
End Page	2143
Type of Use	reuse in a thesis/dissertation
Portion	figures/tables/illustrations
Number of figures/tables /illustrations	1
Format	both print and electronic
Are you the author of this Elsevier article?	No
Will you be translating?	No

Dear Aula,

No problem: you can use it.
Best regards

Dr Sabine Castano

Maître de Conférences
Université de Bordeaux,
CBMN, UMR 5248
Allée Geoffroy Saint-Hilaire
33600 Pessac

Mail: sabine.castano@u-bordeaux.fr
Tel: 05 40 00 68 48 / 05 40 00 33 22

----- Mail original -----

De: aalmusli@uwaterloo.ca
À: "s castano" <s.castano@cbmn.u-bordeaux.fr>
Envoyé: Lundi 25 Avril 2016 16:54:43
Objet: permission to use an image

Dear Dr. Castano,
I am currently writing my PhD dissertation as part of my PhD multidisciplinary program at the Chemistry department at university of Waterloo about the use of non-viral gene delivery systems and part of the characterization is the use of Langmuir monolayers and BAM. For that, I would like to ask the permission to use an image in your publication: Brewster Angle Microscopy and PMIRRAS Study of DNA Interactions with BGTC, a Cationic Lipid Used for Gene Transfer in Langmuir in 2008. This is the scheme that I would like to include in my thesis: Scheme 3

.
Scheme of the DNA Interactions with BGTC/DOPE (3/2) Layer.

Can you please let me know if it is OK with you and if there is any form you would like me to sign to guarantee the proper use and referencing of the scheme?

Thanks,
Aula Al Muslim
PhD Candidate at the department of Chemistry
Office #4024

**JOHN WILEY AND SONS LICENSE
TERMS AND CONDITIONS**

Aug 15, 2016

This Agreement between Aula A Al Muslim ("You") and John Wiley and Sons ("John Wiley and Sons") consists of your license details and the terms and conditions provided by John Wiley and Sons and Copyright Clearance Center.

License Number	3930401218120
License date	Aug 15, 2016
Licensed Content Publisher	John Wiley and Sons
Licensed Content Publication	Journal of Gene Medicine
Licensed Content Title	Gene therapy clinical trials worldwide to 2012 – an update
Licensed Content Author	Samantha L. Ginn,Ian E. Alexander,Michael L. Edelstein,Mohammad R. Abedi,Jo Wixon
Licensed Content Date	Feb 27, 2013
Licensed Content Pages	13
Type of use	Dissertation/Thesis
Requestor type	University/Academic
Format	Print and electronic
Portion	Figure/table
Number of figures/tables	1
Original Wiley figure/table number(s)	Figure. Gene delivery vectors in clinical trials up to 2013
Will you be translating?	No
Title of your thesis / dissertation	Synthesis and Characterization of Dissymmetric gemini surfactants for gene delivery applications
Expected completion date	Sep 2016
Expected size (number of pages)	214
Requestor Location	Aula A Al Muslim 10A Victoria st South Kitchener, ON N2G 1C5 Canada Attn: Aula A Al Muslim
Publisher Tax ID	EU826007151
Billing Type	Invoice
Billing Address	Aula A Al Muslim 10A Victoria st South Kitchener, ON N2G 1C5 Canada

**SPRINGER LICENSE
TERMS AND CONDITIONS**

Aug 15, 2016

This Agreement between Aula A Al Muslim ("You") and Springer ("Springer") consists of your license details and the terms and conditions provided by Springer and Copyright Clearance Center.

License Number	3930410109574
License date	Aug 15, 2016
Licensed Content Publisher	Springer
Licensed Content Publication	The AAPS Journal
Licensed Content Title	Nonviral gene delivery: What we know and what is next
Licensed Content Author	Xiang Gao
Licensed Content Date	Jan 1, 2007
Licensed Content Volume Number	9
Licensed Content Issue Number	1
Type of Use	Thesis/Dissertation
Portion	Figures/tables/illustrations
Number of figures/tables /illustrations	1
Author of this Springer article	No
Order reference number	
Original figure numbers	Figure 1. methods of delivery and the cellular barriers
Title of your thesis / dissertation	Synthesis and Characterization of Dissymmetric gemini surfactants for gene delivery applications
Expected completion date	Sep 2016
Estimated size(pages)	214
Requestor Location	Aula A Al Muslim 10A Victoria st South Kitchener, ON N2G 1C5 Canada Attn: Aula A Al Muslim
Billing Type	Invoice
Billing Address	Aula A Al Muslim 10A Victoria st South Kitchener, ON N2G 1C5 Canada Attn: Aula A Al Muslim